UNIVERSITY OF BELGRADE

FACULTY OF TECHNOLOGY AND METALLURGY

Branislav S. Todić

KINETIC MODELING AND OPTIMIZATION OF FIXED-BED REACTOR FOR FISCHER-TROPSCH SYNTHESIS

Doctoral Dissertation

Belgrade, 2015

UNIVERZITET U BEOGRADU

TEHNOLOŠKO-METALURŠKI FAKULTET

Branislav S. Todić

MODELOVANJE HEMIJSKE KINETIKE I OPTIMIZACIJA REAKTORA SA PAKOVANIM SLOJEM ZA FISCHER-TROPSCH SINTEZU

doktorska disertacija

Beograd, 2015

Members of the thesis committee:

Dr Nikola Nikačević, Associate Professor

University of Belgrade, Faculty of Technology and Metallurgy

(Thesis advisor)

_____

Dr Dragomir Bukur, Full Professor
Texas A&M University

_____

Dr Aleksandar Orlović, Associate Professor
University of Belgrade, Faculty of Technology and Metallurgy

_____

Acknowledgements

I would like to thank my thesis advisors and mentors, Prof Dragomir Bukur and Dr Nikola Nikačević, for their thorough and dedicated guidance. I am grateful for Prof Bukur's persistent comments and drive for excellence through hard work and persistence. I am thankful to Nikola for his reassurances, helping me stay on track with the dissertation, as well as advises and expertize he provided during the last four years.

I thank Dr Aleksandar Orlović for serving as a member of my thesis committee.

I would also like to acknowledge the help and support of my MSc Thesis mentor, Dr Dejan Skala, for recognizing my affinity for reaction engineering and motivating me to enroll in Doctoral studies at Faculty of Technology and Metallurgy.

I am very privileged to have been advised by Prof Gilbert Froment during my work on kinetic model development, for which I thank him.

Heartfelt thanks goes to researchers from Center for Applied Energy Research (University of Kentucky, US): Dr Wenping Ma for his excellent experimental work on cobalt-based catalyst for FTS; Dr Gary Jacobs for advices with analysis, manuscript preparations and positive encouragement; and Prof Burtron Davis for advices and overall project guidance.

In the end, I would like to thank my family, especially my sister Sanja, for their support and help during my studies.

Kinetic modeling and optimization of fixed-bed reactor for Fischer-Tropsch synthesis

Abstract

Fischer-Tropsch synthesis (FTS) is a heterogeneously catalyzed chemical reaction in which a mixture of hydrogen and carbon-monoxide is converted into an array of hydrocarbon products. These products can be used as synthetic liquid fuels (gasoline, diesel, kerosene) or feedstock for the chemical industry. As such, FTS is a key step in the conversion of coal, natural gas and biomass into liquids in large plants all over the world, including plants in Qatar, Malaysia, South Africa etc. Even though FTS has been commercially used for most of the 20th century, many fundamental aspects of this reaction are unclear. The main objectives of the work included in this thesis were: to study the effect of process conditions on FTS product selectivity and distribution with regards to hydrocarbon chain length, develop a detailed model of FTS kinetics (capable of predicting both reactant disappearance and product formation rates) and apply the detailed kinetic model in modeling and optimization of a multi-tubular fixed-bed reactor for FTS.

Most often used catalysts for FTS are iron and cobalt. The experimental data used in this study were obtained in collaboration with Texas A&M University and Center for Applied Energy Research, University of Kentucky, for iron- and cobalt-based catalyst, respectively. The analysis of experimental data for both catalysts showed dependence of product selectivity from process conditions inside the reactor (temperature, pressure, reactant feed ratio and conversion level). These dependences were shown to be related to the chain-growth probability factor (α), which also varies with carbon number. Over the cobalt catalyst, the significant variation of C_1 intermediate growth probability (α_1) at different process conditions and a lack of the same variations for higher C_{2+} chain intermediates, was interpreted as evidence for the existence of separate methanation pathways. The same data presented evidence that the secondary 1-olefin readsorption does not play a major part in determining FTS selectivity. For the iron-based catalysts, similar correlations between variations of growth probability with process conditions were found. However, existence of additional pathways for methane formation and relevance of secondary olefin reactions could not be confirmed for that catalyst.

A detailed model of FTS kinetics was developed using the Langmuir-Hinshelwood-Hougen-Watson methodology. A number of different kinetic models was derived based on the forms of carbide and CO-insertion mechanisms. A concept of chain-length-dependent olefin desorption was derived from fundamentals and used to explain the variation of chain-growth probability and olefin-to-paraffin ratio with carbon number. The parameters of these kinetic models were determined using the hybrid genetic algorithm with the data obtained over the cobalt catalyst and a range of conditions. Different kinetic models were then discriminated based on statistical and physico-chemical criteria. The detailed kinetic model derived from CO-insertion mechanism was selected as the best amongst those tested. The model showed excellent ability to predict the rates of formation of n-paraffin and 1-olefin products, as well as a good ability to predict the disappearance of carbon-monoxide and hydrogen. Typically observed deviations of the experimental data from the Anderson-Schulz-Flory (ASF) product distributions were predicted with this model.

The developed detailed kinetic model was applied in modeling and optimization of fixed-bed reactor for FTS. The reactor model was a simple one-dimensional pseudo-homogeneous fixed-bed reactor, with assumptions of no intra-particle mass and heat transport resistances, gas plug flow and negligible liquid flow. Simulations were performed in order to test the effect of process conditions at the reactor inlet on the reactor performance. In addition, optimization of inlet parameters, including inlet temperature, flow rate and reactant ratio, was conducted in order to maximize the productivity of desired C_{5+} products. In collaboration with Texas A&M University at Qatar, our future work will focus on development of a comprehensive and highly sophisticated models of conventional FTS fixed-bed and novel milli-structured reactor systems by coupling of detailed FTS surface kinetics, realistic heat and mass transfer phenomena inside the catalyst particle with computational fluid dynamics reactor balances for mass, heat and momentum.

Keywords: Fischer-Tropsch synthesis, cobalt catalyst, iron catalyst, product selectivity, product distribution, kinetic modeling, reaction mechanism, fixed-bed reactor.

Academic Expertise: Technological Engineering (Chemical Technology)

Field of Academic Expertise: Chemical Engineering

UDC: 621.039.514:665.652.7

Modelovanje hemijske kinetike i optimizacija reaktora sa pakovanim slojem za Fischer-Tropsch sintezu

Rezime

Fischer-Tropsch sinteza (FTS) je heterogeno katalizovana hemijska reakcija u kojoj se smeša vodonika i ugljen-monoksida pretvara u niz ugljovodoničnih proizvoda. Ti proizvodi se mogu koristiti kao sintetička tečna goriva (benzin, dizel i kerozin) ili sirovine za hemijsku industriju. Kao takva, FTS je ključni korak u konverziji uglja, prirodnog gasa i biomase u tečnosti u velikim postrojenjima širom sveta, uključujući postrojenja u Kataru, Maleziji, Južnoj Africi itd. Iako je FTS veći deo dvadesetog veka bila u komercijalnoj upotrebi, mnogi fundamentalni aspekti ove reakcije su nejasni. Glavni ciljevi istraživačkog rada u sklopu ove disertacije su bili: ispitivanje efekata procesnih uslova na selektivnost i raspodelu FTS proizvoda u odnosu na dužinu ugljovodoničnog lanca, razvoj detaljnog kinetičkog modela FTS (sposobnog da ujedno predskaže brzine nestajanja reaktanata i nastajanja proizvoda) i primena detaljnog kinetičkog modela u modelovanju i optimizaciji višecevnih FTS reaktora sa pakovanim slojem katalizatora.

Najčešće korišćeni katalizatori za FTS su gvožđe i kobalt. Eksperimentalni podaci za gvozdeni i kobaltni katalizator korišćeni u ovoj studiji su dobijeni u saradnji sa Texas A&M Univerzitetom (Texas A&M University) i Centrom za primenjeno istrazivanje energije Univerziteta u Kentakiju (Center for Applied Energy Research, University of Kentucky), respektivno. Analiza eksperimentalnih podataka za oba katalizatora je pokazala zavisnost selektivnosti proizvoda reakcije of procesnih uslova unutar reaktora (temperature, pritiska, odnosa reaktanata u ulaznoj smeši i konverzije reaktanata). Pokazano je da su ove zavisnosti povezane sa verovatnoćom rasta ugljovodoničnog lanca (α), koja se takođe menja sa brojem atoma ugljenika. Značajne varijacije u vrednosti verovatnoće rasta C_1 lančanih intermedijera pri različitim procesnim uslovima, zabeležene sa kobaltnim katalizatorom, kao i odsustvo istih varijacija za duže C_{2+} lančane intermedijere, su interpretirane kao dokaz postojanja dodatnog reakcionog puta za metanaciju. Isti rezultati su poslužili kao dokaz da sekundarne reakcije 1-alkena ne igraju bitnu ulogu u određivanju selektivnosti FTS. Slične korelacije između promena

verovatnoće rasta lanca i procesnih uslova su zapažene i sa gvozdenim katalizatorom. Međutim, postojanje dodatnog reakcionog puta za formiranje metana i važnost sekundarnih reakcija alkena nisu potvrđene za taj katalzator.

Detaljni FTS kinetički model je razvijen primenom Langmuir-Hinshelwood-Hougen-Watson pristupa. Nekoliko različitih kinetičkih modela je izvedeno na osnovu oblika karbidnog mehanizma i mehanizma CO-umetanja. Koncept zavisnosti desorpcije alkena od dužine molekula je izveden iz teorije i korišćen za objašnjenje promene verovatnoće rasta lanca i odnosa alkena i alkana sa različitim brojem C-atoma. Parametri ovih modela su određeni upotrebom hibridnog genetičkog algoritma sa podacima dobijenim sa kobaltnim katalizatorom pri obsegu procesnih uslova. Različiti kinetički modeli su diskriminisani na osnovu statističkih i fizičko-hemiskih kriterijuma. Među testiranim modelima, detailjni kinetički model zasnovan na mehanizmu CO-umetanja je izabran kao najbolji. Model je pokazao odličnu mogućnost predskazavanja brzina formiranja n-alkana i 1-alkena i dobru mogućnost predviđanja brzina nestajanja ugljen-monoksida i vodonika. Model predskazuje tipična odstupanja od Anderson-Schulz-Flory (ASF) raspodele proizvoda.

Izvedeni detaljni kinetički model je primenjen u modelovanju i optimizaciji cevog reaktora sa pakovanim slojem katalizatora za FTS. Korišćeni model reaktora je bio jednostavni jednodimenzioni pseudo-homogeni model reaktora sa pakovanim slojem, sa pretpostavkom da su otpori prenosu mase i toplote unutar čestica katalizatora zanemarljivi, pretpostavljeno je idealno strujanje gasa i zanemarljivo mali protok tečne faze. Efekat različitih procesnih uslova na ulazu na ponašanje reaktora je testiran uz pomoć simulacija. Takođe, sprovedena je optimizacija ulaznih parametara, uključujući ulaznu temperaturu, protok i odnos reaktanata, u cilju povećanja produktivnosti željenih C_{5+} proizvoda. U saradnji sa Texas A&M Univerzitetom u Kataru (Texas A&M University at Qatar), naš budući rad će se fokusirati na razvoj sveobuhvatnih i naprednih modela konvencionalnih cevnih reaktora za FTS, kao i novih mili reaktorskih sistema, kroz povezivanje detaljne kinetike FTS, realističnih prenosa toplote i mase unutar čestica katalizatora sa CFD (computational fluid dynamics) modelima reaktora, koji sadrže bilanse za masu, toplotu i količinu kretanja.

Ključne reči: Fischer-Tropsch sinteza, kobaltni katalizator, gvozdeni katalizator, selektivnost proizvoda reakcije, raspodela proizvoda reakcije, modelovanje kinetike, mehanizam reakcije, reactor sa pakovanim slojem katalizatora.
Naučna oblast: Tehnološko Inženjerstvo
Uža naučna oblast: Hemijsko Inženjerstvo
UDK: 621.039.514:665.652.7

Table of contents:

1. Introduction

One of the greatest challenges that the modern civilization is facing in the 21st century is coping with a growing need for energy and the impact that the increased consumption of unclean energy sources has on the environment. Even though alternative clean and renewable energy sources, such as solar, wind, geothermal etc., have been known and used for a long time, their application in powering our industries and day-to-day life is hindered by many factors. Main of these are high cost of developing the new technologies for their utilization (e.g. thermonuclear fusion) and inefficiency of technologies that are currently used (e.g. solar energy). All of these energy sources have a future, but the transition to them will be gradual and long term. For now the population' energy requirements are met with existing unrenewable energy sources and will continue to be in the following decades. Oil and gas are a big part of these resources. Most projections show that liquid fossil-derived fuels will be used as a main source of energy in transportation throughout the 21st century [1].

In recent years natural gas industry has had a considerable growth due to the larger utilization of shale gas resources. In addition, some of the previously untapped large gas fields in the Middle East and Caucuses have been put into production. This global increase in production of natural gas has also had for a consequence a decrease in gas prices. The energy obtained from 1 USD worth of natural gas is in todays' market significantly higher than that from 1 USD worth of crude oil [1]. However, a major problem of natural gas is its transportation from the source, which is often very remote and inaccessible by pipeline, to the final consumer. One of the ways this is circumvented is by indirectly converting natural gas into synthetic high value liquid oil. This is done through the so-called Gas-to-Liquid (GTL) process (Figure 1.1), where natural gas is first converted to synthetic gas, which is then converted into liquid products. As such, GTL is a part of XTL (X-to-Liquid) processes, where X can stand for coal, natural gas and even biomass. The high energy consumption of the GTL process is acceptable due to the economic viability of the process, which stems from the price difference between natural gas and crude oil.

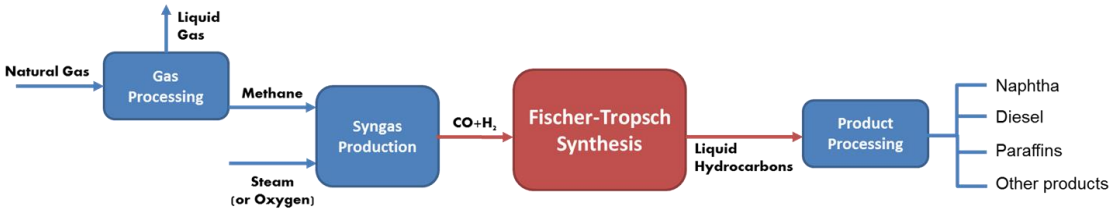

Figure 1.1 - Schematic of the GTL process.

A key part of the GTL process is the Fischer-Tropsch Synthesis (FTS), a heterogeneous chemical reaction in which a mixture of carbon-monoxide and hydrogen is converted into an array of polymerized products, mainly consisting of liquid hydrocarbons (n-paraffins and 1-olefins). These are then processed into a variety of high value products (mainly ultra-clean liquid fuels) in the downstream processes.

Fischer-Tropsch Technology (Past, Present and Future)

The Fischer-Tropsch synthesis has been around for over a century and has a very interesting history. In this time it has gone through several periods of discovery and re-discovery that are mainly liked with the prices and availability of crude oil (Figure 1.2) [2]. In many ways the history of FTS is the history of chemistry and chemical engineering, as well as the 20th century world history.

In 1902 Sabatier and Sanders [3] discovered that CO can be hydrogenated to methane using various metallic catalysts (Fe, Ni, Co etc.). During the 1920s, Fischer and Tropsch [4, 5] later discovered that under mild conditions (250 - 300 °C and 1 atm) and over Co-Fe catalysts, carbon-monoxide and hydrogen can react to give liquid hydrocarbons and even solid paraffins. These publications formed an initial seed of what is to be called Fischer-Tropsch technology. The development of commercial FTS process took place in Germany during the 1930s and early 1940s. Seeing that Germany had no reserves of crude oil of its own, in the period prior to and during World War II, it had invested heavily into the production of synthetic oil through direct coal liquefaction (DCL) and coal-to-liquids (CTL) process. First small pilot plant based on FTS technology was constructed in Mulheim in 1932, followed by larger pilot plant in Oberhausen-Holten

in 1934 with the capacity of about 200 bbl/day [6]. A series of larger CTL plants followed and by 1944 Germany produced about 12000 bbl/day, approximately 10-15% of its total production of liquid synthetic fuels [7]. The general belief during that time was that the global supply of oil is very limited and will be exhausted quite fast. This is why FTS research performed in Germany and data from its industrial plants was considered to be very valuable by the allies, who formed a Technical Oil Mission (TOM) tasked with collecting the documents pertaining to FTS [7, 8]. The files collected by the TOM were later revealed to public trough Texas A&M University in the 1970s.

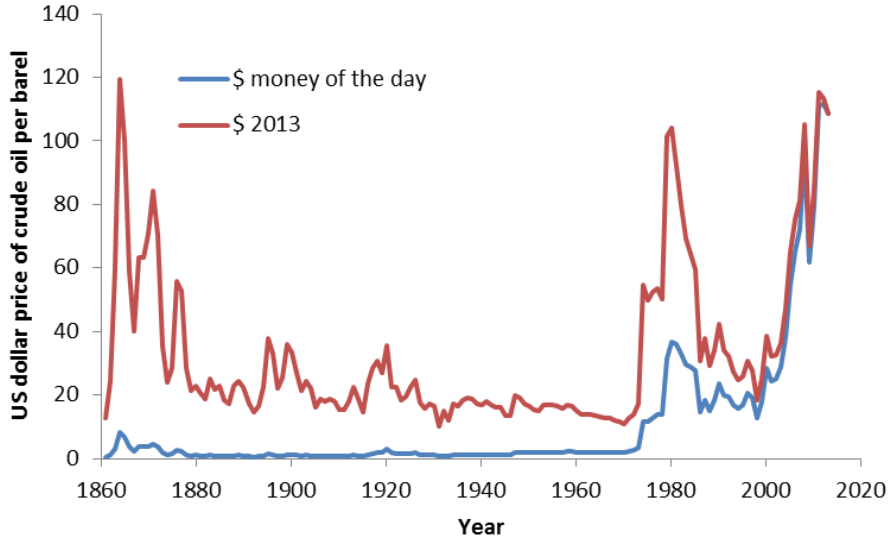

Figure 1.2 – Historical prices of crude oil (Note: 1861-1944 US Average, 1945-1983 Arabian Light posted at Ras Tanura, 1984-2013 Brent dated; Data from Ref. [9])

Research into FTS continued during the early 1950s in both Germany and United States, with several smaller pilot plants. The first GTL plant was constructed in Brownsville, Texas, opened in 1951, with the capacity of 7000 bbl/day. Similarly, in 1955 in Sasolburg, South Africa, a CTL plant was constructed. However, at that time large oilfields were discovered in the Middle East, providing ample supply of cheap oil. Therefore the need to produce synthetic oil via FTS disappeared, resulting in closing of the Brownsville and most other FTS-based plants and in a pause in research into this technology. Since South Africa had an ample supply of coal and limited reserves of oil, together with a complex political situation in which its government was under

international pressure to dismantle the Apartheid system, including trade embargos, the Sasolburg plant continued to function throughout the 1960s and 70s.

The second era of FTS growth and expansion happed in the 1970s and 80s and was initiated by OAPEC (Organization of Arab Petroleum Exporting Countries) oil embargo. Therefore, the western countries had to look for alternatives to cheap Middle Eastern oil, and FTS immediately appeared as a possible solution. During this period support of research into FTS increased dramatically. Initially, much of the work focused on re-discovery of earlier knowledge about the FTS technology, but additional advances were made in the areas of catalyst preparation (relating activity and selectivity with metal loading, promoters, support types etc.) and reactor design [7]. The Sasolburg plant was expanded and joined by two additional plants in South Africa, with combined capacity of about 120 000 bbl/day [2]. In the mid-1980s, once again, the price of crude oil declined and the funding for FTS related research decreased due to its economic unviability. However, this time research has not ceased completely and industry continued to work on development of this technology.

Even with decrease in price of crude oil, two new large scale plants were commissioned in Bintulu, Malaysia, and Mossel Bay, South Africa, by Shell and PetroSA, respectively. These were the first large scale plants which used natural gas, instead of coal, as feedstock. The profitability of these plants significantly increased ever since the price of one barrel of crude oil passed above 30$ in 1999. Since that time the oil price has been well above 30 $/bbl, making GTL economically viable. On the other side, recent discovery of large amounts of shale gas has made the supply of cheap natural gas insured in the foreseeable future. High price of oil coupled with low price of natural gas makes the GTL an industry with very high profit margins. Additionally, local circumstances can also influence decisions to construct GTL plants. Best examples for this is Qatar, with an ample supply of “stranded” natural gas (inaccessible to final consumers by natural gas pipelines), where initially gas was sold as liquefied natural gas (LNG). However, the reduced global prices of natural gas have incented the diversification of use of this resource and the construction of two of the largest GTL plants in the world, Oryx GTL by Sasol and Pearl GTL by Shell (both in collaboration with Qatar Petroleum), with capacities of 34 000 and 140 000 bbl/day, respectively. Similar factors are driving the

construction of other large GTL plants in places such as Uzbekistan, Nigeria and even US (Figure 1.3).

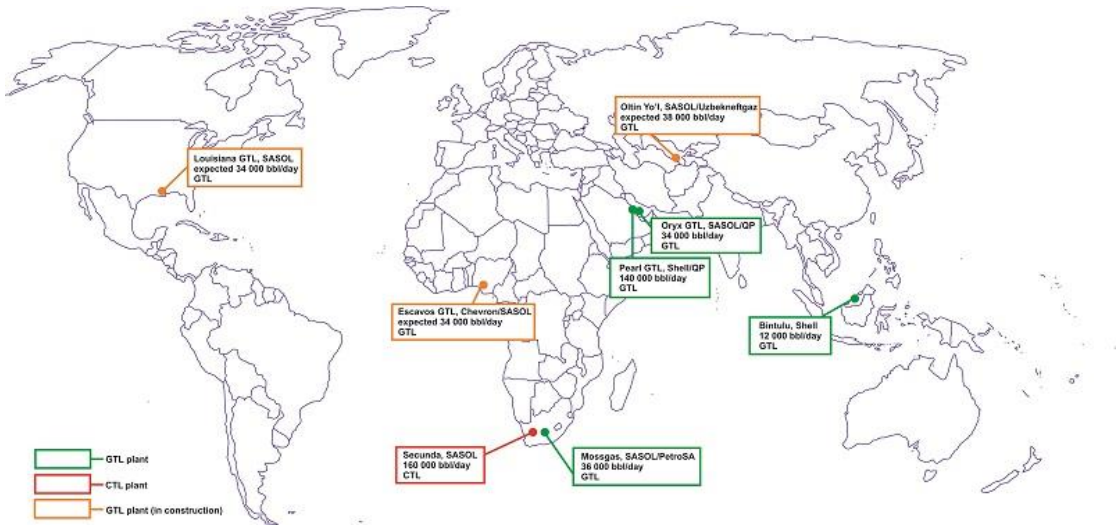

Figure 1.3 – Large scale GTL and CTL plants worldwide.

It was long believed that GTL can be economically viable only on the large scale, meaning that it required large fields of natural gas. The fields of sufficient size exist only in few places worldwide. However, interest into small scale GTL has increased significantly. This has a lot to do with the environmental legislation pressure that the oil companies are under, forcing reduction in flaring of natural gas during oil exploitation. Another factor is the development of a new generation of smaller micro-channel reactors and a more compact processes for GTL that are pioneered by Velosys-Oxford Catalyst and Compact GTL companies [10, 11]. These companies promise profitable modular GTL plats with capacities from 1000 to 15 000 bbl/day.

As long as the supply of cheap natural gas feedstock coming from large gas fields across the world is secured, large scale GTL will be economically competitive and will have a bright future. Small scale GTL is sure to be successful as well, and potentially for an even longer time, since it can be related to the use of flaring natural gas during oil production, as well as utilization of small natural gas fields. If we add BTL, which is more and more used in Europe [12-18], and CTL technology, being commercialized in China [19] [20], we can conclude that the FTS could have a very important role in the global energy future.

Research Motivation and Objectives

The new paradigm of chemical reaction engineering being developed for the 21st century dictates that the major improvement of existing processes, as well as development of new green and more compact processes, requires the use of more sophisticated and fundamental models of chemical reactors [7, 21]. Design of a new generation of FTS commercial chemical reactors will involve science-based understanding of all scales relevant to the FTS process. A good example for this is the replacement of empirical kinetic expressions used to obtain reactant consumption and product selectivity, an approach that was typically used up until now in FTS reactor modeling, with more fundamental detailed kinetic models of FTS, that provide both reactant consumption and product formation rates, and which will be applied in this thesis. Potential benefits include improved product yield, better reactor design and operation, as well as the overall increase in profitability of these units.

Objectives of this thesis include:

- ***Analysis of the effect of process conditions on FTS in terms of activity and product distribution.***

Using experimental data obtained over cobalt- and iron-based catalysts and under relevant FTS conditions, the effects of time on stream, temperature, pressure, reactant feed ratio and conversion level on overall product selectivity, as well as parameters that determine selectivity, i.e. chain growth probability and ratios between different product species, will be analyzed. This will enable us to draw important conclusions about the kinetics of major and minor reactions under FTS conditions for both cobalt- and iron-based catalysts.

- ***Development of a detailed kinetic model of FTS.***

A series of detailed mechanistic models of FTS kinetics over cobalt-based will be derived using the Langmuir-Hinshelwood-Hougen-Watson approach. Their intrinsic kinetic parameters will be estimated using experimental data. Models will be discriminated and the best detailed kinetic model will be chosen based on statistical and physico-chemical criteria.

- ***Application of detailed kinetics in fixed-bed reactor modeling and optimization.***

A one-dimensional pseudohomogenious reactor model including detailed FTS kinetics will be developed. Simulations will be performed in order to determine the result of process parameters on product yields and selectivity. Rigorous optimization of process parameters will be conducted in terms of maximum yield of desired products. Obtained results will be analyzed and compared to available literature data.

2. Literature review

Publications from this chapter

1. Branislav Todic, Vitaly V. Ordomsky, Nikola M. Nikacevic, Andrei Y. Khodakov and Dragomir B. Bukur, "Opportunities for intensification of Fischer–Tropsch synthesis through reduced formation of methane over cobalt catalysts in microreactors", Catalysis Science & Technology, **2015**, 5, 1400.

2.1. Basic studies in FTS

Fischer-Tropsch synthesis (FTS) is reaction between carbon-monoxide and hydrogen over a solid metallic catalyst in which a wide range of organic products is formed. Depending on the catalyst and process conditions the content of various product species can vary, but main products are always n-paraffins and 1-olefins. Minor products formed in FTS include branched hydrocarbons, 2-olefins and various oxygenate species (alcohols, aldehydes, ketones etc.). All of these product species are present in an array of different chain lengths, from those containing only one carbon atom to well over a hundred.

The overall stoichiometry of FTS for hydrocarbon formation can be shown as:

$$CO + (1 + \frac{m}{2n})H_2 \longrightarrow \frac{1}{n} C_n H_m + H_2O \qquad (2.1)$$

However, this portrayal significantly oversimplifies the complexity of FTS kinetics, since the reaction itself consists of a series of elementary steps. These steps can be divided into groups, such as reactant adsorption, chain initiation, propagation and termination etc., which all have its own sub-steps (which will be discussed below). In addition, Eq. (2.1) does not include the formation of oxygenate products (mainly alcohols):

$$nCO + 2nH_2 \longrightarrow C_n H_{2n+1} OH + (n-1)H_2O \qquad (2.2)$$

Under FTS conditions a number of side reactions occur both in parallel and in sequence to the main reaction, involving both reactants and products of FTS. Most notably these

include water-gas shift (WGS) reaction, Boudouard reaction, catalyst oxidation and bulk carbide formation and secondary reactions of FTS products (mainly 1-olefins and alcohols). This is why FTS kinetics is considered to be highly complex. It is made even more difficult to study considering the three-phase nature of the reaction and resistances that can occur with mass and heat transfer in FTS reactors.

Catalysts

Most often used catalysts in FTS are group VIII metals: iron (Fe), cobalt (Co) and ruthenium (Ru). The choice between these catalysts is made on the basis of:

- *Metal cost* – Iron is the cheapest and ruthenium the most expensive catalyst, with current approximate relative cost being Fe (1) < Co (350) < Ru (20000) [22]. Due to its extremely high price and limited availability, ruthenium catalysts are not used in commercial FTS reactors.

- *Catalyst activity and selectivity* - Iron is the least and ruthenium most active FTS catalyst [23]. Iron catalysts have high WGS activity and high olefin content, while cobalt and ruthenium produce more waxy paraffinic products. A good reviews of comparisons between various catalysts in terms of activity and selectivity are given by Davis and co-workers [24, 25] and Bartholomew and Farrauto [7].

- *Feedstock for syngas production* – The feedstock for XTL process can be coal, biomass and natural gas. Coal is the most carbon-rich feedstock and gives syngas with H_2/CO ratios bellow 1. Since stoichiometric ratio for hydrocarbon production is about 2, the ratio in coal-derived syngas needs to be increased by WGS. This makes iron the catalyst of choice for CTL plants. Natural gas on the other side gives syngas with H_2/CO ratios of about 2 making it readily available for FTS. Therefore, the catalyst used in GTL is cobalt.

The cost is also one of the factors determining the form in which catalyst is used, i.e. catalyst design. In order to reduce cost metallic cobalt is usually dispersed over a support which is pre-shaped. This allows for a very high surface area with only 10 to 20 wt. % loading of cobalt. The supports used for cobalt are typically alumina (Al_2O_3), silica (SiO_2)

and titania (TiO_2). Active material in these catalysts is metallic cobalt. Therefore, additives such as noble metal promoters (e.g. Ru, Re and Pt) are added to the cobalt-based catalysts in small amounts (usually up to 0.2 wt. %) in order to promote catalyst reduction and thereby increase activity.

On the other hand, much cheaper iron catalyst is usually used as bulk catalyst with contents of iron around 60 wt. %. To increase the mechanical strength binder materials, such as silica, are used. Iron catalyst usually contain 1 to 5 wt. % of copper (Cu) as a reduction promoter. It is also well known that promotion with alkali metals, most often potassium (K), improves iron catalysts activity, as well as selectivity.

A recent work by Botes et al. [26] gives an excellent comparison of iron and cobalt catalysts from an industrial perspective. A wealth of information about FTS catalyst design, as well as activity and selectivity, can be found in reviews done by Bartholomew and Farrauto [7], Dry [27], Iglesia et al. [28, 29] and Khodakov et al. [30].

Reaction mechanism

Even though FTS is known and utilized in XTL industry for almost a full century, the exact sequence of its elementary steps (i.e. reaction mechanism) is still a subject of considerable debate in the scientific community. What is agreed is that FTS is a polymerization type reaction, consisting of following steps:

1. *Reactant adsorption* – CO and H_2 adsorb to the active surface.
2. *Chain initiation* – Adsorbed reactants produce a C_1 intermediate, which is the chain initiator.
3. *Chain propagation* – Carbon containing species (i.e. monomer) is inserted into the growing chain, increasing its carbon number by one.
4. *Chain termination and desorption* – Product molecule is formed and desorbed from the surface.

5. *Secondary reactions of formed products* – Product molecules can readsorb onto the surface and participate in secondary reactions.

Several authors reviewed the FTS mechanism in detail [7, 23, 31-35]. Here we will give a short summary of proposed mechanisms and a short comparison of the most likely candidates.

Classification of proposed FTS mechanisms can be made according to the growing chain and monomer species to: alkyl [4, 36], CO insertion [37], enolic [38], and alkenyl mechanisms [39].

Alkyl mechanism – This mechanism was initially introduced by Fischer and Tropsch [4] and has since been a part of mechanistic discussions, where number of revisions and alternative forms have been proposed. This is why it is also known as carbide, carbene or CH_x insertion mechanism. The most commonly used form of alkyl mechanism is shown in Figure 2.1. In this mechanism CO dissociates upon adsorption on the surface, whether directly or with the assistance of hydrogen. It is then hydrogenated to a monomeric species CH_x, which is most often believed to be CH_2. Chain initiator is the adsorbed metyl species. Chain propagation proceeds by successive insertion of CH_x species into the growing alkyl chain. Alkyl chain is terminated by hydrogenation, dehydrogenation and hydroxylate to give paraffin, olefin and alcohols, respectively.

It is well known that iron catalysts form carbides, which is why Fischer and Tropsch's proposal of carbide mechanism, where surface carbide played a role of monomer, found large support. However, experiments with labeled carbon in iron-carbide performed by Kummer et al. [40] showed that only a small amount of products originates from carbides. Thus, alternative pathways had to be explored. Brady and Petit [36] modified the carbide mechanism to what is today known as alkyl mechanism by making the CH_2 species the growth monomer. They proposed that C-C bond is formed by CH_2-alkyl reaction. The formation of CH_2 species, as well as propagation, is generally considered to be irreversible in alkyl mechanism [36, 37]. Also, other reaction monomers, as well as initiation and propagation pathways, are also possible within the alkyl mechanism. For example, Ciobica et al. [41, 42] proposed CH species as the monomer.

Currently, various routes for initiation and propagation are being examined using computation chemistry and these studies will be reviewed below.

Termination in alkyl mechanism produces n-paraffins and 1-olefins as main products. An initial flaw of alkyl mechanism was its inability to explain oxygenates formation. Johnston and Joyner [43] proposed that hydroxyl group could be involved in their formation, but these claims were never experimentally substantiated.

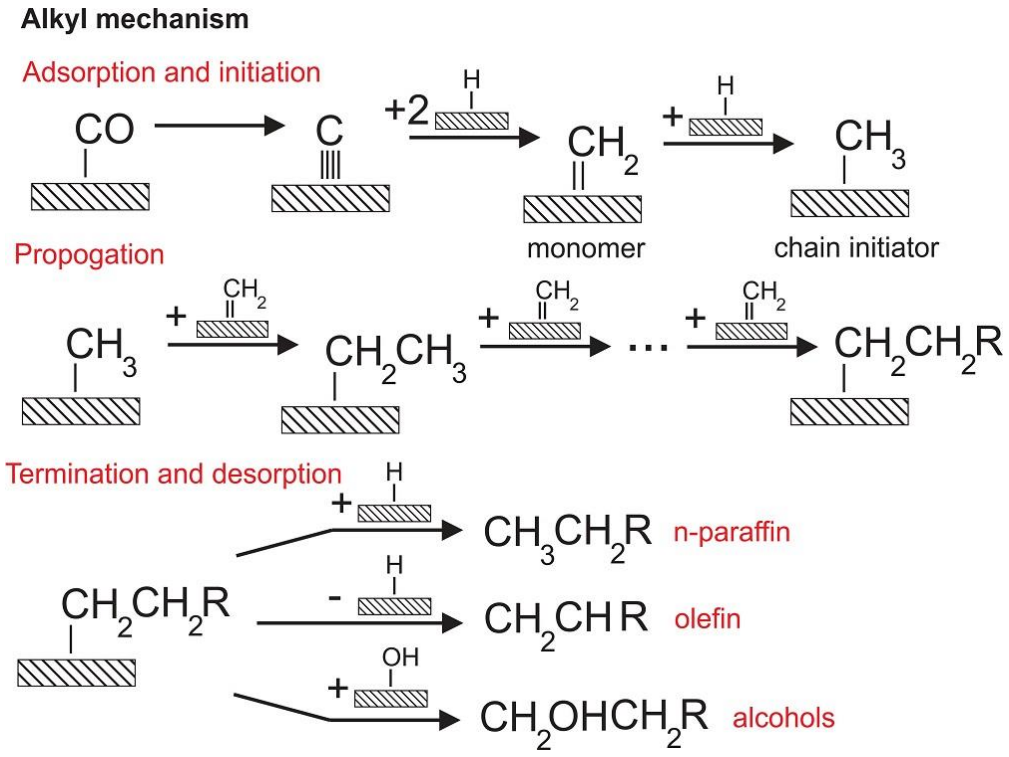

Figure 2.1 – Schematic of the alkyl mechanism

Alkenyl mechanism – Maitlis et al. [39, 44] proposed an alkenyl mechanism for olefin formation in FTS (Figure 2.2). According to it the C-C bond was formed in a reaction between adsorbed methylidyne (CH) and methylene (CH_2). The resulting vinyl species ($CH=CH_2$) is the chain initiator and propagation occurs by successive insertion of CH_2 into the alkenyl (i.e. vinyl) chain. The alkenyl chain is terminated by hydrogenation to form 1-olefin.

This reaction mechanism failed to take into account the formation of primary n-paraffin, for which an additional pathway is required. It is interesting though that very

low energy barrier was predicted for alkenyl mechanism. Ge et al. [45] reported activation energies of 55.9 and 166.5 kJ/mol for Co and Ru catalysts, respectively.

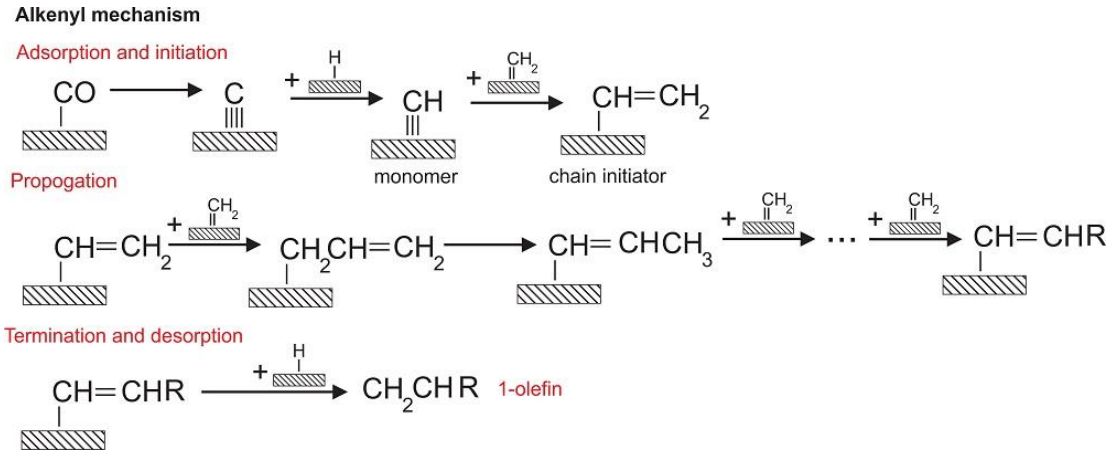

Figure 2.2 - Schematic of the alkenyl mechanism

Enolic mechanism – Storch et al. [46] proposed a mechanism that involved oxygen-containing species and was able to account for oxygenate formation in FTS. According to it, initiation step is the hydrogenation of CO to hydroxycarbine CHOH (i.e. enol). Propagation occurs by reaction of CHOH with the adsorbed enolyc species RCOH, during which water is eliminated. Termination steps yield an array of oxygenate products (alcohols, aldehydes and acids) along with 1-olefin. Similar to alkenyl mechanism, n-paraffins are believed not to be the primary products of FTS, but are formed in secondary 1-olefin reactions.

CO-insertion mechanism – Pichler and Schulz [37] developed a CO-insertion mechanism in FTS. This type of mechanism was previously well-known in organic chemistry. According to this mechanism, CO was first hydrogenated after which C-O bond was severed. Chain propagation occurs by insertion of adsorbed CO into the metal-alkyl bond forming an acyl species CH(OH)R. This is then hydrogenated and oxygen is removed to form another alkyl molecule. Similar to alkyl mechanism, these can terminate by hydrogenation to form n-paraffins or β-hydrogen elimination to form 1-olefin. The main advantage of this mechanism was its ability to explain formation of oxygenates in FTS, as shown in Figure 2.3. Acyl molecules can participate in hydrogenation to n-alcohols or hydrogen elimination to aldehydes. It was long believed that this mechanism

is the most likely candidate for oxygenate formation [33], however recent transient kinetic studies of Schweicher et al. [47, 48] provided some new evidence for CO-insertion as the main mechanism of FTS.

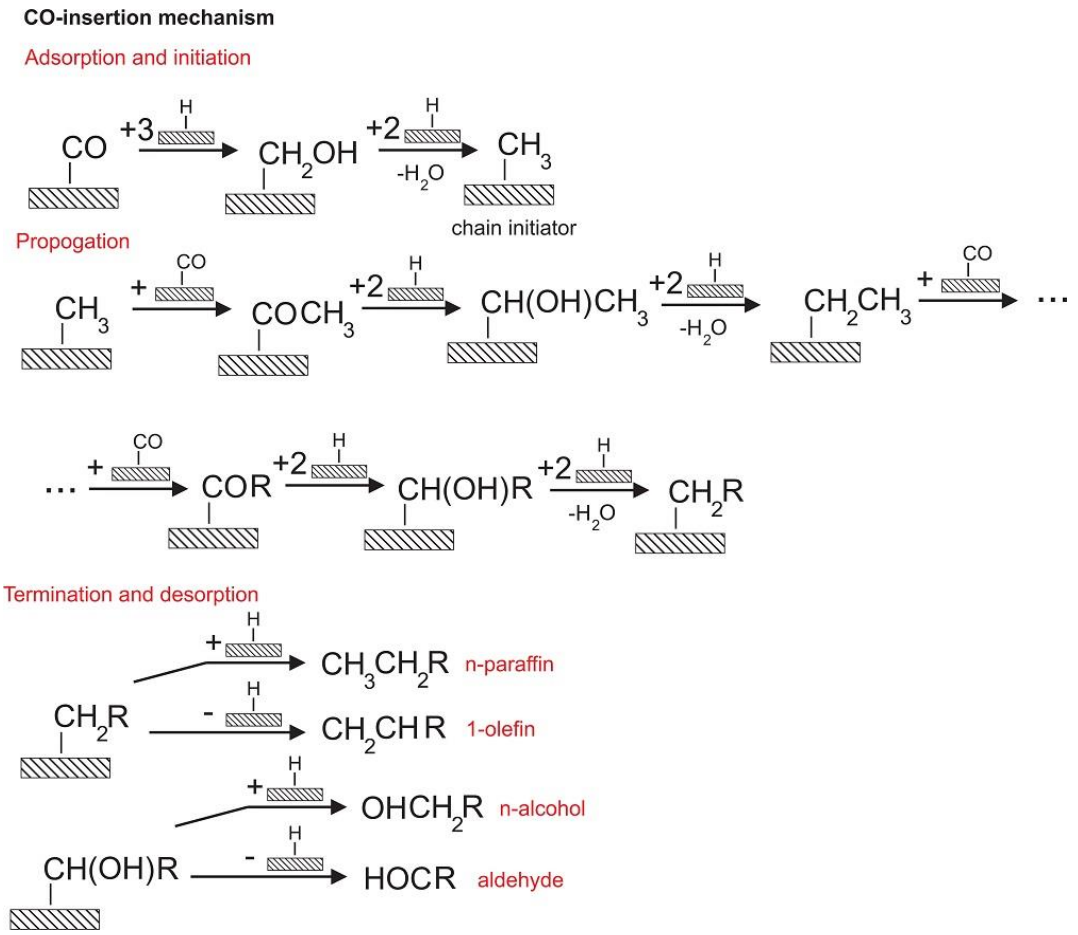

Figure 2.3 - Schematic of the CO-insertion mechanism

Computational studies on FTS mechanism – Substantial number of experimental studies have proposed various forms of FTS mechanism. The carbide mechanism originally proposed by Fischer and Tropsch [4] and modified by Brady and Petit [36], was questioned by the lack of support CO dissociation and metal carbide formation [40]. This led to a series of mechanistic proposals, out of which a CO-insertion mechanism [37] could explain the formation of all typical FTS products (paraffins, olefins, and oxygenates). A debate on the exact series of elementary steps that constitute FTS mechanism is still ongoing. However, aside from experiments it now includes a new computational chemistry dimension. With the development of computers and their

processing power, researchers are now able to perform simulations of surface reactions and perform calculations of their activation energies, using methods such as density function theory (DFT). Based on these it is possible to discriminate between rival elementary steps and determine reaction mechanisms. Reviews of recent computational chemistry studies in FTS were published by Valero and Raybaud [49] and van Santen et al. [50]. These computational studies mainly focused on simulating elementary reactions belonging to FTS initiation (CO-activation) and chain propagation for various catalysts, since simulations of termination steps for long chains could be computationally too demanding.

A number of studies have examined the initiation phase in FTS [42, 51-59]. Figure 2.4 shows possible CO activation steps in the carbide (also referred to as the alkyl or methylene) and the CO-insertion mechanisms. For the classical carbide mechanism, the CO activation step consists of a direct CO dissociation (i.e., the C-O bond is severed before C is hydrogenated), whereas in the CO-insertion pathway CO is first hydrogenated and only then is the C-O bond broken to give the chain starter (CH_3-S). Newer modification of the carbide mechanism assumes that hydrogen assists in the C-O bond scission [53]. Storsæter et al. [52] compared versions of the two mechanisms - carbide (including direct and H-assisted CO dissociation) and CO-insertion - using the UBI-QEP (unity bond index – quadratic exponential potential) method [60] and micro-kinetic modeling of C_1 and C_2 species formation (albeit at somewhat atypical FTS conditions of H_2/CO ratio of 10). Their results showed that the majority of CO reacts in a mechanism including direct hydrogenation of CO, where hydrogenation of CHO is the rate limiting step. Zhuo et al. [53] used DFT techniques with Co (0001) surface and assuming CO and H coverage of 0.2 ML and 0.4 ML, respectively, their results also indicated that CO is first hydrogenated, before C-O bond is severed. They suggested that oxygen elimination from CH_2O is the rate determining step for activation. Ojeda et al. [54] investigation suggested that CO hydrogenation is completely dominant for Co (0001) surface, while for Fe (110) direct dissociation of CO also had minor role. The vast majority of computational studies agree that C-O bond scission proceeds through a series of hydrogenations steps first and that the involvement of surface carbides in FTS is less likely.

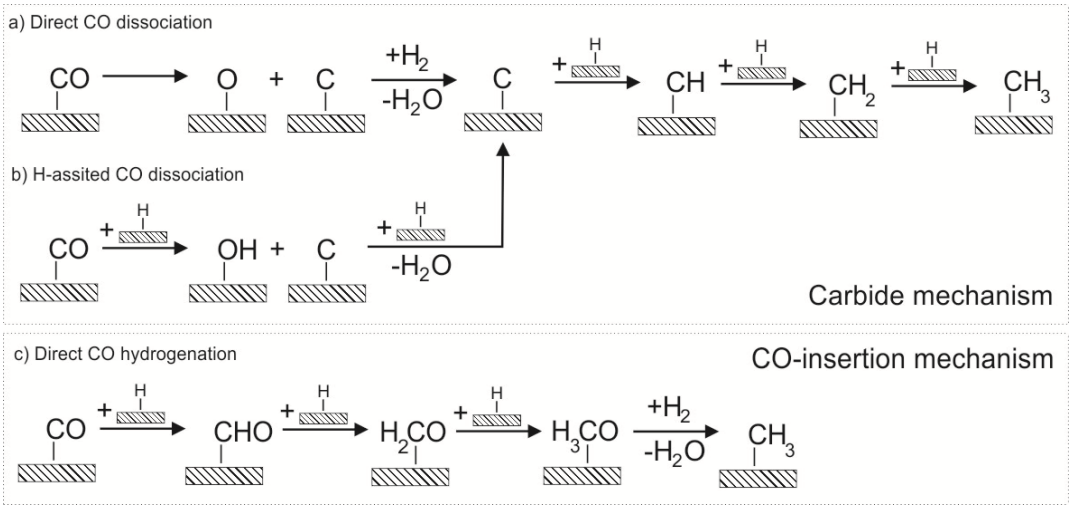

Figure 2.4 - Examples of CO activation pathways: a) direct CO dissociation (carbide mechanism); and b) H-assisted CO dissociation (carbide mechanism); c) CO hydrogenation (CO-insertion mechanism). (Based on elementary steps investigated by Storsæter et al. [52])

Computational chemists have also investigated the propagation steps of FTS, however unlike initiation these is no clear consensus on this topic [41, 50, 53, 61-70]. The research has mainly focus on different forms of CO-insertion and CH_x-insertion (alkyl) mechanism, where some groups favor the first [53, 61, 69, 70], others the later [41, 50, 71] and some believe that the two mechanism coexist in parallel [72]. The research groups which have investigated the alkyl mechanism have compared different possible C-C coupling. For example, Cheng et al. [62] reported $C+CH_3$ and CH_2+CH_2 to be the most favorable on cobalt surface, Li et al. [65] reported CH+CH on iron surface and Liu et al. [66] C+CH on ruthenium surface. Inderwildi et al. [69, 70], Storsæter et al. [52] and Saeys and co-workers [53, 61] comparisons of CO-insertion and alkyl mechanisms showed that CO-insertion is preferred over cobalt catalyst. Their investigations focus also on determining CH_x (x=1-3) species in which CO is inserted into. Storsæter et al. [52] found that the adsorbed CO combines with CH_3 species while Zhuo et al. [53] and Inderwildi et al. [69, 70] found that it combines with CH_2 species. However, due to the different interpretations and a lack of a single comprehensive study, that would take into account all of the potential mechanism forms and alternative combinations of elementary

steps, it is still unclear as to which of the proposed FTS propagation mechanisms is accurate.

An additional difficulty that faces researchers trying to make sense of computational chemistry results and apply them to FTS kinetics is the fact that majority of the results comes from simulations performed on ideal catalyst surfaces. However, in reality catalytic surface is far from ideal and is covered with a number reaction intermediates. Recent study of Zhuo et al. [61] showed that CO coverage used in simulations can have a significant effect on calculated activation energies and therefore impact the selection of "most optimal" sequence of elementary steps.

Influence of process conditions on activity and selectivity

Process parameters, such as time on stream, temperature, pressure, syngas feed ration and conversion level, can have a large influence on activity and selectivity of all FTS catalysts. FTS selectivity is most often expressed in terms of molar, weight and C-atom selectivity towards the undesired product methane and the desired C_{5+} products. Many experimental studies have been published about the effect of process conditions on FTS and here we give a short overview. The effect of process condition variations on Fe- and Co-based catalyst will be analyzed in more depth (based on our own data) in a separate chapter.

Time on stream – The effect of time on stream (TOS) is related to changes to the catalyst surface during FTS and can be equated with deactivation. Several reviews of deactivation over FTS catalysts exist for both cobalt and iron catalyst [7, 73, 74]. The TOS has the largest effect during the initial period of the reaction (up to 100 h), which later decreases but continues to affect both activity and selectivity. Typically, with increasing TOS studies have reported a decrease in reaction rate, increase in methane and decrease in C_{5+} selectivity [75-77]. The causes of deactivation in FTS are complex and several mechanisms at work include: sintering, mechanical attrition, poisoning with sulfur and nitrogen compounds, fouling by carbon and wax compounds and formation of inactive catalyst phases (oxides, carbides and metal-support compounds) [7, 78-84]. Experiments used to report the effect of process conditions and FTS kinetics typically

need to be conducted over a long period of time during which activity and selectivity need to be reproducible [85].

Temperature - As is to be expected, increasing temperature has a positive effect on the rate of FTS. However, in terms of selectivity it leads to an increase in selectivity for light weight products for all FTS catalysts [35, 76, 86-95]. This effect is much more pronounced with cobalt and ruthenium than with iron FTS catalysts [25, 96]. In general, all of the temperature effects are related to intrinsic FTS kinetics. So, the increase in light product selectivity at higher temperature can be viewed as an increase in rates in chain termination compared to propagation. Temperature was also reported to have an effect on olefin content [91, 92, 97, 98], which can tell us about secondary reactions of 1-olefins.

Pressure – Increasing pressure has an overall positive effect on FTS over all catalysts, where FTS reaction rate is increased [31, 76, 90, 99] and selectivity towards lower products is decreased and C_{5+} increased [25, 96, 100-102]. It should be noted though that the influence on selectivity is lower on iron compared to cobalt catalysts [25, 96]. It is thought that the influence if pressure on improving selectivity comes from lowering of hydrogen coverage at higher pressures and higher rates of olefin readsorption due to suppression of olefin hydrogenation at higher CO partial pressures [99].

H_2/CO ratio – The ratio between hydrogen and carbon-monoxide is known to have a very high influence on FTS selectivity [23, 76, 86, 89-91, 94, 103-105]. The increase of H_2/CO ratio leads to an increase in light and decrease in heavy C_{5+} products [23, 76, 86, 89-91, 94, 103]. It also decreases the olefin content due to secondary hydrogenation of 1-olefins [105].

Conversion level – The effect of conversion level is analyzed by varying the space velocity (i.e. inlet flowrate) at constant pressure, temperature and reactant feed ratio. This way two major variables change within the reactor: residence time and partial pressure of water. It is well-known that increasing conversion level leads to lower methane and higher C_{5+} selectivity for cobalt- and ruthenium-based catalysts [29, 94, 106-108]. For iron catalysts conversion has little to no effect on selectivity [76, 91, 92]. However, for all catalyst types (iron, cobalt and ruthenium) it was shown that olefin content (i.e. olefin-to-paraffin ratio) decreases with increased conversion [76, 108, 109].

This is related to the secondary reactions of 1-olefins. Furthermore, it is thought that increases in C_{5+} selectivity observed with increasing conversion for Co and Ru catalysts are caused by secondary 1-olefin readsorption and continued chain growth [29, 108, 110]. Iron is less active in secondary olefin reactions [108], which could explain the relatively constant selectivity at varied conversions for these catalysts. We will discuss secondary reactions in a separate section. Another aspect that affects FTS selectivity over Co (and potentially Ru) is the partial pressure of water, which is known to decrease methane and increase C_{5+} selectivity [111-119]. This is likely due to the decrease of hydrogenation activity and additional methane formation.

FTS product distribution

FTS is a polymerization type reaction and is characterized by a chain growth mechanism in which a C_1 surface species (a monomer) is inserted into the growing C_n chain, where n is the number of carbon atoms in a molecule. This feature of FTS has been used in the past to define the product distribution and predict the selectivity trends of hydrocarbons as a function of the number of carbon atoms in the molecule. Molar fractions of hydrocarbons can be calculated using the Anderson-Schulz-Flory (ASF) model [38, 120]:

$$y_n = (1-\alpha)\cdot\alpha^{n-1} \tag{2.3}$$

where molar fraction of hydrocarbons with n carbon atoms y_n is defined by its length (n) and chain growth probability α, which is independent of chain length. This model is most often presented in its logarithmic form:

$$\log(y_n) = \log(\frac{1-\alpha}{\alpha}) + \log(\alpha)\cdot n \tag{2.4}$$

Eq. (2.4) shows that the slope in a $\log(y_n)$ vs. n plot will be equal to $\log(\alpha)$, i.e. a constant slope for the entire distribution. However, the FTS product distribution very seldom follows the classical ASF distribution and regularly reported deviations from this model are (Figure 1a): a higher-than-expected fraction of methane, a lower-than-anticipated yield of C_2 (caused by the low fraction of ethene), and a positive bend in the

ASF plot (i.e., greater-than-expected yield of higher hydrocarbons due to an increase in chain growth probability with carbon number). These features are reported for all FTS catalysts [23] and are known as non-ASF behavior. Their underlying causes have been the topic of debate for several decades now. Different explanations for the observed shift towards heavier products in the product distribution have been proposed: two parallel FTS mechanisms (including two types of active sites, pathways or growth monomers) [104, 121-123], experimental VLE artifacts and accumulation of heavy products in the reactor [122, 124-126], intra-particle and inter-reactor concentration gradients [127-129], and most notably secondary reactions of 1-olefin [108, 109, 130-136].

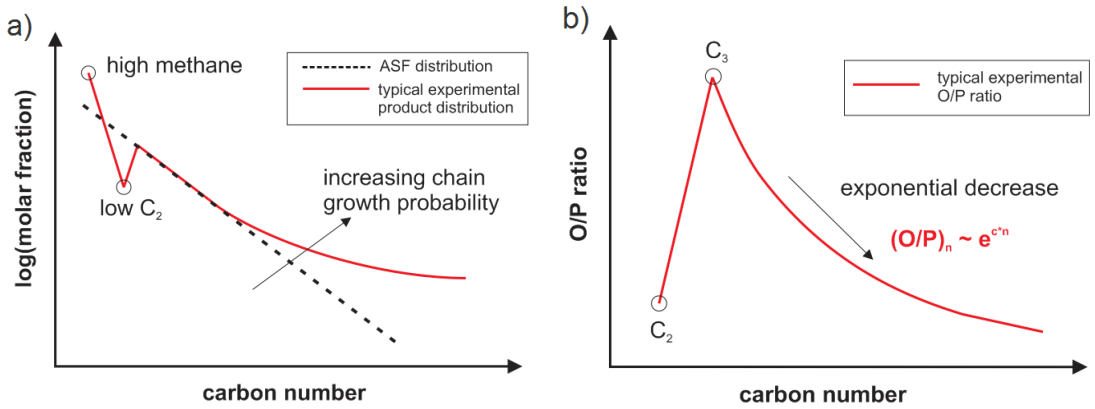

Figure 2.5 - Typical features of experimental product distributions: a) ASF distributions and deviations from it; b) olefin-to-paraffin (O/P) ratio

Initial investigations showed both positive and negative deviations of FTS product distribution from ASF can occur and that experimental artifacts are likely the cause [124, 126, 137-146]. Negative deviations have been attributed to experimental errors in gas chromatography [137]. More importantly, positive deviations are believed to be caused by unsteady-state slurry reactor operation, where heavier molecules spend considerably more time in the slurry compared to the light gas phase ones [147]. This idea was first introduced by Satterfield et al. [138], but the majority of work on the topic comes from Davis and co-workers [124, 126, 142-144]. They believed that if accumulation was accounted for, the product distribution would have a constant α-value and follow the ASF model. This group proposed the use of labeling experiments, in which hydrogen is replaced with deuterium (D_2) for a period of time, to determine the extent of accumulation

in the reactor [126, 142, 143]. The results with deuterium did show significant changes in the observed product distribution and a closer match to ideal ASF [142]. Recently however, same group also published a study on isotopic effect of deuterium in FTS [148]. The results showed that deuterium behaves quite differently than hydrogen in FTS, having a significantly different apparent activation energy (98 kJ/mol compared to 116 kJ/mol for hydrogen) and a higher surface coverage [148]. The occurrence of isotopic effects with D/H exchange is known from previous studies as well [149] and therefore its use in studying of FTS product distribution is questionable. Even though the effect of heavy product accumulation undoubtedly exists, most researchers consider it as minor and focus on more fundamental explanations [23]. This is rationalized by the fact that positive deviations from the ASF occur even in lower carbon number range (below C_{10}), i.e. for molecules that are mainly in gas phase inside the reactor. Therefore, accumulation is thought to have an impact only on heavier C_{15+} products. Botes [150] stated that the bend in the product distribution from Sasol's commercial reactors (with liquid residence time less than 1 day) using iron catalyst "*is so prominent that it can hardly be solely due to reactor artifact"*.

Some researchers believed that the FTS product distribution is determined by two distinct α-values, α_1 in low and α_2 in higher carbon number range [91, 104, 122, 137, 138, 151-154]. This explanation is known as the double-α concept. The two values of α would stem from the two different pathways of FTS. Some initial studies showed the bend in product distribution to be much more pronounced with iron catalysts, while cobalt was thought to follow the ideal ASF distribution [150, 155-157]. This was explained with well-known fact that two types of iron carbides are active in FTS [92, 158, 159], while only metallic cobalt and ruthenium are FTS active [97]. However, today is well known that both cobalt- and ruthenium-based catalysts also display non-ASF behavior [29, 94, 135, 160], so the different catalyst phases could not be the reason for it. Some authors have since justified using the double-α concept through associating it two parallel reaction mechanisms, which feature two different monomers [123]. Another important characteristic of FTS product distributions for all catalyst types is an exponential decrease in the olefin-to-paraffin ratio (OPR) with increasing carbon number (Figure 2.5b). A

common issue of double-α models is their inability to separate between different product types (only total hydrocarbon distribution is predicted) and OPR cannot be predicted.

Another explanation put forward for the non-ASF behavior is the existence of concentration and temperature gradients within the reactor, as well as the catalyst particles [127-129, 144, 161]. The general idea is that the product distribution follows the ASF distribution, i.e. has a constant α-value, if concentrations and temperature are kept constant [129]. However, due to the gradients that exist within fixed-bed reactors, there would be a range of different α-values within these reactors. This means that each point along the reactor bed would have its own characteristic α-value, summing up of which results in a non-ASF product distribution [161]. By analogy, for slurry reactors the intra-particle gradients could cause the same effect [127]. However, this theory is highly questionable due to the fact that many experimental studies conducted in systems without gradients (e.g. well-mixed stirred tank slurry reactors with very small catalyst particle sizes) have shown that non-ASF behavior of FTS products [94, 162]. Therefore, researchers in the field typically favor more fundamental kinetic explanations.

Herington [163] proposed secondary reactions of initially formed olefins (hydrogenation, isomerization and readsorption) as an explanation of the non-ASF behavior. Secondary olefin reactions are an interesting general feature reported for all FTS catalysts [23, 135, 164, 165]. The theory was that initially formed olefins can readsorb onto the FTS active sites and continue with growth, which results in a higher yield of heavy products. This is referred to as olefin readsorption concept. Since higher olefins are hypothesized to readsorb better, due to their higher residence time, this concept can also be used to explain the shape of OPR with carbon number. This is why readsorption concept is the most well-rounded and elegant explanation of the non-ASF distribution and is most often used in modeling of FTS product selectivity [108-110, 130-136, 160, 166-168]. We will discuss these readsorption-based models in more details in the later sections.

The most recent concept proposed to explain the non-ASF product distribution is the chain length dependent olefin desorption, introduced by Botes in 2007 [169]. He argued that Fe-based catalysts exhibit a lower activity for secondary reactions of olefins

[165, 170], negating the olefin readsorption explanation for non-ASF distribution of that catalyst, and proposed an alternative theory based on chain length dependent desorption of olefins. According to this concept the activation energy of 1-olefin desorption rate constant depends exponentially on carbon number, due to linearly increasing activation energy of the 1-olefin desorption. Similar ideas on higher hydrocarbon adsorptivity with increased chain length can be found in older literature as well [97, 171]. This concept will be further explained in later sections. Its advantage is the ability to explain the non-ASF behavior and exponential decrease in OPR with carbon number in simple and mathematically elegant and physically meaningful terms, without the need to use secondary reactions.

Secondary reactions of 1-olefins in FTS

Because secondary reactions 1-olefins are thought to play a major role in determining FTS selectivity [135], it is important to develop a good understanding of them through experiments before adequately applying them in modeling. Both 1- and 2-olefins, as well as alcohols, can participate in secondary reactions, however 1-olefins are far more active in them [172, 173] and because 1-olefins are major products in FTS we often equate FTS secondary reactions with secondary reactions of 1-olefins. The secondary reactions of 1-olefins include: hydrogenation to n-paraffin, isomerization to 2-olefin and readsorption followed by continued growth (Figure 2.6) and cracking to lower products and hydrogenolysis [172, 174]. Note that in this review by readsorption reaction we will refer to olefin readsorption to primary FTS active sites followed by continued chain growth (Figure 2.6). In literature this reaction is also referred to as reincorporation. In is different from hydrogenation and isomerization which take place on a secondary type of sites [174].

The secondary reactions are studied by cofeeding olefins in the reactor along with syngas. These studies are typically conducted with either labeled [165, 175-177] or in most cases unlabeled olefins [28, 153, 164, 170, 178-183]. The first involved using very small amounts of ^{13}C labeled olefins and measuring the radioactivity of outlet products. This way the labeled ^{13}C molecules can tell us exactly how much olefins converted into paraffins, iso-olefins, lower products etc. The studies with unlabeled olefins usually conduct a number of baseline experiments without olefin cofeeding add then experiments

in which olefin is cofed in some significant amount. The activity and selectivity of added olefins is then determined from the comparison to baseline experiments through mass balances. The use of unlabeled olefins in cofeeding studies has been questioned by Davis and co-workers [175, 176], who argued that use of high olefin concentrations can have an effect on competitive adsorption in FTS, increasing the chances for added olefins to participate in secondary reactions. Therefore, the olefin conversions reported in these studies can be misleadingly high and care must be taken when analyzing these results.

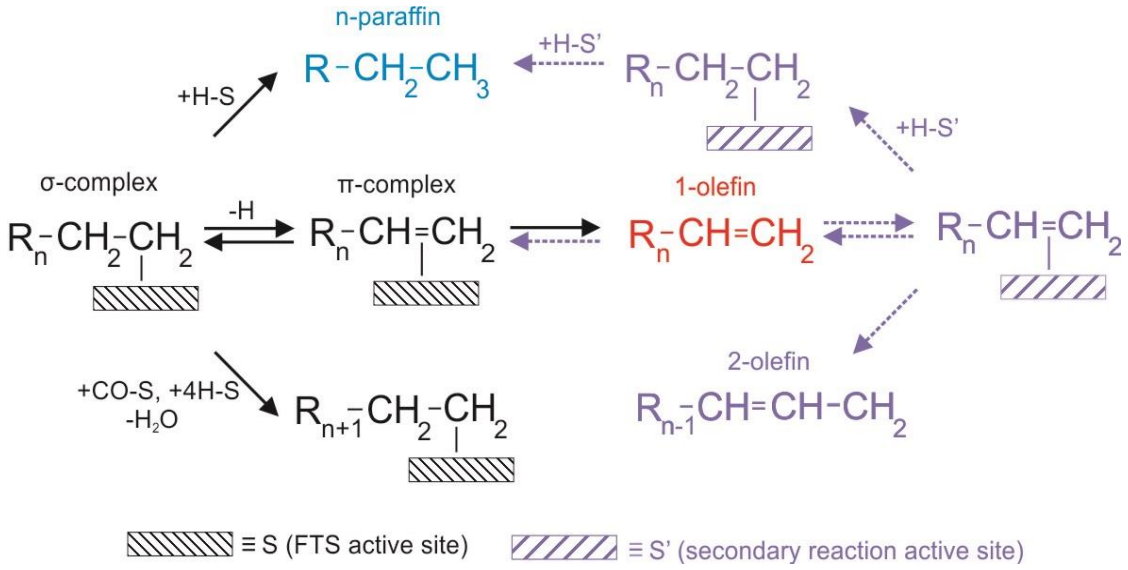

Figure 2.6 – Schematic of primary FTS and secondary olefin reactions

Depending on the type of study, as well as catalyst, reactor and conditions used, the extent and selectivity of olefin secondary reactions vary. The catalyst activity in secondary reactions increases in the order iron < ruthenium < cobalt [108]. Botes [150] stated that this is surprising considering that the increase of chain growth probability with carbon number is more pronounced over Fe than Co catalysts (see Figure 2.7). This is inconsistent with readsorption concept explanation.

It is also important to see how different chain length olefins behave in secondary reactions. All studies agree that ethene in by far the most active olefin [164, 165]. The reactivity of added 1-olefins descends in the order [108]:

ethene >> propene > 1-butene ~ C_{5+} 1-olefins

Ethene exhibits a negative deviation from the ASF and its high reactivity in cofeeding studies is expected. However, based on the readsorption concept it would be expected the reactivity of cofed higher olefins was higher than that of propene and 1-butene.

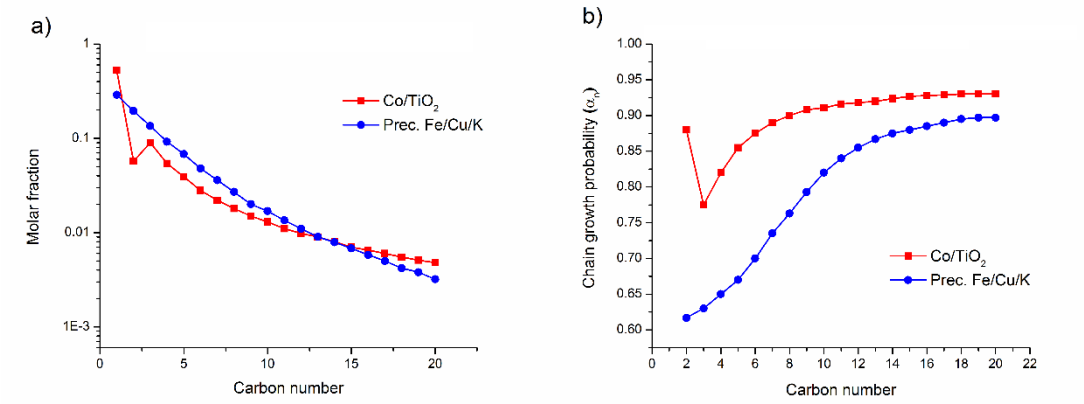

Figure 2.7 - Comparison of typical product distribution behavior for Fe and Co catalysts: a) the deviations from the ASF product distribution; b) increasing chain growth probability with carbon number; (Data from Refs. [28, 86, 152])

Another important issue is that of secondary reaction selectivity. Majority of studies conducted over Fe and Co catalysts report that prevailing secondary reaction is hydrogenation, followed by isomerization and readsorption (i.e. incorporation). [153, 164, 165, 170, 175-177, 179-182]. Schulz et al. [164] stated that readsorption followed with continued chain growth generally constituted below 20% of olefins converted. Some studies even report that readsorpiton of higher olefins is negligible for Fe and very low for Co-based catalysts [175]. Contrary to those results, Iglesia et al. [28] reported that olefins participate in readosrption and further growth in more than 90% of cases with Co and Ru catalysts. This debate is important from the kinetic modeling point of view because typically readsorption-based model require this reaction to be the dominant one, with selectivity close to 100% [153], and will be discussed in more details below. Patzlaff and Gaube [153] analyzed the growth probability of readsorbed cofed olefin over Co and showed it was considerably lower than the typical FTS growth probability (~ 0.6 compared to above 0.9). This result could suggest that the added olefins that readsorbed did not participate in typical FTS chain growth, as readsorption concept states.

It is clear that the secondary reactions of initially formed 1-olefin occur and that they are dependent on catalyst and reaction conditions. However, the nature of these reactions is yet to be clearly resolved. This would require a comprehensive study with cofeeding of a range of labeled 1-olefin molecules under different experimental conditions.

2.2. Modeling of FTS kinetics

Kinetic models of FTS can be classified into three major categories: 1) models of overall reactant consumption – give the overall rate of FTS or syngas or only CO consumption; 2) models of product selectivity – give the product selectivity of various FTS products, either as total hydrocarbons or divided into individual species (n-paraffins, 1- and 2-olefins, etc.); 3) detailed kinetic models – give information about both consumption of CO and H_2 and the formation of all products, including water, n-paraffins, 1-olefins etc. In this section we will give a brief description of different model types with a review of proposed models, their advantages and disadvantages and the overall impact of proposed concepts on FTS kinetic theory.

Models of overall reactant consumption

The kinetic models of overall reactant consumption are very useful in initial design of FTS reactor, including their sizing. There are several ways to ways to present the reactions rate in FTS: as rate of CO consumption ($-R_{CO}$), rate of syngas consumption ($-R_{CO+H2}=-R_{CO}-R_{H2}$) or overall FTS rate ($R_{FTS}=-R_{CO}-R_{WGS}$) [23]. Several reviews of overall FTS kinetic models exist for iron [23, 184, 185] and cobalt catalysts [23, 186, 187]. In general, simple FTS kinetic models can be divided into empirical power law models [35, 97, 184, 188] and more theoretical Langmuir-Hinshelwood-Hougen-Watson (LHHW) type models [160, 185, 187, 189-199].

Iron catalyst - One of the first and the simplest model of FTS kinetics was proposed by Anderson [97]:

$$R_{FT} = k \cdot P_{H_2} \tag{2.5}$$

This model performed satisfactory for conversion up to 60%, however at higher conversion the inverse effect of water partial pressure had to be taken into account for iron-based catalyst. Anderson [97] also proposed an empirical model that included an inhibition term for water:

$$R_{FT} = \frac{k \cdot P_{CO} P_{H_2}}{P_{CO} + a \cdot P_{H_2O}} \tag{2.6}$$

Later, Dry [189] and Huff and Satterfield [185] developed the same model on the basis of a form of combined enol/carbide mechanism [23]. Since then most authors have preferred the use of LHHW approach in model development. This entailed an assumption of FTS mechanism and its elementary steps, most often with assumption of rate determining step (RDS) and pseudo-steady-state hypothesis (PSSH). Van der Laan and Benackers [199] tested a number of reaction mechanisms by deriving kinetic expressions for them through LHHW approach. They showed that even completely different mechanism can lead to identical rate expressions. Their results confirmed that best results are obtained from models derived based on a combined enol/carbide mechanism. The apparent overall FTS activation energies reported in these models are typically in 70 – 105 kJ/mol range [23].

Cobalt catalyst – An empirical model for cobalt catalyst is reported by Zennaro et al. [186]:

$$R_{FT} = k \cdot P_{H_2}{}^{a} P_{CO}{}^{b} \tag{2.7}$$

where a and b are empirical parameters with values of 0.74 and – 0.24. This shows a general trend for cobalt catalyst where hydrogen has a promoting and carbon-monoxide inhibiting effect on FTS reaction rate. LHHW rate expressions were proposed for cobalt catalyst as well. Rautavuoma and van der Baan [196] proposed an expression based on carbide mechanism, in which formation of CH_2 monomeric species was RDS:

$$R_{FT} = \frac{k \cdot {P_{CO}}^{0.5} P_{H_2}}{(1 + k_{CO} P_{CO})^3} \tag{2.8}$$

Sarup and Wojciechowski [193] derived expressions that also included models that included hydrogen inhibition term in denominator. These models were questioned based on statistical significance by Yates and Satterfield [195]. Their models only included CO inhibition term in denominator, since it was believed that CO is the most abundant surface species. Recent study by Botes et al. [197] derived yet another semi-empirical rate equation:

$$R_{FT} = \frac{k \cdot {P_{CO}}^{0.5} {P_{H_2}}^{0.75}}{(1 + k_{CO} {P_{CO}}^{0.5})^2} \tag{2.9}$$

with a "nontraditional" hydrogen reaction order of 0.75, where constant k_{CO} was to be pseudoconstant dependent on hydrogen partial pressure. Overall reaction mechanism was consistent with carbide mechanism with direct CO dissociation step. Some authors have also included a water inhibitor term in their kinetic models [160, 198, 200]. For example, Bhatelia et al. [198] developed a model based on a form of carbide mechanism, that included hydrogen-assisted dissociative adsorption of CO.

Various authors tested various forms of FTS mechanism, for both iron and cobalt catalysts, often arriving at contradicting mechanistic conclusions. This could potentially point to a general weakness of LHHW approach in mechanistic studies [201, 202]. In any case, more fundamental understanding of FTS reaction mechanism is needed before a definitive overall rate expression for FTS can be obtained.

Models of product selectivity

The selectivity models are based on FTS reaction networks (simplified reaction mechanisms, e.g. Figure 2.6) and allow for prediction of FTS selectivity towards various product species. Most selectivity models can be grouped either as the double-alpha models or the olefin readsorpion models. Latter are more frequently used because they calculate selectivity for various product species (paraffin and olefin), while the double-

alpha models predict only the total hydrocarbon formation (lumped paraffin and olefin). Recently Botes [169] proposed a third type of selectivity model for the Fe catalyst, based on the new hypothesis of chain length dependent olefin desorption.

Double-α models – We showed that using the ASF model (Eq. 2.3) the molar fraction of total hydrocarbons with different chain length can be calculated using a single parameter α (i.e. chain growth probability), which corresponds to the logarithm of the slope of log (y_n) vs. carbon number product distribution (Eq. 2.4). However, as shown above, the FTS product distribution deviates from the ideal ASF model. One of the first attempts to explain the positive deviations from the ASF was the inclusion of the second chain growth probability by Huff and Satterfield [122]. They proposed that FTS occurs on two separate sites that have different growth probability α_1 and α_2; and curvature in the product distribution was explained by the superposition of the two chain growth probabilities (Figure 2.8). Similar explanations were proposed by Donelly et al. [152], Dictor and Bell [92], Sarup and Wojciechowski [121] and others [104, 154].

In general the double-α models can be presented as three parameter models:

$$y_n = x(1-\alpha_1)\cdot\alpha_1^{n-1} + (1-x)(1-\alpha_2)\cdot\alpha_2^{n-1} \qquad (2.10)$$

where α_1 is the growth probability in light product range, α_2 is the growth probability in heavy product range and x is the fraction of products following the first α-value. The intersect point between the two α-values is between C_5 and C_{15} depending on the catalyst and process conditions. Typical values of α_1 are 0.5 – 0.7, α_2 0.8 – 0.95.

A deficiency of the double-alpha models is that they do not consider formation of different product species (paraffins and olefins) separately. These models are therefore unable to explain the experimentally observed changes in the OPR with carbon number. In addition, Botes [150] reported low repeatability of double-α model results, due to high covariance between three model parameters. The double-alpha models are not predictive, but are instead typically used as "data fitting" models. Their advantage is simplicity and explicit form.

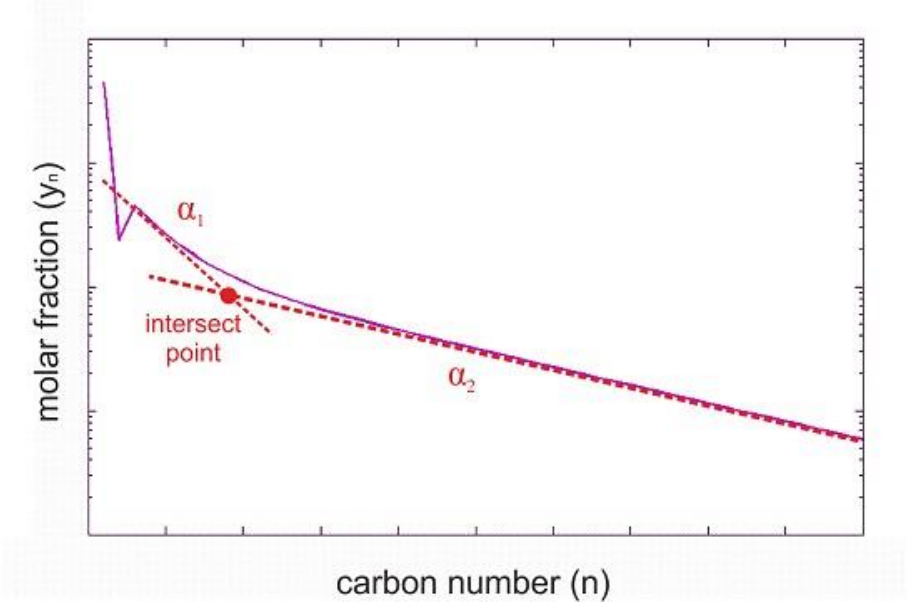

Figure 2.8 – Double-α explanation of the experimentally observed product distribution

Olefin readsorption-based models – Novak et al. [130] first proposed a mathematical model based on olefin readsorption. Their model showed that if the majority of olefins readsorbed and did not hydrogenate or isomerize, the result would be a non-ASF distribution. Additional refinements of this theory were made upon introducing the assumption that secondary reactions of olefins are dependent on chain length, i.e., that they are enhanced by longer reactor residence times of high molecular weight 1-olefins due to their lower diffusivities [29, 108, 110, 135], higher solubilities [131-133, 136, 166-168] in FTS wax, and/or stronger physisorption characteristics [109, 134, 203].

Iglesia et al. [108, 110, 135] proposed a reaction-transport model of product distribution on Ru and Co catalysts, applicable to pellets in packed-bed reactor. This model was based on diffusivity enhanced readsorption, where slow removal of olefin molecules from the catalyst pellet was causing increased residence time with carbon number, which in turn causes higher secondary reactions (readsorption and hydrogenation) of 1-olefin molecules. Diffusion of the products in the particle pores was defined by carbon number dependent Thiele modulus, which was a function of reaction conditions, fluid properties, as well as a structural parameter (χ). This parameter χ was especially useful for catalyst design as it was dependent of average pore radius, pellet

radius and catalyst site density. In addition, Iglesia et al. selectivity model (also known as the Exxon model) also includes CO hydrogenation sub-model, defined in a similar way to readsoprtion model. This takes into account mass transfer of CO inside the catalyst pores, which is very important for large particles in fixed-bed reactors. In should be noted that this was an implicit model that required parallel solving of both fixed-bed reactor model and the selectivity model equations [7, 150]. Model included only three parameters $\beta_{o,n}$, β_p and β_r, i.e. probabilities for chain termination to olefin, paraffin and readsorption, respectively. These parameters were said to be independent of chain length, except for ethene. The model was able to predict both the influence of process conditions and catalyst structure on the product distribution and determine the optimal ranges for C_{5+} selectivity. Using it, Iglesia et al. [108, 135] showed that C_{5+} selectivity can be optimized by varying the structural parameter χ. In the χ range of 10^{17} and 10^{19} m^{-1} the C_{5+} selectivity increased due to the increased rate of olefin readsorption, while above that χ range the C_{5+} selectivity decreased due to high diffusion resistances on CO transfer. However, as pointed out by Botes [150], similar studies by Holmen and co-workers [204] showed that C_{5+} selectivity is constant up to $\chi \sim 10^{19}$ m^{-1} and then decreased presumably because of CO mass transfer limitations. This brought into question the validity of olefin readsopriton approach. Researchers from Shell [205] argued that the kinetic model similar to that of Iglesia et al. [110] could fit non-ASF product distribution, but would do so with parameters without physical meaning. They also proposed reanalysis of Iglesia et al. [29] 1-butene bed residence time studies, according to which data showed no evidence of readsorption but that most of 1-butene hydrogenates to n-butane. This result would is indeed more in line with results of 1-olefin cofeeding studies, as discussed above. However, main critics of Iglesia et al. model focused on the use of exponentially decreasing olefin diffusivity function [23, 131]. They pointed out that the model assumption that $D_n \sim e^{-0.3*n}$ is not based in reality, since experiments by Erkey et al. [206] show a much lower dependency.

Studies published by Zimmerman et al. [133], Schulz et al. [131], Van der Laan and Benackers [132], as well as others, highlighted the importance of chain length dependent 1-olefin solubility on the increased rate of their readsoprtion with carbon number. Among these, particularly popular is the Van der Laan and Benackers model

[132], known as the olefin readsorption product distribution model (ORPDM). This model was developed using Fe-Cu-K/SiO_2 catalyst data obtained under a range of isothermal conditions in a spinning basket reactor. ORPDM was based on carbide mechanism and included elementary steps of reactant adsorption, monomer formation and chain initiation, propagation and termination to paraffins and olefins, as well as readsorption (Figure 2.9). Following the conclusion of previous models, rate of olefin readsorption is said to increase with carbon number because of physisorption and solubility effects. This is done by assuming an empirical relation between olefin liquid phase concentration at the catalyst surface and olefin gas phase partial pressure $C_{olefin}/(P_{olefin}/RT) \sim e^{c*n}$. ORPDM was shown to be able to predict the non-ASF behavior and OPR decrease with carbon number with only three parameters, as well as separate parameters for methane and ethene and solubility parameter c. These parameters were pseudo-kinetic parameters, i.e. dependent on process conditions (pressure, reactant feed ratio and space velocity). It should also be noted that in order to eliminate the olefin concentration term from the kinetic model equations, Van der Laan and Benackers [132] introduced the CSTR mass balance into the ORPDM derivation, making it explicit. Similar to Iglesia et al. model [110], which can only be applied for fixed-bed reactors, ORPDM can be used only for ideal CSTR type reactors. Madon and Iglesia [207] criticized the use of liquid phase concentration in kinetic models, stating that the *"rate of chemical reaction depends only thermodynamic properties, such as chemical potential, activity, or fugacity of reactants and products"* and that *"reaction rates depend on concentrations only in ideal reaction mixtures"*. Since FTS is an example of non-ideal gas-liquid-solid system, it followed that concentration terms cannot be used in kinetic rate expressions. Van der Laan and Benackers model [132] only considered olefin readsorption reaction, but not secondary hydrogenation and isomerization, for which olefin cofeeding studies showed are as major secondary reactions. They also did not mention anything about readsorption selectivity, i.e. probability of readsopriton event. Schulz et al. [131] developed a solubility enhanced olefin readsorption selectivity model that included all secondary olefin reactions (readsorption, hydrogenation and isomerization). Even though Schulz et al. [131] did not discuss selectivity of these reactions, analysis of Patzlaff et al. [153] showed that modeled selectivity towards

readsorption had to be close 100% and that hydrogenation and isomerization are negligible, if the model is to predict non-ASF behavior.

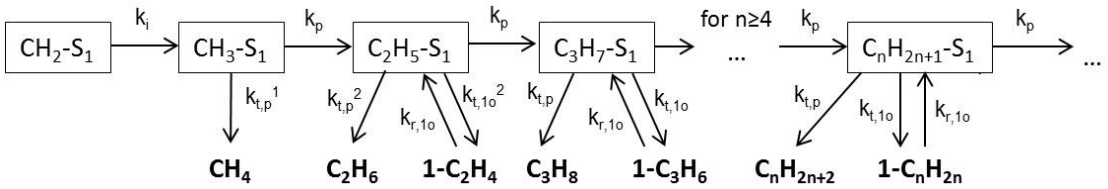

Figure 2.9 – Reaction network of Van der Laan and Benackers model [132]

Physisorption of olefin molecules is also though to promote enhanced olefin readsorption [109, 134, 203, 208]. The higher adsorptivity of heavier molecules increases their residence time near the surface, making for increased probability for readsorption. This concept is based on an experimentally well-known fact that heavier hydrocarbons have higher adsorption enthalpies [209-213]. Kuipers et al. model [109, 134] selectivity model includes 1-olefin readsorption, secondary hydrogenation and hydrogenolisis. It differentiated between chain-growth sites (primary FTS sites) and hydrogenation sites (secondary sites). Authors gave a detailed discussion on how olefin readsoprion is enhanced by three proposed effects of diffusivity, solubility and physisorption. They studied the reaction at 1 bar on Co foil and on Co/SiO_2 catalyst in order to compare how the presence of wax affects product distribution. Even when wax layer was absent at Co foils, OPR still showed exponential decrease with carbon number. This lead to the conclusion that even though diffusivity and especially solubility play a role in olefin readsorption, main reason for the observed characteristics of product distribution is physisorption. Further justification was that "*for reinsertion an olefin had to chemisorb at a vacant site at the surface. Under FT conditions such sites are rare, since surface is covered with a variety of species. Once a chain-growth site becomes vacant, an olefin has to compete with CO and H_2 for its occupation. It is very unlikely that an olefin far removed from the vacant site will reach the site before it has been occupied again. Thus of the olefins inside the reactor only those in the near neighborhood have a chance of readsorbing and therefore the reinsertion rate should be coupled with olefin concentration at the interface in the physisorbed layer (or precursor state) instead of reactor-averaged concentration (i.e. contact time).*" [134] . Kuipers et al. [109, 134] also

performed co-feeding of hexene to further study secondary reactions. Results showed that on both Co-foil and Co-SiO_2 added hexene underwent hydrogenation, but that reincorporation and hydrogenolisis was not observed. This is consistent to the theory that only olefins close to the active site (i.e. in physisorbed layer) can be readsorbed and continue with chain-growth. However, Shell researchers (including Kuipers) [205], later reanalyzed values of kinetic parameters of a very similar model. They concluded that even though at first glance parameters made sense, the values related to readsorption of olefin seem to be "unphysical", with values much higher than expected and stated that "*non-ASF behaviour in the Fischer–Tropsch product distribution does not necessarily imply that secondary growth reactions of a-olefins are occurring to a significant extent*".

Chain length dependent desorption model - Botes [150, 169] was highly critical of olefin readsorption concept. He believed that the discussion about which of the physical phenomena is enhancing olefin readsorpiton (diffusion, solubility or physisorption) has distracted researchers from questioning the concept itself. He pointed out several inconsistencies associated with disparity in the hypothesized 1-olefin behavior in readsorption-based models and their behavior in cofeeding experiments. Most important of which was the high deviations from ASF over iron-based catalysts, even though there is little proof of higher olefin readsoprtion over these catalyst. Because of this he proposed a selectivity model based on a novel chain length dependent desorption concept [169]. Botes model had three basic elementary reactions: chain growth, chain desorption (forming olefins) and chain hydrogenation (forming paraffin). The main assumption was that rates of chain growth and chain hydrogenation to paraffin are independent of chain length, while chain desorption to olefin is a function of carbon number. This carbon number dependence is said to be caused by interaction of the chain with the catalyst surface, resulting in longer residence time of high molecular weight hydrocarbons. He proposed an empirical formula, according to which energy required for desorption E_d is linearly increasing with carbon number (n):

$$E_d = k'n \tag{2.11}$$

where k' is an empirical constant. From this rates of chain desorption (olefin formation), chain hydrogenation (paraffin formation) and chain growth would be:

$$r_d = k_d[C_n^*]e^{-k*n} \tag{2.12}$$

$$r_h = k_h[C_n^*] \tag{2.13}$$

$$r_g = k_g[C_n^*] \tag{2.14}$$

where k_i is reaction rate constant (i = d – desorption, h – hydrogenation, g – growth), $[C_n*]$ surface fraction of a growing intermediate, while k is an exponential dependency of chain length (k=k'/RT). From this it is easy to see that OPR would be exponentially decreasing with carbon number for k > 0:

$$OPR_n = \frac{r_d}{r_h} = \frac{k_d}{k_h} e^{-k*n} \tag{2.15}$$

It also explains the increasing chain-growth probability α_n with carbon number and its asymptotic value at high carbon numbers:

$$\alpha_n = \frac{r_g}{r_g + r_h + r_d} = \frac{k_g}{k_d + k_h + k_d e^{-k*n}} \tag{2.16}$$

Eq. (2.16) shows that initially olefin desorption term $k_d e^{-k*n}$ decreases with carbon number, resulting in increasing α_n, while at high values of n it is essentially negligible and α_n becomes constant. Therefore, both positive deviations from the ASF and OPR behavior are described in a simple and mathematically very elegant way using only three adjustable parameters. Deficiencies of the model were: 1) it completely neglected olefin secondary reactions and was therefore unable to predict changing product formation rates with residence time; 2) did not adequately describe C_1 and C_2 product distribution; and 3) was not based on mechanistic approach, so the validity and physical meaningfulness could not be verified.

In addition to being relatively easy to use, mostly empirical selectivity models offer good precision for the conditions that they are optimized for, but not for the entire

range of industrially relevant conditions. This is because most often they include pseudokinetic parameters dependent on reaction conditions and are therefore not predictive. This is why a different approach was taken in developing detailed kinetic models of FTS, which have been popularized in the last two decades.

Detailed kinetic models

Detailed kinetic models are based on a full sequence of FTS elementary steps that include reactant adsorption, chain initiation, growth and termination. This is different from product selectivity models that include only the later three. It allows detailed kinetic models to predict both reactant consumption and product formation rates. This is why some authors refer to them as comprehensive models. In the 90s and early 2000s the focus was on development of detailed kinetic models for iron-based catalysts [123, 167, 214-222], while more recently that focus has shifted to cobalt-based ones [95, 223-229].

Initial development of detailed models of FTS kinetics happened in the 90s. Precursor to their formation was the model of Zimmerman et al. [133], because unlike previous selectivity models, that only included generic steps of propagation and chain termination to paraffin and olefin, this model also includes adsorption of reactants and chain initiation. Zimmerman et al. model assumed carbide mechanism and the presence of two types of active sites on the catalyst. There was distinction between primary FTS sites and secondary olefin hydrogenation sites. Zimmerman et al. model included the effect of solubility for both inorganic and organic (paraffin and olefin) species. Schulz et al. [131] noted that it "contains no explicit information about the used chain length dependence of solubility of FT products". In addition, model parameters were not optimized, but taken from the literature, which caused for a poor fit of the experimental data. However, due to inclusion of secondary 1-olefin readsorption and hydrogenation, model did show the ability to explain variations in growth probability and 1-olefin/n-paraffin ratio with carbon number.

First model fully based on LHHW approach was developed by Lox and Froment [214]. They derived rate equations for a number of FTS mechanism forms and assumptions of RDS. These models were then optimized using data obtained in a fixed-

bed reactor and discriminated based on statistics and physical meaningfulness of model parameters. It should be noted that their experiments were conducted at inlet H_2/CO ratio between 3 and 6, which is very high for iron catalyst and atypical for FTS operation [215]. These conditions favored hydrogenation reactions and n-paraffin formation, which is why their data showed an apparent constant chain growth probability in relation to carbon number (i.e. ASF distribution). Lox and Froment [214] model therefore did not include any explanation for non-ASF behavior. The importance of this study was development of a strict LHHW methodology for detailed FTS model derivation and rigorous discrimination.

Wang et al. [219] expanded the model of Lox and Froment [214] by including readsorption of 1-olefins. Only 1-olefin readsorption and continued growth was considered, while other secondary reactions were neglected. This was done by introducing an olefin readsortion factor β_n, which is the ratio of rates of olefin readsorption and rate of initial olefin formation. However, the proposed model was not able to account for changes in growth probability and OPR with carbon number. Closer inspection of the model shows that factor β_n was close to zero, i.e. contribution of readsorption to model results was negligible. This was followed by a series of studies on promoted iron catalysts by Li and co-workers [123, 216-218, 220-222]. Yang et al. [222] tested a number of FTS mechanisms with models that included olefin readsorption with the factor β_n. This model was also unable to explain non-ASF behavior and OPR variation, which was explained with the fact that factor β_n was related with olefin partial pressure in the model, while the effect of increased olefin residence time (e.g. through solubility) was not accounted for. Similar model, with similar results, was proposed by Teng et al. [217]. An importance of the latter was that it first introduced oxygenate formation in FTS mechanism [217, 218]. Teng et al. later published a "corrected version" of their model [220] which was able to explain non-ASF behavior, as well as exponentially decreasing OPR with carbon number. This was done by introducing the "non-intrinsic effects" through the assumption that rate constants for 1-olefin and oxygenate formation had an exponential dependency with chain length e^{-c*n}. This exponential function in essence replaced olefin readsorption factor β_n used in earlier models. Even though the authors claimed the exponential dependency term would stem

from olefin readsorption and showed this reaction as one of the steps in the mechanism, there was no explicit explanation as to how this term was derived and introduced into the model equations. Furthermore, Teng et al. model [220] did not include any dependence of olefin concentration, which would be required if one is accounting for olefin secondary reactions. Around the same time, Guo et al. [216] used a similar exponential dependency term in their model, which was able to fit isothermal data from iron-based catalyst, including deviations from the ASF distribution and OPR behavior with chain length. Guo et al. model [216] assumed that both olefin desorption and readsorption constants would be dependent on chain length due to physisorption and had an olefin readsorption factor β_n. However, the good fit of this model was likely due to the exponential dependency in the rate of 1-olefin desorption, while similar to other models readsorption factor β_n only had negligible influence.

Recently, detailed FTS kinetics models were developed for cobalt-based catalysts. Anfray et al. [230] proposed a LHHW model based on the carbide mechanism and solubility enhanced readsorption of 1-olefins. They reported a good prediction of n-paraffin rates, but a poor fit for 1-olefins. The model predicted only a minor effect of 1-olefin readsorption on the product distribution, and experimentally observed increase of chain growth probability and decrease in OPR with carbon number could not be adequately explained. Visconti et al. [95] utilized a micro-kinetic approach assuming that all elementary steps are irreversible. Steady-state balances for each species were solved simultaneously with the reactor model equations; which resulted in highly implicit and complex models. Visconti et al. [95, 223] also included solubility enhanced 1-olefin readsorption concept and, unlike Anfray et al. [230], a good fit of the olefin formation data was reported; however, rates and probabilities of 1-olefin readsorption were not discussed. Kwack et al. [225] model, based on [95], did not predict increasing chain growth probability with increasing carbon number.

It is clear that the detailed FTS kinetic models are more reliable and desirable for application in modeling of FTS reactor, due to their use of intrinsic kinetic parameters optimized for a wide ranges of conditions. However, all of them are based on assumed FTS mechanisms and more mechanistic knowledge is needed in order to develop a completely reliable detailed model of FTS kinetics. As shown in earlier sections, based

on experimental and computation studies there is much debate about the nature of initiation and propagation steps in FTS. In addition, termination steps and a role of olefin secondary reactions on product distribution must be carefully scrutinized.

2.3. Industrial FTS reactors

There are two general types of FTS technology: high and low temperature Fischer-Tropsch (HTFT and LTFT), where the latter is typically used in GTL industry [2, 7]. Temperatures typically used in HTFT are 320 to 350 °C, whereas LTFT usually operates in the 200 to 240 °C range. Main difference is that HTFT is a two-phase (gas-solid) process, where liquid exists only in catalyst particle pores, while LTFT is characterized by a three-phase (gas-liquid-solid) operation. HTFT is performed in fluidized-bed reactor, which is operated so that liquid condensation is avoided (higher temperatures and lower α values). Therefore, the heaviest HTFT products are in the gasoline/diesel fuel fraction (up to C_{20}). Temperature in HTFT is kept bellow 350 °C in order to avoid excess carbon formation, which is detrimental for the catalyst [231]. LTFT is mainly conducted within two types of commercial reactors: slurry bubble column (SBCR) and multi-tubular fixed-bed reactors (MTFBR). These reactors are depicted in Figure 2.10. The SBCR consists of a vertical column filled up to certain level with liquid hydrocarbons (i.e. slurry or wax), and the gas phase in introduced trough a sparger at the bottom. The gas bubbles mix the slurry phase as they move upwards, removing the need for mechanical mixing. Small size catalyst particles are diluted in the liquid slurry phase, which is continuously removed from the reactor. Therefore, in SBCR technology catalyst needs to be separated from the slurry. MTFBR process is somewhat simpler, since it does not involve catalyst/slurry separation and recycle. In the MTFBR larger catalyst particles are used to form a fixed-bed. These reactors consist of a several thousands of small diameter tubes. Gas phase goes into the reactor from the top reacting with the catalyst to form both gas and liquid phase products, which trickle down the packed bed.

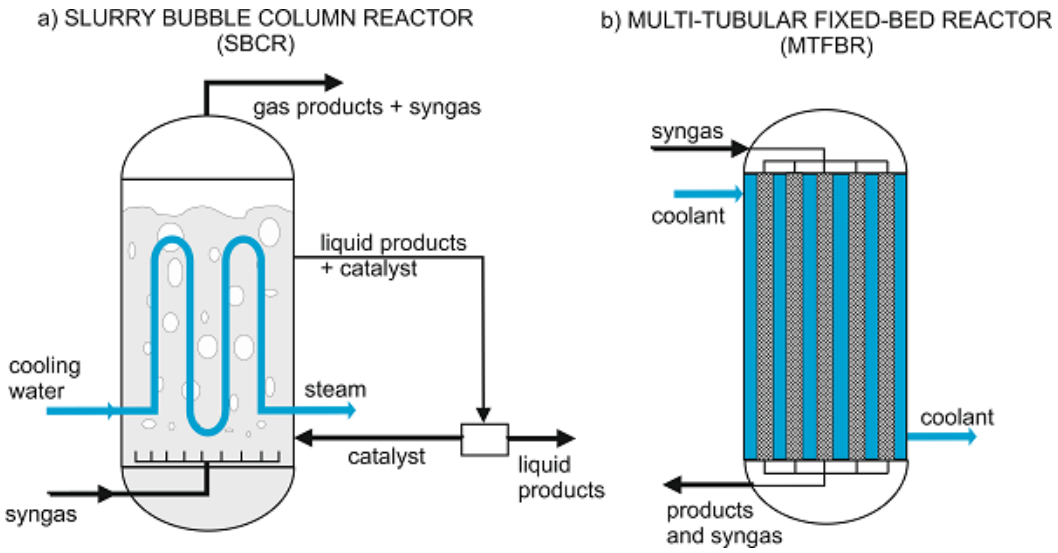

Figure 2.10 - Commercially used industrial reactors types for low temperature FTS: a) slurry bubble column reactor; b) multi-tubular fixed-bed reactor.

The FTS reaction is highly exothermic and the removal of heat presents one of the main challenges when choosing the reactor type. However, other issues that also have to be considered are catalyst effectiveness due to mass transfer resistances, catalyst deactivation and regeneration, pressure drop etc. The differences between these reactor types have already been discussed elsewhere [231-233]. The major downsides of SBCR are difficult scale-up, separation of active catalysts from the wax and catalyst deactivation due to attrition, while the drawbacks of MTFBR are high capital cost, poor heat removal, high mass transfer resistances and high pressure drop [234]. In this work we will mainly focus on the fixed-bed design. Several useful reviews of FTS reactor technologies and their historic development exist in the literature [2, 7, 26, 34, 231, 232, 235, 236].

Design, modeling and optimization of fixed-bed FTS reactors

Multi-tubular fixed-bed reactors (MTFBRs) are the most often used as commercial FTS reactors. They are used in plants around the world, including South Africa, Qatar and Malaysia, as part of Sasol ARGE and Shell Middle Distillate Synthesis process. These reactors consist of several hundred to well over ten thousand tubes, with 2 to 5 cm diameters. The use of such narrow tubes, coupled with turbulent fluid flow, allows for high heat transfer coefficients. Good reaction heat transfer from the packed bed

to the cooling fluid is a key factor in the optimal FTS reactor operation. Since iron is less active and therefore produces less heat, tubes up to 5 cm diameter are used, whereas for cobalt catalysts narrower tubes are more optimal. Considering that high gas space velocities are needed to achieve turbulent flow, a part of the tail gas is recycled into the reactor. Because of water deactivation issues, single pass syngas conversions are typically kept around 60% for both cobalt and iron catalysts. However, recycling of unconverted syngas increases the overall conversion to above 90%. Some industrial patents also suggest recycling of liquid products in order to improve temperature uniformity inside the bed, as well as to potentially improve product selectivity [237, 238]. Catalyst particles used in the fixed-bed are in the 1 to 3 mm diameter range. The particles larger than 0.2 mm are known to exhibit mass transfer difficulties [30]. The use of large particles MTFBRs means that a part of catalyst activity is sacrificed in order to maintain acceptable pressure drop within the tubes.

A number of modeling studies of conventional fixed bed and fewer studies of milli-structured FTS reactors exist in the literature [99, 188, 190, 239-246]. Modeling of fixed bed reactors for FTS over Fe-based catalyst was first done in the late 70's by Atwood and Bennett [190], by applying a simple kinetic model in a one-dimensional pseudo-homogeneous model of FBR. Later studies over iron [188, 239] developed two-dimensional pseudo-homogeneous reactor models, assuming plug-flow and utilizing empirical selectivity models of kinetics. Only Wang et al. [247] applied detailed Langmuir-Hinshelwood-Hougen-Watson (LHHW) model of FTS kinetics, including reactant disappearance and product formation, as a part of one-dimensional heterogeneous FBR model. All of the above mentioned reactor modeling studies used Fe as catalyst of choice and neglected the effect of liquid formation on heat transfer and pressure drop calculation. However, this effect was later shown to be significant [248]. De Swart et al. [248] first modeled FTS multi-tubular fixed bed configuration that utilizes Co-based catalyst (higher activity and C_{5+} selectivity compared to Fe catalysts [96]). Their one-dimensional heterogeneous reactor model showed that the effect of liquid presence is very important and cannot be neglected as assumed by previous models. In the last few years the interest in modeling of conventional FTS fixed bed reactor modeling based on cobalt catalysts has increased [241-245]. Most recently, computational fluid

dynamics (CFD) methods were applied, coupled with empirical selectivity models [243, 244], leading to improved representation of fluid behavior inside the packed bed.

The interaction between physical phenomena (liquid/gas phase behavior and interstitial flow patterns, intra-particle diffusion and heat transfer, etc.) and chemical phenomena (intrinsic FTS surface kinetics) is very delicate and proposed reactor models have not captured the full level of detail needed for comprehensive understanding of these reactor systems. Considering the high dependency of FTS reaction rate and selectivity on reaction conditions, which are variable along the fixed bed, the importance of reliable kinetics cannot be underestimated. The most rational solution in this case is the use of models that take into account the complexity of FTS reaction pathways and species involved [7], i.e. detailed LHHW kinetic models. Overall, the truly optimal reactor design can be archived by using detailed knowledge of reaction kinetics, coupled with precise mass, energy and momentum balances.

While developing a reliable FTS reactor model one has to consider the multitude of scales at which different processes occur (Figure 2.11) and to select the comparable level of detail for all of the aspects. In addition, appropriate level of detail and sophistication needs to be applied throughout reactor modeling, eliminating simplifications and empirical correlations that could potentially diminish the models' ability to describe the reactor performance in a realistic and physically meaningful way. An example of commonly used simplification is the neglecting of liquid phase presence and application of empirical Ergun's equations for pressure drop, which result in serious misrepresentation of the pressure drop within the packed bed [231]. A more detailed approach would include the kinetic model capable of predicting liquid heavy products formation and couple it with gas-liquid phase equilibrium and Navier-Stokes equations (using CFD methods), resulting in a much more reasonable estimate of pressure drop. Two-dimensional heterogeneous CFD models would provide more accurate representation of heat distribution throughout the reactor bed, allowing for comparisons and selection of the optimal configuration based on effective heat removal, which is a limiting design factor with conventional fixed bed FTS reactors.

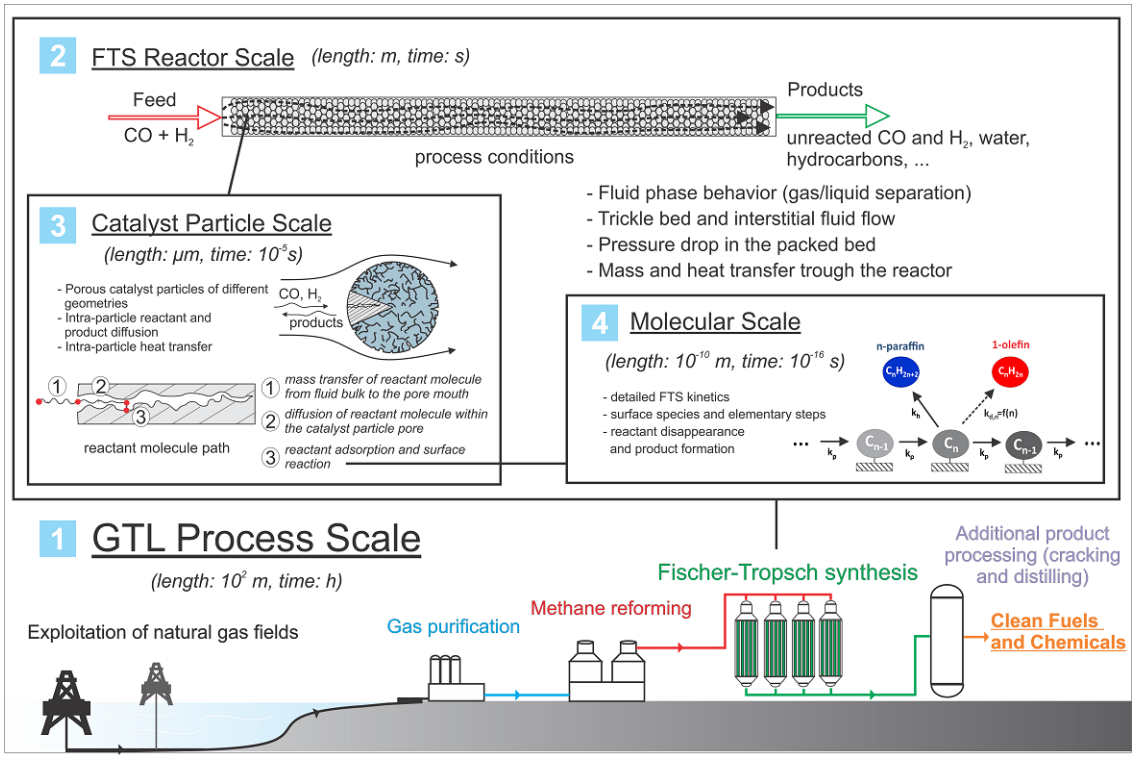

Figure 2.11 - Chemical reaction engineering multi-scale approach to GTL process and development of FTS reactors ([1] GTL process scale → [2] FTS reactor scale → [3] Catalyst particle scale → [4] Molecular scale).

Although optimization of FTS reactor design parameters and operating conditions could be highly beneficial for practical application, scientific contributions to this topic are scarce [249-257]. Advanced optimization approaches are used and vary from deterministic Non-Linear Programming (NLP) methods such as Sequential Quadratic Programming (SQP) and Levenberg-Marquardt (LM) [250-253] to stochastic global optimization methods such as Genetic Algorithm (GA) and Differential Evolution (DE) [249, 254-256] and their combinations. However, reactor models used in these studies do not apply all of the precise descriptions of the occurring phenomena. Either they use basic kinetics or too simplified transport models. Moreover, intensified mill-structured reactors have not been optimized so far.

So far all efforts in reactor modeling were focused on steady-state operation of FTS reactors and little is known about the dynamics of FTS conventional fixed bed operation [258, 259] and especially novel milli-structured configurations. Therefore

dynamic models of mentioned reactor configurations need to be established in order to study the various aspects of reactor dynamics, particularly for control design purposes.

2.4. Intensification of FTS process

As it was discussed in the Introduction, XTL plants that utilize FTS reactors are most often made on the large scale. GTL plants require very high capital investments (in order of billion dollars US) and the capacity needed to pay off these investments is above 30 000 bbl/day. This is why GTL plants can be placed only in locations with sufficient natural gas reserves. Process intensification aims at reducing the size of the plant, and by doing that reduce the capital investment needed, while maintaining the desired capacity and most importantly economic viability of these plants [260]. This way plant capacity can also be drastically reduced, enabling the utilization of smaller gas fields, as well as associated gas.

The design and construction of this new generation of smaller GTL plants is pioneered by Velocys Inc. Current technology proposed by them is based on coated microchannel reactors with "super active" cobalt-based catalysts [10]. Similar solution is also offered by Compact GTL [11].

In this section we will focus on exploring the options for intensification via reduced methane production for cobalt-based catalysts, i.e. improved yield of desired products, by better understanding of methane formation kinetics allowing for selection of optimal catalysts, process conditions and reactor configurations.

Higher-than-expected methane formation in FTS over cobalt-based catalysts

As explained above, methane formation in FTS does not follow the expected ASF distribution. Higher-than-expected methane formation in FTS on cobalt catalysts can be due to the mechanistic and kinetic reasons, reactor and reaction conditions. Several

concepts explaining non-ASF behavior of methane have been proposed and include: high surface mobility of methane precursor [35], hydrogenolysis of higher hydrocarbons by successive demethylation [109], lower activation energy for methane formation compared to other products [52, 229], and existence of different pathways for methanation reaction [261, 262]. A recent review of Yang et al. [25] discusses some of these concepts and offers an in depth review of the effect of CO conversion level on methane selectivity over various FTS catalyst. Perhaps the most accepted kinetic explanation for high methane is the existence of two different sites, i.e. FTS active sites and specific sites for methanation, or different reaction pathways [174, 263, 264]. According to Schulz [174], the methanation reaction is mainly happening on active sites with different coordination than that of FTS active sites. Lee and Bartholomew [263] showed that support could play a role, where spillover CO and H species could react to form CH_xO complex, which then diffuses to FTS active metal sites and produces methane trough decomposition. According to their study, increase in catalyst loading lead to a decrease in this secondary methanation reaction and favoring of FTS pathway. Further evidence for the hypothesis of separate methanation pathway is given by addition of water and ammonia, which both seem to inhibit secondary methane formation [118, 265]. Similar behavior is observed for 1-olefin hydrogenation and isomerization, which are also believed to happen on a secondary type of active sites [164, 174]. Further evidence for the hypothesis of separate methanation pathway is given by addition of water and ammonia, which both seem to inhibit secondary methane formation [118, 265].

The effect of water on FTS with cobalt catalyst is somewhat controversial and conflicting results have been reported [101, 200, 266-268]. Even though all studies seem to agree that water addition causes reduction in methane selectivity, its effect on reaction rate and catalyst deactivation are a matter of debate [101, 197, 200]. Large partial pressures of water are known to irreversibly deactivate cobalt based catalysts [73] as well as increased methane selectivity [106], most likely due to the formation of methanation sites [119, 174]. Smaller amounts of added water (less than ~ 20 vol% in the feed) can either increase or decrease the rate of FTS, depending on the catalyst support, promoters, loading etc. [200]. Water is believed to have a positive effect on rate trough: better reagent

diffusion in water [112], washing out of carbon species from the surface [160] and intrinsic kinetic effects [116, 269].

Ammonia addition also reduces FTS catalyst activity. Recently, Pendyala et al. [265] reported that high concentrations of ammonia reduces the methane selectivity and enhance the C_{5+} yield over cobalt-alumina catalyst. The addition of both water and ammonia also results in higher 1-olefin selectivity [164, 265]. The proposed explanation is that these molecules block catalytic sites for hydrogen adsorption thereby reducing hydrogenation activity. Alternatively, the adsorption of water and ammonia onto sites on which secondary methane formation and 1-olefin reaction (hydrogenation and isomerization) occur could also explain the observed trends in selectivity.

Cobalt catalyst properties (such as particle size, phase and addition of promoters) have been shown to affect methane selectivity. The cobalt particle size does not affect the catalyst activity (turn over frequency, TOF) in the ~10 to 200 nm range, as well as methane selectivity, however bellow 10 nm TOF is decreased and methane selectivity increased [26, 29, 270, 271]. This difference between smaller (bellow ~10 nm) and larger (10 to 200 nm) cobalt particles was attributed with surface coverage of CO, H and CHx. As measured by SSITKA (Steady State Isotopic Transient Kinetic Analysis) smaller particles had increased coverage of atomic coverage hydrogen, while in the range above 10 nm those coverages did not change with particle size [270]. Different phases of cobalt crystals (hcp and fcc) also exhibit different behavior and hcp is generally believed to be favorable both in terms of TOF and selectivity [272]. The addition of noble metal promoters is well known enhance the rate of FTS, but recent study by Ma et al. [273] shows that they potentially could be used to enhance selectivity. In their study rhenium was highlighted as the promoter that had the most positive effect on both catalyst activity and selectivity.

Methane selectivity in FTS can also be affected by phenomena that are not intrinsically kinetics, but depend on reactor configuration. Here we most often talk about mass and heat transport phenomena. Fixed-bed reactor configuration is particularly affected by poor mass and especially heat transport, leading to increased methane selectivity. The influence of these phenomena cannot be decoupled from that of intrinsic

kinetic features (e.g. poor heat removal causes high temperature, which in turn causes higher conversion with high partial pressure of water, which irreversibly deactivates the catalyst). The mass transfer limitations change the concentration of reactants close to the catalyst surface, thereby changing the intrinsic kinetics with effective one. The rates at which hydrogen and carbon-monoxide diffuse into the catalyst pellets are different, where later diffuses faster [206]. Severe mass transfer resistance will therefore cause surface saturated in hydrogen and without enough carbon-monoxide (high effective H_2/CO ratio), causing poor performance in terms of selectivity. Catalyst pellets with diameter lower than 200 nm do not experience mass transfer issues; however these can be expected for pellet sizes typically used in industrial fixed-bed reactors (1 – 3 mm). Conventional fixed-bed FTS reactors, with tube diameter typically above 2 cm, also often experience temperature gradients and hot spots due to poor heat removal. As shown above, high temperature favors the production of methane and other light products; and at very high temperatures catalyst is deactivated and methane becomes the main product [73]. However, the occurrence of mass and heat transport limitations can be avoided by the use of modern intensified reactor configurations, i.e. microreactors.

Microreactors for FTS

Micro-reactors, as the name suggests, represent the reactors with characteristic sizes (of tubes of channels) in the order of micro-meters [274, 275]. They also provide a significant reduction in reactor dimensions, compared to conventional reactors, allowing for a significant reduction in capital costs (Figure 2.12).

Microreactors for FTS have recently received a lot of attention from both academic and industrial research community [276]. They offer potential to minimize mass and heat transport resistances that are present in conventional fixed bed reactors and which lead to higher methane selectivity. Several types of microreactors are available for FTS (Figure 2.13), including: 1) reactors with microstructured catalyst (e.g. monoliths and foams); 2) coated microchannel reactors (or catalytic plate reactors), in which catalyst is coated over the walls of microchannels; and 3) micro- and milli-fixed bed reactors, in

which sufficiently small catalyst particles are loaded into the packed bed, allowing for micro-scale flow characteristics.

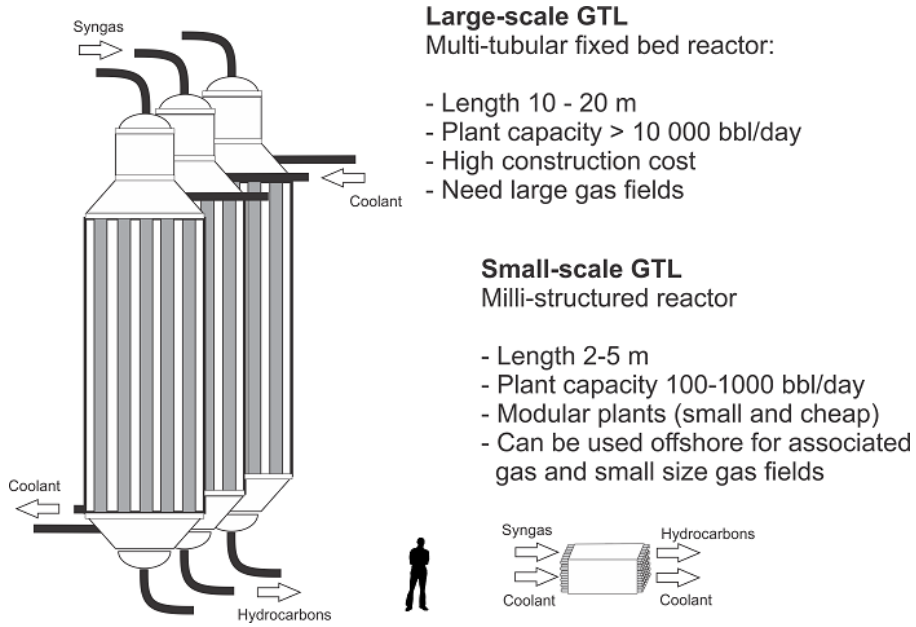

Figure 2.12 - Comparison of large-scale multi-tubular fixed bed and small-scale milli-structured FTS reactors.

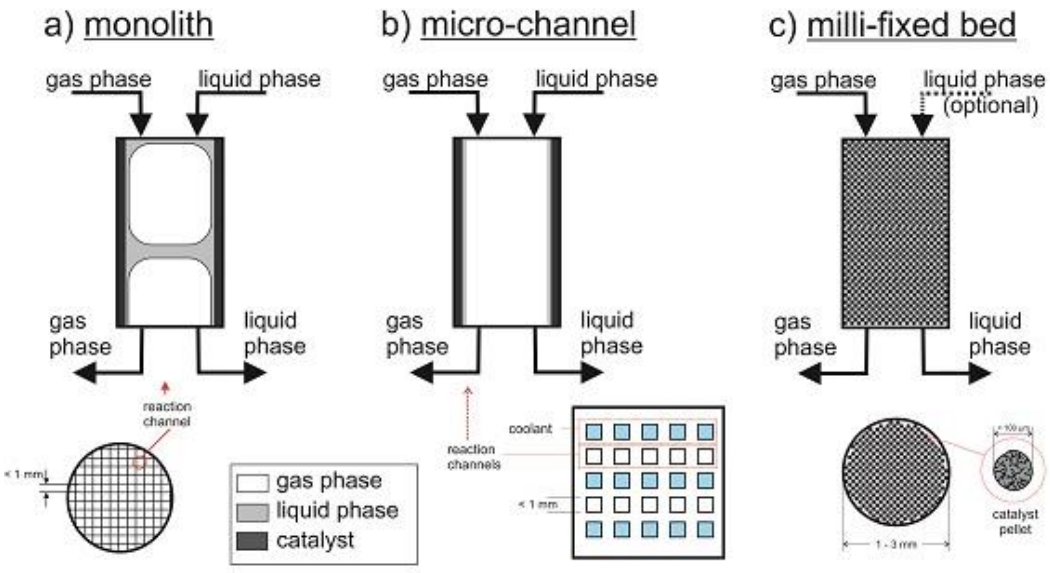

Figure 2.13 – Microreactors for FTS (flow pattern and cross-sections): a) monolith microstructured catalyst reactor; b) micro-channel reactor; c) milli-fixed bed reactor.

The principal advantage of microreactors is enhanced heat transfer which is often problematic in conventional centimetric fixed bed reactors. The temperature control can be particularly demanding during the reactor start up, when the uncontrollable temperature surge can affect the catalyst structure. Because of the enhanced heat transfer, more active catalysts with much higher hydrocarbon productivities can be used in the microreactors. One of the main disadvantages when dealing with conventional reactors is the chaotic nature of fluid dynamics within them, i.e. turbulent fluid flow between catalyst pellets within the fixed-bed and gas bubble and liquid phase behavior within a slurry bubble column reactor. Microstructured catalysts and reactors overcome this by having regular spatial structures, allowing for simplification of fluid behavior (e.g. to laminar flow) and thus better control of physical heat, mass and momentum transport phenomena [277]. Microstructured catalysts are formed by coating a structured support, such as honeycomb monolith, with a thin layer of catalyst. This way the catalyst and reactor really become inseparable entities, since the structured catalyst is placed inside the reactor as a whole and not the sum of individual catalyst pellets. A monolith catalyst consists of many parallel channels, which are separated by thin walls, coated with the active catalyst [278]. In this type of structure the heterogeneous gas-liquid mixture flow pattern is known as the Taylor flow [279]. Taylor flow is characterized by elongated gas bubbles, whose typical equivalent diameter is significantly larger than that of channel diameter. The gas bubbles are separated by liquid flow. A very thin layer of liquid also separates the gas bubbles from the walls coated with catalyst. This means that the reactant molecules from the gas phase will have to travel a very short distances to reach the active catalyst surface, allowing for very small mass transfer resistances. By analogy, similar can be said for heat transport resistance, where heat is very easily removed from the coated catalyst walls, compared to conventional fixed-bed catalyst particles. It should be noted though, that sometimes achieving Taylor flow regime requires high liquid flow rates. Therefore, the use of liquid phase recycle is needed in a monolith loop reactor [237, 238]. The monolith structure offers a very high open cross-section area, for fluid to flow through, considering the reactor volume, allowing for a very low pressure drop. Similar characteristics can be achieved with other types of microstructured catalysts, such as foams, wire and fibers.

Holmen and co-workers [238, 280, 281] first used monolith, coated with Re-promoted Co/Al_2O_3 catalyst, for FTS applications. Their results showed that the C_{5+} selectivity and olefin/paraffin ratios depended on coat loading, i.e. thickness of coated catalyst layer, due to the occurrence of transport limitations. However, both activity and selectivity of cordierite monoliths, with catalyst layer thickness of 40 – 50 μm, was comparable with the classical powder catalyst (< 90 μm) [280]. Hilmen et al. [280] showed that methane and C_{5+} selectivities are 8.9 and 82.5%, respectively, for monolithic cobalt catalyst with layer thickness of 40 μm, compared to 8.3 and 82.3% for powder catalyst used in a slurry reactor. Almeida et al. [282] showed that increasing catalyst loading from 255 to 908 mg (i.e. increasing coating layer thickness) caused increase in methane selectivity from 20.8 to 27.1% for monoliths, even though the overall CO conversion increased from 19.2 to 58.2%. Using Krischna and Sie [283] approach to multiphase reactor selection, de Deugd et al. [276] analyzed several reactor types and found the monolithic reactor to be especially fitting for FTS application. Several research groups used monolith catalysts for FTS in the past decade [238, 246, 280, 284-300]. Kapteijn et al. [286] showed the effect that the monolith catalyst washout layer thickness (from 20 to 100 μm) has on FTS activity and selectivity. Similar to previous reports [280], their results showed that the FTS activity and selectivity are intrinsically kinetic for layers up to 50 μm, while thicker layers exhibit clear signs of diffusion limitations. This study showed that activity and selectivity of FTS can be tuned by optimizing the thickness of monolith catalysts washcoat layer.

Even though monolith support was most frequently used for FTS applications, other structured catalyst supports (e.g. foam and wire) have been demonstrated to have similar performance characteristics [301]. General conclusion that can be made is that the structured catalysts typically perform similarly, or in some cases even better, compared to conventional catalysts in terms of activity and selectivity. However, the biggest drawback of structured catalysts is the low activity compared to reactor volume. In other words, these reactors hold a very low amount of active catalyst material to provide sufficiently high product yield. Most recently carbon nanofibers (CNF) have been proposed as a support for catalytic reactions and especially FTS in order to enhance the activity per reactor volume, due to their larger surface area [290, 302, 303]. However, the

issue of these catalysts was rapid deactivation at industrial FTS conditions [303]. This issue was addressed by Zhu et al. [302], who applied Co catalyst on SiO_2 support coated on carbon nanofiber structure, using the sol-gel method. The application of uniformed SiO_2 layer increased the catalyst stability.

Another type of FTS microreactors are the micro-channel reactors. These reactors are very similar to monolith in their general design and have been studied by several research groups [289, 301, 304]. This technology has also been extensively used by the industry [305-307]. Micro-channel reactors consist of a large number of parallel rectangular channels, which are coated with a thin layer of active catalyst, most often sorted into blocks. Due to their high surface area-to-volume ratio, they offer high mass and heat transfer coefficients, several times larger compared to conventional reactor technologies [308]. This in turn enables operation at severe process conditions needed to achieve best activity and selectivity, such as increased temperature, conversion level and pressure. Coolant fluid flows through the parallel uncoated channel rows (Figure 2.13b). Unlike monoliths, fluid flow in these FTS reactors is laminar. This technology was initially employed for FTS by Velosys [305-307]. Velocys researchers reported methane selectivity for these reactors at about 9%, which is similar to slurry phase experiments with powder catalysts and monoliths with thin catalyst layers. Their fabrication is relatively simple and consists of stacking many thin sheets with solid walls one on top of another. This leads to cost effective manufacturing and robust design [306]. Guettel and Turek [237] compared conventional reactors (fixed-bed and slurry) with novel micro-channel and monolith reactors using mathematical modeling. Their analysis focused on reactor effectiveness and the effect of mass and heat transfer on effectiveness. The simulation results showed that slurry reactors exhibit a tenfold higher effectiveness compared to fixed-bed and require both less active catalyst mass and reactor volume, due to better mass transfer characteristics and isothermal operation. Monolith catalyst reactor exhibited the same similar yield-to-reactor volume compared to fixed-bed reactor, but no heat transfer issues. However, both slurry bubble column and monolith reactor suffer from practical issues; removal of catalyst particles from liquid products in the slurry reactor and high liquid recycle flow rate needed in monolith reactor for heat removal. On the other side, Guettel and Turek [237] showed that micro-channel reactors do not have

such issues and exhibit very high reactor efficiency, due to negligible heat and mass transfer resistances. However, the very low catalyst mass-to-reactor volume ratio meant that their productivity with conventional catalysts is not high enough for industrial application. However, their application is possible with the new generation of highly active catalyst, reported by the Oxford Catalyst Group [309]. Such micro-channel reactors with highly active catalyst are already being tested on industrial scale by Velocys plc. (integration of Oxford Catalysts and Velocys).

Almeida et al. [282, 301] studied the performance of different structured catalyst (monolith, micromonolith and foam) to powder catalyst and micro-channel block reactors. Their results showed similar or better performance of micro-channel technology compared to structured catalysts, in terms of catalyst effectiveness and methane and C_{5+} selectivity, at similar process conditions. Their results showed that microchannel reactors had methane selectivity ranging from 5.0 to 18.1%, depending on the loading, while monoliths and foams typically exhibited methane selectivity of ~ 20% [282]. Recently, Holmen et al. [289] reviewed and compared different microreactor types used by their group in previous studies (monolith, carbon nanofibers and micro-channel reactors). Results for these reactor types show comparable CO consumption and hydrocarbon formation rates. The micro-channel reactor showed the highest reaction rates on the basis of Co mass and catalyst mass, but was outperformed by micro-structured carbon nanofiber catalyst in terms of CO conversion per reactor volume. They also point out that monoliths and carbonfiber structured catalysts *"are relatively easy to handle (shape to any type) and can be used in fixed-bed reactors directly"*, while micro-channel reactors *"need to a larger extent to be designed and fabricated to the purpose, but they offer possible advantages in terms of control and safe operation of the vessel, if the parallelized/compartmented approach is maintained throughout"*.

The most significant downside to coated FTS microreactors (micro-channel and structured catalyst reactors) is the above mentioned low catalyst mass to reactor volume ratio, resulting in low hydrocarbon yield. However, others disadvantages, such as difficult reactor wall coating procedures and the need for specially designed catalysts for coating [234]. This is why some authors have looked into the possibility of using micro- and milli-fixed bed reactors, in order to reap the mass and heat transport benefits of microreactors,

as well as high catalyst mass to reactor volume of fixed bed [234, 310]. An additional advantages of such configurations is the ability to use tried and proven catalysts, easy reactor loading and possibility of catalyst replacement [234]. As expected, the main issue with these reactors is a very high pressure drop, due to the loading of very small catalyst pellets into the bed. However, Knochen et al. [310] showed that the acceptable pressure drop can achieved with catalyst pellets as small as 100 μm, while maintaining high catalyst effectiveness. They also showed that tubes as large as 3 mm can be utilized to benefit from high heat transfer. Therefore, this type of configuration also displays much better control and deactivation characteristics compared to conventional reactors.

Recommendations for intensification of FTS in terms of selectivity

Based on our analysis of experimental results (which will be discussed later in this work), obtained under a range of typical FTS conditions, it seems that the best way to improve C_{5+} selectivity is to reduce this extra methane formation [103]. Methane selectivity can be affected by influencing the kinetics of its formation. This can be done in several ways, i.e. by changing the catalyst, as well as the process conditions within the reactor and within the catalyst pellets.

First, better understanding of methane formation kinetics is needed. As pointed out before, methane deviates from ASF FTS kinetics most likely because of the existence of several formation pathways. One experimental method that could help elucidate methane kinetics is the steady-state isotopic transient kinetic analysis (SSITKA). In this technique, one of the reactants is abruptly replaced by its labeled isotope. For SSITKA application in FTS, usually labeled ^{13}CO is used, since D_2 exhibits isotopic effects [311]. There have been several investigations in which SSITKA was used to study the FTS reaction mechanism [261, 311, 312]. It is interesting however that SSITKA studies are typically performed at conditions favoring methane formation, i.e. low pressure and high H_2/CO ratios. Therefore, extrapolation of SSITKA results in the analysis of overall FTS kinetics (as done so far) is questionable, since it is based on analyzing methane formation, which deviates from overall FTS ASF distribution. However, its application in analyzing

the kinetics of methane formation kinetics within FTS is undoubtedly justified. To our knowledge, this type of study was only performed by Govender et al. [313]. They proposed a mechanistic kinetic model for methane formation over Fe-based catalysts, consisting of two parallel methane formation pathways. This is something that requires further consideration and such detailed kinetic models of methane formations should be derived for Co-based FTS catalysts as well.

Having reliable FTS methane formation kinetic models would help analyze the effect of process conditions on methane selectivity and reduce the selectivity towards this undesired product by helping to choose the optimal set of conditions. Second important implication of this viewpoint is that one could conceivably control the methanation rate through catalyst design by shutting down the additional methanation pathways [103]. An ideal catalyst would produce methane only through FTS reaction (i.e. have CH_4 selectivity close to 1%). Methane selectivity could therefore be reduced by optimizing the size of cobalt catalyst nano-sized crystals [271], metallic cobalt phase composition and support structure [272], as well as selection of optimal catalyst loading [263] and catalytic promoters [273]. Methane selectivity could also be reduced by optimizing the size of cobalt catalyst nano-sized crystals, metallic cobalt phase composition and support structure.

Third improvement in methane selectivity, and FTS intensification as a whole, is the use of knowledge of methane formation kinetics in reactor design. As described above, mass transfer resistances could play a huge role in determining FTS product selectivity for conventional fixed-bed reactors, since the concentrations of reactants near the active catalytic sites are often very different from those inside the reactor fluid bulk. By applying new microreactor concepts, with intensified mass transfer, these concentration gradients can be minimized. Some characteristics of different FTS microreactor types are summarized in Table 1. The use of such reactors would also benefit from improved heat transfer, enabling better temperature control which in turn would result in lower catalyst deactivation and more stable product distribution over time.

Table 2.1 - Comparison of main characteristics of microreactors (data from Refs. [280, 299, 306]).

Characteristic		Monolith	Micro-channel	Micro fixed-bed
Surface area	Rank	2	3	1
	m^2/g	160	N/A	184
Porosity	Rank	2	1	3
	%	89	N/A	<70
Heat transfer	Rank	2	1	3
	W/cm^2	N/A	1-20	~ 1
Mass transfer	Rank	2	1	3
Pressure drop	Rank	2	1	3
Catalyst loading	Rank	2	3	1

Conclusions

There are still many unknowns regarding the fundamental nature of FTS and best ways it can be affected to maximize the yield of desired products. Some of the most important questions pertaining to kinetics are: the mechanism of FTS initiation and propagation, secondary pathways for methane formation, termination of chain growth, formation of main products and the role secondary 1-olefin reactions etc.

The available literature data suggests that the catalytic performance of cobalt FT catalysts and product selectivity depend on catalyst, operation conditions and the reactor configuration. This also suggests possible ways for improving long-chain hydrocarbon productivity and reducing methane formation.

It is important to gain better understanding of intrinsic FTS kinetics and develop kinetic models for more reliable prediction of both reactant consumption and product formation rates in FTS. Such knowledge would provide opportunities to greatly improve catalyst design and reactor configurations.

3. Effect of process conditions on the FTS product distribution

Publications from this chapter

1. Branislav Todic, Wenping Ma, Gary Jacobs, Burtron H. Davis, Dragomir B. Bukur, "Effect of process conditions on the product distribution of Fischer–Tropsch synthesis over a Re-promoted cobalt-alumina catalyst using a stirred tank slurry reactor", *Journal of Catalysis*, **2014**, 311, 325.

Conducting experiments and collecting data for Fischer-Tropsch synthesis in a laboratory reactor setup was not a part of this thesis. Experimental data used in this work for analysis of process conditions effect on product distribution and kinetic modeling was obtained in Prof. Dragomir Bukur's lab at Texas A&M University (experiments with iron-based catalyst conducted by Dr. Lech Nowicky) and in Prof. Burtron Davis's lab at Center for Advanced Energy Research, University of Kenticky, (experiments with cobalt-based catalyst conducted by Dr. Wenping Ma).

Original contribution of this author (Branislav Todić) in this Chapter will be to critically analyze the effect of various process parameters (i.e. temperature, pressure, reactant feed ratio, conversion level and time on stream) on various aspects of FTS product selectivity. Here we will analyze the delicate interplay between the kinetics of various parallel reactions (FTS, WGS and olefin secondary reactions), at different process conditions, which determines the overall selectivity of FTS products. The main goal in FTS is high selectivity of desired C_{5+} products and reduced methane selectivity. Proper selection of process conditions is important in achieving this goal. Even though there is a number of studies and reviews describing how variation of each process parameter (temperature, pressure, reactant feed ratio and conversion level) affects overall FTS selectivity for both iron [23, 29, 76, 90, 91, 98, 314-316] and cobalt catalysts [88, 89, 94, 223], questions about the reasons for the observed behaviors have not been fully answered.

We will analyze the basic parameters of FTS in terms of carbon number: selectivity, growth probability and ratios between products, and ways they vary with

conditions. Based on these results, conclusions are drawn about reaction pathways of primary FTS reactions, secondary 1-olefin reactions as well as WGS. In addition we look for the most optimal set of process conditions that result in high conversions, efficient syngas utilization, high hydrocarbon yields and low catalyst deactivation.

3.1. Precipitated iron catalyst

The catalysts of choice for industrial FTS are cobalt and iron. If the raw resource being used is coal, then the preferred catalyst is usually iron [24, 26]. One of the main features of iron FTS catalysts is their WGS activity, which provides additional hydrogen for FTS, which is needed in the case of coal-derived syngas. Coal-derived syngas has a H_2/CO ratio well below 2, the latter being an approximate stoichiometric H_2/CO ratio needed in FTS. The product distribution over iron-based catalysts, similar to other FTS catalysts, deviates from standard ASF distribution (Figure 3.1a). However, as we previously shown, C_1 and C_2 fall much closer to ASF values compared to cobalt-based catalyst. α_n values typically range between 0.6 and 0.9 (Figure 3.1b). OPR can range greatly depending on process conditions, primarily H_2/CO ration (Figure 3.1c).

Analyzing the effect of process conditions (temperature, pressure, reactant feed ratio and conversion level) on FTS product formation selectivity over Fe-based catalyst is complex because of the competing effects of several parallel reactions, including primary FTS reaction, secondary 1-olefin reactions and WGS. Apparent product distribution features, such as growth probabilities, 1-olefin-to-n-paraffin ratios and selectivities with carbon number, are dependent on the mutual interplay of the kinetics of these reactions. With Fe-based catalysts the effect of WGS is very significant. This reaction affects concentrations (partial pressures) of CO, H_2, CO_2 and H_2O in the system and changes kinetics of both primary FTS and 1-olefin secondary reactions.

Because of this complexity and unknown nature of kinetics over Fe-based catalyst, it is impossible to design an experiment in which only one process parameter affecting kinetics is varied, while all others are kept constant. The observed FTS behavior will therefore reflect a lumped effect of several process parameters (e.g. increasing T and

changing partial pressures of reactants). Through careful consideration of the combined effect of these variations, such as the magnitude of process condition change, and the expected kinetic implication of such changes we will try to shed more light on variation of selectivity with process conditions.

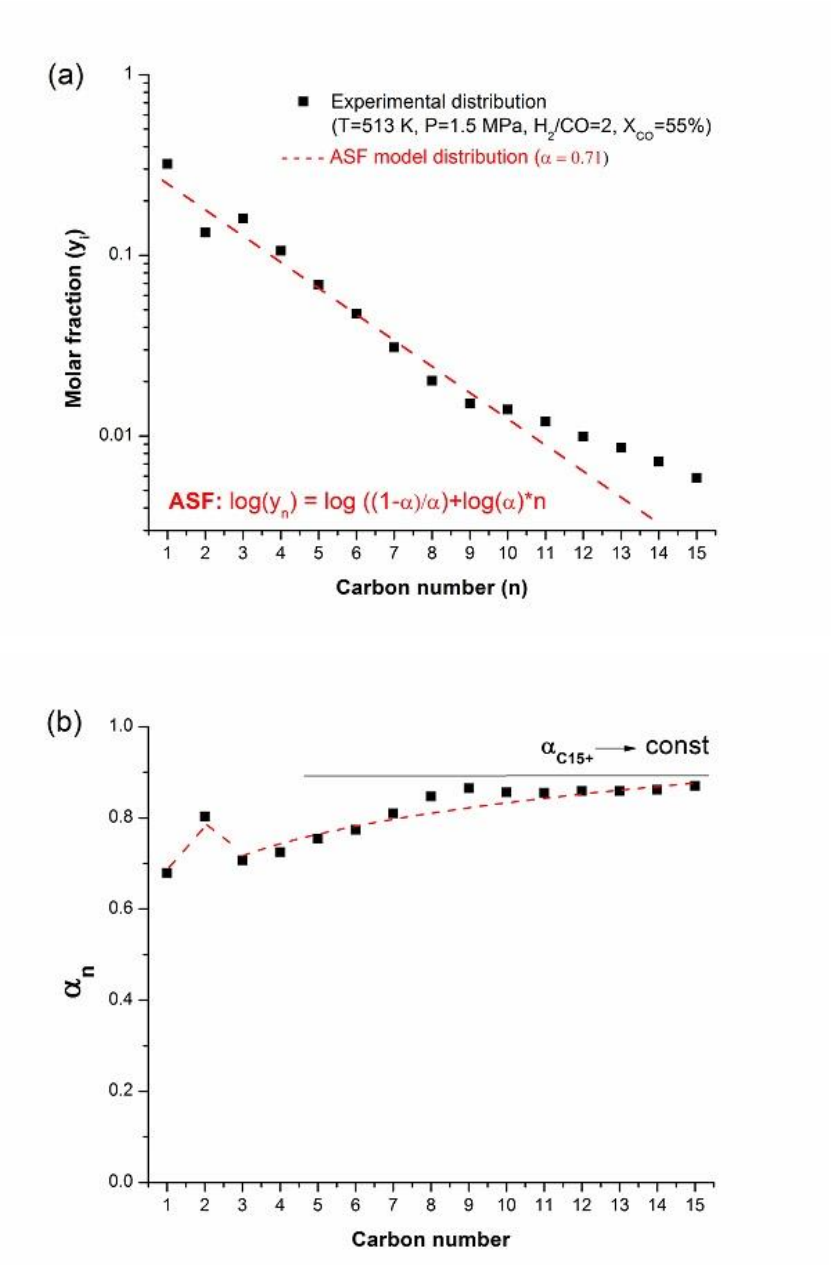

Figure 3.1 - FTS product distribution features over precipitated iron catalyst: a) molar fraction with carbon number (ASF plot); b) chain growth probability (α_n) with carbon number; (continued on next page).

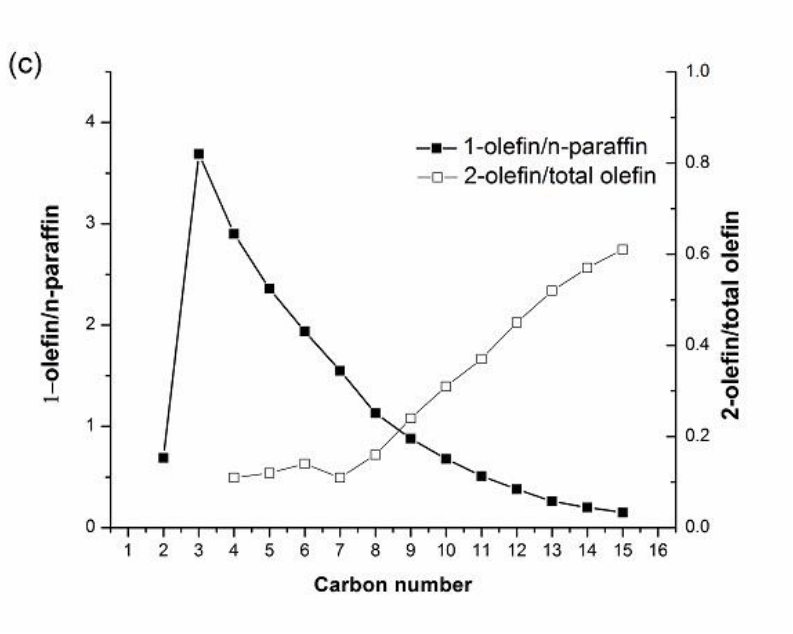

Figure 3.1 – (continued): c) 1-olefin/n-paraffin and 2-olefin/total olefin ratio with carbon number. (Process conditions: T = 513 K, P = 1.5 MPa, H_2/CO = 2, X_{CO} = 55%).

Experimental data

In total 27 sets of data at different process conditions were obtained in three separate runs, involving 12, 7 and 8 mass balances, respectively. The conditions and selected result are summarized in Table 3.1. Three reaction temperatures (T = 493, 513 and 533 K), four pressures (P = 0.8, 1.5, 2.25 and 2.5 MPa), two synthesis gas feed molar ratio (H_2/CO = 0.67 and 2) were achieved. The gas space velocity (SV) was varied from 0.52 to 23.5 $Ndm^3/g\text{-}Fe/h$ to obtain a wide range of conversions (X_{CO} = 9 to 84%). More details on the catalyst preparation and activation and reactor system and operating procedures can be found elsewhere [103].

Following formulas were used to calculate conversions and selectivities:

- CO conversion (% by moles)

$$X_{CO} = 100\% \times \frac{(\text{Moles of CO at inlet}) - (\text{Moles of CO at outlet})}{(\text{Moles of CO at inlet})} \qquad (3.1)$$

- CO_2 selectivity (% by moles)

$$S_{CO_2} = 100\% \times \frac{\text{Moles of } CO_2 \text{ at outlet}}{(\text{Moles of CO at inlet}) - (\text{Moles of CO at outlet})} \quad (3.2)$$

- CH_4 selectivity (% by mass in hydrocarbons)

$$S_{CH_4} = 100\% \times \frac{\dot{m}_{CH_4}}{\dot{m}_{HC,total}} \quad (3.3)$$

where $\dot{m}_{CH_4}$ is the mass flowrate of methane and $\dot{m}_{HC,total}$ is the total mass flowrate of hydrocarbons.

- C_n selectivity (% by mass in hydrocarbons) for n = 2, 3 and 4

$$S_{Cn} = 100\% \times \frac{\dot{m}_{C_n}}{\dot{m}_{HC,total}} \quad (3.4)$$

where $\dot{m}_{C_n}$ is the mass flowrate of hydrocarbons with n carbon atoms.

- C_5^+ selectivity (% by mass in hydrocarbons)

$$S_{C_{5+}} = 100\% \times \sum_{n=5}^{50} \frac{\dot{m}_{C_n}}{\dot{m}_{HC,total}} \quad (3.5)$$

The above formulas assume that there is no carbon dioxide in the feed.

- Mole fractions of hydrocarbons (product distribution) with n carbon atoms

$$y_n = \frac{F_n}{F_{HC,tot}} \quad (3.6)$$

where F_n is the molar flowrate of hydrocarbons with *n* carbon number and $F_{HC,tot}$ is the total hydrocarbon flowrate.

The chain growth probabilities for hydrocarbons having n carbon atoms (α_n) were calculated as:

$$\alpha_n = \frac{\sum_{i=n+1}^{\infty} F_i}{\sum_{i=n}^{\infty} F_i} \tag{3.7}$$

1-olefin to n-paraffin and 2-olefin to total olefin ratios for different chain lengths were calculated as follows:

$$1-olefin\ /\ n-paraffin = \frac{F_n^{1-olefin}}{F_n^{n-paraffin}} \tag{3.8}$$

$$2-olefin\ /\ total\_olefin = \frac{F_n^{2-olefin}}{F_n^{olefin}} \tag{3.9}$$

Table 3.1 - Reaction conditions and selectivity results for iron-based catalyst.

Run	No.	TOS	T	P	Inlet H_2/CO	Outlet H_2/CO	SV	X_{CO}	X_{H2}	X_{CO+H2}	UR	P_{CO}	P_{H2}	P_{H2O}	P_{CO2}	Selectivity (C-atom %)			
		h	K	MPa			NL/g-	%	%	%	-	MPa	MPa	MPa	MPa	CH_4	C_2-C_4	C_{5+}	CO_2
1	1[b]	78	533	1.50	0.67	0.58	4.0	54	60	57	0.74	0.63	0.37	0.08	0.33	4.6	19.8	75.6	43.9
	2	101	533	1.50	0.67	0.84	1.7	84	80	82	0.64	0.31	0.26	0.06	0.71	5.9	22.2	71.9	43.8
	3	126	533	1.50	0.67	0.56	9.2	27	39	31	0.98	0.82	0.46	0.06	0.11	6.4	27.4	66.2	34.8
	4	164	513	1.50	0.67	0.54	2.0	39	51	45	0.88	0.76	0.41	0.09	0.18	5.2	22.9	71.9	37.1
	5	215	513	1.50	0.67	0.58	1.0	56	62	59	0.74	0.62	0.36	0.07	0.36	5.4	26.7	67.8	45.3
	6	238	513	1.50	0.67	0.58	5.5	14	25	18	1.22	0.87	0.50	0.05	0.04	7.1	28.2	64.7	27.7
	7[b]	270	533	1.50	0.67	0.56	4.0	46	54	50	0.79	0.69	0.39	0.08	0.26	5.3	22.5	72.2	44.4
	8	310	513	1.50	2.00	2.63	4.2	46	29	36	1.26	0.34	0.89	0.11	0.08	11.2	36.0	52.8	28.5
	9	368	513	1.50	2.00	2.18	10.8	22	15	18	1.35	0.43	0.93	0.06	0.02	10.1	33.9	56.0	20.1
	10[b]	505	533	1.50	0.67	0.56	4.0	46	55	50	0.80	0.69	0.39	0.08	0.25	4.9	21.2	73.9	42.6
	11	606	533	2.25	0.67	0.50	6.1	36	52	43	0.96	1.13	0.57	0.14	0.25	6.0	25.6	68.4	38.5
	12	654	533	2.25	0.67	0.79	1.0	84	81	83	0.65	0.43	0.34	0.17	1.01	5.9	23.7	70.4	45.0
2	13	92	533	1.50	2.00	5.27	7.1	77	39	52	1.02	0.17	0.89	0.14	0.19	10.3	26.5	63.2	34.3
	14	122	533	1.50	2.00	3.91	10.1	66	34	46	1.02	0.23	0.89	0.14	0.15	9.8	26.5	63.6	34.7
	15	146	533	1.50	2.00	2.54	23.5	41	25	32	1.22	0.36	0.90	0.11	0.07	9.7	29.2	61.1	28.8
	16	191	513	1.50	2.00	2.92	5.8	55	34	42	1.25	0.30	0.87	0.15	0.10	8.7	28.0	63.3	28.1
	17	240	533	2.50	0.67	0.48	6.7	43	60	50	0.93	1.32	0.63	0.21	0.36	4.2	21.3	74.6	35.9
	18	268	533	2.50	0.67	0.53	17.1	20	37	27	1.24	1.51	0.80	0.15	0.10	4.9	21.5	73.6	25.6
	19	313	533	2.50	0.67	0.54	2.0	70	76	72	0.73	0.88	0.47	0.23	0.83	5.0	23.7	71.3	40.4
3	20	101	493	1.50	0.67	0.56	4.1	11	25	16	1.55	0.89	0.50	0.05	0.02	5.0	18.5	76.5	18.1
	21	143	493	1.50	0.67	0.50	0.5	34	51	41	1.00	0.79	0.39	0.11	0.14	4.5	26.7	68.8	35.1
	22	170	493	1.50	2.00	2.03	9.5	13	12	13	1.78	0.47	0.95	0.04	0.01	15.3	36.6	48.1	12.1
	23	198	493	1.50	2.00	4.17	0.6	72	42	54	1.16	0.18	0.77	0.29	0.14	7.3	25.2	67.5	29.9
	24	238	533	0.80	2.00	8.52	1.5	84	32	54	0.76	0.06	0.49	0.05	0.13	14.0	29.0	57.0	43.7
	25	268	533	0.80	2.00	2.42	9.0	35	21	25	1.22	0.21	0.50	0.03	0.03	10.5	30.3	59.2	30.8
	26	292	513	0.80	0.67	0.61	5.5	9	17	13	1.25	0.47	0.29	0.02	0.01	4.7	17.5	77.9	28.7
	27	318	513	0.80	0.67	0.61	0.7	50	54	54	0.73	0.34	0.21	0.04	0.17	3.9	16.5	79.6	48.7

Note: b – baseline condition

Effect of time on stream

The catalyst was initially tested at a set of baseline conditions (533 K, 1.5 MPa, 4 NL/g-Fe/h, H_2/CO = 0.67) in order to observe reproducibility. The catalyst in Runs 1 and 2 was tested at baseline conditions up to 80 h on stream, whereas in Run 3 from 50 to 73 h on stream. Results of all three tests at the baseline conditions and during the initial period are shown in Figure 3.2. Syngas conversion (Figure 3.2a) and methane and C_5^+ hydrocarbon selectivities (Figure 3.2b) during the first 80 h of testing were very similar in all three tests. It was observed that conversion and selectivity reach an approximately constant value after about 50 h on stream.

The catalyst was also tested at baseline conditions several times during all runs in order to assess the extent of catalyst deactivation. Measurements were repeated throughout the Run 1and at the end of the Runs 2 and 3. Conversion and selectivity are shown in Figure 3.3. The catalyst activity (conversion) decreased slightly in all three tests (Figure 3.2a). Methane selectivity increased whereas C_5^+ selectivity decreased slightly with time, similar to literature reports [75-77] (Figure 3b). In addition, product distribution with carbon number was analyzed for Run 1 (mass balances 1, 7 and 10 in Table 3.1). Total hydrocarbon and 1-olefin distributions for these conditions are shown in Figure 3.4a and b, respectfully. It can be seen that besides the catalyst activity, its selectivity, i.e. product distribution, has not changed significantly during Run 1.

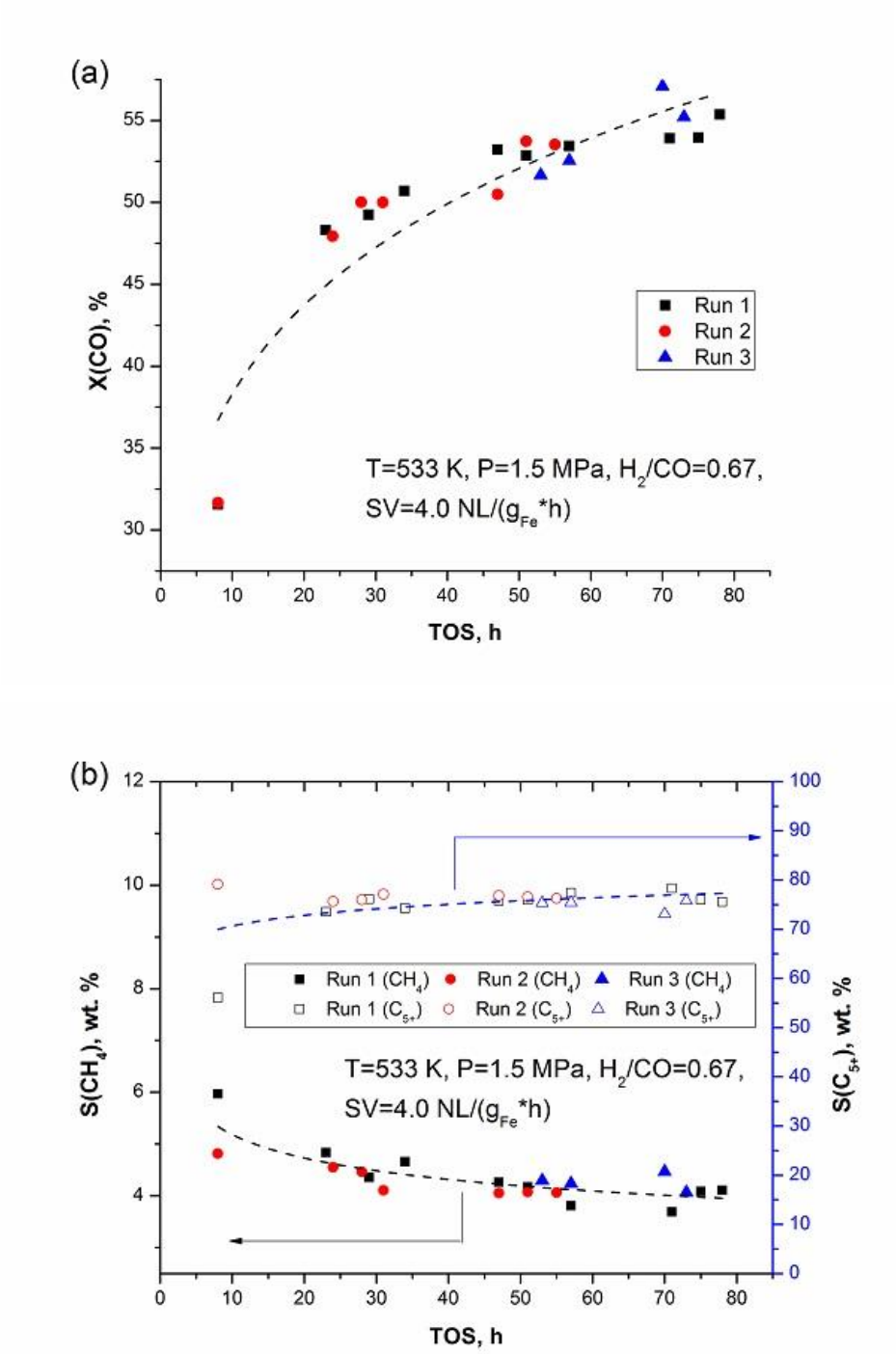

Figure 3.2 - Effect of time at the baseline conditions (initial period): (a) Syngas conversion, (b) Methane and C_5^+ selectivity. (Process conditions: T = 513 K, P = 1.5 MPa, H_2/CO = 2, X_{CO} = 55%).

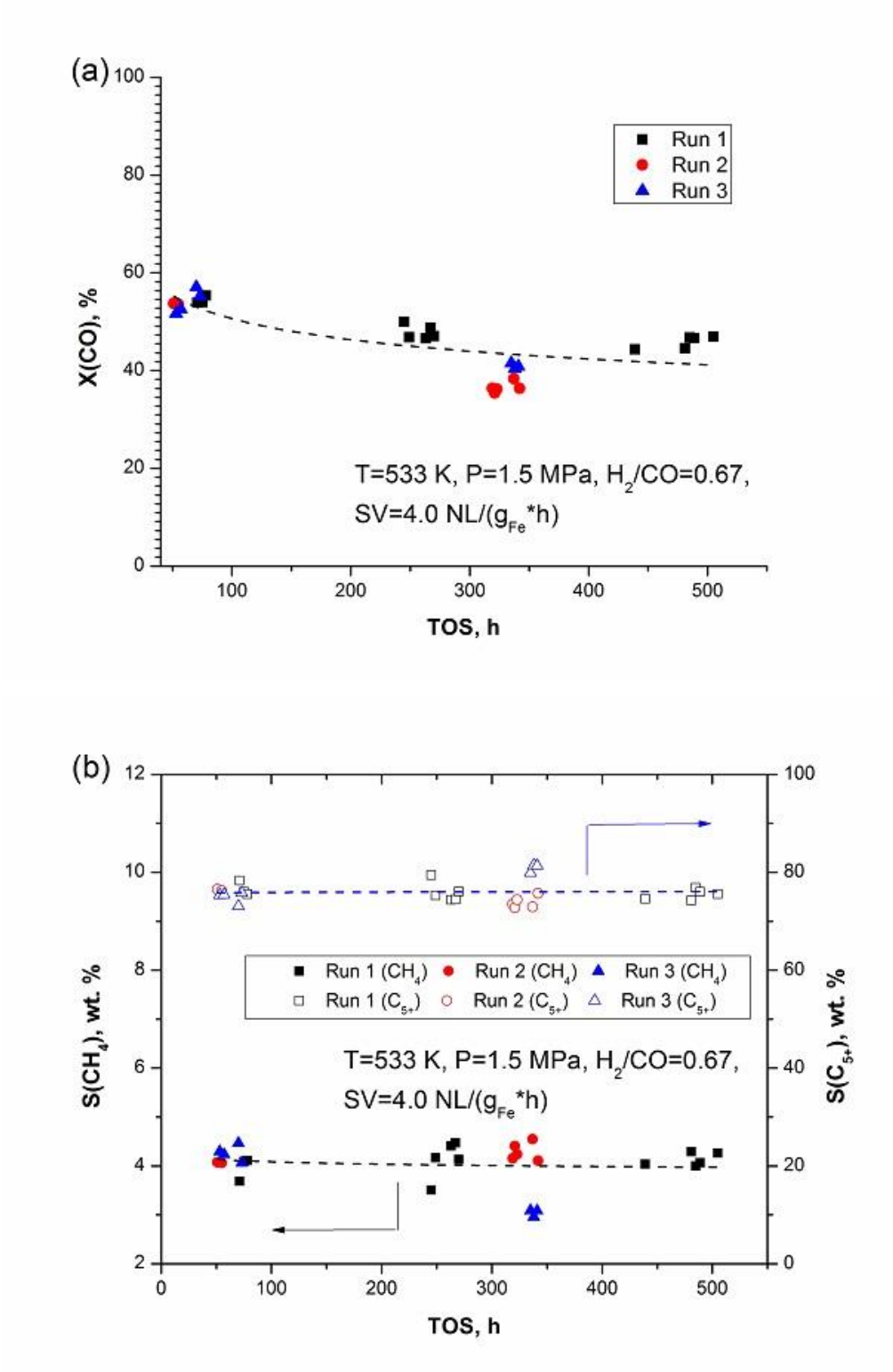

Figure 3.3 - Effect of time at the baseline conditions (normal process period): (a) Syngas conversion, (b) Methane and C_5^+ selectivity. (Process conditions: T = 513 K, P = 1.5 MPa, H_2/CO = 2, X_{CO} = 55%).

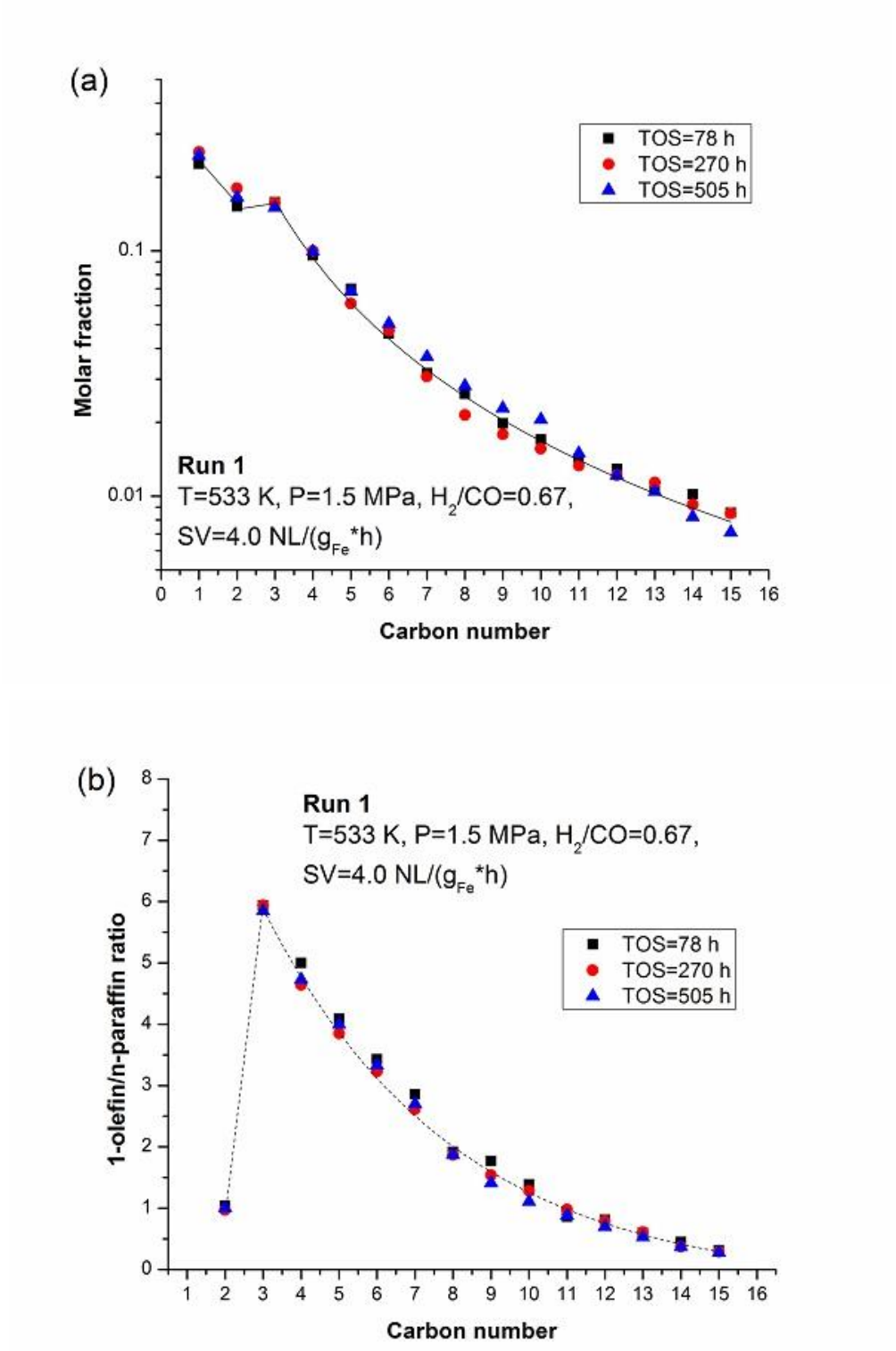

Figure 3.4 - Effect of time at the baseline conditions: (a) mole fractions of total hydrocarbon; (b) 1-olefin-to-n-paraffin ratio with carbon number. (Process conditions: T = 513 K, P = 1.5 MPa, H_2/CO = 2, X_{CO} = 55%).

Water-gas-shift reaction

A measure of WGS activity is the amount of CO_2 formed in the reactor. In order to be able to understand and at least partially eliminate the effect of WGS kinetics on FTS products we will first analyze how WGS activity varies with process conditions.

A useful property to look at when studying WGS is the usage ratio (UR):

$$UR = (Moles\ of\ H_2\ consumed) / (Moles\ of\ CO\ consumed) \quad (3.10)$$

In the absence of the WGS reaction, the usage ratio is 2, whereas if all water produced by FTS is consumed by the WGS reaction, the usage ratio is 0.5 and the CO_2 selectivity is 50% (assuming that CO is not consumed in any other reactions). Therefore, the change of UR always has an opposite trend compared to CO_2 selectivity.

The effect of temperature and conversion of the limiting reactant (H_2 for H_2/CO = 0.67 feed gas, CO for H_2/CO = 2 feed gas) is shown in Figure 3.5a and b. The usage ratio decreases whereas the CO_2 selectivity increases with an increase in conversion (at constant temperature) or with an increase in temperature (at constant conversion of the limiting reactant). This trend is the same regardless of feed composition (H_2/CO = 0.67 in Figure 3.5a, or H_2/CO = 2 in Figure 3.5b). From the stoichiometry it is expected that the extent of WGS reaction (secondary or consecutive reaction) will increase with increase in conversion, which is manifested in decrease of the usage ratio and increase in CO_2 selectivity. The increase in WGS activity (higher CO_2 selectivity and lower UR) with increase in temperature (at constant conversion) is a kinetic effect.

The effect of reaction pressure is shown in Figure 3.5c and d. The extent of the WGS reaction increases (lower UR and higher CO_2 selectivity) with an increase in conversion or with a decrease in total pressure, which is a kinetic effect.

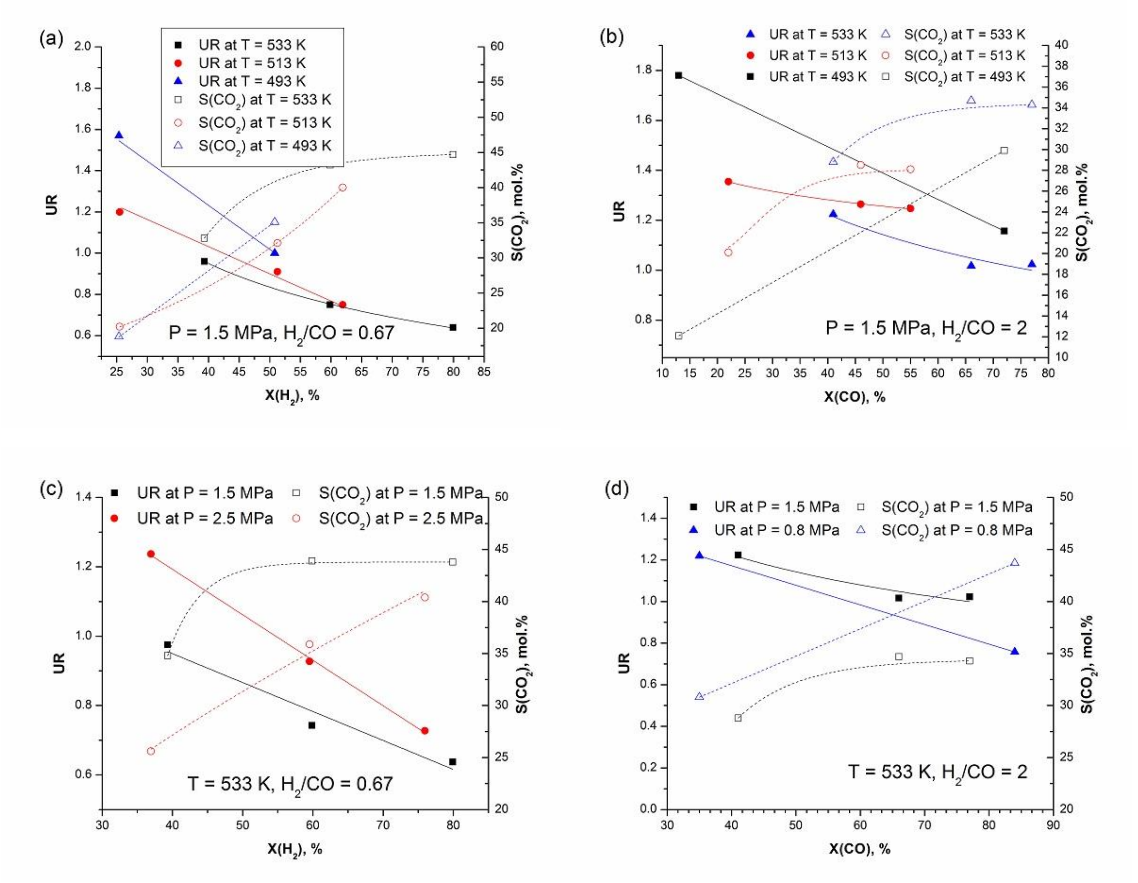

Figure 3.5 - The effect of process conditions on UR and CO_2 selectivity: a) effect of T at low H_2/CO; b) effect of T at high H_2/CO; c) effect of P at low H_2/CO; d) effect of P at high H_2/CO;

Effect of reactant feed ratio

For inlet H_2/CO ratio of 0.67, the limiting reactant is hydrogen, while in the case of H_2/CO = 2 the limiting reactant is carbon-monoxide. The H_2/CO ratio inside the reactor corresponds to the ratio at the outlet. In this part we will only compare the effect on selectivity of low vs. high H_2/CO ratio, which remain far enough apart regardless whether we are looking at inlet or outlet reactant ratios.

Our data shows that the increase in H_2/CO feed ratio results in higher selectivity of light products (CH_4 and C_2-C_4) and decrease in C_{5+} selectivity (Figure 3.6a). These trends are typically observed with all FTS catalysts [23, 76, 90, 91, 103]. This is related

to decrease of chain growth probability with increasing H_2/CO ratio both at the inlet and inside the reactor (Figure 3.6b) [104]. A logical interpretation is that the increase in H_2/CO causes an increase in H surface coverage in relation to monomer coverage resulting in an increased rate of chain termination.

Similar to previous reports [105], our results showed that OPR decreases significantly and selectivity towards 2-olefins increases with increasing H_2/CO ratio (Figure 3.6c). Decrease in 1-olefins is caused by increases in both primary and secondary hydrogenation reactivity. An effect that could have influence on the decrease of OPR with increasing H_2/CO is the reduction in CO partial pressure, due to inhibiting properties of CO to secondary hydrogenation. For the conditions showed in Figure 3.6 the CO conversion was kept constant with increasing H_2/CO, which meant SV was increased simultaneously. Lower residence time at high H_2/CO condition would have decreased the secondary reactivity of 1-olefins, i.e. increased OPR. However since OPR decreased it is evident that increasing H_2/CO had a more significant effect compared to the residence time.

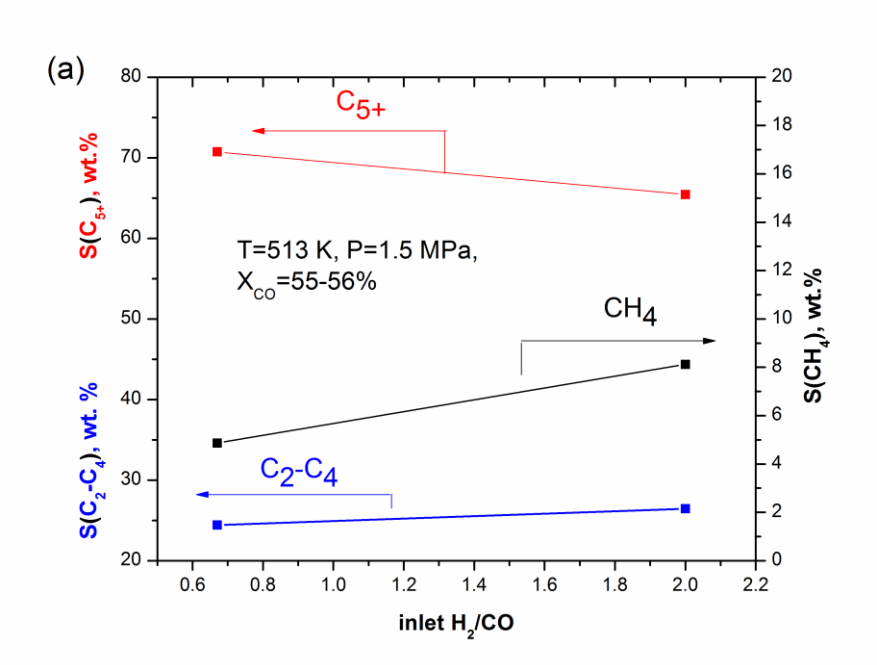

Figure 3.6 - Effect of feed ratio on: (a) chain growth probability with carbon; (Process conditions: T = 513 K, P = 1.5 MPa, X_{CO} = 55 – 56 %). (continued on next page)

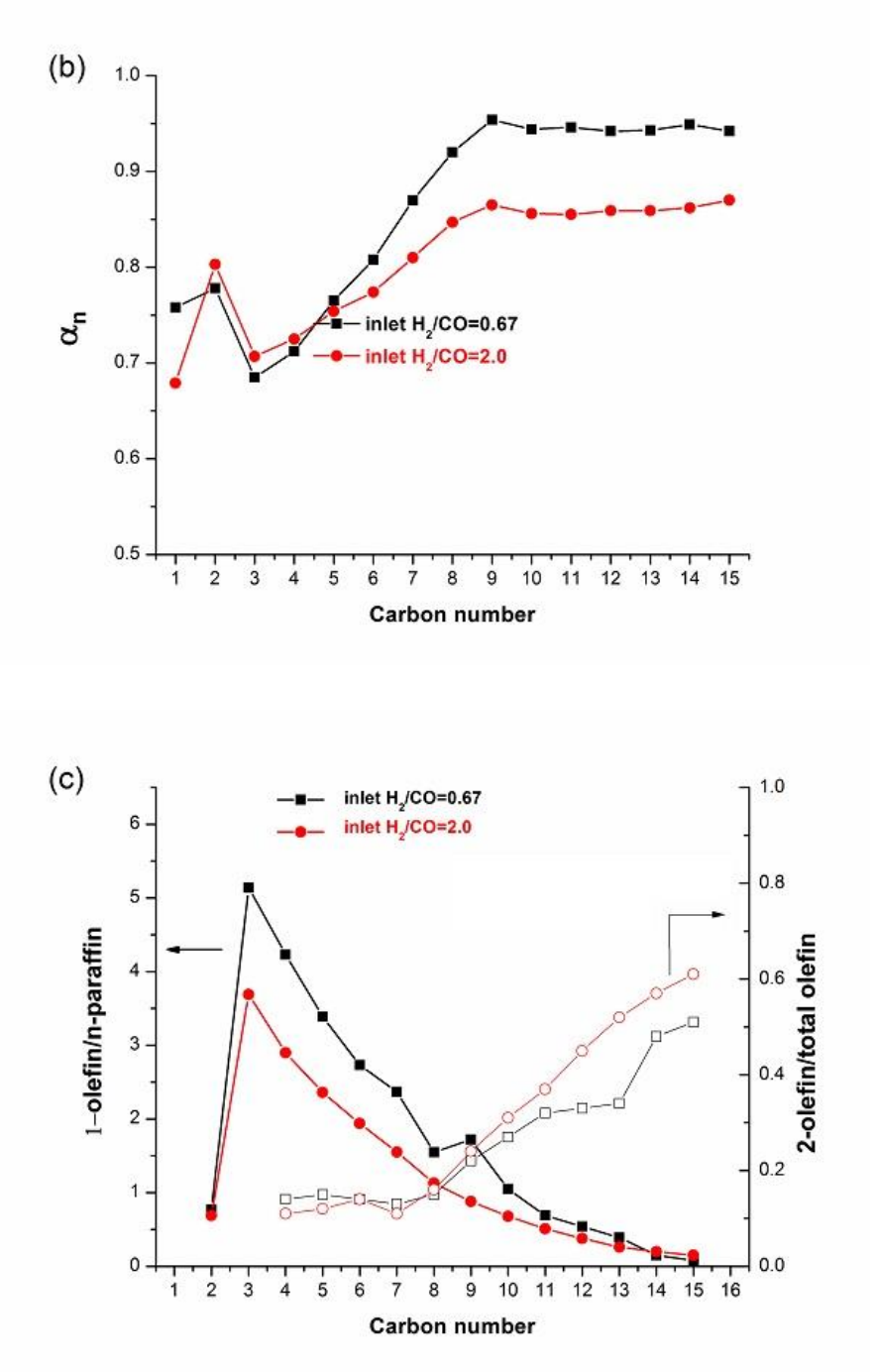

Figure 3.6 - Effect of feed ratio on: (b) 1-olefin-to-n-paraffin with carbon number with carbon number; (c) selectivity of CH_4, C_2-C_4 and C_{5+}. (Process conditions: T = 513 K, P = 1.5 MPa, X_{CO} = 55 – 56 %).

Effect of temperature

The effect of temperature for Fe catalyzed FTS reaction has been reported many times in the literature. The consensus is that with increasing temperature amount of light products increases, while heavy products decrease [35, 76, 90-93] and is linked to a decrease in chain growth probability. However, this effect is much more pronounced with cobalt and ruthenium than with iron FTS catalysts [25, 96]. On the other hand, the increasing of T is sometimes reported to increase olefin content [91, 92, 97] and sometimes decreases it [91, 98]. Our experiments showed that α_n typically slowly decreased with increase in T (Figure 3.7b). This explains trends showed in Figure 3.7a, where methane selectivity increases, whereas higher hydrocarbon selectivities decrease with increasing T.

Kinetically the growth probability is determined by the ratio between rates of chain propagation ($R_{p,n}$) and termination reactions ($R_{t,n}$):

$$\alpha_n = \frac{R_{p,n}}{R_{p,n} + R_{t,n}} \tag{3.11}$$

The rates of these surface reactions are determined by corresponding rate constants and surface coverages of monomeric species and atomic hydrogen, which all vary with changing temperature. The main effect of temperature would be to change rate constants of FTS chain propagation and termination that determine α_n (Eq. 3.11). The reaction with higher activation energy will respond faster to changes in T. The implication of decreasing α_n with T is that chain termination has a higher activation energy than chain propagation. However, relatively slow decrease of α_n with temperature (within the tested range 493-533 K) suggests that the difference between the two activation energies is relatively small.

Our data showed mixed results for OPR with changing T, which is consistent with literature studies [91, 92, 97, 98]. The analysis of T effect on OPR is difficult because of a number of temperature related process that would affect OPR. The effects that could cause increase of OPR with increasing T are:

1) Higher activation energy of chain hydrogenation (n-paraffin formation) compared to desorption to 1-olefin.
2) Increased FTS reaction rate with T causes increase in partial pressure of water, which inhibits secondary olefin reactions, leading to higher OPR [182].
3) Potentially WGS activity changes could also affect OPR. Decrease of K_{WGS} with T would be followed by an increase in CO and H_2O partial pressures, which inhibit secondary reactions and increase OPR.

It should also be pointed out that residence time in our study decreased with increasing T, which would favor the increase of OPR due to lower extent of secondary olefin reactions. Also interesting is that even though the OPR remained relatively constant with temperature, the amount of 2-olefins increases (Figure 3.7c). This could mean that the activation energy for 2-olefin formation is higher compared to those for 1-olefin and n-paraffin formation.

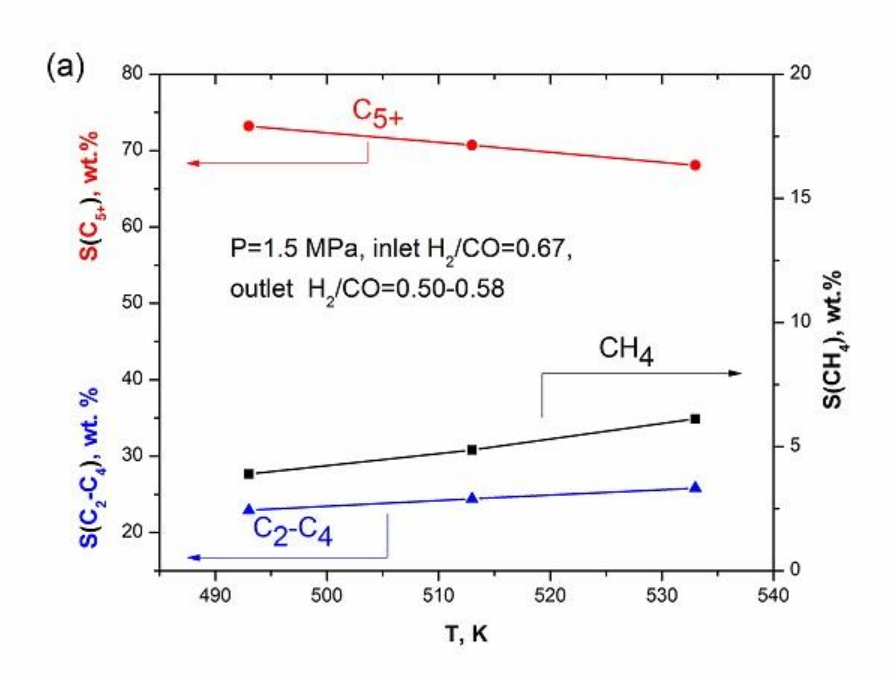

Figure 3.7 - Effect of temperature on: (a) chain growth probability with carbon number; (Process conditions: P = 1.5 MPa, inlet H_2/CO = 0.67, outlet H_2/CO = 0.50 – 0.58, X_{CO} = 27 – 46 %). (continued on next page)

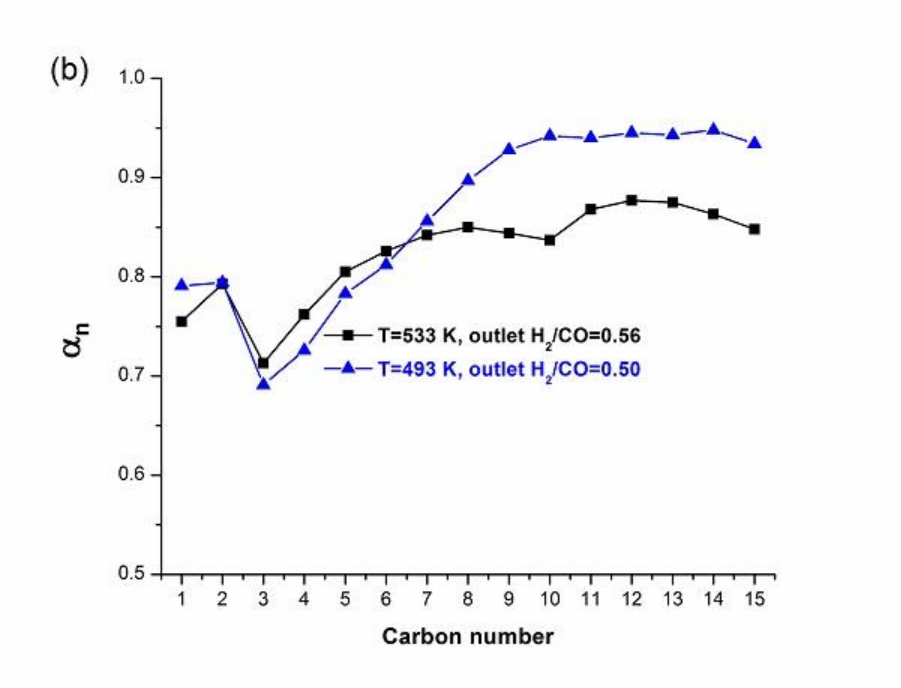

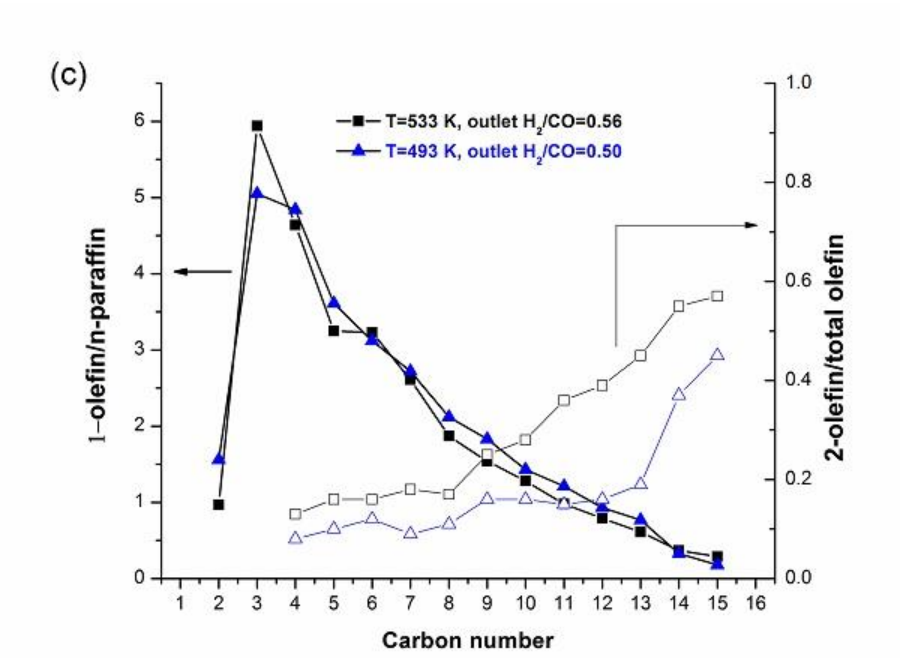

Figure 3.7 – (continued) Effect of temperature on: (b) 1-olefin-to-n-paraffin with carbon number with carbon number; (c) selectivity of CH_4, C_2-C_4 and C_{5+}. (Process conditions: P = 1.5 MPa, inlet H_2/CO = 0.67, outlet H_2/CO = 0.50 – 0.58, X_{CO} = 27 – 46 %).

Effect of pressure

It is well know that total pressure has a positive effect on FTS reaction rate [31, 76, 90, 99]. A positive effect has also been reported on FTS product selectivity, decreasing methane and increasing C_{5+}, for cobalt-based catalysts [99, 103]. For iron catalysts the same effect has been reported [76], but the influence of total pressure on selectivity for this catalyst is much smaller than for cobalt [25, 96]. Botes et al. [96] studied the effect of syngas pressure on methane selectivity at constant outlet H_2/CO of 2 showing no variations of methane selectivity between 4 and 25 bar.

Figure 3.8 shows the detailed product distribution features as a function of pressure between 1.5 and 2.5 MPa (temperate and inlet feed ratio are kept constant and conversion is within a small range). Selectivity towards light products (methane and C_2-C_4) decreased and C_{5+} selectivity increased with pressure (Figure 3.8a). These changes can be related to variations in α_n (Figure 3.8b), which shows slight increase with increasing pressure. The reason for this behavior can be explained in terms of kinetics as a decrease of hydrogen to carbon-monoxide coverage ratio. Dinse et al. [99] showed that the decrease of hydrogen to carbon-monoxide coverage ratio favors propagation over chain termination via hydrogenation, therefore causing increase in α_n.

We would like to point out that for conditions in our experiments the outlet H_2/CO ratio was not constant at different total pressure; it decreased with increasing P. This would also cause a decrease of H/CO surface coverage ratio and the observed product selectivity variations. Therefore, it can be expected that at a constant outlet H_2/CO ratio the effect of changing P on selectivity would have been much lower, as stated by Botes [96].

Our data showed increase of OPR with increasing P (Figure 3.8c). This trend can be seen as contribution of several parallel processes:

1) Decrease in primary n-paraffin formation by chain hydrogenation due lower outlet outlet H_2/CO ratio.

2) Decrease in secondary 1-olefin reactions due to lower outlet (and surface) H_2/CO ratio, because H_2 promotes secondary hydrogenation and CO suppresses secondary reactions altogether [164].
3) Higher water partial pressure due to higher total pressure suppresses secondary reactions of 1-olefins [118].

Increased partial pressure of in-situ formed 1-olefins would have increased rate of their secondary reactions, however this effect seems to be minor in comparison to factors that suppress secondary reactions and increase OPR. The 2-olefin content, i.e. 2-olefin/total olefin ratio, also decreased with increasing pressure (see Figure 3.8c). Dictor and Bell [92] and Egiebor et al. [155, 156] reported that internal olefins are formed through secondary reactions of 1-olefins over iron-based catalysts. This explanation would be consistent with our results, since 2-olefins content is decreasing, while OPR is increasing, with increasing pressure.

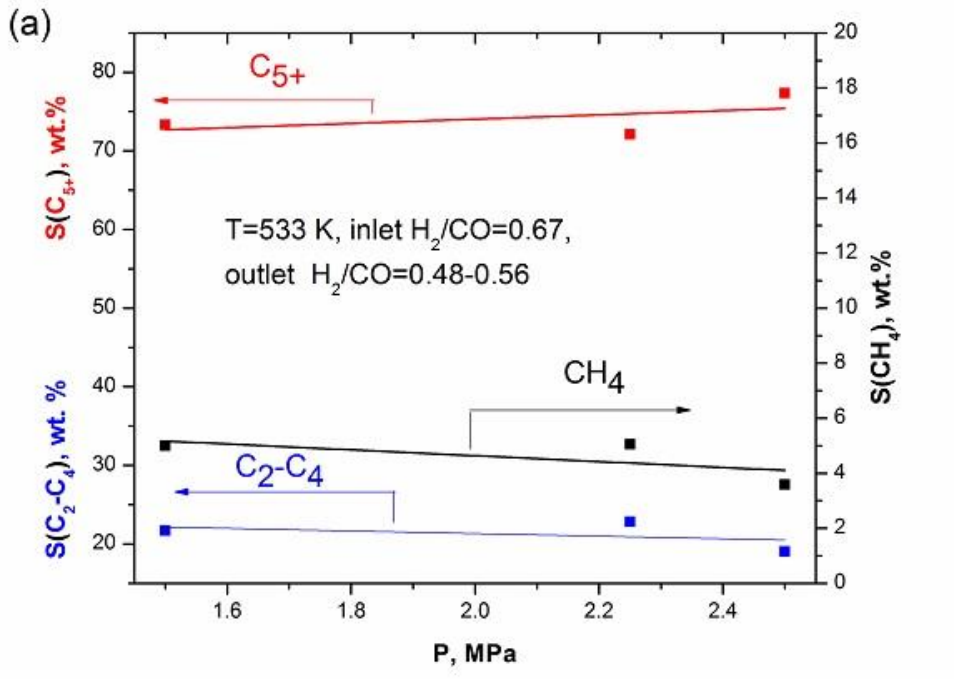

Figure 3.8 - Effect of pressure on: (a) chain growth probability with carbon number. (Process conditions: T = 533 K, inlet H_2/CO = 0.67, outlet H_2/CO = 0.48 – 0.56, X_{CO} = 36 – 46 %). (continued on next page)

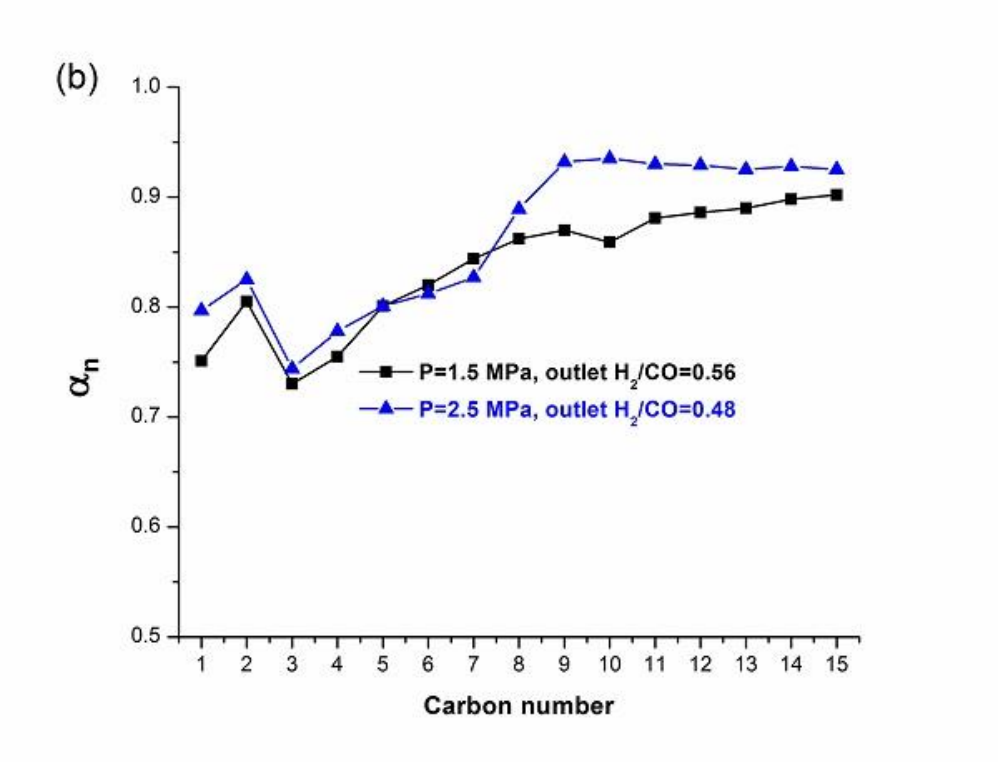

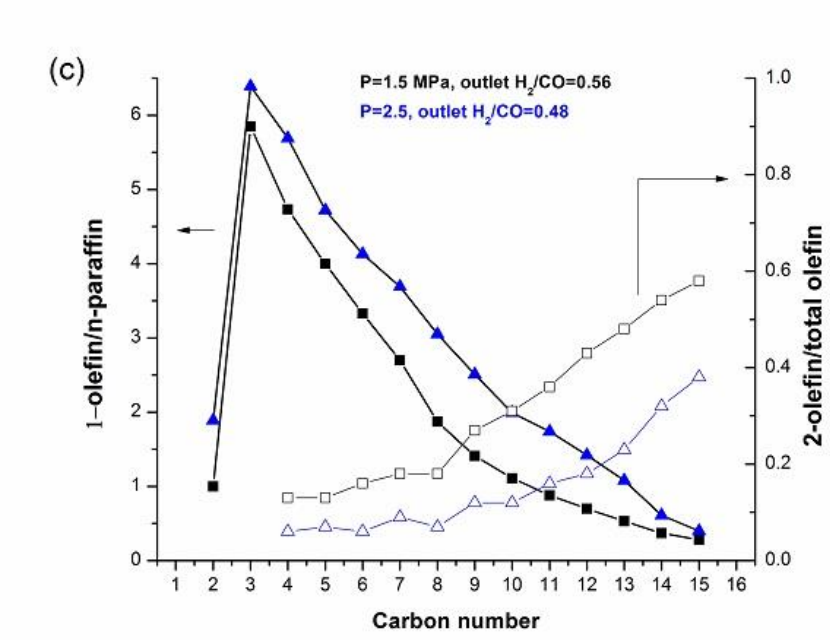

Figure 3.8 – (continued) Effect of pressure on: (b) 1-olefin-to-n-paraffin with carbon number with carbon number; (c) selectivity of CH_4, C_2-C_4 and C_{5+}. (Process conditions: T = 533 K, inlet H_2/CO = 0.67, outlet H_2/CO = 0.48 – 0.56, X_{CO} = 36 – 46 %).

Effect of conversion level

Conversion level at fixed values of temperature, pressure and feed ratio was controlled by varying the space velocity in 0.5 to 23.5 NL/(g_{cat}*h) range. CO conversions from 9 to 84% were achieved. For the majority of data varying space velocity did not have a significant effect on hydrocarbon product selectivity (Figure 3.9a and b), i.e. typically CH_4 and C_{5+} selectivity remains relatively constant with different conversions (i.e. residence time). Bukur et al. [76] reported the same result. This is consistent with relatively constant chain growth probabilities at different conversions (Figure 3.10a) [91, 92]. WGS activity increases significantly with conversion, as already discussed (see Figure 5), which is caused by the increased partial pressure of water at higher conversions, resulting in a higher concentration of H_2, i.e. higher H_2/CO ratio. As shown previously, H_2/CO ratio can have a significant effect on growth probabilities (Figure 8b) OPR decreases with increase in residence time (Figure 3.10b) due to 1-olefin secondary reactions (hydrogenation, isomerization and readsorption). From Figure 3.10b we see that the amount of 2-olefins in the products increases with increased residence time and for high carbon number range (above C_{10}) 2-olefins are the dominant olefinic products [105].

Oxygenate formation

Up to this point we looked at results only considering hydrocarbons. However, products containing oxygen atoms (mainly alcohols) are formed as well. Thus, oxygenates are a minor product of FTS with iron-based catalyst and depending on the process conditions their content can vary [23].

Figure 3.11a shows the molar flowrates of different chain length oxygenates together with flowrates of hydrocarbon products. Some studies suggest that oxygenates cannot be neglected when analyzing the product distribution of low weight molecules, mainly C_1 and C_2, since this leads to more significant observed deviation from ASF [137]. This is shown to be true in our results as well (Figure 3.11b), where total molar flowrates including oxygenates approach ASF distribution compared to flowrates of hydrocarbons only. It is also interesting to note that oxygenates and olefins have a different slope

compared to n-paraffin in the range above C_8 (Figure 11a). This refers to the so-called "break in the ASF" or non-ASF behavior. Wojciechowski [317] interpreted this as proof that n-paraffins have two different termination steps, one with addition of hydrogen atoms and one with the addition of methyl group to the growing chain, while olefin and oxygenates only have one. Huff and Saterfield [122] hypothesized that some molecules (including oxygenates, olefins and lighter paraffins) are created on separate type of active sites, compared to the heavier paraffins. Additional explanations for these differences in slopes with carbon number are the existence of secondary reactions with 1-olefin and oxygenates [165, 318], as well as the dependence of 1-olefin desorption rates on chain length [167, 169]. Though the later theory was only applied to 1-olefins and not oxygenates.

The oxygenate content can be calculated in relation to hydrocarbons as:

$$Oxygenates\,(wt.\%) = 100\% \times \frac{\dot{m}_{Oxygenates}}{\dot{m}_{Oxygenates} + \dot{m}_{HC,total}} \qquad (3.12)$$

where $\dot{m}_{Oxygenates}$ and $\dot{m}_{HC,total}$ are mass flowrates of oxygenates and hydrocarbons, respectively.

Oxygenate products formed in FTS mainly have low carbon numbers and the amount of formed oxygenates quickly declines with carbon number. The oxygenate slope in the ASF plot is steeper compared to n-paraffin and 2-olefin, and is similar to that of 1-olefins (see Figure 3.11a). This could suggest some similarities in the formation of oxygenates and 1-olefins in FTS. Both species are well-known to participate in secondary reactions. Tau et al. [173] showed that added n-alcohols undergo hydrogenolysis to corresponding n-paraffin, dehydrogenation to aldehyde or ketone, as well as reincorporation and continued chain growth to hydrocarbons. The chain-length dependency of n-alcohol secondary reactions is likely the reason for the lack of higher oxygenate products. Our results showed that oxygenate flowrates decrease with increasing residence time (Figure 3.13), which is an indirect proof of oxygenate secondary reactivity.

The effect of process conditions on oxygenate formation is rarely reported in the literature due to the difficulty to analyze relatively low amounts of these products [23, 319]. Our results showed decrease in oxygenate content with increasing temperature and decrease with increasing reactant feed ratio (Figure 3.12). An increase in oxygenates content was reported as well for higher pressures [23], however our results showed complex behavior for pressure variations, potentially dependent to some extent on the variation of partial pressures due to WGS.

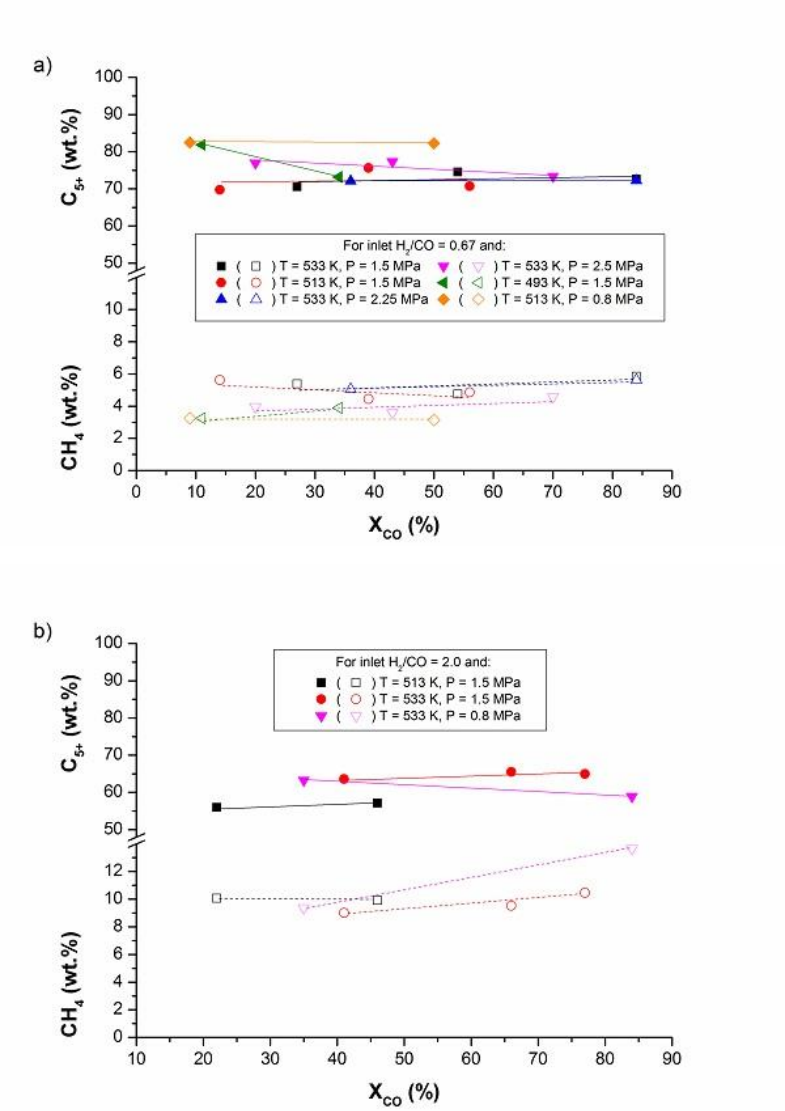

Figure 3.9 - Variation of CH_4 and C_{5+} product selectivity with CO conversion level for selected conditions: a) data at inlet H_2/CO = 0.67 and different T and P; b) data at inlet H_2/CO = 2.0 and different T and P; (Note: Lines connect points with same T, P and inlet H_2/CO).

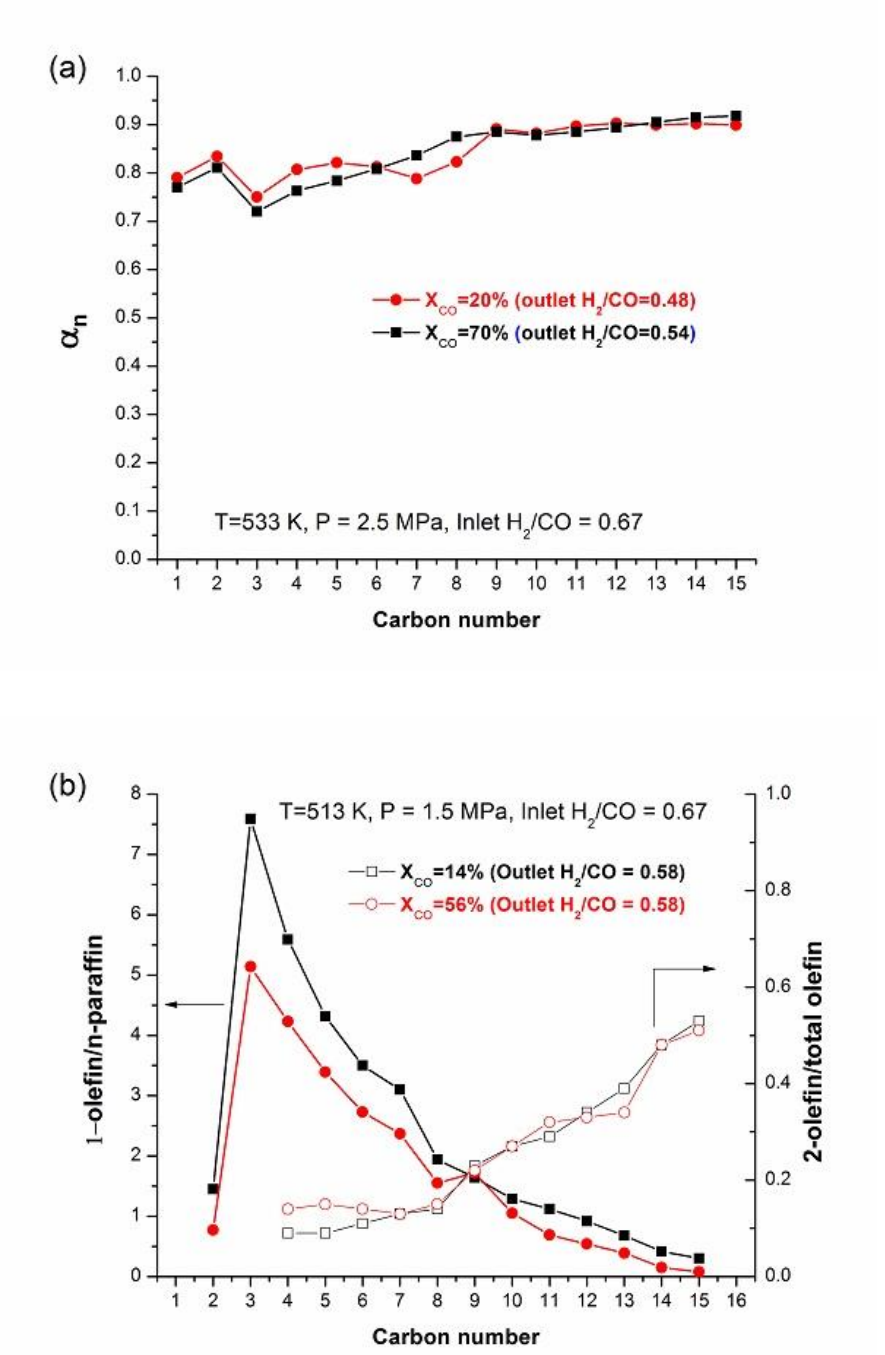

Figure 3.10 - Variation of main product formation features with carbon number and residence time: a) chain growth probability (T = 533 K, P = 2.5 MPa and inlet H_2/CO = 0.67); b) 1-olefin-to-n-paraffin ratio and 2-olefin-to-total olefin ratio with carbon number (T = 513 K, P = 1.5 MPa and inlet H_2/CO = 0.67).

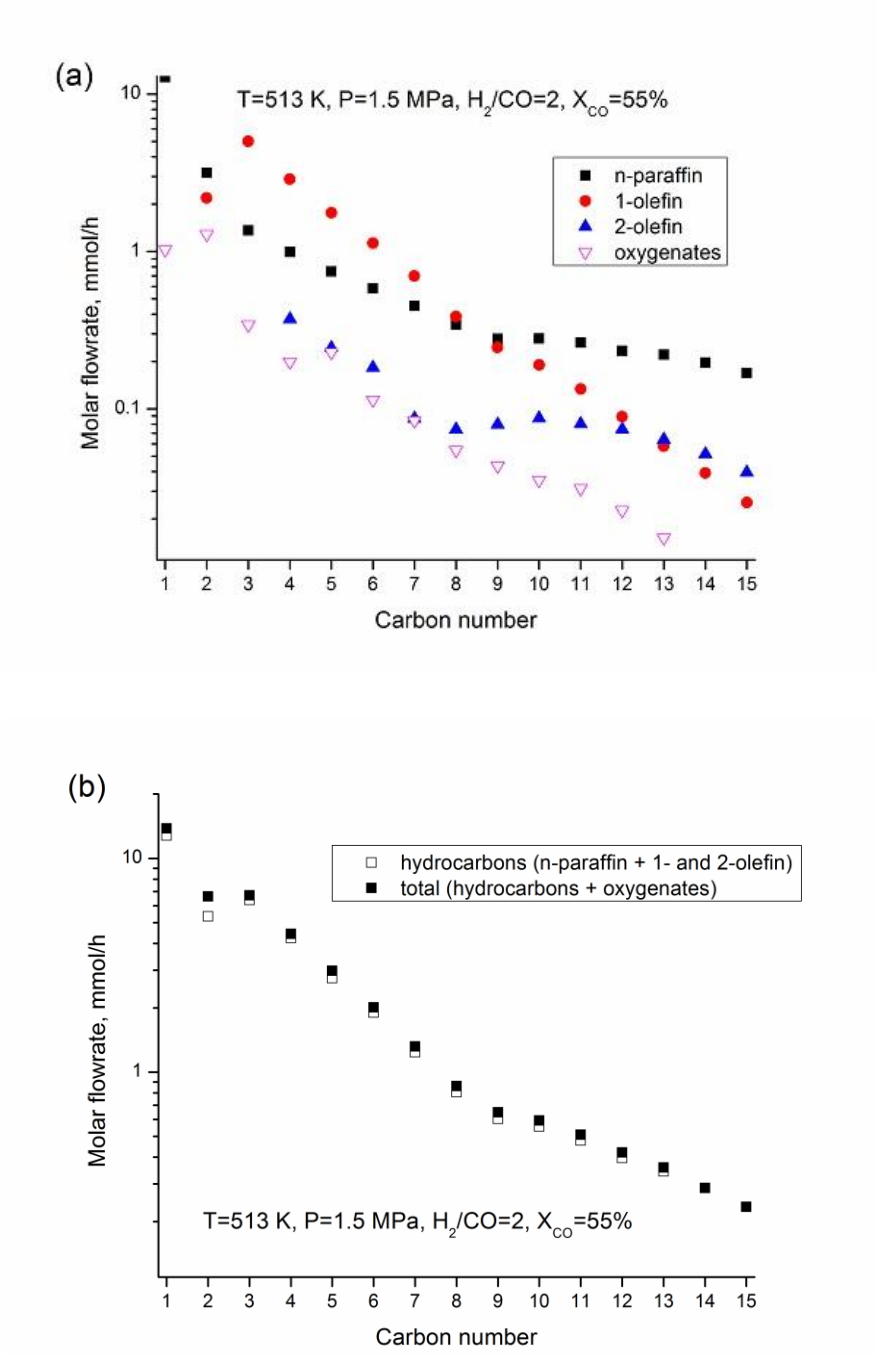

Figure 3.11 - Oxygenates as minor products in FTS: a) Molar flowrates of different FTS product species; b) Hydrocarbon and total product molar flowrates. (Process conditions: T = 513 K, P = 1.5 MPa, $H_2/CO = 2$, $X_{CO} = 55\%$).

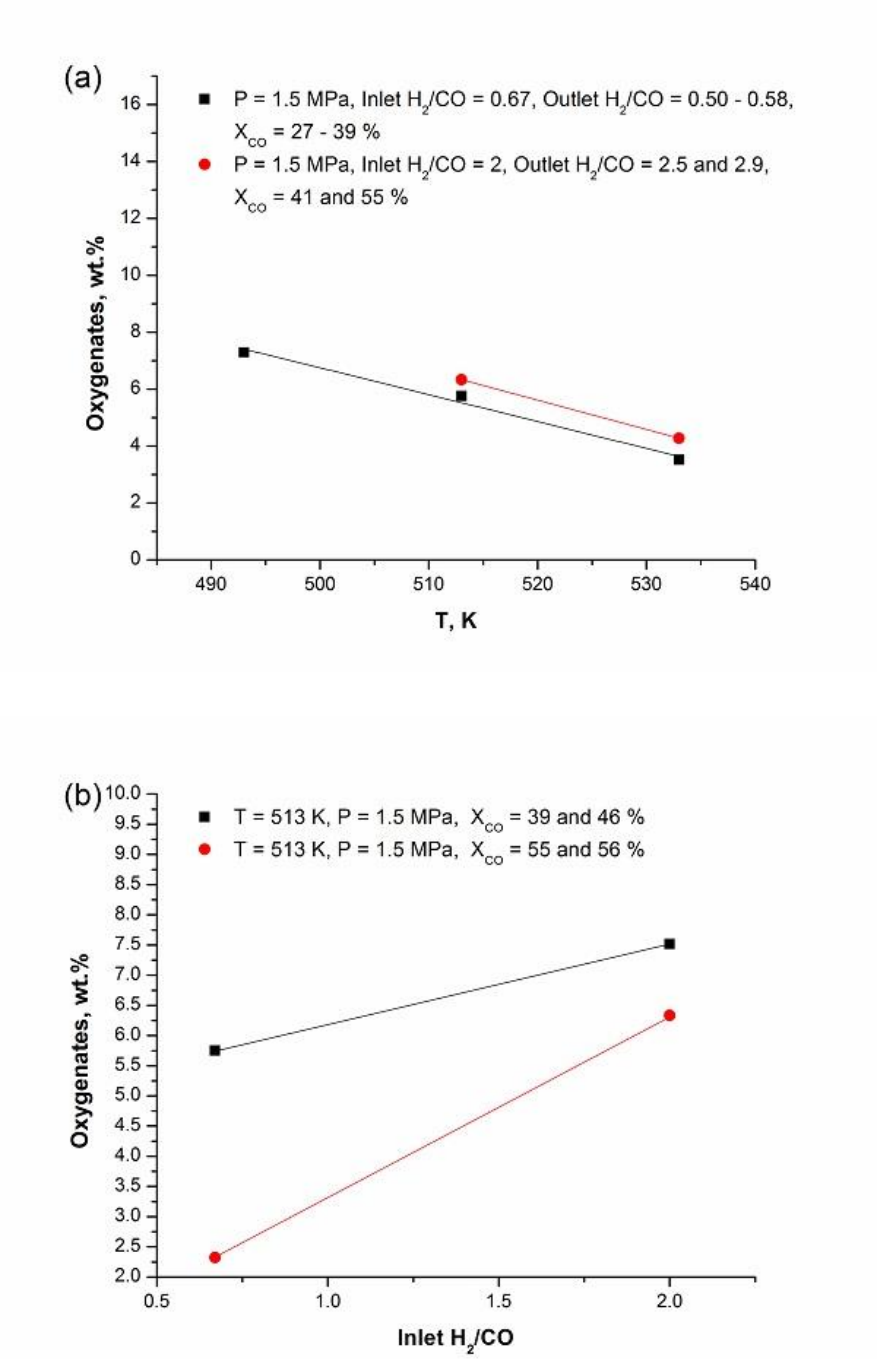

Figure 3.12 - Effect of process conditions on the oxygenate selectivity: a) Effect of temperature; b) Effect of inlet H_2/CO ratio.

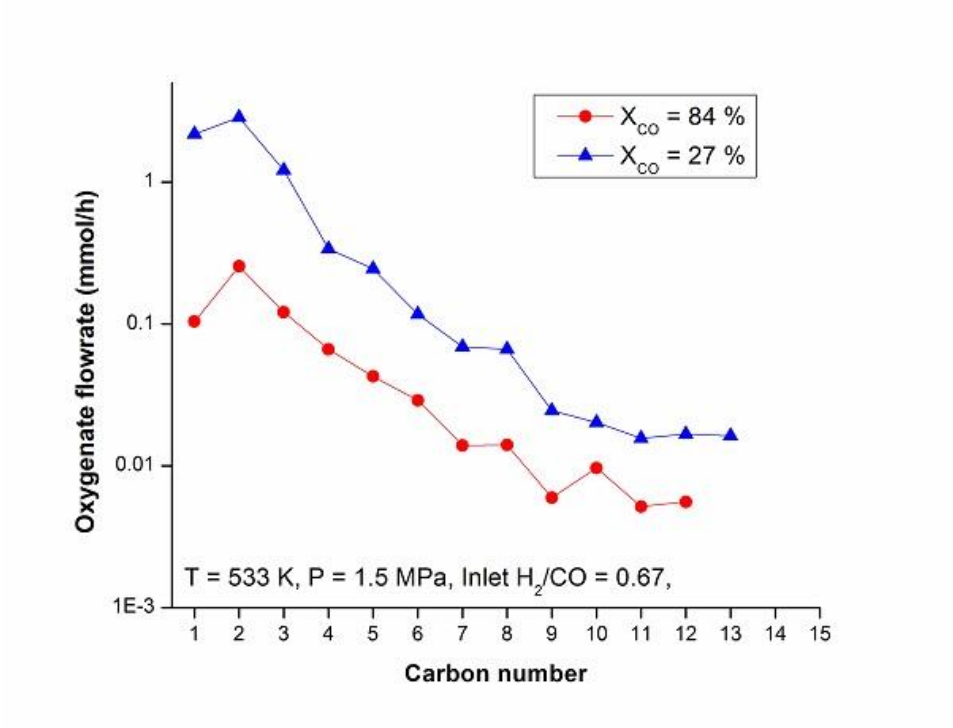

Figure 3.13 - Effect of residence time on the oxygenate formation. (Process conditions: T = 533 K, P = 1.5 MPa, H_2/CO = 0.67).

Selecting the optimal reaction conditions for iron-based catalyst

One of the main goals when designing an FTS reactor is to achieve the highest possible yield of desired hydrocarbon products per mass of catalyst inside the reactor and per volume of syngas fed into the reactor. This depends heavily on the selection of reactor conditions. However, it is also important to achieve overall plant efficiency in terms of both costs and productivity. In this section we present some thoughts on this issue, stemming for the analysis of our data.

For iron-based catalysts consideration of WGS is very important, since it affects the partial pressures of reactants, thereby affecting reaction rates and selectivity. One of the most important process parameters is the reactant feed ratio (H_2/CO). WGS creates hydrogen and consumes carbon-monoxide, and therefore increases the H_2/CO ratio inside the reactor. It is this ratio inside the reactor (i.e. at the outlet of stirred tank slurry reactor) that controls rates and selectivity. Figure 3.14 shows how outlet H_2/CO ratio changes with

conversion level for two levels of inlet H_2/CO ratio tested in our study (0.67 and 2). This figure also includes data from two literature sources [184, 320]. One can clearly see that if inlet H_2/CO ratio is 2, the WGS activity is higher and, under all conditions tested, the outlet H_2/CO ratio drastically increases with conversion level. Higher outlet (i.e. reactor) H_2/CO ratio leads to higher methane and lower C_{5+} selectivity. From a kinetic point of view, it is clear that one should not operate at H_2/CO ratio much higher that the stoichiometric FTS ratio, since the resulting products will mainly consist of methane. With the inlet H_2/CO ratio equal to 0.67, even with very high conversion levels, outlet ratio remained below 1, allowing for high C_{5+} selectivity. Similar result was shown by Davis [321]. From the two feed ratio tested, a low inlet H_2/CO ratio (0.67) seems to be a better option. The same inlet ratio of 0.67 was utilized by Kölbel et al. [322], who conducted the reaction at high conversion (about 90% CO and syngas conversions), relatively low syngas pressure (1.1 MPa for laboratory and 1.2 MPa for demonstration plant) and relatively high temperature (~540 K). The focus of their work was to design an iron-based catalyst slurry phase reactor with high productivity of liquid fuels. They reported producing yields of 176 g of hydrocarbons per Nm^3 of syngas, out of which about 130 g were liquid fuels. Researchers from Sasol attempted to replicate these results but failed [232, 323]. Steynberg et al. [323] stated that the amount of hydrocarbons that should be produced at such high conversions would be expected to be higher than 178 g (i.e. above 200 g). In addition they believed that Kölbel et al. reported high conversion was actually single-pass conversion of 50-60% with recycle of unconverted gas [322]. These type of medium level single-pass conversion levels with gas recycle, accompanied with high pressures (25 bars and higher) and relatively high inlet H_2/CO ratio (1.25 – 2), have been reported in the literature as process conditions pertaining to industrial reactors [7, 232, 241, 323, 324].

The high conversion is avoided in order to keep the partial pressure of water low, since water severely influences iron catalyst deactivation due to sintering and oxidation [325, 326]. Maintaining low water content inside the reactor is considered to be crucial for iron catalyst longevity, thus relevant for plant operating costs. Therefore it is also important to look at the variation of water partial pressure with process conditions. Figure 3.15 shows variation of partial pressure of water with conversion level for different

process conditions. Typically water partial pressure increases with conversion level for a given temperature, pressure and reactant feed ratio. However, several sets of conditions, at low inlet H_2/CO ratio of 0.67 and total pressure of 1.5 MPa, show that partial pressure of water reaches a maximum at moderate 40 – 60 % syngas conversions and then decreases at higher conversions. Particularly interesting is mass balance No. 2 from Table 1, with T = 533 K, P = 15 bar, inlet H_2/CO = 0.67 and syngas and CO conversions of 82 and 84%, respectively. Similar results was observed in the data of Zimmerman et al. [184] (also see Figure 3.15). Here we achieved high single-pass conversion with very low partial pressure of water. The usage ratio (UR) was 0.64, which is very close to the inlet H_2/CO ratio, meaning that in terms of syngas usage efficiency this set of process conditions was very good. These conditions are similar to the set of conditions used in Kölbel et al. study [322] and a number of studies conducted by Bukur and co-workers [184, 327-329] (all using carbon-rich syngas with H_2/CO ratio of 0.67).

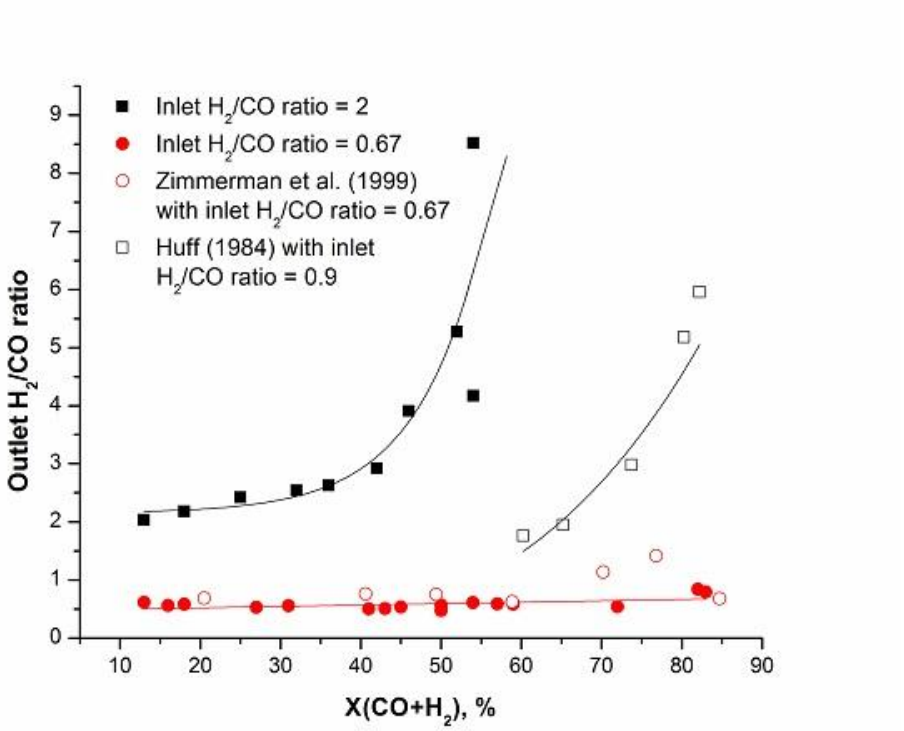

Figure 3.14 - Variation of outlet H_2/CO ratio with different conversion levels. (Note: temperature, pressure and space velocity are varied; Additional data from Zimmerman et al. [184] and Huff [320]).

A significant portion of the costs associated with constructing and operating a CTL plant is related to the preparation of syngas, i.e. gasification of coal. There are three main types of gasifiers used for this purpose: 1) fixed-bed (e.g. Sasol-Lurgi gasifier); 2) fluidized-bed (e.g. Kellog-Rust-Westinghouse gasifier); and 3) entrained flow (Texaco and Shell gasifiers). There are many differences between these gasifiers, but one of the primary ones is the content of produced syngas. Sasol-Lurgi gasifier produces syngas with H_2/CO ratio between 1.7 and 2, which is said to be optimal or close to optimal for Sasol's low temperature FTS process with inlet H_2/CO ratio between 1.25 and 2 (the exact ratio used by Sasol has not been reported). On the other side, other gasifier types produce a much more carbon-rich syngas. The entrained flow gasifiers having typical syngas H_2/CO ratios of 0.4 – 0.9, respectively, which depends on the coal quality. As previously stated, syngas with ratio of 0.67 was used by Kölbel and coworkers in their Rheinpreussen pilot plant [322]. One of the key technical issues entrained flow gasifiers is the high temperature of raw syngas produced (above 1200 °C). However, if the heat from cooling of raw gas is used in the production of high pressure water steam, then the cold gas efficiency of Texaco and Shell gasifiers goes up to 95% [330]. They are therefore highly competitive with Sasol-Lurgi process in terms of efficiency. In the 80s and early 90s, US DOE funded a series of studies by the MITRE Corporation [331-336], which showed that, compared to the alternative technologies present at the time, using Shell gasifier with carbon-rich syngas in a slurry phase FTS reactors for CTL process is not only economically feasible but also desirable. Reason listed by Sasol for not using carbon-rich syngas was that even though this type of syngas can be tolerated, "the reactors and catalysts are more expensive when aiming for high level of overall conversion" [236]. This probably refers to the high deactivation of iron catalysts (oxidation and sintering) caused reactor water content at high single-pass conversions. However, syngas with 0.7 H_2/CO ratio was used in studies conducted at DOE's FTS slurry reactor pilot plant at La Porte, which showed relatively stable activity and selectivity [337]. Furthermore, Bukur and co-workers [184, 327-329] conducted a number of long-term studies (lasting up to 500 h and in some cases longer) with different precipitated iron FTS catalysts using inlet H_2/CO ratio of 0.67.Their results showed that the catalyst deactivation was very gradual, even at high conversions. Even though the results regarding partial pressure of water were not analyzed in these studies, it is likely that they were relatively low, which allowed for

stable activity. Therefore, the combination of carbon-rich syngas with high single-pass conversions in FTS slurry reactors cannot be ignore as potentially more optimal solution for CTL applications in the future.

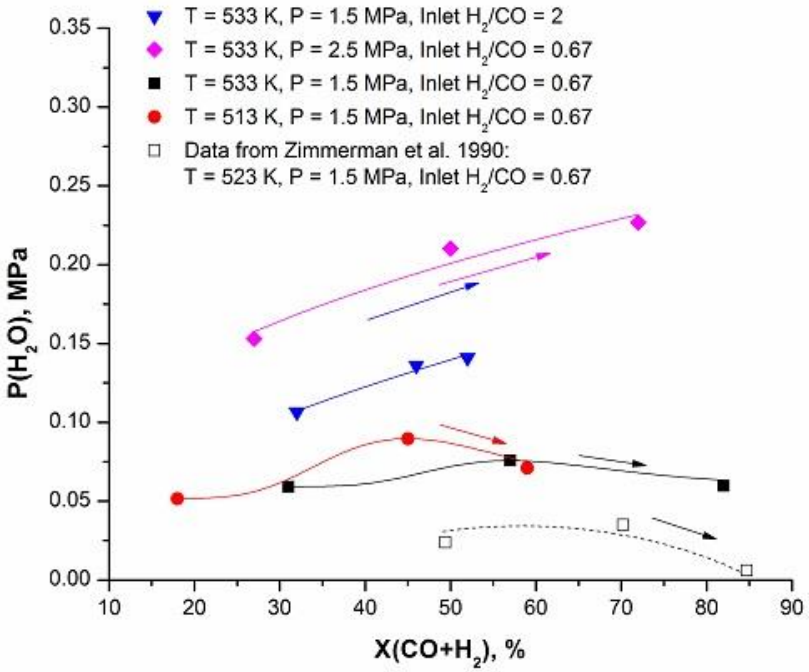

Figure 3.15 - Effect of process conditions on the water partial pressure (Additional data from Zimmerman et al. [184]).

Conclusions

Variations in FTS hydrocarbon selectivity, as a result of changes in process conditions, are related to changes in chain growth probabilities. Studying these probabilities can lead to better understanding of intrinsic kinetics of FTS surface reactions. In this study we showed that increasing temperature and H_2/CO feed ratio decreases the growth probabilities, leading to increased methane and lower C_{5+} selectivity. Pressure increase was shown to have a positive, albeit slight, effect on selectivity. Conversion effect on selectivity is complex and selectivity towards methane and C_{5+} does not seem to be significantly affected by variations in residence time. Considering all of the conditions tested we can conclude that values of C_1 and C_2 growth probabilities are close to those of C_{3+} species and do not exhibit significantly different behavior at different process conditions. Unlike cobalt FTS catalysts where C_1 is the

dominant cause for selectivity changes, with iron catalyst all of the growth probabilities seem to change in parallel and contribute to selectivity shifts.

Process conditions determine the content of different hydrocarbon species, primarily n-paraffin, 1- and 2-olefin, as well as oxygenate formation. As seen from variations of 1-olefin/n-paraffin ratio, increasing residence time and H_2/CO ratio favored secondary 1-olefin reactivity and resulted in a lower OPR. The effect of pressure and temperature on 1-olefin content was shown to be smaller and more complex. 2-olefin content in olefins increases with increasing residence time, temperature and H_2/CO ratio, while pressure increase has the opposite effect. Oxygenate formation was most affected by temperature and H_2/CO ratio variations. Decrease of oxygenate content at higher residence time is related to their participation in secondary reactions.

The results of our study show that FTS product selectivity can be tailored to a certain degree by choosing the appropriate process conditions. We showed several potential benefits of operating FTS slurry reactors at 0.67 syngas H_2/CO ratio, including: improved selectivity due to low H_2/CO ratio inside the reactor, low partial pressure of water at high single-pass conversions, efficient utilization of syngas (i.e. usage ratio equivalent to H_2/CO feed ratio) and the ability to switch to the more efficient and cost effective types of coal gasification technologies.

However, due to complexities related to the unknown kinetics of FTS and WGS, as well as secondary reactions, additional research covering an even wider range of conditions (especially inlet H_2/CO ratios) is required in order to realize the full potential of iron-based catalysts.

3.2. Rhenium promoted cobalt-alumina catalyst

Cobalt based catalysts are used in commercial FTS reactors for gas-to-liquids (GTL) processes, because they exhibit high activity and good selectivity towards the desired C_{5+} products, and have low intrinsic activity for the water-gas shift reaction. The FTS product distribution over cobalt-based catalysts very seldom follows the classical ASF distribution (see Figure 3.16a) and regularly reported deviations from this model are: a higher-than-expected fraction of methane, a lower-than-anticipated yield of C_2 (caused by the low fraction of ethene), and a positive bend in the ASF plot, i.e., greater-than-expected yield of higher hydrocarbons due to an increase in chain growth probability with carbon number, (Figure 3.16b). The rates of 1-olefin formation have a much steeper decrease with carbon number compared to n-paraffin (Figure 3.16c), which results in an exponentially decreasing OPR with carbon number (Figure 3.16d).

There are still many questions which need to be answered in order to better understand how the FTS product distribution is governed, some of which are:

1) What is the extent and selectivity of 1-olefin secondary reactions and how do they affect FTS product distribution?
2) How to explain high methane formation and is there a special relation between the formation of C_1 intermediate and process conditions? Can the deviation in C_1 selectivity from ASF behavior be controlled, perhaps by shutting down the methanation route, such that it is only formed via the FTS pathway?
3) Is water involved in changes of product selectivity and what are the mechanistic reasons for this?
4) What is the reason for the increasing growth probability and decreasing OPR with carbon number?
5) How does the longer residence time of heavy products (i.e. product hold-up) affect observed product distribution and how to decouple the influence of these effects?

In this section we discuss some useful clues and possible answers to these questions.

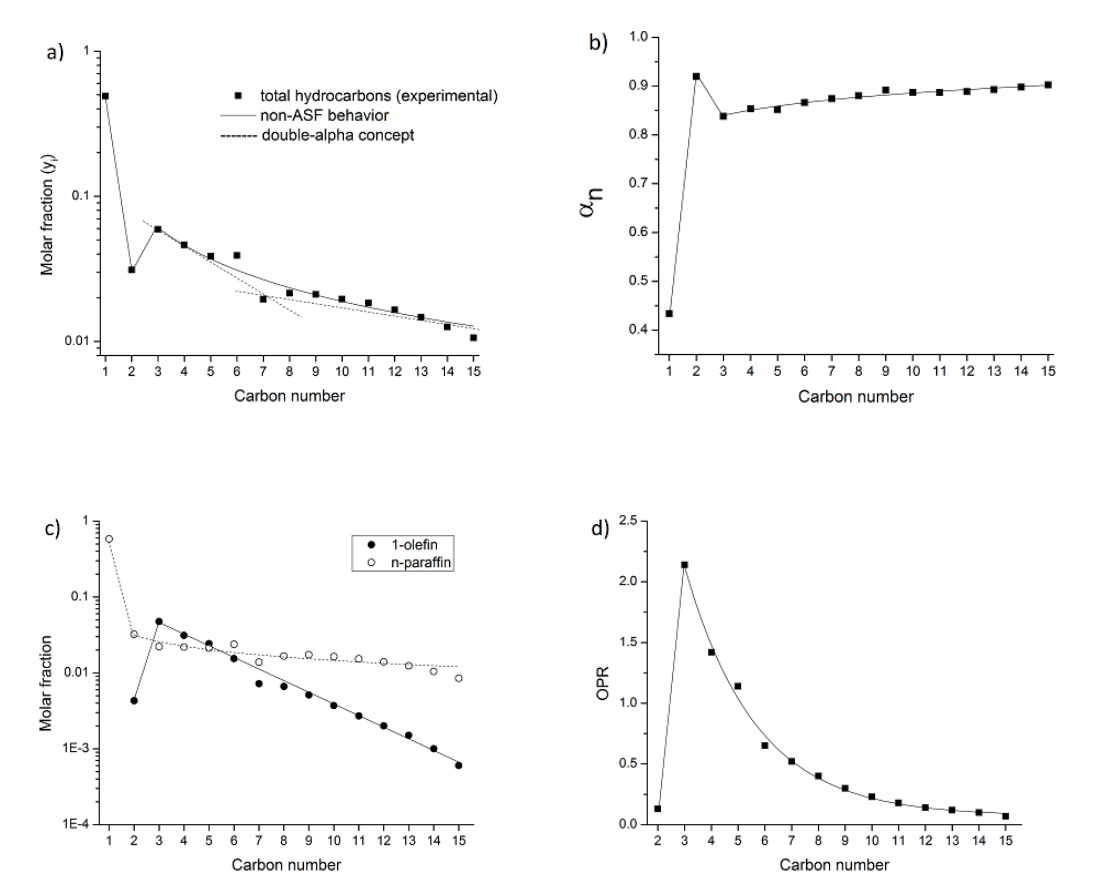

Figure 3.16 - FTS product distribution over 0.48%Re-25% Co/Al_2O_3 (at 493 K, 1.5 MPa, H_2/CO = 2.1, 8 NL/g_{cat}/h): a) log-scale molar fractions (y_i) vs. carbon number; b) chain growth probabilities with carbon number (α_n); c) log-scale molar fractions of 1-olefin and n-paraffin vs. carbon number; and d) 1-olefin-to-n-paraffin ratio (OPR) with carbon number.

Experimental data

The experiments were conducted over a 0.48%Re-25%Co/Al_2O_3 catalyst prepared by a slurry impregnation method. The experimental design and procedures used in this work can be found elsewhere [229]. A 1-L stirred tank slurry reactor was loaded with ~ 14g of catalyst with pellets in the sieving range of 44-90 μm in order to minimize heat and mass gradients and allow for intrinsic kinetic measurements. Co cluster size was 10.3 nm. The product distribution data were collected at three temperatures (478, 493, 503 K), two pressures (1.5 and 2.5 MPa), two H_2/CO feed ratios (1.4 and 2.1) and a range

of CO conversions (16 – 62 %). Available conditions and selectivities at these conditions are shown in Table 3.2.

Conversions and CO_2 selectivity were calculated using Eqs. (3.1) and (3.2). For hydrocarbon selectivities (C_1 – C_4), the following formula was used:

$$S_n(\%) = \frac{n * F_n}{F_{CO}^{in} - F_{CO}^{out} - F_{CO_2}^{out}} * 100\% \tag{3.13}$$

where S_n is the selectivity towards hydrocarbons containing n carbon atoms, F_n is the molar flow rate of hydrocarbons having n carbon atoms, F_{CO}^{in} and F_{CO}^{out} are molar flow rates of CO at the inlet and outlet of the reactor, and F_{CO2}^{out} is the molar flow rate of carbon dioxide.

Selectivity to heavier C_{5+} products (S_{C5+}) was calculated based on the difference method using the selectivities of C_1 to C_4:

$$S_{C_{5+}}(\%) = 100 - (S_{C1} + S_{C2} + S_{C3} + S_{C4}) \tag{3.14}$$

Note that selectivity to CO_2 is typically below 1% so it can be neglected in this calculation.

The chain growth probabilities for chains of different length (α_n) were calculated using Eq. (3.7). Note that hydrocarbon products up to C_{50} were used in applying Eq. (3.7). Due to the difficulties related to collection of C_7 species, the values of α_n were calculated after the molar flowrate data in the region around C_7 was smoothed. However, this procedure did not include or affect C_1-C_4 species.

1-olefin to n-paraffin ratios for different chain lengths (OPR_n) were calculated using Eq. (3.8).

Table 3.2 - Experimental process conditions and selectivity over 0.48% Re-25% Co/ Al_2O_3.

No	Run	TOS (h)	T (K)	P (MPa)	inlet H_2/CO mol/mol	WHSV NL/(g_{cat}*h)	X_{CO} (%)	(-R_{CO}) mol CO/(gcat*s)	outlet H_2/CO mol/mol	P_{CO} (MPa)	P_{H2} (MPa)	P_{H2O} (MPa)	S_{C1} %	S_{C2} %	S_{C3} %	S_{C4} %	S_{C5+} %	S_{CO2} %
1	1	173	493	1.5	2.1	8.0	45.5	5.25E-02	2.1	0.37	0.77	0.30	7.09	0.88	2.61	2.79	86.63	0.38
2		197		1.5	2.1	6.3	54.6	4.96E-02	2.1	0.34	0.70	0.39	7.11	0.96	2.67	2.80	86.46	0.54
3		221		1.5	2.1	14.0	24.3	4.92E-02	2.1	0.43	0.91	0.14	8.35	0.99	2.90	2.98	84.78	0.34
4		246		1.5	1.4	5.6	34.1	3.56E-02	1.0	0.57	0.59	0.30	4.80	0.69	2.34	2.46	89.71	0.55
5		293		1.5	2.1	8.0	41.3	4.76E-02	2.1	0.38	0.79	0.27	7.54	0.95	2.72	2.85	85.93	0.41
6		318		1.5	1.4	3.6	42.3	2.83E-02	0.9	0.56	0.48	0.42	4.36	0.70	2.37	2.57	90.01	0.94
7		342		2.5	2.1	15.0	26.0	5.63E-02	2.1	0.70	1.47	0.26	8.24	1.07	3.46	3.33	83.90	0.37
8		367		2.5	2.1	6.1	56.7	4.98E-02	2.1	0.55	1.14	0.69	6.32	1.07	3.14	3.19	86.27	0.48
1*	2	117	493	1.5	2.1	8.0	43.2	4.99E-02	2.1	0.38	0.79	0.28	7.90	0.99	2.92	3.02	85.17	0.37
9		158	478	1.5	2.1	3.7	43.1	2.33E-02	2.1	0.38	0.78	0.29	6.40	0.91	3.04	3.08	86.57	0.31
10		181		1.5	2.1	7.4	23.1	2.51E-02	2.1	0.44	0.92	0.12	7.02	0.85	2.97	3.02	86.14	0.24
11		209		1.5	2.1	1.9	62.3	1.76E-02	2.1	0.30	0.62	0.50	5.56	0.95	2.98	3.10	87.42	0.59
12		231		1.5	1.4	4.9	18.0	1.67E-02	1.3	0.60	0.75	0.13	5.52	0.71	2.79	2.85	88.13	0.42
13		253		1.5	2.1	3.7	37.4	2.03E-02	2.1	0.40	0.82	0.24	6.73	0.89	2.98	2.99	86.41	0.30
14		278		1.5	1.4	1.7	39.6	1.29E-02	0.9	0.56	0.53	0.37	3.82	0.68	2.58	2.72	90.21	0.59
15		303		1.5	1.4	1.0	48.1	9.08E-03	0.8	0.53	0.42	0.49	3.43	0.74	2.73	2.79	90.31	1.14
1*	3	125	493	1.5	2.1	8.0	43.4	4.98E-02	2.1	0.39	0.80	0.29	7.95	1.06	1.98	3.14	85.87	0.40
16		148	503	1.5	2.1	11.3	43.3	7.11E-02	2.0	0.38	0.77	0.29	10.3	1.36	3.60	3.85	80.94	0.60
17		171		1.5	2.1	20.0	23.5	6.83E-02	2.0	0.44	0.9	0.13	12.1	1.48	4.13	4.17	78.16	0.49
18		198		2.5	2.1	22.5	27.6	9.03E-02	2.0	0.71	1.45	0.27	11.0	1.39	4.18	4.05	79.42	0.43
19		222		2.5	2.1	11.5	52.5	8.77E-02	2.1	0.57	1.18	0.63	8.44	1.24	3.49	3.74	83.09	0.55
20		249		1.5	2.1	11.3	41.6	6.83E-02	2.1	0.38	0.78	0.27	10.4	1.46	3.79	4.09	80.24	0.63
21		270		1.5	1.4	18.1	15.7	5.35E-02	1.2	0.61	0.75	0.11	8.68	1.20	3.67	3.70	82.75	0.66
22		293		1.5	1.4	5.4	39.6	4.01E-02	0.9	0.56	0.51	0.36	6.66	1.03	3.13	3.41	85.77	1.18
23		317		2.5	1.4	18.1	16.0	5.44E-02	1.2	1.03	1.23	0.21	9.32	1.30	4.17	4.16	81.06	0.62
24		366		2.5	1.4	4.8	44.6	4.02E-02	0.8	0.92	0.73	0.74	5.40	1.00	3.18	3.34	87.09	1.25

Note: * - Initial period condition

Effect of time on stream

During the start-up period in FTS experiments over Co-based catalysts there is a period of rapid decrease in activity [73]. Change of conversion with time on stream (TOS) is shown in Figure 3.17a. In order to reach relatively stable activity an initial period at constant conditions (493 K, 1.5 MPa, H_2/CO = 2.1, 8 $NL/g_{cat}/h$) of about 120 h was required for all runs. Decreases in activity during the initial period were accompanied by increases in selectivity towards methane and decreases in C_{5+} selectivity (Figure 3.17b). After the initial period, a relatively stable state in catalyst activity and selectivity was reached. This was followed by a period in which process conditions where changed as shown in Table 3.2.

For Runs 1, 2 and 3 different temperatures were used, i.e. 493, 478 and 503 K, respectively. Specific baseline conditions during these runs were repeated at different times on stream (TOS) to assess the catalyst activity (i.e., extent of deactivation). TOS did not significantly affect the product distribution [229]. However, the trend of decreasing activity and changing selectivity typically continued during the entire run and deactivation was possibly even enhanced by frequent changes in process conditions. In all runs, during the period in which process conditions were varied (300 - 400 h in which catalyst activity decreased by about 20%) CH_4 increased and C_{5+} selectivity decreased by approximately 2%. WGS activity typically exhibited a small increase with TOS. The effect of TOS was taken into account when comparing the product distribution at different conditions, so that the focus was on conditions that are closer in TOS and activity.

Due to problems with heavy product accumulation, the analysis focused on C1-C15 hydrocarbons, and changes in product distribution with time are shown in Figure 3.18. It can be seen that hydrocarbon product distribution did not change significantly with time in spite of deactivation.

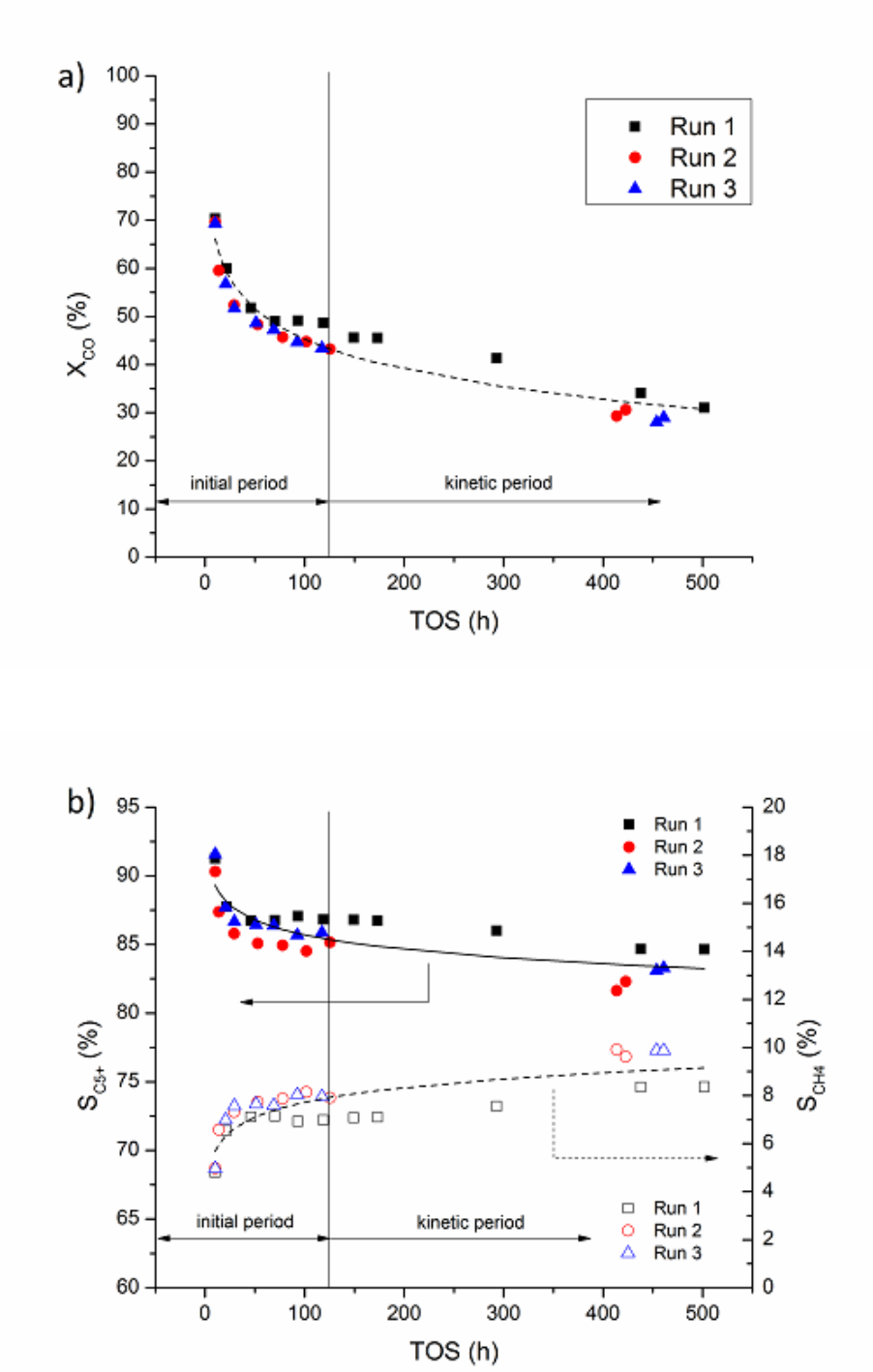

Figure 3.17 - Effect of time on stream (baseline conditions: 493 K, 1.5 MPa, H_2/CO = 2.1, 8 NL/g_{cat}/h) on: a) CO conversion and b) C_{5+} and methane selectivity.

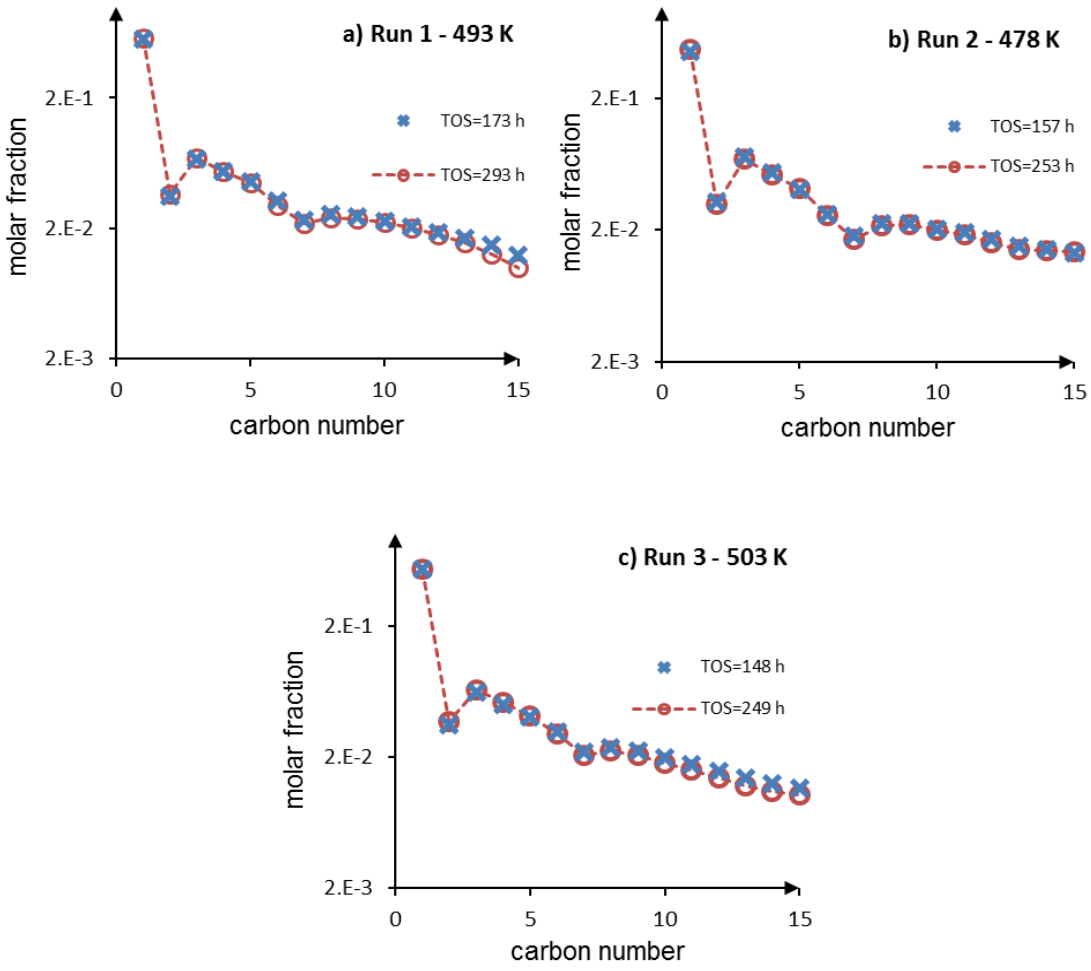

Figure 3.18 - Reproducibility of hydrocarbon product distribution at replicated conditions during the kinetic period: a) Run 1 (493 K, 1.5 MPa, H_2/CO = 2.1, 8 $NL/g_{cat}/h$); b) Run 2 (478 K, 1.5 MPa, H_2/CO = 2.1, 3.7 $NL/g_{cat}/h$); c) Run 3 (503 K, 1.5 MPa, H_2/CO = 2.1, 11.3 $NL/g_{cat}/h$).

Effect of temperature

A typical trend over all FTS catalysts is that an increase in temperature is accompanied by an increase in selectivity towards light products and a decrease in heavier C_{5+} products [86-89]. As shown in Figure 3.19, at constant pressure, H_2/CO ratio and similar CO conversions, our data exhibits this behavior as well. For the lighter products (Figure 3.19a), methane selectivity is shown to be the highest and C_2 selectivity the lowest, both however exhibiting a clear increase when increasing the temperature from

478 to 503 K. Figure 3.19b shows the decline of selectivity towards C_{5+} in the 478 - 503 K range. Even though most studies over Co-based catalysts report an increase in selectivity towards light products (i.e., a decrease in heavy hydrocarbon production) [87, 89], some authors state that selectivity is not strongly dependent on temperature in their examined temperature ranges [94, 95]. This difference is probably due to the intrinsic kinetic nature of the chain growth process, where rates of propagation and termination are determined by rate constants, which are in turn exponential functions of temperature (i.e., Arrhenius dependency). Therefore, the differences between changes in rates of chain propagation and termination with variations in temperature are responsible for the observed variations in selectivity. In other words, as the temperature increases, the rate of chain termination increases faster relative to that of chain propagation. This could be caused by slightly higher activation energies of termination steps compared to those of propagation. Another undesired kinetic effect related to increases in temperature is that of the increase in the rate of water-gas-shift (WGS) reaction, evident from increases in CO_2 selectivity (Figure 3.19b).

In order to further analyze the effect of temperature on the FTS product distribution, variations in the main products as a function of carbon number (Figure 3.20) were investigated. The mole fraction of methane is the highest and fractions of heavy products are lowest at 503 K, while the opposite trend exists at 473 K (Figure 3.20a). If we compare chain growth probabilities from Figure 3.20b, we can see that α_n values tend to be higher at lower temperature, which is something that is again well documented for all FTS catalysts [86]. This relates to the above mentioned relative changes in termination and propagation rates as defined by ASF kinetics. The changes in OPR with changing temperature are relatively small, but seem to be present, especially at 503 K (Figure 3.20c). These decreases in OPR have been suggested to be caused by increased rates in secondary reactions of 1-olefins at higher temperatures [89], but alternative kinetic explanations cannot be excluded. The reported activation energies for olefin formation are usually 10-20 kJ/mol higher than those of paraffin formation [92], while secondary reactions of 1-olefins are reported to have a very high activation energy (approximately 150 kJ/mol) [164]. Thus, increasing temperature would most significantly increase the

rates of secondary olefin reactions. The observed minor decrease in OPR with temperature is likely caused by variations in secondary reactions of olefins.

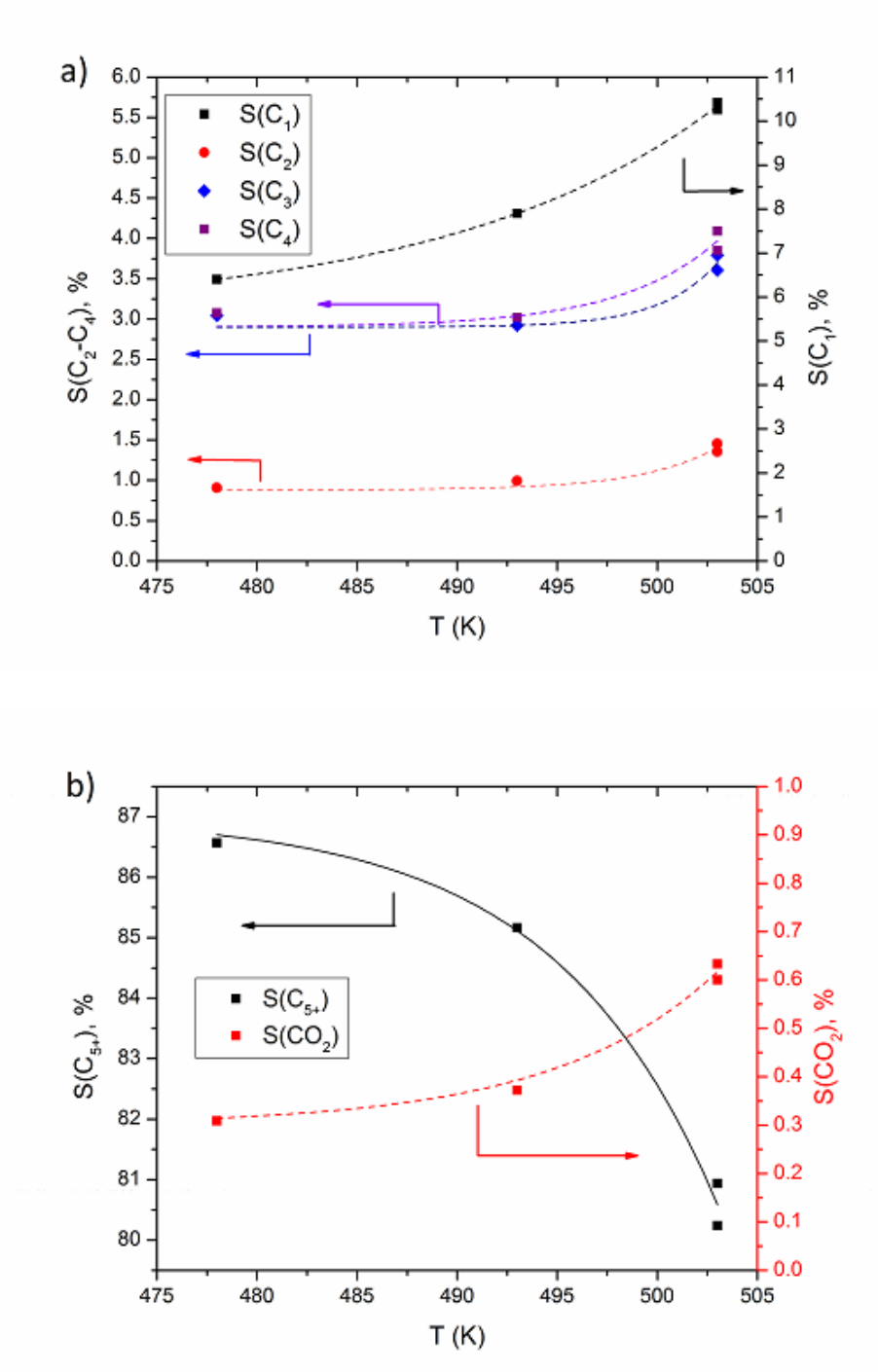

Figure 3.19 - Effect of varying reaction temperature (at P = 1.5 MPa, H_2/CO = 2.1 and $X_{CO} \approx 43\%$) on: a) C_1, C_2, C_3 and C_4 selectivity and b) C_{5+} and CO_2 selectivity.

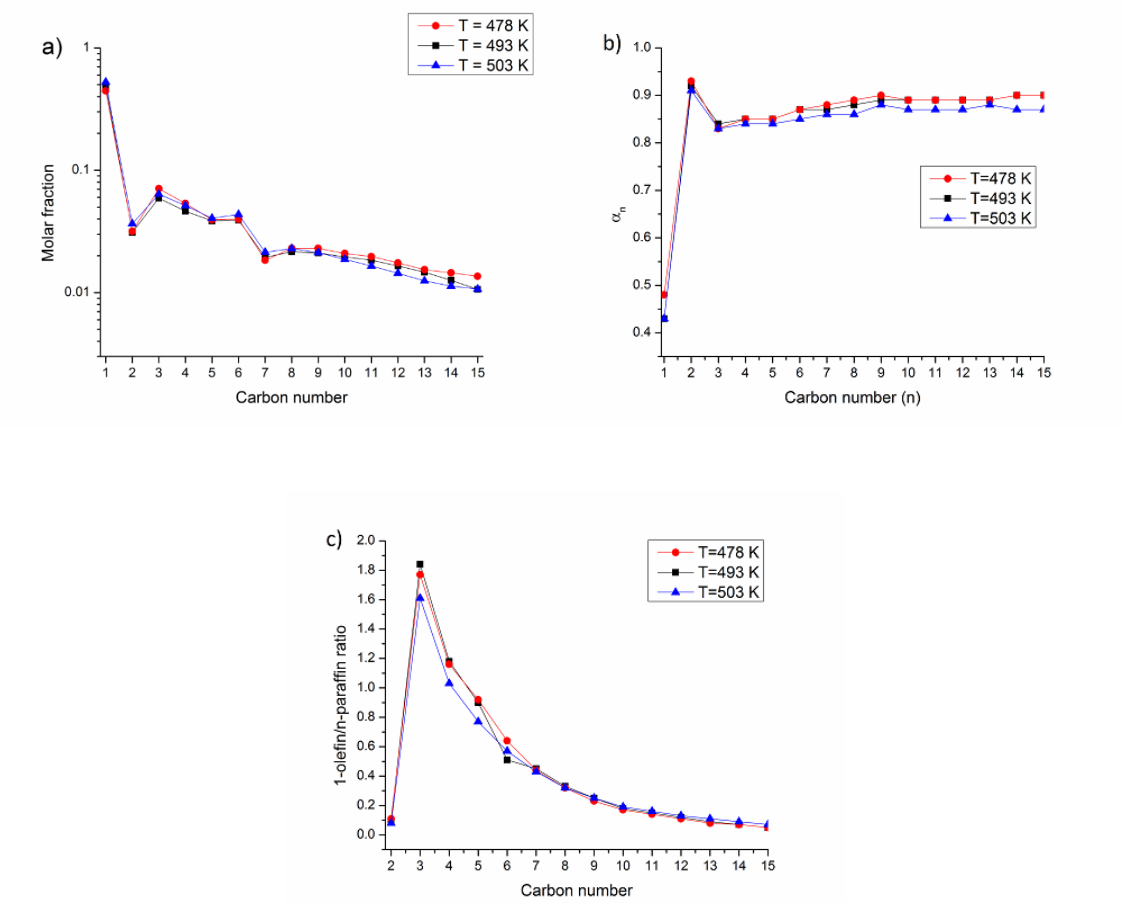

Figure 3.20 - Effect of varying process temperature (at P = 1.5 MPa, H_2/CO = 2.1 and X_{CO} = 41.3-43.3%) on: a) hydrocarbon molar fractions with carbon number; b) chain growth probabilities (α_n) with carbon number; and c) 1-olefin/n-paraffin ratio with carbon number.

Effect of pressure

Increasing the total pressure has a positive effect on FTS reaction rate and selectivity [101]. Typically, increases in pressure lead to lower methane and higher C_{5+} selectivities [100, 101] and our results are consistent with this trend (Figure 3.21). WGS activity slightly decreased when increasing pressure from 1.5 to 2.5 MPa. Similar to our results, a recent study with a Co/SiO_2 catalyst performed by Dinse et al. [102] showed that if pressure is increased from 1 to 10 atm there is a subsequent decrease in C_1 and C_2-C_4 accompanied by an increase in C_{5+} selectivity. Dinse et al. [102] hypothesized that

this shift was caused by a combined effect of pressure in enhancing the olefin readsorption rate and decreasing the hydrogen coverage that, in turn, decreased the rate of termination; the net result was an increase in chain growth probability, resulting in a higher yield of heavier products. To analyze this, the change in growth probability with pressure was plotted (Figure 3.22a). In contrast to the above mentioned explanation, our results, obtained at higher pressures (1.5 and 2.5 MPa), show that α_n values remain almost constant at different pressures. The only change observed was a small increase in α_1 with increasing pressure.

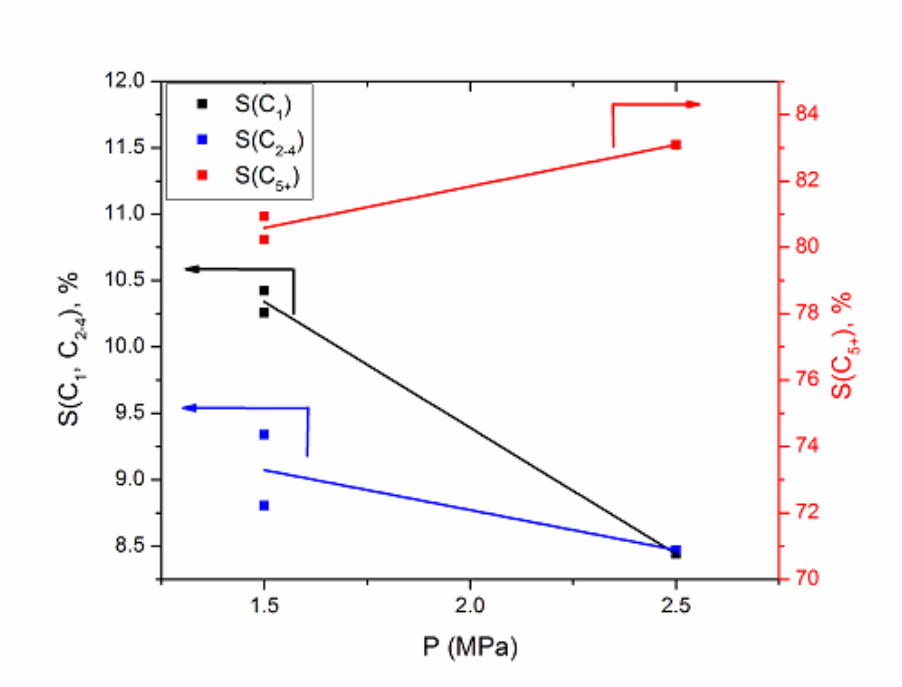

Figure 3.21 - Effect of varying total pressure (at T = 503 K, H_2/CO = 2.1 and WHSV = 11.3 and 11.5 NL/g_{cat}/h) on C_1, C_{2-4} and C_{5+} selectivity.

Our results showed that for certain conditions OPR slightly decreased when pressure was increased from 1.5 to 2.5 MPa (Figure 3.22b), while maintaining the residence time (i.e., space velocity) constant. However, at other conditions the opposite trend was observed as well, especially in the C_2-C_5 range. Because increasing pressure decreases the hydrogen coverage [338], and thus decreasing the rate of primary chain hydrogenation to n-paraffin, we would expect to see an increase in OPR with increased pressure. In addition, increasing total pressure causes the partial pressure of water to

increase, which suppresses secondary 1-olefin hydrogenation and also raises the OPR. Opposing these two effects is the effect of increasing 1-olefin partial pressure due to increased total pressure, which results in a higher rate of secondary reactions (i.e., lower OPR). Therefore, the influence of pressure on the OPR is complex and determined by several competing effects.

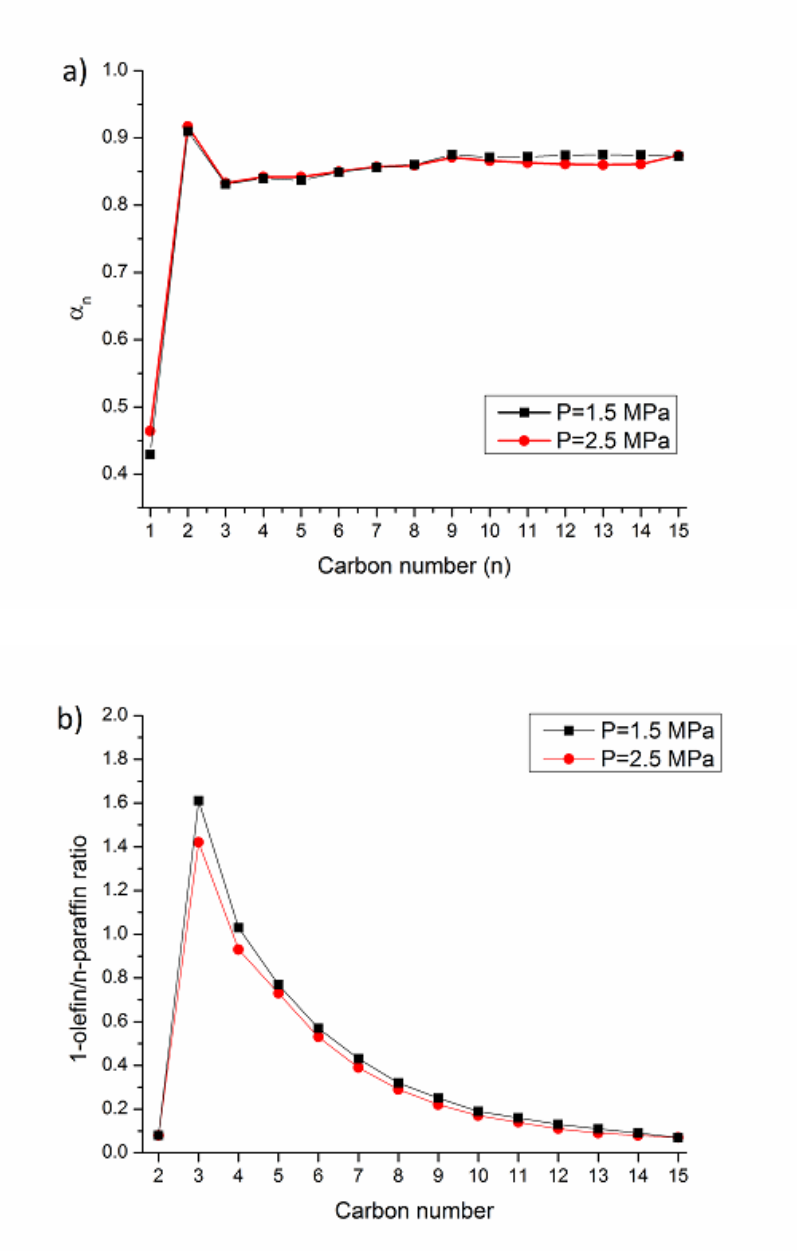

Figure 3.22 - Effect of varying total pressure (at T = 503 K, H_2/CO = 2.1 and WHSV = 11.3 and 11.5 NL/g_{cat}/h) on: a) chain growth probabilities (α_n) with carbon number and b) 1-olefin/n-paraffin ratio with carbon number.

Effect of reactant feed ratio

We analyzed the effect of H_2/CO ratio on the product distribution by reducing the inlet reactant feed ratio from 2.1 to 1.4. Outlet H_2/CO ratios correspond to those inside the reactor, and depending on the conversion level varied between 0.79 - 1.25 and 2.04 - 2.14 for inlet ratios of 1.4 and 2.1, respectively (Table 3.2). Lowering the H_2/CO ratio leads to an increase in C_{5+} selectivity and a reduction in the selectivity to methane and lower C_2-C_4 hydrocarbons (Figure 3.23). This is an effect that is generally reported in the literature [86, 89, 94]. The selectivity to CO_2 typically doubled when reducing the reactant feed ratio from 2.1 to 1.4, but it still remains quite low, with a maximum value of 1.2%.

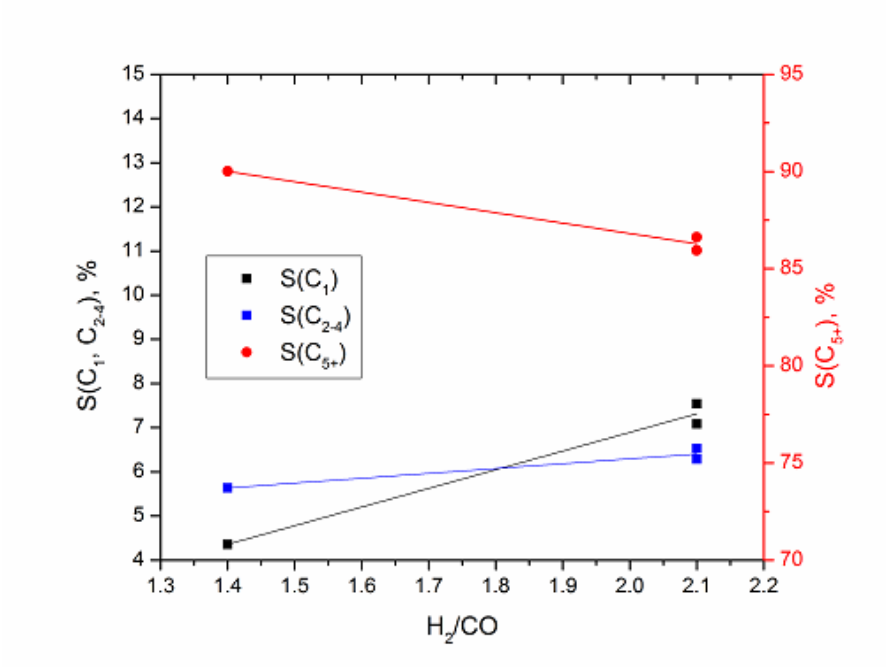

Figure 3.23 - Effect of varying H_2/CO feed ratio (at T = 493 K, P = 1.5 MPa and X_{CO} = 41.3 - 45.5%, outlet H_2/CO ratio = 0.9 and 2.1) on C_1, C_{2-4} and C_{5+} selectivity.

The hydrocarbon distribution at different H_2/CO ratios is shown in Figure 3.24a. A decrease in H_2/CO ratio from 2.1 to 1.4 causes a decrease in the methane fraction and a parallel shift upwards for C_{2+} products. Some authors believe that the increase in formation of heavier hydrocarbons is caused by a combined effect of a decrease in the termination probability due to lower primary hydrogenation rates, and an enhancement in

1-olefin readsorption due to the higher CO partial pressure [86, 89]. Contrary to that view, Yates and Satterfield [94] reported that feed ratio mainly affects the rate of methane formation, while the formation of heavier products is not significantly affected. Our results suggest that the reason for changing selectivity with feed ratio lies in the fact that only α_1 seems to be significantly altered by the change in feed ratio, while other α_n values remain unchanged (Figure 3.24b). On the other hand, the OPR is also affected and increases when H_2/CO is reduced from 2.1 to 1.4 (Figure 3.24c). The explanation for this could be due to reductions in both primary and secondary hydrogenation rates to n-paraffins; however, variations in primary hydrogenation rates (i.e., chain termination to n-paraffin) would have affected the values of growth probabilities. Since the α_{C2+} values remained largely constant, the changes in OPR are most likely caused by secondary hydrogenation of 1-olefins.

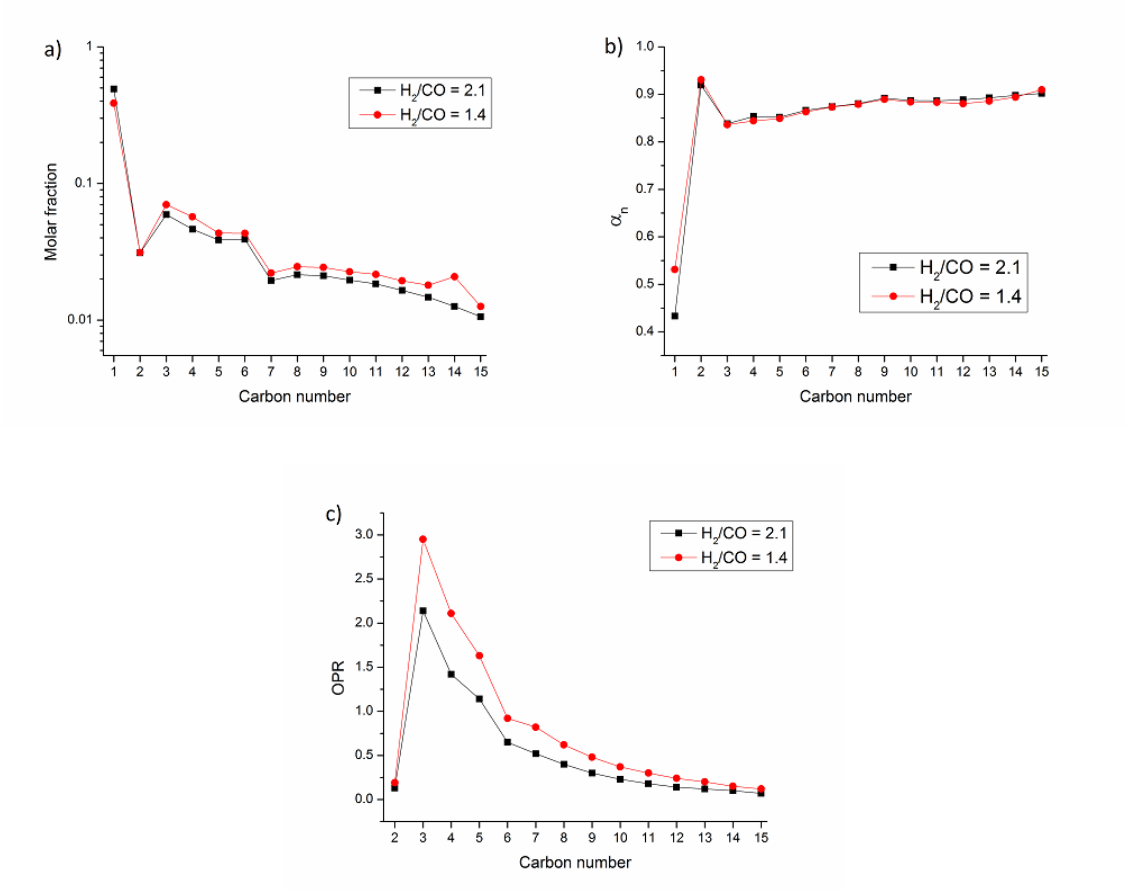

Figure 3.24 - Effect of varying H_2/CO feed ratio (at T = 493 K, P = 1.5 MPa and X_{CO} = 41.3 - 42.3%, outlet H_2/CO ratio = 0.9 and 2.1) on: a) hydrocarbon molar fractions with carbon.

Effect of conversion level

This study focused on the effect that changing CO conversion from low to moderately high conversion levels (X_{CO} = 16 – 62 %) has on the FTS product distribution. This range of single-pass conversions is typically used in industry, while the implications of operating at higher conversions are discussed elsewhere [106, 107]. Our results showed a linear increase in C_{5+} and decreases in CH_4 and C_{2-4} selectivities with increasing CO conversion (i.e., decreasing space velocity) as displayed in Figure 3.25. This is a trend that is generally well known [29, 94, 106, 107]. Increasing conversion also led to increased WGS activity.

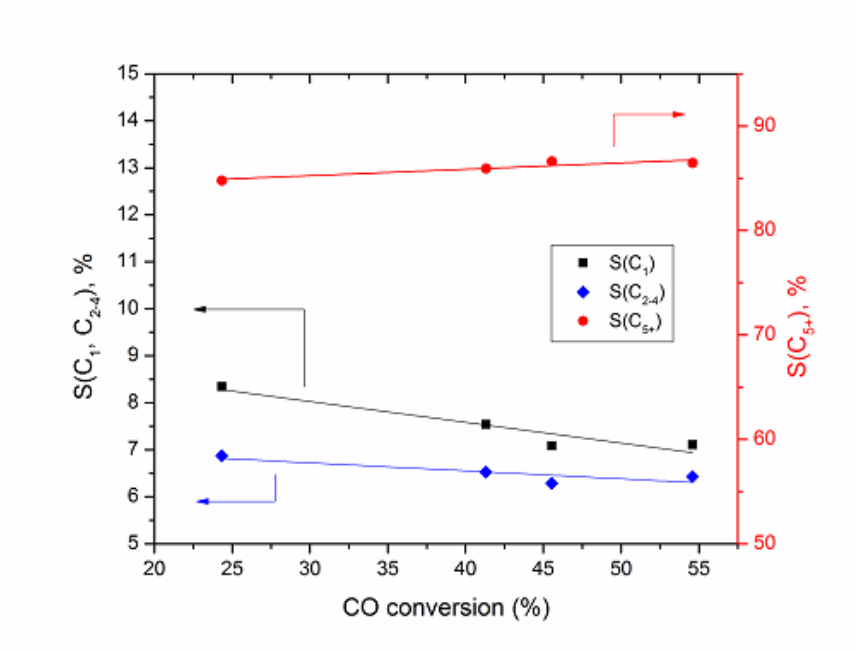

Figure 3.25 - Effect of varying CO conversion (at T = 493 K, P = 1.5 MPa and H_2/CO = 2.1) on C_1, C_{2-4} and C_{5+} selectivity.

A widely accepted explanation for the increase in the yield of heavier (C_{5+}) hydrocarbons is that the in-situ formed 1-olefins can readsorb on the surface and continue with chain growth [23, 108, 163]. The extent of secondary readsorption of 1-olefins is then related to the residence time of the molecule, which would depend on the space velocity (i.e., conversion level), and the chain length of the molecule, which determines diffusivity, solubility and/or physisorption characteristics as a function of molecular weight [86]. The increase in C_{5+} selectivity with increasing conversion is accompanied

by a decrease in the 1-olefin/n-paraffin ratio (Figure 10a), which is caused by a decrease in the 1-olefin formation rate due to secondary reactions, and a relatively constant formation rate for n-paraffins. Therefore, an explanation involving 1-olefin secondary reactions is a logical one, and it is most often referred to when discussing the effect of conversion level and/or residence time. In a study of titania support Ru and Co catalysts by Iglesia et al. [28], which utilized a fixed bed reactor setup, the reported increase in C_{2+} chain growth probabilities with conversion level was attributed to diffusion enhanced 1-olefin readsorption. However, Holmen and coworkers [119, 339-341] recently questioned the importance of secondary olefin readsorption based on experiments with various Co-based catalysts. Lögdberg et al. [119] proposed an interesting new explanation, in which the increase in C_{5+} selectivity, and decrease in CH_4 selectivity, was the result of high intrinsic chain growth probabilities, where α_1 would be especially important, and olefin readsoprtion was considered to have only a small effect. The increase in chain growth probabilities (α_n) for higher carbon numbers was rationalized by Lögdberg et al. [119] by the potential existence of a different type of FTS active site, one responsible for methanation and formation of some of the lighter hydrocarbons, and one responsible for growth and formation of heavy C_{5+} hydrocarbons. Their ideas were consistent with the so-called double-alpha concept, which generally cannot explain the exponential decreases in OPR with carbon number (Figure 3.26a).

In order to better understand the causes for the change in product selectivity with conversion level (i.e., residence time), the effect of changes in conversion on growth probabilities at fixed temperature, pressure and H_2/CO ratio were analyzed. If the residence time dependent olefin readsorption effect is dominant, one would expect to see an increase in α_n for the C_{2+} range with increasing conversion, as reported by Iglesia et al. [28], while if readsorption is negligible and α_1 is the most important parameter (as per Lögdberg et al. [119]), one should expect to see α_1 increase with conversion. Our results showed that the C_{2+} growth probabilities at fixed temperature, pressure and H_2/CO ratio and with changing conversions (Figure 3.26b) did not typically increase, but were relatively constant. This aspect will be discussed further in the following section.

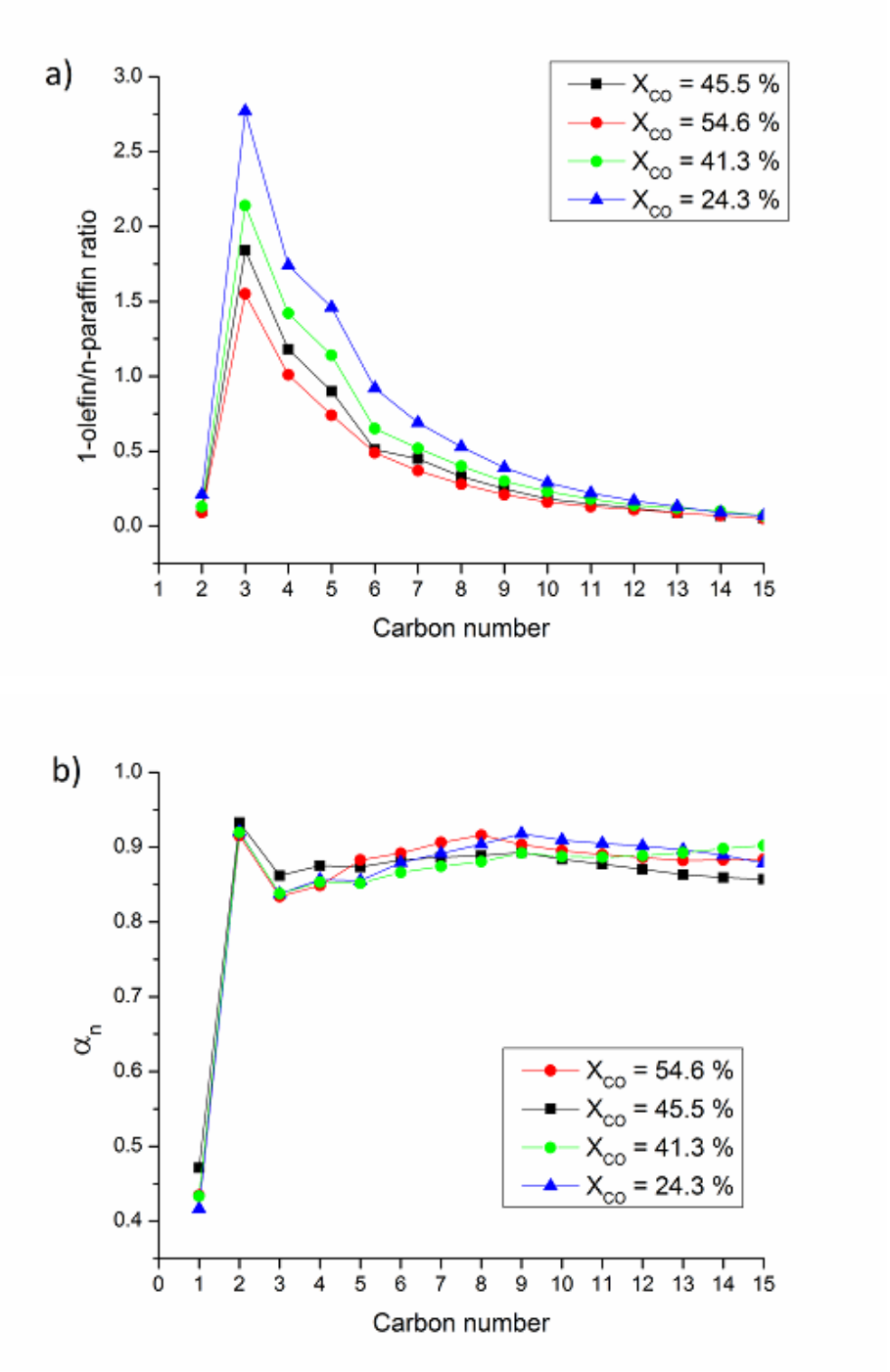

Figure 3.26 - Effect of varying CO conversion (at T = 493 K, P = 1.5 MPa and H_2/CO = 2.1): a) 1-olefin/n-paraffin ratio (OPR) with carbon number; b) chain growth probabilities with carbon number (α_n).

Effect of olefin secondary reactions

As explained above, secondary reactions of initially formed 1-olefins from FTS are usually thought to have a large influence on the FTS product distribution. Our results at different H_2/CO feed ratios and conversion levels, as well as pressures and temperatures to a smaller extent, show clear evidence for the existence of some of these reactions. However, one of the unresolved issues is which of the secondary reactions is the dominant pathway: hydrogenation or readsorption followed by continued chain growth (sometimes also referred to as reinsertion) [108, 150, 164]. Iglesia et al. [108] proposed that readsorption is the dominant secondary reaction and stated that for heavy olefins the probability of this reaction would have to be very high (above 90%) and that hydrogenation of in-situ formed olefins is negligible. Schulz and Claeys [164] questioned this opinion based on the results of their olefin co-feeding study, which showed secondary hydrogenation to be the dominant reaction, followed by isomerization, whereas secondary readsorption was found to be typically below 20%. Different olefin co-feeding studies reported even lower selectivity towards readsorption [175, 176]. Schulz and Claeys [131] proposed a model of product distribution that included all secondary reactions (hydrogenation, isomerization and readsorption). However, as Patzalaff and Gaube [153] pointed out, this model also required that olefin readsorption be the main secondary reaction, with readsorption probability almost at 100%, which is contrary to the experimental evidence by Schulz and Claeys [164].

Figure 2.6 shows a schematic representation of chain growth and termination steps to form the main products, as well as 1-olefin secondary reactions. The chain growth is considered to be irreversible [342], while 1-olefin readsorption is included, so that the chain growth probability α_n can be defined as:

$$\alpha_n = \frac{R_{p,n}}{R_{p,n} + R_{t,n}^{n-par} + R_{t,n}^{1-ole}(1-\beta_n)} = \frac{k_p[C_m - S]}{k_p[C_m - S] + k_t^{n-par}[H - S] + k_t^{1-ole}(1-\beta_n)} \qquad (3.15)$$

where $R_{p,n}$ is the rate of chain C_n-S propagation, $R_{t,n}^{n-par}$ rate of C_n-S primary hydrogenation to n-paraffin and $R_{t,n}^{1-ole}$ rate of 1-olefin desorption with readsorption probability of β_n. The constants k_p, k_t^{n-par} and k_t^{1-ole} are kinetic rate constants of

propagation, hydrogenation and desorption, respectively, $[C_m - S]$ is the monomer surface coverage and $[H - S]$ is the coverage of atomic hydrogen. From Eq. (3.15) we see that any potential increase in the rate of olefin readsorption with process conditions would result in increases in α_n. An increase in primary hydrogenation, caused by increases in hydrogen coverage, would result in a decrease in α_n.

Our results showed that the temperature and pressure changes did not significantly affect OPR and that these factors do not seem to have a major effect on secondary reactions. On the other hand, H_2/CO feed ratio (Figure 3.24) and conversion level (i.e. residence time, Figure 3.26) show a significant effect on secondary reactions and changes in these conditions resulted in major changes in OPR.

Increasing conversion, while keeping T, P and H_2/CO constant, leads to a higher extent of secondary reactions of 1-olefins due to higher residence times of these molecules. In order to discriminate among different secondary reactions, we looked at how molar fractions of different products change with the residence time. Figure 3.27 shows molar fractions for C_2, C_4, C_8 and C_{12} molecules at different conversions. Molar fractions of 1-olefins decreased with increasing conversion, whereas those of 2-olefins increased steadily with increasing conversion. It is interesting to note that 2-butene (Figure 3.27b) was not even observed at lower conversions, which might suggest that it is only formed by a secondary reaction pathway. Figure 3.27 also shows that there is a trend of increasing molar fraction for total C_{2+} hydrocarbons with increasing conversion. For C_{3+} products this increase is usually assumed to come from readsorption and continued chain growth of olefins having lower chain length (e.g., higher C_8 in Figure 3.27c could be said to come from a higher extent of readsorption of C_2-C_7 olefins). However, we also see an increase in the fraction of C_2 at higher conversions, which could not be caused by readsorption, as ethylene is the lowest olefin. This would suggest a different reason for the change in selectivity with conversion level.

Results also indicate that growth probabilities did not significantly vary with conversion level. To further analyze this, we plotted Figure 3.28 using $C_{1\text{-}4}$ growth probabilities at all of the available conditions. Not only were C_{2+} growth probabilities relatively constant for different conversion levels, but they only varied within a small

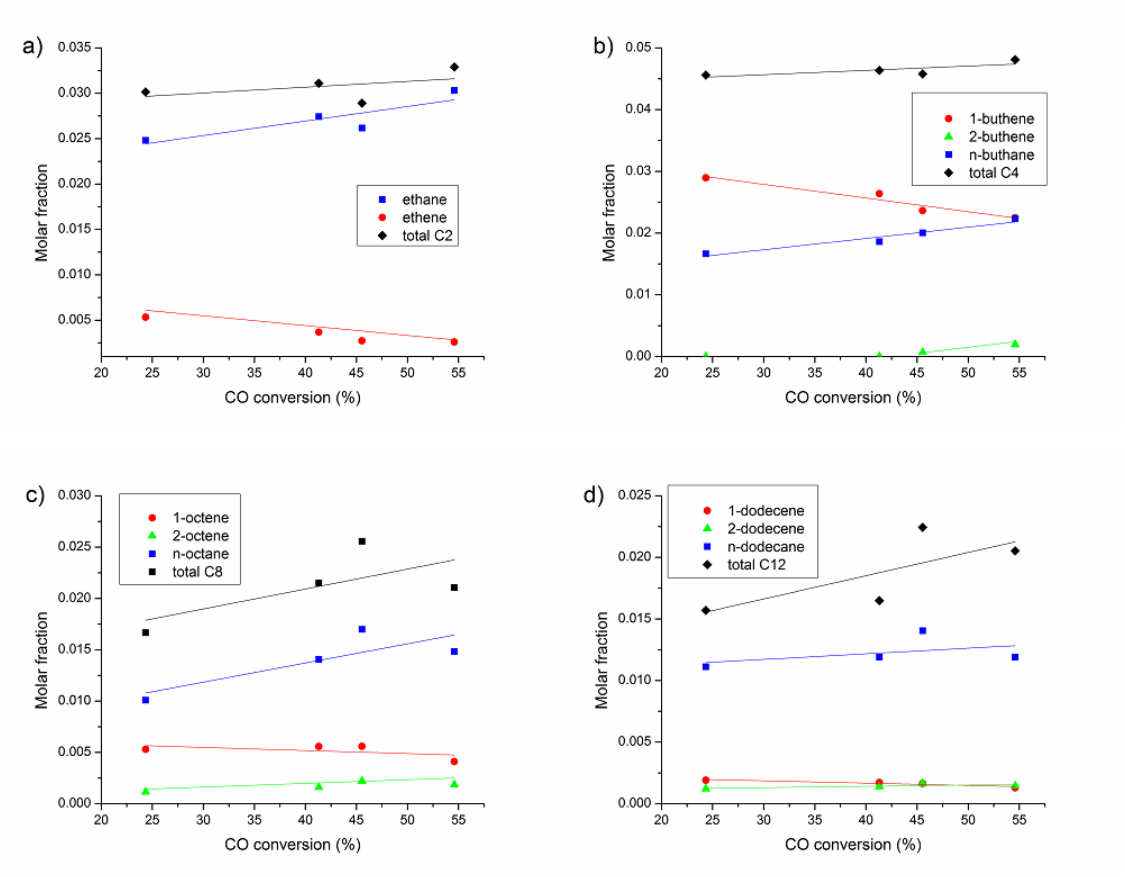

Figure 3.27 - Variation of hydrocarbon molar fraction at different CO conversions (at T = 493 K, P = 1.5 MPa and H_2/CO = 2.1) for: a) C_2; b) C_4; c) C_8; and d) C_{12}.

range for all of the conditions studied. Growth probabilities of higher C_{5+} chains exhibited the same trend as well (not shown here). Since α_{2+} shows no significant variation at different values of residence time we believe that the intrinsic FTS chain growth is not significantly affected by olefin readsorption. If this secondary reaction had a more significant effect, we would expect to see an increase in α_{2+} values with conversion. On the other hand, while maintaining T, P and inlet H_2/CO constant and changing only conversion, α_1 exhibits a clear increasing trend (one set of data at constant T, P, inlet H_2/CO and varying X_{CO} conditions is marked in Figure 3.28, but other sets have almost parallel trendlines). This trend of α_1 is in contrast to that observed for a Ru/TiO_2 catalyst as observed by Madon et al. [343], which showed a constant value of α_1 with residence time. The scatter in the values of α_1 is due to the fact that, unlike α_{2+}, the

growth probability of C_1 is highly dependent on process conditions. These results are consistent with the study of Lögdberg et al. [119] and bring additional evidence that the main reason for the variations in selectivity with process conditions lies in the kinetics of C_1 formation.

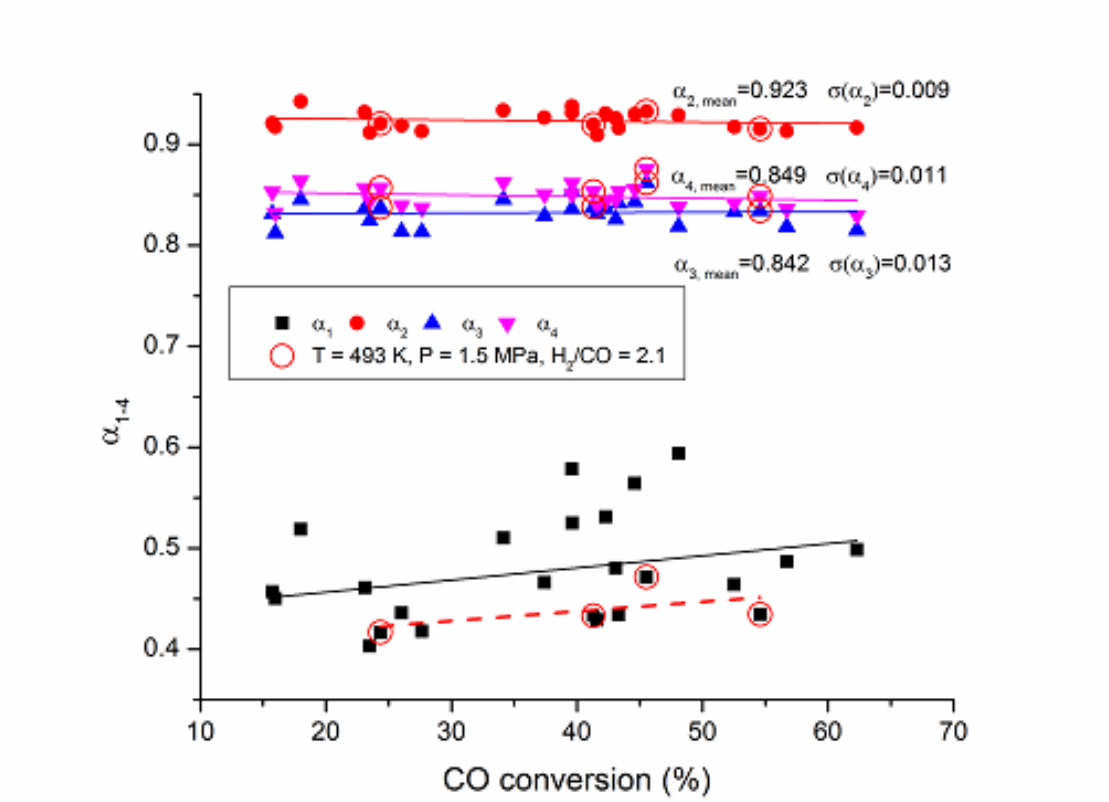

Figure 3.28 - Variation of chain growth probabilities αn (n = 1 – 4) at different CO conversions for the range of studied conditions (σ – standard deviation).

It is also interesting to note that the slope of 1-olefin formation does not significantly change with changing conversion (Figure 3.29). If we assume that the difference in the slopes of 1-olefins and n-paraffins comes from secondary reactions which are a function of residence time of molecules with different chain length, one would expect to see a change in the 1-olefin slope with residence time. This result might imply that secondary 1-olefin reactions do not significantly depend on chain length in the C_{3+} range for the range of conditions studied, as some co-feeding results suggest [108], and that the reason for the difference in the slopes of 1-olefin and n-paraffin is intrinsically kinetic. However, it is very difficult to analyze the effects that secondary reactions of 1-

olefins have on the product distribution without actually co-feeding labeled olefins of different chain lengths and observing the results. A recent study by Gnanamani et al. [175], where labeled 1-pentene was co-fed, showed behaviors consistent with our conclusion, i.e. effect of readsorption is negligible, while hydrogenation and isomerization are dominant for cobalt catalyst. This approach would need to be extended to molecules of different chain lengths and at different process conditions in order to further improve our understanding of these reactions.

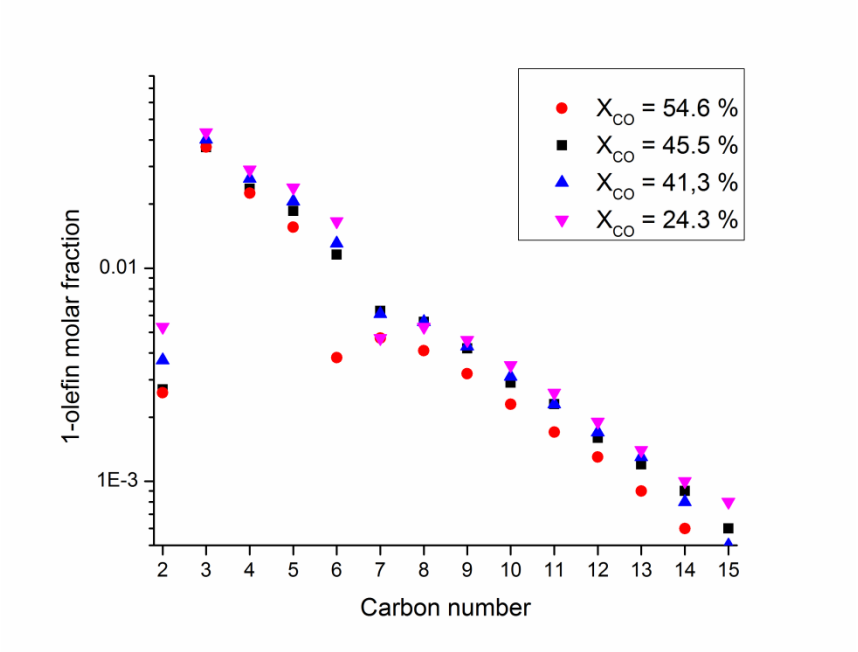

Figure 3.29 - Comparison of 1-olefin molar fraction changes with carbon number at different CO conversions (at T = 493 K, P = 1.5 MPa and H_2/CO = 2.1).

Importance of methane formation and growth of C_1

An additional evidence that 1-olefin readsorption does not play a major role in determining FTS product distribution, presented by Holmen and co-workers [119, 344], was the lack of correlation between changes in OPR and C_{5+} selectivity. Lögdberg et al. [119] found clear correlations between chain growth probabilities (α_n) and different selectivities, which could have been expected considering the polymerization nature of FTS product formation. They also found that the greatest variation at different process

conditions was in α_1, and therefore its influence on the selectivity of C_{5+} is much more significant than that of other growth probabilities. The relation between the C_1-C_4 growth probabilities (α_1-α_4) at different conditions with C_{5+} selectivity for our data set is shown in Figure 3.30. A clear positive correlation for all α_n values (including C_5, C_6, etc., not shown here) and C_{5+} selectivity exists and is consistent with the results of Lögdberg et al. [119]; it shows that the correlation between α_1 and S_{C5+} is dominant and that varying α_1 has the biggest impact on S_{C5+}.

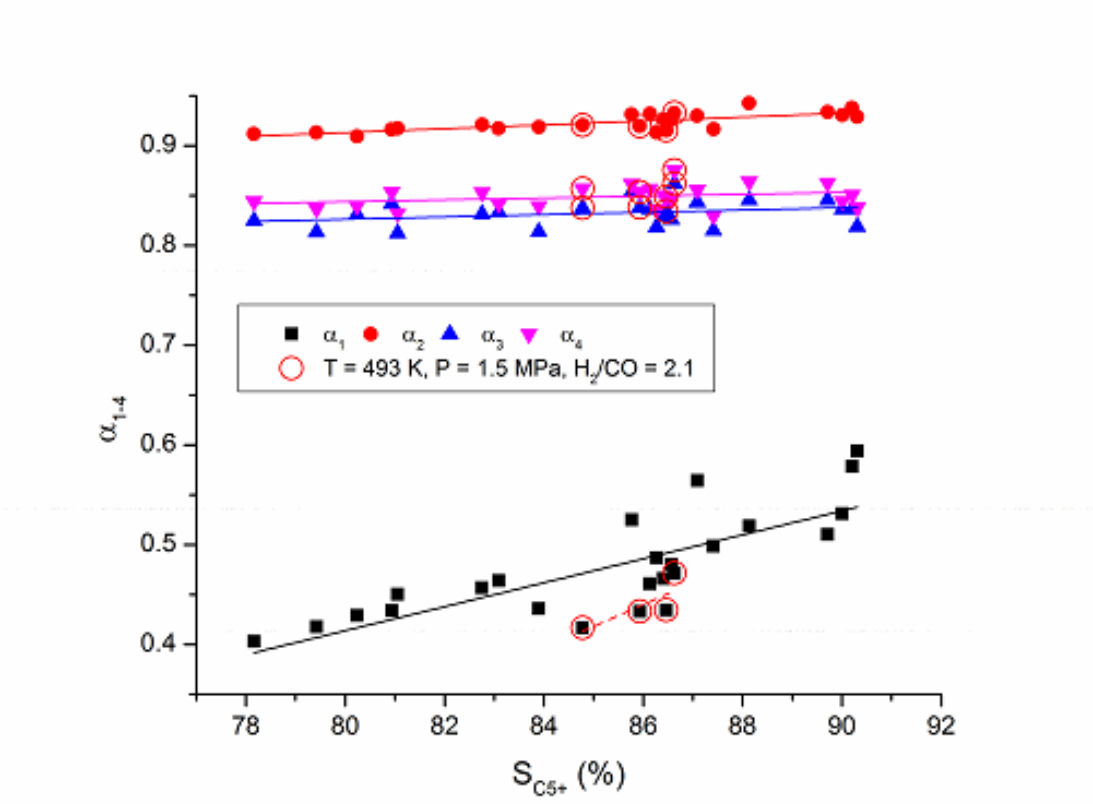

Figure 3.30 - Correlation between chain growth probabilities αn (n = 1 – 4) and C_{5+} selectivity for the range of studied conditions.

We analyzed how changes in process conditions affect α_1 in order to gain a better understanding of which process parameters have the greatest impact on C_{5+} selectivity. Figure 3.31 shows that all process conditions affect α_1. Increasing the temperature and H_2/CO feed ratio will have a decreasing effect on growth of C_1, while increasing pressure and conversion cause α_1 to increase. Because high values of α_1 are needed to obtain a higher C_{5+} product yield, understanding intrinsic kinetics of chain initiation and C_1 growth

in FTS becomes even more important. In order to find a way to control α_1 we need to know what is the cause for the excess production of methane, compared to the methane formed from typical ASF kinetics governing the FT pathway. Several hypotheses have been proposed to explain this non-ASF feature and they include: high surface mobility of methane precursor and the fact that methane is thermodynamically the most favored product [35], hydrogenolysis of higher hydrocarbons by successive demethylation [109], low activation energy for methane formation [229], different pathways for methane formation [261, 262]; however, the dominant explanation seems to be the presence of two different sites (FTS active sites and specific sites for methanation) [174, 263, 264]. Schulz [174] postulated that methanation occurs mainly on metallic sites with different coordination compared to the FTS active sites. Lee and Bartholomew [263] found evidence for the existence of secondary path for methane formation, where spillover of CO and H to the support results in formation of a CH_xO complex, which diffuses to metal sites and decomposes to give methane. Their results showed that methane formation is a function of metal loading and reduction temperature and that increasing metal loading causes an increase in methane formation by the FTS pathway. Based on our results, obtained under a range of typical FTS conditions, it seems that the best way to improve C_{5+} selectivity is to reduce this extra methane formation. This is something that requires further consideration, but useful insights about the kinetics of methane formation could potentially be deduced from SSITKA studies typically performed at conditions favoring methane formation, i.e. low pressure and high H_2/CO ratios [261, 311, 312].

One important implication of this viewpoint is that one could conceivably control the methanation rate through catalyst design by shutting down that pathway; in an ideal catalyst, then, the methane selectivity would be closer to that predicted by a single alpha model for FTS. In recent studies, it was observed that methane selectivity depends somewhat on the promoter that is used [273], and that Ag provides an interesting, albeit slight, decrease in methane selectivity even with respect to an unpromoted Co catalyst [345, 346].

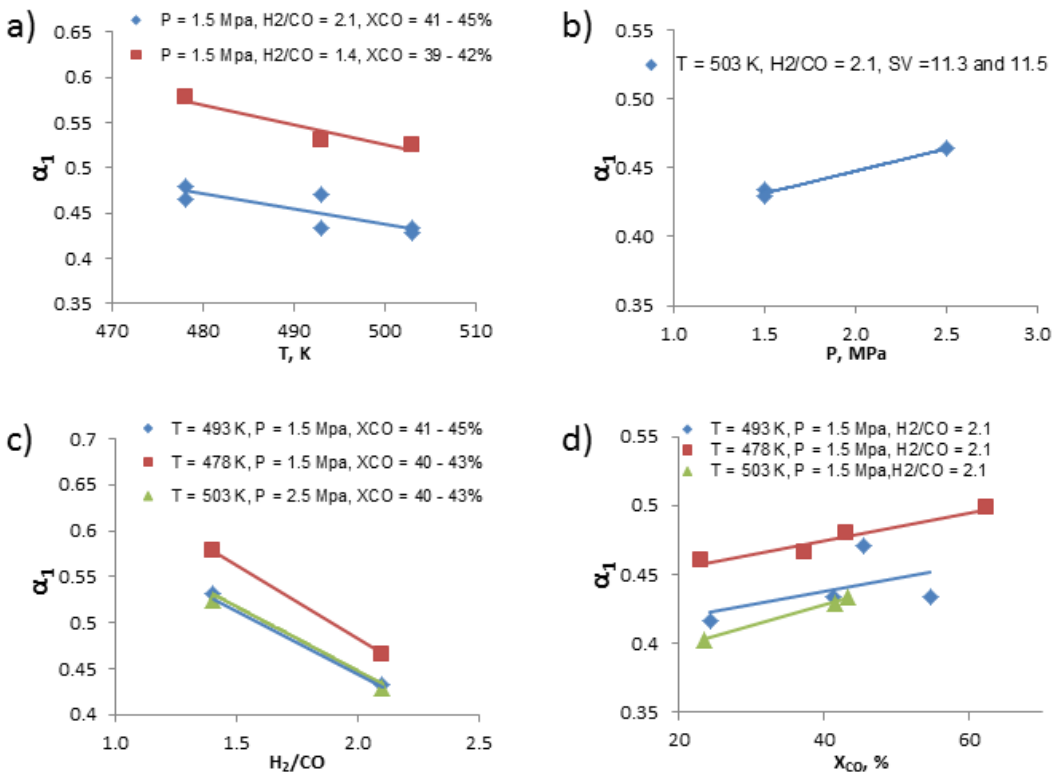

Figure 3.31 - Variation of C_1 chain growth probability (α_1)at different: a) temperature; b) pressure; c) H_2/CO feed ratio; and d) CO conversions.

Effect of water on FTS selectivity

Another important variable that influences FTS selectivity is the partial pressure of water. While the effect of water on FTS reaction rate is somewhat controversial and seems to depend on the catalyst support [106], the change of water partial pressure is well known to have an effect on C_{5+} and CH_4 selectivity [101, 106, 107, 119, 347, 348]. Our results show that increasing the water partial pressure is correlated with increased selectivity towards C_{5+} (Figure 3.32) and a decrease in methane formation. Also, the increase of water partial pressure is known to inhibit olefin secondary reactions and its effect is competing with the effect of residence time, where the latter tends to be more dominant [348]. The most common explanation for the effect water on C_{5+} and CH_4 is that secondary hydrogenation and isomerization are inhibited, while readsorption is unaffected or even enhanced [348]. Our data indicate that olefin readsorption as a whole has only a negligible effect and that both C_{5+} and CH_4 selectivity are primarily determined

by α_1, so it follows that water could induce a change in selectivity by affecting C_1 growth probability. However, it should be pointed out that in our analysis variations in water partial pressures were caused by changes in conversion level, so additional kinetic effects could have contributed to the results.

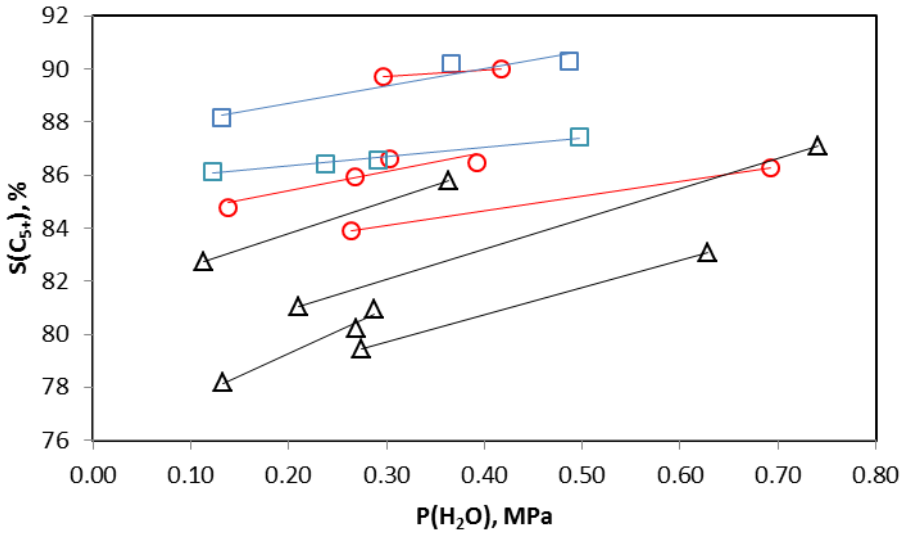

Figure 3.32 - Correlation between the partial pressure of water and C_{5+} selectivity (● - Run 1; ■ – Run 2; ▲ – Run 3; lines are connecting points at same T, P and H_2/CO).

Several researchers have studied this problem by externally adding water to the reactor feed [101, 119, 348-350]. The advantage of these studies was that only water partial pressure could be varied, while keeping other process parameters (e.g., conversion) constant. Bertole et al. [349] reported an increase in a single α, calculated for the C_{8+} range, with partial pressure of water, which they correlated with an increase in the surface concentration of active carbon. They calculated the amounts of active carbon by using the number of labeled C-atoms in methane and selectivity to methane. However, considering that methane deviates significantly for the typical polymerization scheme that other FTS products exhibit, it is questionable whether the conclusions drawn from its formation can be extrapolated for the entire spectrum of FTS products. Lögdberg et al. [119] showed that co-feeding water resulted in a significant increase in α_1, albeit the growth probability of C_2 seemed to be unaffected while α_3 and α_4 exhibited negligible decreases. It is

possible that water partial pressure does not significantly impact intrinsic FTS propagation probabilities as much as it attenuates the additional methane that is formed (i.e., the deviation observed in the ASF plot) and by that changes α_1. The adsorption of water on the secondary active sites responsible for methanation, i.e. inhibition of this reaction by water, and the corresponding increase in α_1 could be the intrinsic kinetic reason for most of the selectivity changes related to water.

Intrinsic kinetic explanations for deviations from the ASF distribution

The difference in the slopes of formation of two main types of products (Figure 3.16c) is the apparent reason why the total hydrocarbon distribution exhibits a bend, i.e. non-ASF behavior (Figure 3.16a). If we accept that both 1-olefins and n-paraffins are the primary products of FTS [174] and that they have a common precursor [311], then a simple polymerization scheme would yield the same slopes (i.e., parallel distributions) for n-paraffins and 1-olefins, and this would result in a classical ASF distribution. A probable reason for deviation from the ASF model is a rapid decrease in 1-olefin formation with carbon number, but additional concepts that explain non-ASF behavior, e.g. double-alpha and the effect of product accumulation, exist as well. As shown above, the lack of variation in C_{2+} growth probability values with changes in conversion level suggests that the reactor residence time dependent olefin readsorption (e.g., solubility, vapor pressure, and diffusion enhanced) could only have a negligible effect on the FTS selectivity. Kuipers et al. [109, 134] postulated that the physisorption layer could function as an "umbilical cord" keeping the olefins close to the surface after the chemical bond is broken and increasing the probability for readsorption with increased chain length. This means that effectively 1-olefin surface residence time would be increased, and not only their reactor residence time; in this case 1-olefin desorption from the physisorbed layer is considered a rate determining step. Therefore, this concept implies the existence of a mass transfer limitation, which is something experimental co-feeding studies do not seem to support [164, 351]. In addition, the driving force for desorption from the physisorbed layer would include a 1-olefin concentration term, which has to depend on the reactor residence time. However, this is not consistent with our experimental results, as explained

above. A somewhat similar explanation, chain length dependent olefin desorption, was introduced by Botes [150, 169] for an Fe-based catalyst. He argued that the activation energy for the olefin desorption step increases with increasing chain length, due to weak physical interactions [229]. This intrinsic kinetic concept included an exponential dependency of carbon number in the olefin desorption rate, which was suggested to be the key in explaining the OPR and growth probability behavior as a function of carbon number. Our recent kinetic modeling studies [228, 229] show that this concept can be used to predict trends of increasing chain growth probability and the exponential decrease of 1-olefin-to-n-paraffin ratio with carbon number over Co-based catalyst. The probable cause for an increase in activation energy of 1-olefin desorption could be the formation of a π-complex stabilized by weak Van der Waals forces [62, 351, 352]. A low yield of ethylene and its high reactivity in secondary reactions compared to higher olefins might be explained by the stronger chemical bond of its π-complex with the surface [353]. In this type of scheme the termination rate determining steps would be desorption to 1-olefin from the π-complex and hydrogenation of the adsorbed σ-complex to n-paraffin (Figure 2.6), consistent with results of previous studies [354]. However, the chain length dependent 1-olefin desorption is still a relatively new concept in terms of FTS product distribution kinetics and additional studies are needed to further validate it. As discussed below, alternative explanations are also possible.

Conclusions

We can draw the following conclusions about cobalt catalyst from the presented study:

- Most of the variations in selectivity of C_1 and C_{5+} with process conditions can be traced back to changes in C_1 intermediate growth probability (α_1). Increasing α_1 leads to a decrease in CH_4 and an increase in C_{5+} selectivity. Our experimental results show that the greatest influence on α_1 can be achieved by decreasing the H_2/CO feed ratio, but that decreasing temperature, increasing pressure and increasing conversion also result in increases of α_1 as well. The mechanistic reasons for this change are still not understood, but the most plausible explanation seems to be the existence of a secondary pathway for the production of extra methane that is responsible for the deviation from ASF behavior.

This pathway is most likely severely inhibited by water, resulting in lower methane selectivity at higher partial pressures of water (e.g., at higher levels of conversion or during water co-feeding).

- The chain growth probabilities for C_{2+} hydrocarbons do not significantly change with process conditions. The lack of α_{C2+} variation with residence time suggests that 1-olefin readsorption and continued chain growth could only have a minor effect on the FTS product distribution over the examined catalyst and conditions used. Consistent with the literature on 1-olefin co-feeding, secondary hydrogenation and to a smaller extent isomerization of 1-olefins seem to be the dominant 1-olefin secondary reaction, and they are most sensitive to changes in the H_2/CO feed ratio and conversion level (i.e. residence time).
- The typical deviations from the classical ASF distribution in the C_{3+} range, i.e. increasing α_n and an exponential decrease of OPR with carbon number, have been observed in our experiments. Since n-paraffins and 1-olefins exhibit differences in their formation rates as a function of chain length (i.e., resulting in different slopes), the apparent kinetic data could be modeled by applying a chain length dependency on the desorption rates of 1-olefins. However, other kinetic explanations are possible and this aspect requires further study. Additionally, in future work, the effect of product accumulation must be examined further in order to decouple its influence from the kinetic data.

4. Detailed kinetic model of FTS

Publications from this chapter

1. Branislav Todic, Tejas Bhatelia, Wenping Ma, Gary Jacobs, Burtron H. Davis, Dragomir B. Bukur, "Kinetic Model of Fischer−Tropsch Synthesis in a Slurry Reactor on Co−Re/Al_2O_3 Catalyst", *Industrial and Engineering Chemistry Research*, **2013**, 52, 669.
2. Branislav Todic, Wenping Ma, Gary Jacobs, Burtron H. Davis, Dragomir B. Bukur, "CO-insertion mechanism based kinetic model of the Fischer–Tropsch synthesis reaction over Re-promoted Co catalyst", *Catalysis Today*, **2014**, 228, 32.

Even though some selectivity models can describe product distributions very well, their shortcoming is failing to provide a deeper understanding of FTS reaction kinetics. A distinct advantage of detailed kinetic models over hydrocarbon selectivity models is that the detailed kinetic model has a more realistic interpretation of the FTS reaction mechanism, and product formation rate equations contain the intrinsic kinetic parameters.

In this study, we employed coupling of the mechanistic approach based on various forms of the carbide mechanism and a form of the CO-insertion mechanism with Botes's [169] concept of chain-length-dependent olefin desorption. This yields a kinetic model capable of describing experimentally obtained product distributions, including previously described trends with carbon number.

4.1. Carbide mechanism based detailed kinetic models

Carbide-based mechanisms

The carbide mechanism is the one most often used in kinetic modeling. The main characteristic of this mechanism is that the hydrocarbons are formed by successive addition of a building unit of one carbon atom (and no oxygen atom) into the growing chain. Ten different interpretations of the carbide mechanism were taken from the literature [222] and coupled with the chain-length-dependent olefin desorption concept to

derive kinetic models (designated FTS-I to FTS-X). Table 4.1 provides the FTS-I reaction pathway, while others can be found in Table 4.2.

Table 4.1 - FTS-I reaction pathway and kinetic parameters.

No.	Elementary reaction	kinetic constant
1^{RDS}	$CO + H\text{-}S \rightarrow H\text{-}S\text{-}CO$ $CO + CH_3\text{-}S \rightarrow CH_3\text{-}S\text{-}CO$ $CO + C_nH_{2n+1}\text{-}S \rightarrow C_nH_{2n+1}\text{-}S\text{-}CO$	$\mathbf{k_1}$
2	$H\text{-}S\text{-}CO + H_2 \leftrightarrow H\text{-}S\text{-}C + H_2O$ $CH_3\text{-}S\text{-}CO + H_2 \leftrightarrow CH_3\text{-}S\text{-}C + H_2O$ $C_nH_{2n+1}\text{-}S\text{-}CO + H_2 \leftrightarrow C_nH_{2n+1}\text{-}S\text{-}C + H_2O$	$\mathbf{K_2}$
3	$H\text{-}S\text{-}C + H_2 \leftrightarrow H\text{-}S\text{-}CH_2$ $CH_3\text{-}S\text{-}C + H_2 \leftrightarrow CH_3\text{-}S\text{-}CH_2$ $C_nH_{2n+1}\text{-}S\text{-}C + H_2 \leftrightarrow C_nH_{2n+1}\text{-}S\text{-}CH_2$	$\mathbf{K_3}$
4	$C_nH_{2n+1}\text{-}S\text{-}CH_2 \leftrightarrow C_nH_{2n+1}\,CH_2\text{-}S$	$\mathbf{K_4}$
5^{RDS}	$CH_3\text{-}S + H_2 \rightarrow CH_4 + H\text{-}S$ $C_nH_{2n+1}\text{-}S + H_2 \rightarrow C_nH_{2n+2} + H\text{-}S$	$\mathbf{k_{5M}}$ $\mathbf{k_5}$
6^{RDS}	$C_2H_5\text{-}S \rightarrow C_2H_4 + H\text{-}S$ $C_nH_{2n+1}\text{-}S \rightarrow C_nH_{2n} + H\text{-}S$	$\mathbf{k_{6E}}$ $\mathbf{k_{6n}}$
7	$H_2 + 2S \leftrightarrow 2H\text{-}S$	$\mathbf{K_7}$

Table 4.2 - Reaction pathways of different FTS models (FTS II-X).

FTS-II

No.	Elementary reaction | constant	
1	$CO + S \leftrightarrow CO\text{-}S$	K_1
2	$CO\text{-}S + H_2 \leftrightarrow H_2CO\text{-}S$	K_2
3	$H_2CO\text{-}S + H_2 \leftrightarrow CH_2\text{-}S + H_2O$	K_3
4	$H_2 + 2S \leftrightarrow 2H\text{-}S$	K_4
5*	$CH_2\text{-}S + H\text{-}S \rightarrow CH_3\text{-}S + S$ $CH_2\text{-}S + C_nH_{2n+1}\text{-}S \rightarrow C_nH_{2n+1}\,CH_2\text{-}S + S$	k_5
6*	$CH_3\text{-}S + H\text{-}S \rightarrow CH_4 + 2S$ $C_nH_{2n+1}\text{-}S + H\text{-}S \rightarrow C_nH_{2n+2} + 2S$	k_{6M} k_6
7*	$C_2H_5\text{-}S \rightarrow C_2H_4 + H\text{-}S$ $C_nH_{2n+1}\text{-}S \rightarrow C_nH_{2n} + H\text{-}S$	k_{7E} $k_{7,n}$

FTS-III

No.	Elementary reaction | constant	
1	$CO + S \leftrightarrow CO\text{-}S$	K_1
2	$CO\text{-}S + H_2 \leftrightarrow H_2CO\text{-}S$	K_2
3	$H_2CO\text{-}S + H_2 \leftrightarrow CH_2\text{-}S + H_2O$	K_3
4	$H_2 + 2S \leftrightarrow 2H\text{-}S$	K_4
5*	$CH_2\text{-}S + H\text{-}S \rightarrow CH_3\text{-}S + S$ $CH_2\text{-}S + CH_3\text{-}S \rightarrow CH_3CH_2\text{-}S + S$ $CH_2\text{-}S + C_nH_{2n+1}\text{-}S \rightarrow C_nH_{2n+1}\,CH_2\text{-}S + S$	k_5
6*	$CH_3\text{-}S + H_2 \rightarrow CH_4 + H\text{-}S$ $C_nH_{2n+1}\text{-}S + H_2 \rightarrow C_nH_{2n+2} + H\text{-}S$	k_{6M} k_6
7*	$C_2H_5\text{-}S \rightarrow C_2H_4 + H\text{-}S$ $C_nH_{2n+1}\text{-}S \rightarrow C_nH_{2n} + H\text{-}S$	k_{7E} $k_{7,n}$

FTS-IV

No.	Elementary reaction | constant	
1	$CO + S \leftrightarrow CO\text{-}S$	K_1
2	$CO\text{-}S + H_2 \leftrightarrow H_2CO\text{-}S$	K_2
3	$H_2CO\text{-}S + H_2 \leftrightarrow CH_2\text{-}S + H_2O$	K_3
4	$H_2 + 2S \leftrightarrow 2H\text{-}S$	K_4
5*	$CH_2\text{-}S + CH_2\text{-}S \rightarrow CH_2CH_2\text{-}S + S$ $CH_2\text{-}S + C_nH_{2n}\text{-}S \rightarrow C_nH_{2n}\,CH_2\text{-}S + S$	k_5
6	$C_nH_{2n}\text{-}S + H\text{-}S \leftrightarrow C_nH_{2n+1}\text{-}S + S$	K_6
7*	$CH_3\text{-}S + H\text{-}S \rightarrow CH_4 + S$ $C_nH_{2n+1}\text{-}S + H\text{-}S \rightarrow C_nH_{2n+2} + S$	k_{7M} k_7
8*	$C_2H_5\text{-}S \rightarrow C_2H_4 + H\text{-}S$ $C_nH_{2n}\text{-}S \rightarrow C_nH_{2n} + S$	k_{8E} $k_{8,n}$

FTS-V

No.	Elementary reaction | constant	
1	$CO + S \leftrightarrow CO\text{-}S$	K_1
2	$CO\text{-}S + H\text{-}S \leftrightarrow HCO\text{-}S$	K_2
3	$HCO\text{-}S + H\text{-}S \leftrightarrow C\text{-}S + H_2O\text{-}S$	K_3
4	$H_2O\text{-}S \leftrightarrow H_2O + S$	K_4
5	$C\text{-}S + H\text{-}S \leftrightarrow CH\text{-}S + S$	K_5
6	$CH\text{-}S + H\text{-}S \leftrightarrow CH_2\text{-}S + S$	K_6
7*	$CH_2\text{-}S + H\text{-}S \rightarrow CH_3\text{-}S + S$ $CH_2\text{-}S + CH_3\text{-}S \rightarrow CH_3CH_2\text{-}S + S$ $CH_2\text{-}S + C_nH_{2n+1}\text{-}S \rightarrow C_nH_{2n+1}\,CH_2\text{-}S + S$	k_7
8*	$CH_3\text{-}S + H\text{-}S \rightarrow CH_4 + 2S$ $C_nH_{2n+1}\text{-}S + H\text{-}S \rightarrow C_nH_{2n+2} + 2S$	k_{8M} k_8
9*	$CH_3\text{-}S + H\text{-}S \rightarrow CH_4 + 2S$ $C_nH_{2n+1}\text{-}S \rightarrow C_nH_{2n} + H\text{-}S$	k_{9E} $k_{9,n}$
10	$H_2 + 2S \leftrightarrow 2H\text{-}S$	K_{10}

FTS-VI

No.	Elementary reaction | constant	
	$CO + H\text{-}S \leftrightarrow H\text{-}S\text{-}CO$	
1	$CO + CH_3\text{-}S \leftrightarrow CH_3\text{-}S\text{-}CO$ $CO + C_nH_{2n+1}\text{-}S \leftrightarrow C_nH_{2n+1}\text{-}S\text{-}CO$	K_1
2*	$H\text{-}S\text{-}CO + H_2 \rightarrow H\text{-}S\text{-}C + H_2O$ $CH_3\text{-}S\text{-}CO + H_2 \rightarrow CH_3\text{-}S\text{-}C + H_2O$ $C_nH_{2n+1}\text{-}S\text{-}CO + H_2 \rightarrow C_nH_{2n+1}\text{-}S\text{-}C + H_2O$ $H\text{-}S\text{-}C + H_2 \leftrightarrow H\text{-}S\text{-}CH_2$	k_2
3	$CH_3\text{-}S\text{-}C + H_2 \leftrightarrow CH_3\text{-}S\text{-}CH_2$ $C_nH_{2n+1}\text{-}S\text{-}C + H_2 \leftrightarrow C_nH_{2n+1}\text{-}S\text{-}CH_2$	K_3
4	$C_nH_{2n+1}\text{-}S\text{-}CH_2 \leftrightarrow C_nH_{2n+1}\,CH_2\text{-}S$	K_4
5*	$CH_3\text{-}S + H_2 \rightarrow CH_4 + H\text{-}S$ $C_nH_{2n+1}\text{-}S + H_2 \rightarrow C_nH_{2n+2} + H\text{-}S$	k_{5M} k_5
6*	$C_2H_5\text{-}S \rightarrow C_2H_4 + H\text{-}S$ $C_nH_{2n+1}\text{-}S \rightarrow C_nH_{2n} + H\text{-}S$	$k_{6E,}$ $k_{6,n}$
7	$H_2 + 2S \leftrightarrow 2H\text{-}S$	K_7

FTS-VII

No.	Elementary reaction | constant	
	$CO + H\text{-}S \leftrightarrow H\text{-}S\text{-}CO$	
1	$CO + CH_3\text{-}S \leftrightarrow CH_3\text{-}S\text{-}CO$ $CO + C_nH_{2n+1}\text{-}S \leftrightarrow C_nH_{2n+1}\text{-}S\text{-}CO$	K_1
2	$H\text{-}S\text{-}CO + H_2 \leftrightarrow H\text{-}S\text{-}C + H_2O$ $CH_3\text{-}S\text{-}CO + H_2 \leftrightarrow CH_3\text{-}S\text{-}C + H_2O$ $C_nH_{2n+1}\text{-}S\text{-}CO + H_2 \leftrightarrow C_nH_{2n+1}\text{-}S\text{-}C$ $H\text{-}S\text{-}C + H_2 \rightarrow H\text{-}S\text{-}CH_2$	K_2
3	$CH_3\text{-}S\text{-}C + H_2 \rightarrow CH_3\text{-}S\text{-}CH_2$ $C_nH_{2n+1}\text{-}S\text{-}C + H_2 \rightarrow C_nH_{2n+1}\text{-}S\text{-}CH_2$	k_3
4	$C_nH_{2n+1}\text{-}S\text{-}CH_2 \rightarrow C_nH_{2n+1}\,CH_2\text{-}S$	K_4
5	$CH_3\text{-}S + H_2 \rightarrow CH_4 + H\text{-}S$ $C_nH_{2n+1}\text{-}S + H_2 \rightarrow C_nH_{2n+2} + H\text{-}S$	k_{5M} k_5
6	$C_2H_5\text{-}S \rightarrow C_2H_4 + H\text{-}S$ $C_nH_{2n+1}\text{-}S \rightarrow C_nH_{2n} + H\text{-}S$	k_{6E} $k_{6,n}$
7	$H_2 + 2S \leftrightarrow 2H\text{-}S$	K_7

FTS-VIII

No.	Elementary reaction | constant	
1	$CO + S \leftrightarrow CO\text{-}S$	K_1
2	$CO\text{-}S + S \leftrightarrow C\text{-}S + O\text{-}S$	K_2
3	$C\text{-}S + H_2 \leftrightarrow CH_2\text{-}S$	K_3
4	$O\text{-}S + H_2 \leftrightarrow H_2O$	K_4
5	$H_2 + 2S \leftrightarrow 2H\text{-}S$	K_5
6*	$CH_2\text{-}S + H\text{-}S \rightarrow CH_3\text{-}S + S$ $CH_2\text{-}S + CH_3\text{-}S \rightarrow CH_3CH_2\text{-}S + S$ $CH_2\text{-}S + C_nH_{2n+1}\text{-}S \rightarrow C_nH_{2n+1}\,CH_2\text{-}S + S$	k_6
7*	$CH_3\text{-}S + H_2 \rightarrow CH_4 + 2S$ $C_nH_{2n+1}\text{-}S + H_2 \rightarrow C_nH_{2n+2} + 2S$	k_{7M} k_7
8*	$C_2H_5\text{-}S \rightarrow C_2H_4 + H\text{-}S$ $C_nH_{2n+1}\text{-}S \rightarrow C_nH_{2n} + H\text{-}S$	$k_{8E,}$ $k_{8,n}$

FTS-IX

No.	Elementary reaction | constant	
	$CO + H\text{-}S \rightarrow H\text{-}S\text{-}CO$	
1*	$CO + CH_3\text{-}S \rightarrow CH_3\text{-}S\text{-}CO$ $CO + C_nH_{2n+1}\text{-}S \rightarrow C_nH_{2n+1}\text{-}S\text{-}CO$ $H\text{-}S\text{-}CO + H_2 \leftrightarrow H\text{-}S\text{-}C + HO\text{-}S$	k_1
2	$CH_3\text{-}S\text{-}CO + H_2 \leftrightarrow CH_3\text{-}S\text{-}C + HO\text{-}S$ $C_nH_{2n+1}\text{-}S\text{–}CO + H_2 \leftrightarrow C_nH_{2n+1}\text{-}S\text{–}C + HO\text{-}S$	K_2
3	$C_nH_{2n+1}\text{-}S\text{-}C + H\text{-}S \leftrightarrow C_nH_{2n+1}\text{-}S\text{-}CH$	K_3
4	$C_nH_{2n+1}\text{-}S\text{-}CH + H\text{-}S \leftrightarrow C_nH_{2n+1}\text{-}S\text{–}CH_2$	K_4
5	$C_nH_{2n+1}\text{-}S\text{-}CH_2 \leftrightarrow C_nH_{2n+1}\,CH_2\text{-}S$	K_5
6	$HO\text{-}S + H\text{-}S \leftrightarrow H_2O$	K_6
7*	$CH_3\text{-}S + H\text{-}S \rightarrow CH_4 + 2S$ $C_nH_{2n+1}\text{-}S + H\text{-}S \rightarrow C_nH_{2n+2} + 2S$	k_{7M} k_7
8*	$C_2H_5\text{-}S \rightarrow C_2H_4 + H\text{-}S$ $C_nH_{2n+1}\text{-}S \rightarrow C_nH_{2n} + H\text{-}S$	k_{8E} $k_{8,n}$
9	$H_2 + 2S \leftrightarrow 2H\text{-}S$	K_9

FTS-X

No.	Elementary reaction | constant	
	$CO + H\text{-}S \leftrightarrow H\text{-}S\text{-}CO$	
1	$CO + CH_3\text{-}S \leftrightarrow CH_3\text{-}S\text{-}CO$ $CO + C_nH_{2n+1}\text{-}S \leftrightarrow C_nH_{2n+1}\text{-}S\text{-}CO$ $H\text{-}S\text{-}CO + H_2 \rightarrow H\text{-}S\text{-}C + HO\text{-}S$	K_1
2*	$CH_3\text{-}S\text{-}CO + H_2 \rightarrow CH_3\text{-}S\text{-}C + HO\text{-}S$ $C_nH_{2n+1}\text{-}S\text{–}CO + H_2 \rightarrow C_nH_{2n+1}\text{-}S\text{–}C + HO\text{-}S$	k_2
3	$C_nH_{2n+1}\text{-}S\text{-}C + H\text{-}S \leftrightarrow C_nH_{2n+1}\text{-}S\text{-}CH$	K_3
4	$C_nH_{2n+1}\text{-}S\text{-}CH + H\text{-}S \leftrightarrow C_nH_{2n+1}\text{-}S\text{–}CH_2$	K_4
5	$C_nH_{2n+1}\text{-}S\text{-}CH_2 \leftrightarrow C_nH_{2n+1}\,CH_2\text{-}S$	K_5
6	$HO\text{-}S + H\text{-}S \leftrightarrow H_2O$	K_6
7*	$CH_3\text{-}S + H\text{-}S \rightarrow CH_4 + 2S$ $C_nH_{2n+1}\text{-}S + H\text{-}S \rightarrow C_nH_{2n+2} + 2S$	k_{7M} k_7
8*	$C_2H_5\text{-}S \rightarrow C_2H_4 + H\text{-}S$ $C_nH_{2n+1}\text{-}S \rightarrow C_nH_{2n} + H\text{-}S$	k_{8E} $k_{8,n}$
9	$H_2 + 2S \leftrightarrow 2H\text{-}S$	K_9

Chain length dependent 1-olefin desorption

One of the key assumptions of our models is that the 1-olefin desorption rate constant depends exponentially on carbon number, due to linearly increasing activation energy of the 1-olefin desorption [169]. This dependency is caused by the weak Van der Waal's (VdW) interactions of the 1-olefin precursor, a π-complex (Figure 2.6), with the catalyst surface. Nguyen et al. [352] modeled olefin adsorption on the surface of a zeolite. Coupling density function theory (DFT) and statistical thermodynamic calculations, the authors showed that inclusion of weak Van der Waal's forces leads to linearly increasing chemisorption energy with chain length. Cheng et al. [62, 351] also followed the same general idea and a theoretical approach (based on an ab-initio DFT study) and showed that adding VdW interactions increases the chemisorption energy of 1-olefin and, in turn, leads to the explanation of non-ASF product distribution and decrease of OPR with carbon number.

In our recent study [229] we showed that the linear dependency of the heats of chemisorption of 1-olefins with carbon number results in a linear dependency of desorption activation energy:

$$E_{d,o}^{n} = E_{d,o}^{0} + \Delta E * n \tag{4.1}$$

This is then used to directly derive the 1-olefin desorption rate constant, which has an exponential dependency with carbon number:

$$k_{d,n} = k_{d,0} * e^{c*n} \tag{4.2}$$

Constant c in equation (2) is related to the weak VdW interactions by the following relation:

$$c = -\frac{\Delta E}{R*T} \tag{4.3}$$

where ΔE is the contribution of VdW interactions of the chain with the surface for every C-atom (or CH_2-group).

The formation of 1-olefin molecule consists of two steps: β-hydrogen elimination from the growing chain (C_nH_{2n+1}-S, σ-complex) and desorption of the π-complex, whereby the latter is considered to be rate limiting. Our mechanism groups these two steps into a hypothetical one-step desorption process (Figure 4.1) [355]. As the chain length increases, the VdW attractive forces cause an increase in the activation energy for

the one-step desorption of 1-olefin ($E^n_{d,o}$ in Figure 4.1), which is followed by a decreased probability in 1-olefin formation. Therefore, we will see a higher residence time of the adsorbed alkyl chain (σ-complex) on the surface, which is in equilibrium with the π-complex, and this in turn results in a higher probability for chain growth and hydrogenation to n-paraffin with increasing chain length.

Potential secondary reactions of initially formed 1-olefins are hydrogenation, isomerization and readsorption. These reactions are not considered in the present models.

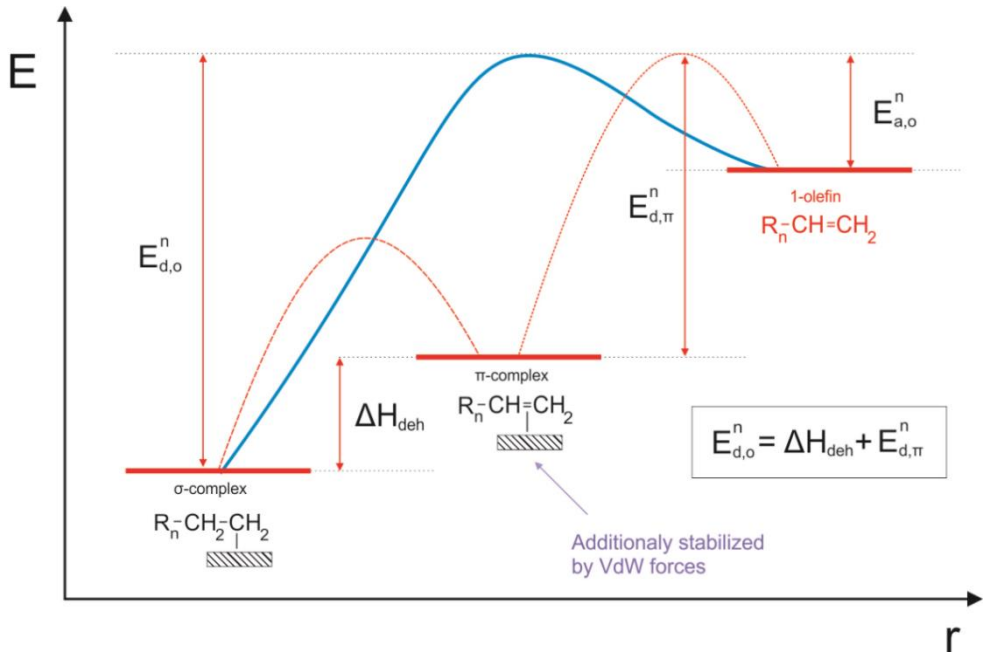

Figure 4.1 - Potential energy diagram for the 1-olefin desorption step.

Derivation of rate equations

The derivation starts with a form of carbide mechanism and uses the LHHW approach to relate the rate of hydrocarbon formation with the partial pressures of reacting gases and intrinsic kinetic (rate and equilibrium) constants of elementary reactions. The methodology applied has been well established by authors who developed detailed kinetic models of FTS in the past, mainly Lox and Froment [214] and Li and co-workers.[216, 217, 219-222] The derivation makes use of the following assumptions:

- only one type of FTS active site is present on the Co catalyst surface;
- the total number of active sites on the catalyst surface is constant;
- the concentrations of surface intermediates and vacant sites are at steady state;
- methane and ethylene have different formation rate constants than other n-paraffins and 1-olefins, respectively;
- rate constants of chain propagation and hydrogenation to n-paraffin are independent of carbon number;
- the rate constant of chain desorption to form 1-olefin is exponentially dependent on carbon number (Equation 4.2); and
- elementary steps for the formation of n-paraffins and 1-olefins are rate determining steps (RDS), as is one of the elementary steps involved in chain propagation or monomer formation. All other elementary steps are considered to be quasi-equilibrated.

We will give an example of model derivation for model FTS-I. Elementary reactions are given in

Table 4.1. It is assumed that elementary steps 1, 5 and 6 are rate determining steps, while the other steps are considered to be sufficiently rapid to be pseudo-equilibrated. Rates of formation of n-paraffin and 1-olefin with n number of C-atoms can be written as:

$$R_{C_nH_{2n+2}} = k_5[C_nH_{2n+1} - S]P_{H_2} \qquad n \geq 2 \qquad (4.4)$$

$$R_{C_nH_{2n}} = k_{6,0}e^{c\cdot n}[C_nH_{2n+1} - S] \qquad n \geq 3 \qquad (4.5)$$

where $[C_nH_{2n+1} - S]$ is a surface fraction of adsorbed species C_nH_{2n+1}-S.

Methane and ethylene are assumed to have different formation rate constants:

$$R_{CH_4} = k_{5M}[CH_3 - S]P_{H_2} \qquad (4.6)$$

$$R_{C_2H_4} = k_{6E,0}e^{c\cdot 2}[C_2H_5 - S] \qquad (4.7)$$

The chain growth probability factor for a molecule having n number of carbon atoms (α_n) is defined as:

$$\alpha_n = \frac{[C_n H_{2n+1} - S]}{[C_{n-1} H_{2n-1} - S]} \qquad n \geq 3 \qquad (4.8)$$

The pseudo-steady-state hypothesis (PSSH) is applied for the fraction of C_nH_{2n+1}-S surface intermediate:

$$-\frac{d[C_n H_{2n+1} - S]}{dt} = -k_1 P_{CO}[C_{n-1} H_{2n-1} - S] + k_1 P_{CO}[C_n H_{2n+1} - S] + k_5 P_{H_2}[C_n H_{2n+1} - S] + k_{6,0} e^{c \cdot n}[C_n H_{2n+1} - S] = 0 \qquad n \geq 3 \quad (4.9)$$

Rearranging equation (4.9) and combining it with (4.8) reduces to the following form:

$$\alpha_n = \frac{k_1 P_{CO}}{k_1 P_{CO} + k_5 P_{H_2} + k_{6,0} e^{c \cdot n}} \qquad n \geq 3 \qquad (4.10)$$

where α_n is dependent on n through the exponential term in the denominator.

Because methane and ethylene have different termination rate constants, growth probabilities for n=1 and n=2 should be defined separately. Using the same PSSH approach, these probabilities can be written as:

$$\alpha_1 = \frac{[CH_3 - S]}{[H - S]} = \frac{k_1 P_{CO}}{k_1 P_{CO} + k_{5M} P_{H_2}} \qquad (4.11)$$

$$\alpha_2 = \frac{[C_2 H_5 - S]}{[CH_3 - S]} = \frac{k_1 P_{CO}}{k_1 P_{CO} + k_5 P_{H_2} + k_{6E} e^{c \cdot 2}} \qquad (4.12)$$

From the definition of growth probability, Equation (S.4), it follows:

$$[C_n H_{2n+1} - S] = \alpha_n \cdot [C_{n-1} H_{2n-1} - S] = \alpha_{n-1} \cdot \alpha_n \cdot [C_{n-2} H_{2n-3} - S] = ... = \alpha_1 \cdot \alpha_2 \cdot \prod_{i=3}^{n} \alpha_i \cdot [H - S] \qquad (4.13)$$

The fraction of adsorbed hydrogen H-S can be linked with the fraction of vacant sites S from the equilibrium relation for step 7:

$$K_7 = \frac{[H-S]^2}{P_{H_2}[S]^2} \tag{4.14}$$

$$[H-S] = \sqrt{K_7 P_{H_2}}[S] \tag{4.15}$$

Substituting (4.15) into (4.13) results in the following expression:

$$\begin{aligned}&[C_n H_{2n+1} - S] = \alpha_n \cdot [C_{n-1} H_{2n-1} - S] = \alpha_{n-1} \cdot \alpha_n \cdot [C_{n-2} H_{2n-3} - S] = ... = \\ &\alpha_1 \cdot \alpha_2 \cdot \prod_{i=3}^{n} \alpha_i \cdot [H-S] = \alpha_1 \cdot \alpha_2 \cdot \prod_{i=3}^{n} \alpha_i \cdot \sqrt{K_7 P_{H_2}} \cdot [S]\end{aligned} \tag{4.16}$$

Calculation of the fraction of vacant sites S requires relating it to partial pressures and kinetic constants through a site balance. The assumption made here is that deactivation is negligible (i.e., the total number of active catalytic sites does not decrease over time).

$$\begin{aligned}&[S] + [H-S] + [H-S-CO] + [CH_3 - S - CO] + \\ &\sum_{i=3}^{n} [C_{i-1} H_{2i-1} - S - CO] + [H-S-C] + [CH_3 - S - C] + \sum_{i=3}^{n} [C_{i-1} H_{2i-1} - S - C] + \\ &[H-S-CH_2] + [CH_3 - S - CH_2] + \sum_{i=3}^{n} [C_{i-1} H_{2i-1} - S - CH_2] + [CH_3 - S] + \\ &[C_2 H_5 - S] + \sum_{i=3}^{n} [C_{i-1} H_{2i-1} - S] = 1\end{aligned} \tag{4.17}$$

Using equilibrium relations and equations (4.11)-(4.16) we can obtain the following equations for the fractions of sites covered by certain intermediates:

$$[H-S-CH_2] = \frac{1}{K_4}[CH_3 - S] = \frac{1}{K_4}\sqrt{K_7 P_{H_2}}\alpha_1 \cdot [S] \tag{4.18}$$

$$[CH_3 - S - CH_2] = \frac{1}{K_4}[C_2 H_5 - S] = \frac{1}{K_4}\sqrt{K_7 P_{H_2}}\alpha_1 \alpha_2 \cdot [S] \tag{4.19}$$

$$[C_{n-1} H_{2n-1} - S - CH_2] = \frac{1}{K_4}[C_n H_{2n} - S] = \frac{1}{K_4}\sqrt{K_7 P_{H_2}}\alpha_1 \alpha_2 \prod_{i=3}^{n} \alpha_i \cdot [S] \tag{4.20}$$

$$[H-S-C] = \frac{1}{K_3 P_{H_2}}[H-S-CH_2] = \frac{1}{K_3 K_4 P_{H_2}}\sqrt{K_7 P_{H_2}}\alpha_1 \cdot [S] \tag{4.21}$$

$$[CH_3 - S - C] = \frac{1}{K_3 P_{H_2}}[CH_3 - S - CH_2] = \frac{1}{K_3 K_4 P_{H_2}} \sqrt{K_7 P_{H_2}}\, \alpha_1 \alpha_2 \cdot [S] \tag{4.22}$$

$$[C_{n-1}H_{2n-1} - S - C] = \frac{1}{K_3 P_{H_2}}[C_{n-1}H_{2n-1} - S - CH_2] = \frac{1}{K_3 K_4 P_{H_2}} \sqrt{K_7 P_{H_2}}\, \alpha_1 \alpha_2 \prod_{i=3}^{n} \alpha_i \cdot [S] \tag{4.23}$$

$$[H - S - CO] = \frac{1}{K_2}\frac{P_{H_2O}}{P_{H_2}}[H - S - C] = \frac{1}{K_2 K_3 K_4}\frac{P_{H_2O}}{P_{H_2}^2} \sqrt{K_7 P_{H_2}}\, \alpha_1 \cdot [S] \tag{4.24}$$

$$[CH_3 - S - CO] = \frac{1}{K_2}\frac{P_{H_2O}}{P_{H_2}}[CH_3 - S - C] = \frac{1}{K_2 K_3 K_4}\frac{P_{H_2O}}{P_{H_2}^2} \sqrt{K_7 P_{H_2}}\, \alpha_1 \alpha_2 \cdot [S] \tag{4.25}$$

$$[C_{n-1}H_{2n-1} - S - CO] = \frac{1}{K_2}\frac{P_{H_2O}}{P_{H_2}}[C_{n-1}H_{2n-1} - S - C] = \frac{1}{K_2 K_3 K_4}\frac{P_{H_2O}}{P_{H_2}^2} \sqrt{K_7 P_{H_2}}\, \alpha_1 \alpha_2 \prod_{i=3}^{n} \alpha_i \cdot [S] \tag{4.26}$$

Replacing equations (4.11)-(4.15) and (4.18)-(4.26) into (4.16) and rearranging it we obtain the equation for the fraction of vacant sites as a function of partial pressures and kinetic constants:

$$[S] = 1/\{1 + \sqrt{K_7 P_{H_2}} + \sqrt{K_7 P_{H_2}} \cdot (1 + \frac{1}{K_4} + \frac{1}{K_3 K_4 P_{H_2}} + \frac{1}{K_2 K_3 K_4}\frac{P_{H_2O}}{P_{H_2}^2}) \cdot (\alpha_1 + \alpha_1 \alpha_2 + \alpha_1 \alpha_2 \sum_{i=3}^{n} \prod_{j=3}^{i} \alpha_j)\} \tag{4.27}$$

Substituting (4.27) into (4.10) and (4.12) into Equations (4.4)-(4.7) we obtain the following rate equations:

$$R_{CH_4} = k_{5M} K_7^{0.5} P_{H_2}^{1.5} \alpha_1 \cdot [S] \tag{4.28}$$

$$R_{C_nH_{2n+2}} = k_5 K_7^{0.5} P_{H_2}^{1.5} \alpha_1 \alpha_2 \prod_{i=3}^{n} \alpha_i \cdot [S] \qquad n \geq 2 \tag{4.29}$$

$$R_{C_2H_4} = k_{6E,0} e^{c \cdot 2} \sqrt{K_7 P_{H_2}}\, \alpha_1 \alpha_2 \cdot [S] \tag{4.30}$$

$$R_{C_nH_{2n}} = k_{6,0} e^{c \cdot n} \sqrt{K_7 P_{H_2}} \alpha_1 \alpha_2 \prod_{i=3}^{n} \alpha_i \cdot [S] \qquad n \geq 3 \qquad (4.31)$$

Equations (4.26)-(4.30) coupled with the equations for chain growth probabilities (4.9)-(4.11) represent model FTS-I equations. Same derivation procedure is applied to obtain rate equations of other detailed kinetic models based on carbide mechanism (Table 4.2), as well as model based on CO-insertion, which is discussed below.

Parameter estimation and model discrimination

Reactor model – Experimental data obtained over Re-promoted cobalt-alumina catalyst was used in the estimation of kinetic parameters. The range of conditions used to obtain the experimental points was discussed in the section on the effect of process conditions on the product distribution of cobalt-based catalyst (Chapter 3, Section 3.2). Experiments were conducted in a reactor that can be idealized as a continuously stirred tank reactor (CSTR), with catalyst particles of sufficiently small diameter so that the physical transport resistances can be neglected. Rate of product formation can be calculated as:

$$R_i^{\exp} = \frac{F_i}{W} \qquad (4.32)$$

where i is the product species (i = CH_4, C_2H_4, C_2H_6, …), $R_i^{\exp}$ the experimental reaction rate of i, F_i the molar flow-rate of product species i at the reactor outlet and W the catalyst mass. Species used in our modeling are C_1-C_{15} n-paraffins and C_2-C_{15} 1-olefins. Minor FTS products, like 2-olefins and oxygenates, are not considered.

Optimization methodology **-** Optimal values of different rival model parameters were estimated by minimizing a multi-response objective function [356]:

$$F_{obj} = \sum_{i=1}^{N_{resp}} \sum_{j=1}^{N_{\exp}} \left(\frac{R_{i,j}^{\exp} - R_{i,j}^{cal}}{R_{i,j}^{\exp}} \right)^2 \qquad (4.33)$$

where N_{resp} is the number of responses (n- paraffin and 1-olefin species, $N_{resp} = 29$) and $N_{\exp}$ is the number of experimental balances (conditions, $N_{\exp} = 24$). $R_{i,j}^{\exp}$ and $R_{i,j}^{cal}$ are experimental and calculated formation rates of species i in a balance j, respectively. Weighting factors were not used in the objective function, because of lack of availability of sufficient number of replicate balances, needed to calculate them.

To avoid getting trapped in a local minimum, the genetic algorithm (GA) is used as a global optimization tool, followed by the Levenberg-Marquardt (LM) method for refined local optimization [222, 357]. Another advantage of using this approach is that the GA does not require any initial guesses for the parameters. The local optimization with LM utilizes parameters estimated by the GA as initial guesses. The algorithm of the MATLAB program used for kinetic parameter estimation can be found in Figure 4.2.

The parameter estimation was first performed with isothermal data at 478, 493 and 503 K for all 10 models. Various models were discriminated based on the results of isothermal estimations. The best models at isothermal conditions were selected and non-isothermal estimation was performed on them. Based on the statistical and physicochemical tests, a final model was selected [214].

Statistical and physicochemical tests **-** Different models were compared and discriminated based on various statistical tests and the physicochemical significance of estimated kinetic parameters.

The accuracy of the model fit relative to the experimental data was obtained by statistical analysis using the mean absolute relative residual (MARR) [136, 222]:

$$MARR = \sum_{i=1}^{N_{resp}} \sum_{j=1}^{N_{\exp}} \left| \frac{R_{i,j}^{\exp} - R_{i,j}^{cal}}{R_{i,j}^{\exp}} \right| \times \frac{1}{N_{resp} \cdot N_{\exp}} \times 100\% \qquad (4.34)$$

The significances of the overall regression and estimated kinetic parameters were evaluated by the F-test and t-test, respectively. The error covariance needed for these tests was calculated from replicate baseline conditions at 493 K.

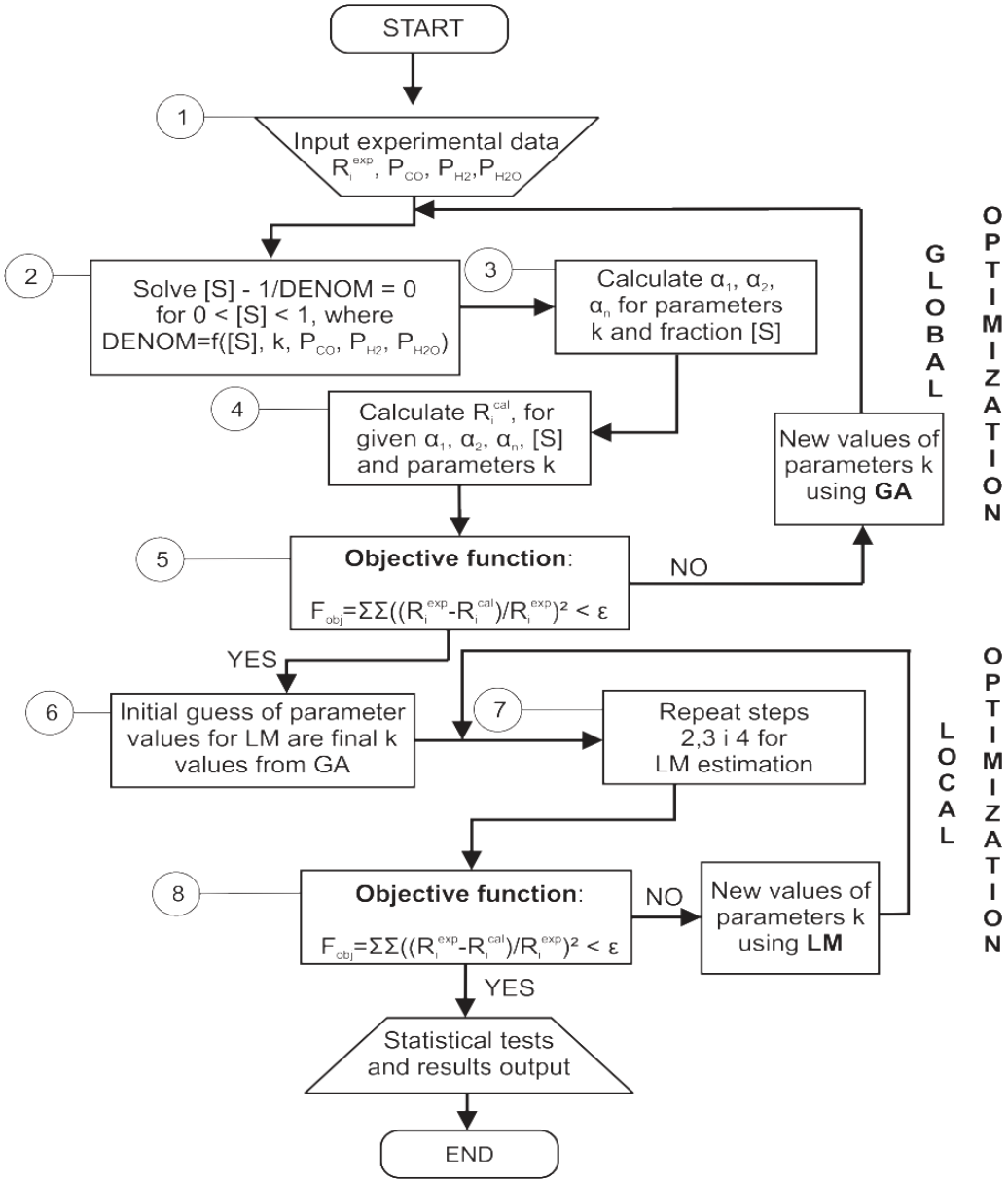

Figure 4.2 – Kinetic modeling parameter estimation algorithm.

All model parameters are intrinsic kinetic constants. Therefore, in addition to providing a good fit of the experimental data, the model parameters must satisfy physicochemical laws. Physicochemical constraints that have to be satisfied are [356, 358, 359]:

- Kinetic rate constants k_i have to obey the Arrhenius temperature dependency, with activation energy:

$$E_{a,i} > 0 \tag{4.35}$$

- Adsorption is an exothermic process so that the adsorption enthalpy has to satisfy:

$$-\Delta H^{0}_{a,i} > 0 \tag{4.36}$$

- The adsorption entropy has to satisfy two conditions [360]:

$$0 < -\Delta S^{0}_{a,i} < S^{0}_{g,i} \tag{4.37}$$

$$41.8 < -\Delta S^{0}_{a,i} < 51.4 + 1.4 \cdot 10^{-3} \Delta H^{0}_{a,i} \tag{4.38}$$

where $S^{0}_{g,i}$ is the standard entropy of a gaseous species i, $\Delta S^{0}_{a,i}$ is the standard adsorption entropy and $\Delta H^{0}_{a,i}$ is the heat of adsorption.

Isothermal parameter estimation and initial model discrimination - The kinetic model parameters (reaction rate constants k_i, the equilibrium and adsorption constants K_i and parameter c) were first estimated at isothermal conditions (478, 493 and 503 K) for 10 rival models (FTS-I to FTS-X). The searching interval in the GA for kinetic parameters k_i (rate and equilibrium constants) was set to $10^{-20} < k_i < 10^{20}$, which is considered to be a very wide range in accordance with transition state theory [357]. The parameter c was constrained between -1 and 0.

The initial model discrimination was based on the overall fit of isothermal data based on MARR values (Equation 4.34). The best models were FTS-III, FTS-X and FTS-I, with MARR of 21.2, 22.5 and 25.5%, respectively. These models were then used in parameter estimation and discrimination using the data at all temperatures simultaneously.

Non-isothermal parameter estimation and final model selection - The parameters are activation energies $E_{a,i}$, reaction and adsorption enthalpies ΔH_i, preexponential factors A_i and a weak interaction contribution to 1-olefin desorption energy ΔE. The total number of points used simultaneously in non-isothermal estimation was 696 (24 mass balances with 29 responses). In this estimation, the Arrhenius law was directly introduced, as well as the expression for the equilibrium constant [214]:

$$k_i(T) = A_i \exp(-\frac{E_{a,i}}{RT}) \quad (4.39)$$

$$K_i(T) = A_i \exp(-\frac{\Delta H_i}{RT}) \quad (4.40)$$

In order to obtain realistic values of activation energies and heats of adsorption, the estimation of these parameters were constrained to a range of literature values. Carbon monoxide and hydrogen adsorption enthalpy bounds were -50 to -200 and -10 to -100 kJ/mol [85, 361], respectively. Activation energies of chain propagation (and/or initiation), n-paraffin hydrogenation and 1-olefin desorption were kept within the ranges 50 to 150, 70 to 120 and 80 to 150 kJ/mol, respectively [92, 123, 214, 219, 222, 362]. Values of A_i were searched in a wide range of 10^{-20} to 10^{20}. Considering the values reported for weak Van der Waals interactions on metallic surfaces [210, 351, 363], the parameter ΔE was kept in a physically reasonable range of 0 - 10 kJ/mol/CH_2.

Non-isothermal parameter estimation was followed by statistical and physicochemical tests for the evaluations of models FTS-I, FTS-III and FTS-X. Although models FTS-III and FTS-X produced a good fit of the data, both returned parameters that did not satisfy physicochemical constraints for the adsorption entropy (Equation 4.37) and, as such, were discarded. Model FTS-I was consistent with physical laws and produced a good fit to the experimental data. It was chosen to be the best among the models tested.

Results and discussion

Estimated model parameters **-** Estimated parameter values of the model FTS-I are given in Table 4.3. The MARR value was 26.6 %, and the F-test showed that the model fit is statistically meaningful. Moreover, the t-test showed that all parameters are statistically different from zero [356].

Table 4.3 - Estimated parameter values for model FTS-I using the data at all temperatures.

Parameter	Value	Unit	Parameter	Value	Unit
A_1	1.83E+010	mol/(g_{cat}*h*MPa)	A_6	7.47E+08	mol/(g_{cat}*h)
E_1	100.4	kJ/mol	E_6^0	97.2	kJ/mol
A_2	5.08E+00	-	A_7	1.00E-03	MPa^{-1}
ΔH_2	8.68	kJ/mol	ΔH_7	-25.0	kJ/mol
A_3	2.44E+01	MPa^{-1}	A_{5M}	8.43E+05	mol/(g_{cat}*h*MPa)
ΔH_3	9.44	kJ/mol	E_{5M}	63.0	kJ/mol
A_4	2.90E+00	-	A_{6E}	7.03E+08	mol/(g_{cat}*h)
ΔH_4	7.9	kJ/mol	E_{6E}^0	108.8	kJ/mol
A_5	4.49E+05	mol/(g_{cat}*h*MPa)	ΔE	1.12	kJ/mol/CH_2
E_5	72.4	kJ/mol	MARR	26.6 %	

**Results of statistical tests: $F_c = 86.4 > F_{0.05}(19, 48) = 1.82$, lowest $t_c = 12.3 > t_{0.05}(19) = 1.70$*

The heat of hydrogen adsorption (ΔH_7) was -25 kJ/mol, and is similar to the reported value of -15 kJ/mol for Co-catalysts [54]. The activation energy for CO activation step (E_1), or the overall FTS energy barrier, was estimated to be 100.4 kJ/mol, which is in the middle of reported values (80-120 kJ/mol) for cobalt-based catalysts [85]. Because experimental and modeling studies have thus far not reported activation energies for termination steps on Co-catalysts, we will base our comparison to existing values for the Fe-catalysts. The paraffin formation activation energy, E_5 = 72 kJ/mol, is comparable, but slightly lower than the reported values of 80-90 kJ/mol by Dictor and Bell [92], 94 kJ/mol by Lox and Froment [214], 87 kJ/mol by Wang et al. [219] and 74 kJ/mol by Chang et al. [221].

In the present study methane was assigned a separate rate constant because of its well-known higher formation rate. One of the explanations for this is that methane has a lower energy barrier for formation compared to other paraffins. Our results also corroborate this, since the value for E_{5M} was found to be 63 kJ/mol. Because of the lower activation energy for this step methane formation from CH_3-S is more favored over chain growth, compared to higher surface chains (i.e. C_nH_{2n+1}-S with $n \geq 2$) [52]. In contrast, ethylene is known to have a lower formation rate and was therefore also provided with a

separate rate constant parameter in the model. By analogy this can likely be attributed to a higher activation energy for ethylene formation compared to other 1-olefins, caused by the higher binding strength of ethylene as discussed by Goda et al. [353]. Our results tend to confirm this view, as activation energies for ethylene and 1-olefin desorption steps (E_{6E}^0 and E_6^0) of 108 and 97 kJ/mol, respectively, were obtained from fitting of the data by the model. It is also worth noting that the olefin formation activation energies estimates are consistent with reported values in the 100-130 kJ/mol range [92, 214, 222].

Chain length dependency of 1-olefin desorption - Recognizing that the model incorporates chain-length-dependency for 1-olefin desorption, note that the activation energy E_6^0 is only a part of the activation energy of 1-olefin desorption that is independent of chain length. The actual activation energy of 1-olefin desorption is a linear function of carbon number and is different for each molecule (Equation 4.4), increasing by a value of ΔE per every CH_2 group:

$$E_{d,o}^{n}\left(\frac{kJ}{mol}\right) = 97.2 + 1.12 * n \qquad (4.41)$$

The postulated cause for this change is a weak Van der Waal's type interactions of the 1-olefin chain with the catalyst surface.[353] Recently, De Moor et al.[41] and Nguyen et al. [352] used statistical thermodynamics and computational chemistry methods to study 1-olefin adsorption on zeolites and demonstrated that including weak Van der Waals interactions with the surface indeed causes a linear increase in adsorption strength. The contribution of these forces to the strength of adsorption has been estimated to be as high as 6-8 kJ/mol/C-atom for Co-catalysts [351].

Therefore, even though weak compared to the energy of a chemical bond between an olefin chain and the active site, the cumulative effect of these forces with increasing chain length cannot be neglected. Weitkamp et al. [171] hypothesized that this could affect chain growth probability. Cheng et al. [62, 351] showed that inclusion of these interactions leads to an exponentially decreasing olefin-to-paraffin ratio and increasing chain growth probability with carbon number. Our model is in agreement with these results and shows that the change in the activation energy for the 1-olefin desorption step, caused by weak Van der Waals forces, is $\Delta E = 1.1$ kJ/mol/C-atom. This leads to a constant

c = -0.26 to -0.28 (Equation 4.3) which matches the values reported previously [108, 109, 131, 132].

Mechanism and surface species - Model FTS-I is based on a form of carbide FTS mechanism proposed by Lox and Froment [214]. Wang et al. [219] and Kim et al. [362] also used this mechanism in modeling of FTS kinetics. It is different than most commonly used forms of carbide mechanism and includes several Eley-Rideal type steps (Steps 1, 2, 3 and 5). It postulates that chain initiation proceeds by adsorption of CO on an active site with adsorbed hydrogen (H-S) (Step 1), which is considered to be a slow step and has some similarities with the H-assisted CO dissociation concept [54]. H-S-CO is subsequently hydrogenated with molecular hydrogen to H-S-CH_2 (Steps 2 and 3) and transformed to chain starter CH_3-S (Step 4). Chain propagation occurs by adsorption of CO on the active site that already contains a coverage of C_nH_{2n+1}-S (n = 1, 2 …) to form C_nH_{2n+1}-S-CO [364], followed by subsequent hydrogenation to C_nH_{2n+1}-S-CH_2 and transformation to $C_{n+1}H_{2n+3}$-S. These steps have some similarity with the chain propagation steps in the CO-insertion mechanism, because CO directly reacts with the adsorbed chain [52]. However the difference is that CO is first hydrogenated to CH_2 and only then inserted into the chain, which is consistent with the carbide mechanism. Hydrogenation of C_nH_{2n+1}-S to n-paraffin and desorption to 1-olefin are rate determining steps [354, 365].

A mechanistic LHHW kinetic model provides relevant information about species that exist on the catalyst surface. Therefore, this model provides calculated surface coverage for all species considered to be involved in the FTS carbide mechanism. Calculated coverage of adsorbed species which contain CO from our model varies between 10 and 45% depending upon the process conditions. This can be related to experimental and modeling studies which show that under FTS reaction conditions the most dominant surface species is adsorbed CO, with reported coverage in the 20 to 65% range [52, 53, 354]. The reported experimental hydrogen coverage is lower than the CO coverage (less than 10%) [311, 366] whereas in our model it is around 4%.

Model predictions of the experimental rates - Figure 4.3a shows a comparison between experimental and calculated rates of methane, of C2-C4 and C5-C15

hydrocarbon formation. The majority of the data points are within a reasonable range of error, and the calculated C_5-C_{15} rates are in a good agreement with the experimental data. The rates of carbon-monoxide and hydrogen consumption were calculated for given conditions by summing up calculated rates of hydrocarbon formations in accordance with reaction stoichiometry:

$$R_{CO} = \sum_{n=1}^{\infty} n \times (R_{C_nH_{2n+2}} + R_{C_nH_{2n}}) \tag{4.42}$$

$$R_{H_2} = \sum_{n=1}^{\infty} \left[(2n+1) \times R_{C_nH_{2n+2}} + 2n \times R_{C_nH_{2n}} \right] \tag{4.43}$$

The comparison between calculated and experimental rates for CO and H_2 consumption is shown in Figure 4.3b. Higher errors for these two species are due to the fact that they were not used in the objective function, and they were more affected by catalyst deactivation than the hydrocarbon species, as well as the fact that Equations (4.42) and (4.43) do not include formation rates of minor products (e.g. oxygenates) and heavy hydrocarbon products (> C_{15}). However, in spite of this the estimates are still within a reasonable error range.

The model provides a good prediction of the main products (n-paraffin and 1-olefin) over a wide range of conditions used. In addition to providing a good fit of n-paraffin and 1-olefin formation (Figure 4.4a, d, g), the model is also able to account for other features observed in the experiments. For example, higher methane and lower ethylene formation are also predicted.

Consistent with the literature [23, 131] calculated chain-growth probabilities α_n increased from 0.8 to 0.95 for C_3 to C_{15} hydrocarbons (Figure 4.4b, e, h). An exponential decrease in the 1-olefins to n-paraffins ratio (OPR) for C_{3+} hydrocarbons is also predicted by the proposed model (Figure 4.4 6c, f, i).

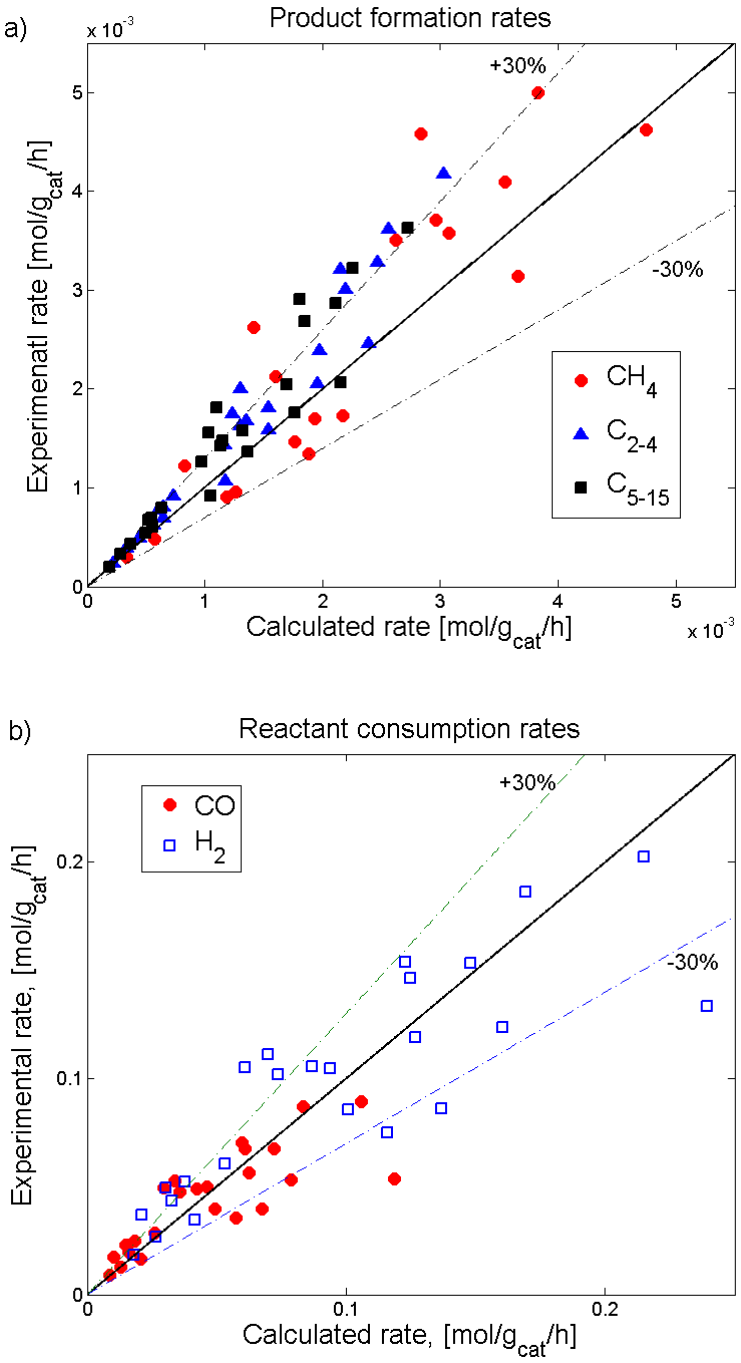

Figure 4.3 - Comparison between experimental and calculated rates of: a) methane, C2-4 and C5+ formation; b) CO and H2 consumption.

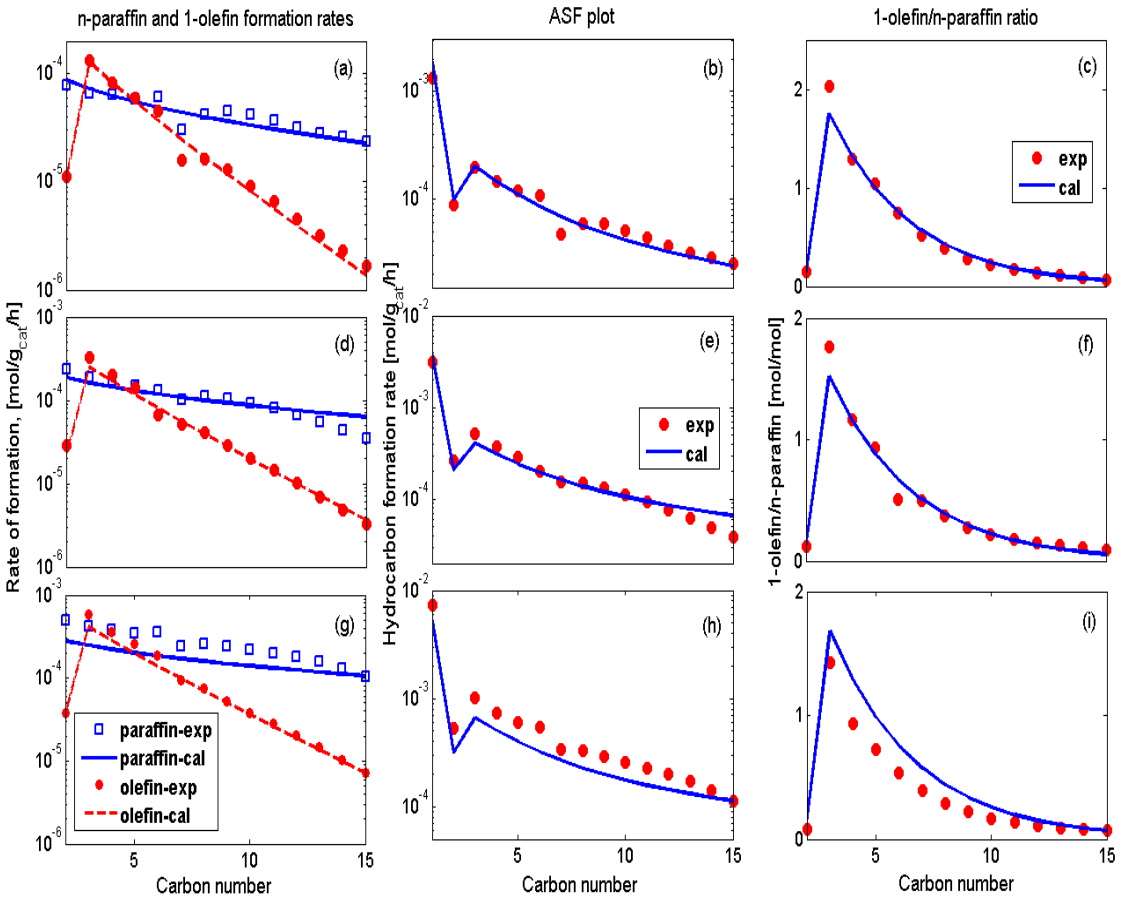

Figure 4.4 - Comparison between experimental and calculated product distributions for: a-c) T = 478 K, P = 1.5 MPa, H_2/CO = 2.1, WHSV = 3.7 NL/g_{cat}/h, X_{CO} = 37%; d-f) T = 493 K, P = 2.5 MPa, H_2/CO = 2.1, WHSV = 6.1 NL/g_{cat}/h, X_{CO} = 57%; g-i) T = 503 K, P = 2.5 MPa, H_2/CO = 2.1, WHSV = 11.5 NL/g_{cat}/h, X_{CO} = 52%.

4.2. CO-insertion based detailed kinetic model

The results of model discriminations of carbide-based detailed kinetic models pointed to a model with a mechanism which included a rate determining step that resembled that found in forms of CO-insertion mechanism. Because of this we considered CO-insertion mechanism as an additional candidate for detailed model development.

Storsæter et al. [52] compared versions of the two mechanisms - carbide (including direct and H-assisted CO dissociation) and CO-insertion - using the UBI-QEP (unity bond index – quadratic exponential potential) method [60] and micro-kinetic modeling of C_1 and C_2 species formation. Their results showed that the chosen CO-insertion pathway had a lower activation barrier compared to both direct and H-assisted CO dissociation mechanisms that were utilized. Based on these findings, they suggested that the CO-insertion mechanism is likely the main mechanism of FTS. The kinetic model shown in this section is based on the mechanism used by Storsæter et al. [52], with a few modifications (e.g. grouping of elementary steps of the same type) that are made in order to reduce the number of model parameters and facilitate calculation of products higher than C_2.

The elementary steps of the FTS mechanism and associated rate and equilibrium constants used in the model derivations are shown in Table 4.4. Steps 1 and 2 are the adsorption equilibrium steps for CO and H_2, respectively. Activation of adsorbed CO by hydrogenation to CHO-S and insertion of CO-S into the growing chain (C_nH_{2n+1}-S) are grouped into Step 3. This combined step is assumed to be rate determining and its kinetic rate constant is independent of chain length. It is followed by a series of fast hydrogenation steps in which the inserted CO is hydrogenated to CH_2, forming an extended chain $C_nH_{2n+1}CH_2$-S (Steps 4 and 5). Water formation and its removal from the surface (Step 6) are considered to be fast and at pseudo-equilibrium. Normal paraffins are formed by hydrogenation of the adsorbed alkyl chain in Step 7. Formation of 1-olefin is by dehydrogenation (β-hydrogen elimination) of C_nH_{2n+1}-S followed by desorption (Step 8). These two steps are combined into a one-step desorption process [355], which is dependent on chain length as described above.

Model equations

The final equations of the CO-insertion mechanism based detailed kinetic model are summarized below.

The chain growth probabilities are dependent on carbon number and can be calculated as:

$$\alpha_1 = \frac{k_3 K_1 P_{CO}}{k_3 K_1 P_{CO} + k_{7M}\sqrt{K_2 P_{H_2}}} \tag{4.44}$$

$$\alpha_2 = \frac{k_3 K_1 P_{CO}[S]}{k_3 K_1 P_{CO}[S] + k_7\sqrt{K_2 P_{H_2}}[S] + k_{8,E}e^{c\cdot 2}} \tag{4.45}$$

$$\alpha_n = \frac{k_3 K_1 P_{CO}[S]}{k_3 K_1 P_{CO}[S] + k_7\sqrt{K_2 P_{H_2}}[S] + k_{8,0}e^{c\cdot n}} \qquad n \geq 3 \tag{4.46}$$

where [S] is the fraction of vacant sites and is calculated by solving the site balance:

$$[S] = 1/\{1 + K_1 P_{CO} + \sqrt{K_2 P_{H_2}} + (\frac{1}{K_2^2 K_4 K_5 K_2}\frac{P_{H_2O}}{P_{H_2}^2} + \sqrt{K_2 P_{H_2}}) \cdot (\alpha_1 + \alpha_1\alpha_2 + \alpha_1\alpha_2\sum_{i=3}^{n}\prod_{j=3}^{i}\alpha_j)\} \tag{4.47}$$

Note that Equation (4.47) is an implicit non-linear function of a single variable [S]. It is solved in the 0 to 1 range with the MATLAB *fminbnd* algorithm (based on golden section search and parabolic interpolation methods).

Rates of product formation can be calculated as:

$$R_{CH_4} = k_{7M} K_2^{0.5} P_{H_2}^{0.5} \alpha_1 \cdot [S]^2 \tag{4.48}$$

$$R_{C_nH_{2n+2}} = k_7 K_2^{0.5} P_{H_2}^{0.5} \alpha_1\alpha_2 \prod_{i=3}^{n}\alpha_i \cdot [S]^2 \qquad n \geq 2 \tag{4.49}$$

$$R_{C_2H_4} = k_{8E,0} e^{c\cdot 2} \alpha_1\alpha_2 \cdot [S] \tag{4.50}$$

$$R_{C_nH_{2n}} = k_{8,0} e^{c\cdot n} \alpha_1\alpha_2 \prod_{i=3}^{n}\alpha_i \cdot [S] \qquad n \geq 3 \tag{4.51}$$

Same as for carbide mechanism based kinetic models, model parameters were estimated using a hybrid genetic algorithm and experimental data obtained with Re-promoted cobalt catalyst. They were analyzed for statistical significance and physicochemical meaningfulness.

Table 4.4 - Elementary steps of the CO-insertion mechanism used in kinetic model derivation.

No.	Elementary step	Rate and equilibrium constants	
1)	$CO + S \leftrightarrow CO\text{-}S$		K_1
2)	$H_2 + 2S \leftrightarrow 2H\text{-}S$		K_2
3^{RDS})	$CO\text{-}S + H\text{-}S \rightarrow CHO\text{-}S + S$ $CO\text{-}S + CH_3\text{-}S \rightarrow CH_3CO\text{-}S + S$ $CO\text{-}S + C_nH_{2n+1}\text{-}S \rightarrow C_nH_{2n+1}\,CO\text{-}S + S \quad n = 2, 3, \ldots$		k_3
4)	$CHO\text{-}S + H\text{-}S \leftrightarrow CH_2O\text{-}S + S$ $CH_3CO\text{-}S + H\text{-}S \leftrightarrow CH_3CHO\text{-}S + S$ $C_nH_{2n+1}\,CO\text{-}S + H\text{-}S \leftrightarrow C_nH_{2n+1}\,CHO\text{-}S + S \quad n = 2, 3, \ldots$		K_4
5)	$CH_2O\text{-}S + 2H\text{-}S \leftrightarrow CH_3\text{-}S + OH\text{-}S + S$ $CH_3CHO\text{-}S + 2H\text{-}S \leftrightarrow CH_3CH_2\text{-}S + OH\text{-}S + S$ $C_nH_{2n+1}\,CHO\text{-}S + 2H\text{-}S \leftrightarrow C_nH_{2n+1}\,CH_2\text{-}S + OH\text{-}S + S \quad n = 2, 3, \ldots$		K_5
6)	$OH\text{-}S + H\text{-}S \leftrightarrow H_2O + 2S$		K_6
7^{RDS})	$CH_3\text{-}S + H\text{-}S \rightarrow CH_4 + 2S$ $C_nH_{2n+1}\text{-}S + H\text{-}S \rightarrow C_nH_{2n+2} + 2S \quad n = 2, 3, \ldots$		k_{7M} k_7
8^{RDS})	$C_2H_5\text{-}S \rightarrow C_2H_4 + H\text{-}S$ $C_nH_{2n+1}\text{-}S \rightarrow C_nH_{2n} + H\text{-}S \quad n = 3, 4, \ldots$		k_{8E} $k_{8,n}$

Note: RDS – rate determining step

Results and discussion

Estimated parameters and quality of model predictions - Table 4.5 shows the estimated values of model parameters. The results of the t-test show that all of the parameters are statistically different from zero. The physicochemical tests show that the parameters are consistent with physicochemical laws [356] - i.e. activation energies have positive values and heats of reactant adsorption are negative. In order to further analyze the meaningfulness of these values, we compare the relevant activation energies and enthalpies to literature values.

The activation energy of the chain propagation step (Step 3 in Table 4.4) is also the overall energy barrier of FTS. It was estimated to be 93 kJ/mol, which is within the reported range of 80-120 kJ/mol [85]. The activation energies for n-paraffin and 1-olefin,

as well as methane and ethene formation, are very similar to values obtained using the carbide mechanism [229]. The estimated heats of reactant adsorption and enthalpies of elementary reactions are low. This may be related to high surface coverage of CO [61], as discussed below. Lower activation energy of methane formation compared to other n-paraffins explains the higher yield of this species. Additional reasons that could also explain high selectivity towards methane, e.g. existence of pure methanation sites [174] or separate methane formation pathways [263], were not included in this model. DFT studies [351, 353] showed that ethene is more strongly adsorbed to the surface than the higher 1-olefins, which would result in its higher desorption activation energy. This is the reason why our model, consistent with the experimental results, predicts a low rate of ethene formation as compared to other 1-olefins. It should be noted that low ethene formation has often been ascribed to its high reactivity in secondary reactions as evidenced from ethene cofeeding studies [86, 174]. The hypothesis that ethene adsorbs to the surface more strongly can also provide an explanation for the high reactivity of externally added ethene molecules.

Table 4.5 - Estimated values of CO-insertion based model parameters and statistical results.

Parameter	Value	Unit	Parameter	Value	Unit
A_1	$6.59*10^{-5}$	MPa-1	ΔH_1	-48.9	kJ/mol
A_2	$1.64*10^{-4}$	MPa-1	ΔH_2	-9.4	kJ/mol
A_3	$4.14*10^{8}$	mol/(g_{cat}*h)	E_3	92.8	kJ/mol
A_4	$3.59*10^{5}$	-	ΔH_4	16.2	kJ/mol
A_5	$9.81*10^{-2}$	-	ΔH_5	11.9	kJ/mol
A_6	$1.59*10^{6}$	MPa	ΔH_6	14.5	kJ/mol
A_7	$4.53*10^{7}$	mol/(g_{cat}*h)	E_7	75.5	kJ/mol
A_8	$4.11*10^{8}$	mol/(g_{cat}*h)	E_8	100.4	kJ/mol
A_{7M}	$7.35*10^{7}$	mol/(g_{cat}*h)	E_{7M}	65.4	kJ/mol
A_{8E}	$4.60*10^{7}$	mol/(g_{cat}*h)	E_{8E}	103.2	kJ/mol
ΔE	1.1	kJ/mol/CH_2	MARR	23.5	%

* Statistical results: $F_c = 90.1 > F_{0.05}(11, 47) = 1.70$, lowest $t_c = 72.59 > t_{0.05}(21) = 1.72$

The weak physical interactions with the catalyst surface cause the activation energy for the 1-olefin desorption step to increase from 100 kJ/mol by 1.1 kJ/mol for very C-atom in the molecule. It is important to note that the value of approximately 1 kJ/mol/CH_2 for the contribution of weak Van der Waal's forces is consistent with our

understanding of these interactions. From this value, we can calculate value of constant c, appearing in the term e^{c*n}, as approximately - 0.27, which is in a very good agreement with the literature values for cobalt FTS catalysts [86, 229].

Fit quality of the model for C_1-C_{15} n-paraffins and C_2-C_{15} 1-olefins is shown in Figure 4.5 for selected conditions at the three temperatures tested. Overall, the MARR value for the 29 species considered is 23.5%. Compared to our previous study [229], which was based on the Lox and Froment [214] form of the carbide mechanism and had MARR = 26.6%, there is a slight improvement in the fit quality. Results of the F-test show that the model fit is statistically meaningful. Consistent with previous results, the model reliably predicts changing growth probability with carbon number (0.8 to 0.95 in C_3-C_{15} hydrocarbon range). Deviations of C_1 and C_2 in the total hydrocarbon distribution are well predicted as shown in Figure 4.5. The exponential drop in OPR with carbon number in C_3-C_{15} range is also accounted for. It might be possible to further improve the model performance by including the olefin secondary reactions to the kinetic scheme; however, that would lead to an increase in model complexity and number of parameters.

Rates of reactant disappearance can be calculated from the product formation rates utilizing the reaction stoichiometry. Due to the fact that the CO insertion mechanism has approximately zeroth order dependence with respect to CO and half order dependence with respect hydrogen, a reasonable agreement is obtained between the model predicted and experimentally measured reactant rates. MARR values are 18.0 and 17.8% for CO and H_2, respectively.

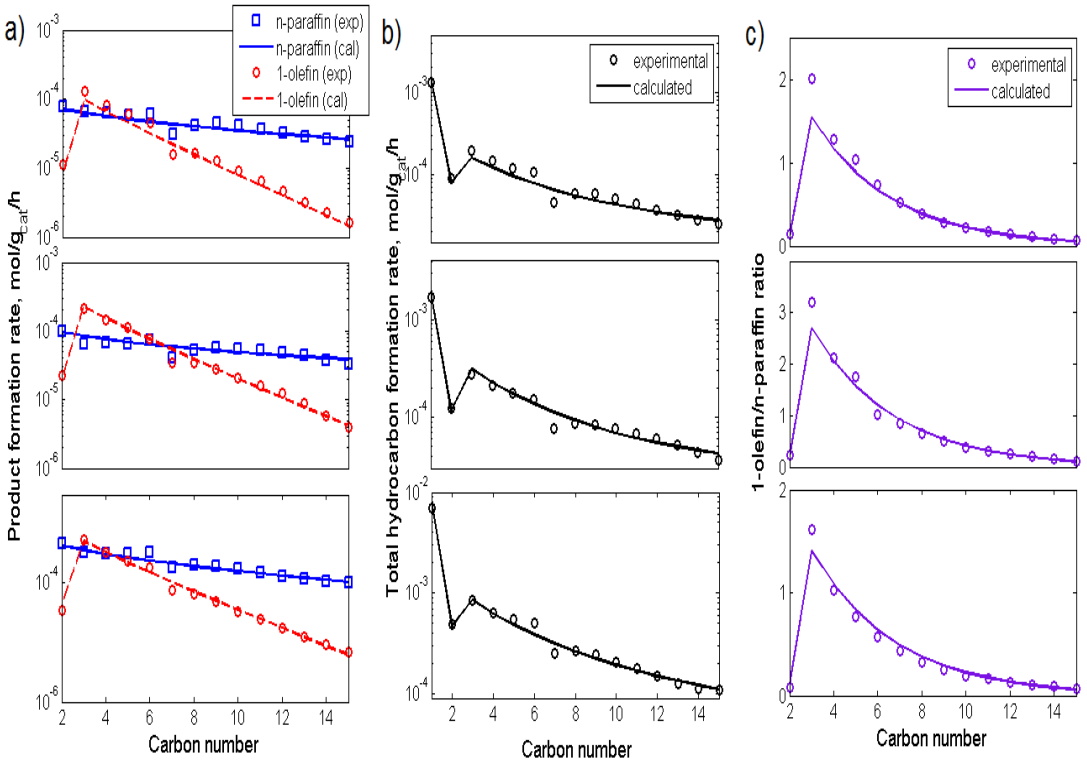

Figure 4.5 - Experimental and calculated product distributions: a) n-paraffin and 1-olefin formation rates; b) total hydrocarbon formation, i.e. ASF plot; c) 1-olefin-to-n-paraffin ratio (Process conditions: fist row - T = 478 K, P = 1.5 MPa, H_2/CO = 2.1, WHSV = 3.7 NL/g_{cat}/h, X_{CO} = 37%; second row - T = 493 K, P = 1.5 MPa, H_2/CO = 1.4, WHSV = 5.6 NL/g_{cat}/h, X_{CO} = 34%; third row - T = 503 K, P = 1.5 MPa, H_2/CO = 2.1, WHSV = 11.3 NL/g_{cat}/h, X_{CO} = 42%).

FTS reaction mechanism, surface species and implications to kinetic modeling - Even though CO-insertion has long been recognized as a plausible main pathway for FTS, the proposed kinetic models have typically not utilized this concept. Majority of FTS kinetic models utilizing the LHHW approach are simple CO disappearance models [193, 195], where selection of carbide mechanism as the basis for derivation has a distinct advantage; all CO disappearance is due to C_1 species formation, which in turn only involves three to five elementary steps. The model derivation is more complex if CO-insertion mechanism is used because CO is consumed not only to initiate chain growth (C_1 species), but also during propagation, where CO is inserted into the growing chain. Therefore, it becomes necessary to define the surface concentration of the growing chains,

which is in turn related to the chain termination steps. Thus, a more comprehensive approach is required to take into account all of the necessary elementary steps of the FTS reaction mechanism.

One of the advantages of using a structured LHHW approach compared to more empirical selectivity models is the ability to obtain information about the surface coverage of various species and their changes with varying process conditions. Surface coverages of adsorbed CO and H can be calculated from the model as:

$$[CO-S] = K_1 P_{CO}[S] \tag{4.52}$$

$$[H-S] = \sqrt{K_2 P_{H_2}}[S] \tag{4.53}$$

where [S] is the fraction of vacant sites defined by Eq. (4.47). The concentration of growing chains on the surface is determined by chain growth probabilities and is given by:

$$[R-S] = \sqrt{K_2 P_{H_2}}(\alpha_1 + \alpha_1\alpha_2 + \alpha_1\alpha_2 \sum_{i=3}^{n}\prod_{j=3}^{i}\alpha_j)[S] \tag{4.54}$$

Figure 4.6 shows the predicted surface coverage for a selected (baseline) condition. Under all conditions used in this study, the model predicts that adsorbed CO is the most abundant surface species, covering 40-80% of total active sites. SSITKA (steady state isotopic transient kinetic analysis) experiments of van Dijk et al. [311, 354] show that about 65% of the surface is covered with adsorbed CO. High coverage of CO is a prerequisite for the CO-insertion mechanism to be favored over the carbide FTS mechanism [50]. Significant coverage of growing chain intermediates and vacant sites is also predicted by the model with average values of 17 and 14%, respectively. SSITKA studies usually report chain coverage lower than 10% [203, 311]. Contrary to these the coverage of atomic hydrogen is usually disregarded in the experimental transient kinetic studies, mainly due to difficulties related to kinetic isotope effects. Therefore our knowledge of it mostly comes from micro-kinetic models (e.g., Storsæter et al. [52]), which are in turn most often determined under methanation conditions (high H_2/CO ratio and low pressure), giving an atomic H coverage usually above 10%. A recent SSITKA

study by den Breejen et al. [270] showed that even at H_2/CO = 10 and P = 1.85 bar, hydrogen covered only about 10% of the surface. If the tests were conducted under realistic FTS conditions (i.e. $H_2/CO \leq 2$ and $P \geq 10$ bar) one would expect a decrease in atomic H surface coverage. Similar conclusion can be made from DFT studies [54] which show that increasing CO coverage reduces H_2 adsorption enthalpy, and would then result in a decrease of H coverage. Our model predicts the H coverage of around 1%. This is mainly due to the fact that the employed mechanism assumes that most of the reactions in which hydrogen is consumed are fast.

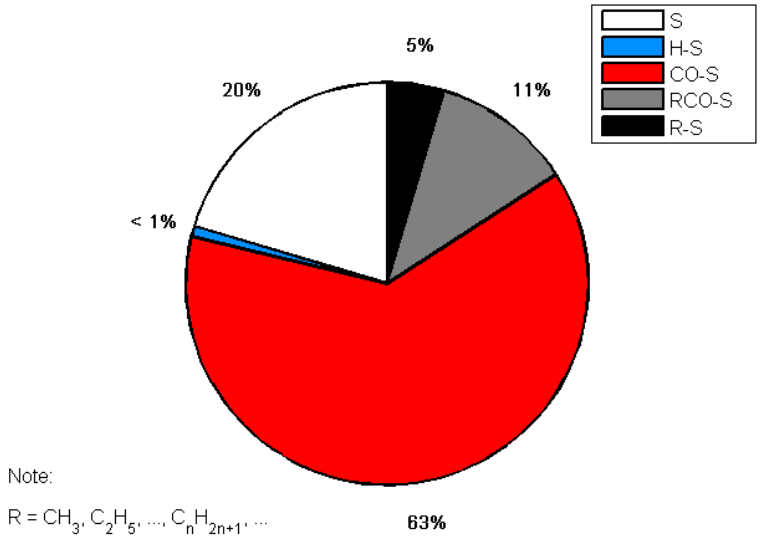

Figure 4.6 - Calculated fractions of surface intermediates at T = 493 K, P = 1.5 MPa, H_2/CO = 2.1, WHSV = 8 NL/g_{cat}/h, X_{CO} = 45%.

4.3. Deviations from the ASF distribution and importance of the exponential chain-length-dependence

Accounting for typical experimental deviations from ASF and variations of OPR with carbon number has been a challenging issue in the development of mechanistic LHHW models of FTS kinetics. Wang et al. [219] and Yang et al. [222] included the olefin readsorption concept into their models for Fe catalysts and expressed the olefin concentration in terms of partial pressures but the models were unable to account for

experimental deviations from the ASF distribution and trends in OPR with increase in carbon number. A model developed by Anfray et al. [230] included solubility enhanced olefin readsorption by using liquid phase concentrations of reactants and readsorbing olefin species, but the agreement between the model predictions and experimental data for olefins was not good (Co FTS catalyst).

Botes [169] identified that the olefin formation rate is directly proportional to e^{c*n} and only models which included this term could adequately describe the observed product distributions. Guo et al. [216] used a model based on olefin readsorption and included an olefin formation rate constant dependence on chain length $k_{ole,n}= k_{ole,0}*e^{-(E+a*n)/RT}$, where the constant a accounts for a non-intrinsic physisorption effect. No theoretical justification for this type of rate equation was provided. Guo's model provided a good fit of the data, including deviations from the ASF distribution and OPR variation with carbon number. The estimated olefin readsorption rate constant was two orders of magnitude lower than the corresponding forward reaction constant, and it is likely that the addition of a rate constant dependent on chain length had a far more significant effect on the model predictions than the inclusion of 1-olefin readsorption term. Teng et al. [217, 220] proposed two models based on the same reaction mechanism. The first model [217] included the 1-olefin readsorption term and the model predictions followed a classical ASF distribution. In the subsequent model Teng et al. [220] replaced the mechanistically derived readsorption rate equation with an equation containing e^{c*n}, in the forward reaction rate for olefin formation. However, it is worth noting that the reversible reaction was not considered in the model derivation. This model was also able to account for non-ASF behavior and the experimental OPR. The models by Guo et al. [216] and Teng et al. [220] as well as the model used in this study show that addition of an exponential term e^{c*n} directly into the olefin formation rate law is essential in order to obtain good agreement with experimental results.

The key consequence of including the chain length dependent 1-olefin desorption concept in our kinetic models is the appearance of the e^{c*n} term in the 1-olefin formation rate equation (Eq. 4.51). Because the n-paraffin formation rate equation (Eq. 4.49) does not have such a term, the olefin-to-paraffin ratio (OPR) will, in line with the experimental results, be an exponentially decreasing function of carbon number (Figure 4.7a). Even

more interesting is that if we define the chain growth probability using the standard definition, we obtain:

$$\alpha_n = \frac{R_{prop}}{R_{prop} + R_{n-par} + R_{1-ole}} = \frac{k_3[CO-S]}{k_3[CO-S] + k_7[H-S] + k_{8,0}e^{c \cdot n}} \qquad n \geq 3 \qquad (4.55)$$

Having the e^{c*n} term (where c is a constant approximately equal to - 0.3), means that as the carbon number increases, the term e^{c*n} will decrease, causing α_n to increase. Therefore, chain growth probability (α_n) will follow the trend plotted in Figure 4.7b. Having a continuously increasing α_n with carbon number means that the positive bend in total hydrocarbons is predicted, as is expected from the experimental data (Figure 4.7c). It is also interesting to point out that after a certain carbon number is reached (above C_{15}), the contribution from the e^{c*n} term essentially becomes zero, resulting in a constant value of chain growth probability for heavy hydrocarbons (α_{inf}). If we drew another constant growth probability in the low carbon range (α_0) in Figure 4.7c, as per the double-alpha theory [152], one could say that the bend in ASF is caused by the superposition of these two distinct growth probabilities. However, the chain length dependent 1-olefin desorption approach explains both features of carbon number dependent product distribution i.e., decreasing OPR and increasing chain growth probability (bend in ASF distribution) with increasing carbon number in a straightforward and explicit way.

As Botes [150, 169] pointed out the vast majority of kinetic modeling studies discussing appearance of olefin secondary reaction fail to provide explicit predictions of selectivity of such reactions. If these info were provided, they could then be compared with the selectivity results of olefin cofeeding studies to improve our understanding of the subject. However, the scientific debate focused almost entirely on the reasons for the hypothesized increase in olefin readsorption with carbon number, which has potentially distracted the research on this topic from other more important questions. Some of these questions are: 1) How many of the initially formed 1-olefins participate in secondary reactions? 2) How many of 1-olefin molecules that participate in secondary reaction will go through hydrogenation, isomerization and most importantly readsorption? 3) How many of 1-olefins need to readsorb in order for this to be the cause of non-ASF and decreasing OPR, and how would then the probability of readsorption change with carbon

number? Answers to the first two questions can be inferred from various experimental olefin cofeeding studies [134, 153, 164, 165, 170, 175, 203], while the answer to the third one requires a better understanding of olefin readsorption theory.

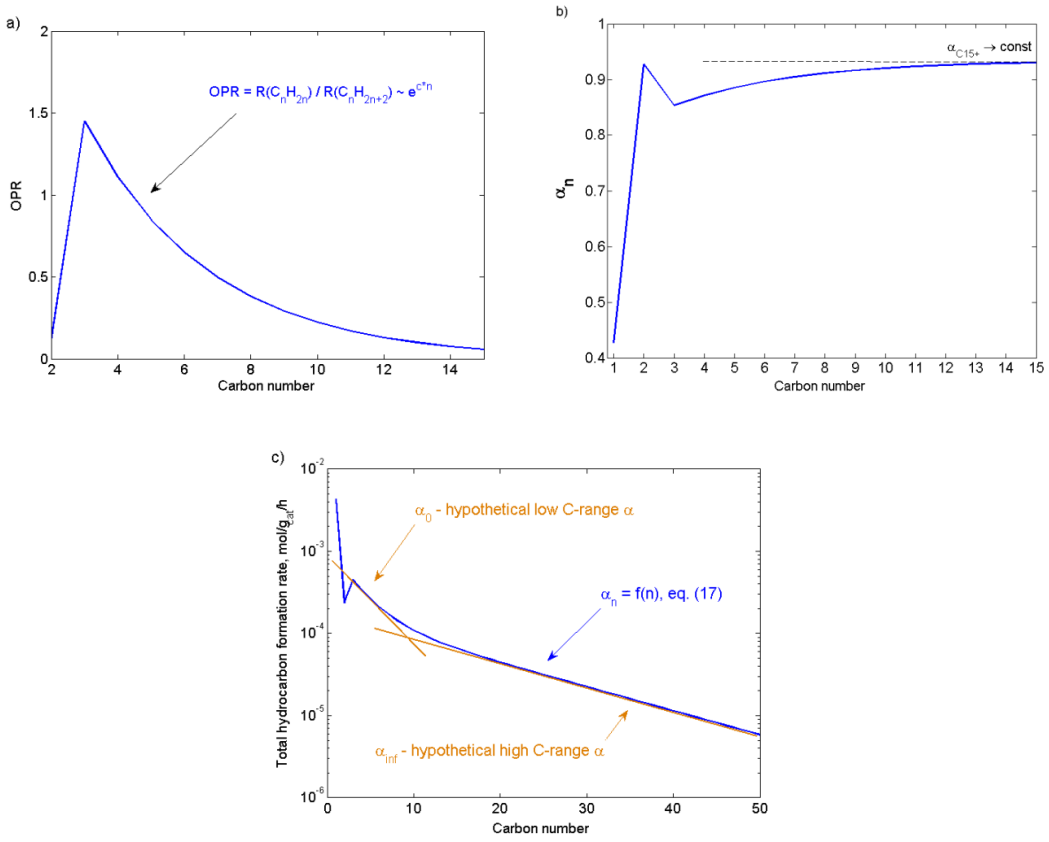

Figure 4.7 - Simulation of FTS product distribution behavior with carbon number (at T = 493 K, P = 1.5 MPa, H_2/CO = 2.1, WHSV = 8 NL/g_{cat}/h, X_{CO} = 45%): a) 1-olefin/n-paraffin ratio (OPR); b) chain growth probability (α_n); c) total hydrocarbon distribution (ASF) plot.

Answer to the third question can be found by mathematical modeling of 1-olefin readsorpiton and comparison to the reported modeling values, as well as the results of olefin cofeeding studies. We analyzed the problem backwards from known outcomes, i.e. increasing chain growth probability and decreasing OPR with carbon number, to determine the probability of readsorption. First we include the 1-olefin readsorption step in a mechanistic model (similar to our own). It is assumed that the readsorbed chain is

indistinguishable from in-situ formed chain. 1-olefin formation (Step 8 from Table 4.4) step becomes:

$$C_nH_{2n+1}\text{-}S \leftrightarrow C_nH_{2n} + H\text{-}S \tag{4.56}$$

Rate of C_{3+} 1-olefin formation is defined as:

$$R_{C_nH_{2n}} = k_{ole}^{for}[C_nH_{2n+1} - S] - k_{ole}^{re}C_{C_nH_{2n}}[H - S] \tag{4.57}$$

where k_{ole}^{for} and k_{ole}^{re} are forward and reverse rate constants of 1-olefin formation, classically described as independent of carbon number. $C_{C_nH_{2n}}$ is a general 1-olefin concentration term and depending on what approach is used to "enhance" the readsopriton it could be partial pressure, liquid phase concentration or fugacity; it is meant to focus on readsorption as an idea, rather than the causes for its potential enhancement with carbon number. If we rearrange Eq. (4.57) we get:

$$R_{C_nH_{2n}} = k_{ole}^{for}[C_nH_{2n+1} - S] \cdot (1 - \frac{k_{ole}^{re}C_{C_nH_{2n}}[H - S]}{k_{ole}^{for}[C_nH_{2n+1} - S]}) \tag{4.58}$$

$$\beta_n = \frac{k_{ole}^{re}C_{C_nH_{2n}}[H - S]}{k_{ole}^{for}[C_nH_{2n+1} - S]} \tag{4.59}$$

$$R_{C_nH_{2n}} = k_{ole}^{for}[C_nH_{2n+1} - S] \cdot (1 - \beta_n) \tag{4.60}$$

Term β_n is the probability of 1-olefin readsorption (ratio of 1-olefins that readsorb and those that are initially formed). It was first introduced in a mechanistic kinetic model of FTS by Wang et al. [219] If we compare Eq. (4.60) with Eq. (4.51) in our model we see that the fast drop in the 1-olefin formation rate with carbon number would be caused by the decrease in $(1-\beta_n)$ term (i.e. increasing readsorption probability β_n) in the readsorption approach and is caused by $e^{c \cdot n}$ term in our model. All other terms appearing in the Eqs. (4.60) and (4.51) are either independent of chain length (kinetic rate constants) or equal (chain surface coverage). Note that generally $e^{c \cdot n}$ term would just be introduced empirically, and not from chain length dependent 1-olefin desorption concept. Above we showed that having an $e^{c \cdot n}$ term directly in the 1-olefin rate equation leads to a good

prediction of increasing growth probability and exponentially decreasing OPR with carbon number (Figure 4.7). From this it follows that readsorption model can only give the correct prediction of this behavior if $(1-\beta_n) \approx e^{c \cdot n}$, and therefore the 1-olefin readsorption probability function with carbon number needs to exhibit the following trend:

$$\beta_n \approx 1 - e^{c \cdot n} \tag{4.61}$$

If constant is e.g. c = - 0.27, then Eq. (4.61) can be plotted as in Figure 4.8. Notice that the behavior of 1-olefin readsorption probability described in Figure 4.8 follows all of the qualitative trends typically attributed to classical olefin readsoprtion theory models, i.e. minimum at C3, increased probability of readsorption with increasing carbon number and readsorption of practically all heavy olefins. Therefore we can see that this is the behavior that 1-olefins need to obey if their readsorption is to cause the observed product distribution. This also implies that readsorption is the dominant secondary reaction of 1-olefin, and that hydrogenation and isomerization are, as stated by Iglesia et al. [108], negligible in comparison.

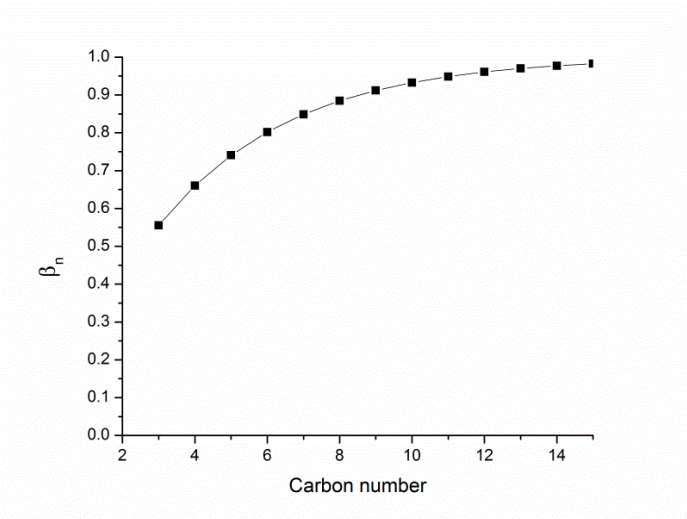

Figure 4.8 - Change of readsorption probability (β_n) with carbon number needed by mechanistic readsorption models to fit the non-ASF and exponentially decreasing OPR.

Question that follows is: How realistic is it to expect 1-olefins to behave as the readsorption theory suggests (Figure 4.8)? Based on results of their comprehensive cofeeding study that included 1-olefins of various chain lengths at various conditions, Schulz and Claeys [164] showed that hydrogenation and isomerization are much more dominant secondary reactions compared to readsorption, which was generally shown to be below 20% of the total 1-olefin conversion. Same type of discrepancy between the behavior of cofed olefins and hypothesized behavior of in-situ formed olefins in their readsorption based model was also noted by Iglesia et al. [108]. Therefore, it seems unlikely that the observed non-ASF behavior and OPR decrease with carbon number is caused by secondary 1-olefin readsorption and continued chain growth. The concept that is physically more meaningful is the chain length dependent desorption concept used in our models.

4.4. Conclusions

Data from experiments performed over a Re-promoted Co/Al_2O_3 catalyst over a range of process conditions was used to determine the detailed kinetic model of FTS. Several LHHW models were derived based on the different forms of carbide FTS mechanism, as well as a model based on CO-insertion mechanism. Implementation of the later mechanism lead to a more complex form of the kinetic model, but improved fit is obtained compared to a form of carbide mechanism. Considering the growing amount of experimental and theoretical evidence in support of CO-insertion mechanism, this work shows that kinetic models can be based on CO-insertion and emphasizes that this possibility needs to be considered further. The estimated model parameters are found to be physically and statistically meaningful. The model predicts that adsorbed CO is the most abundant species on the surface, which is consistent with experimental measurements.

This model provided a good fit of the n-paraffin and 1-olefin formation rates, as well as a reasonable prediction of the reactant consumption rates, for the studied conditions. Our results showed that the increasing chain growth probability and the decreasing olefin-to-paraffin ratio with increase in carbon number can be explained by including the chain length dependent 1-olefin desorption effect. The activation energy of

1-olefin desorption step is linearly dependent on carbon number due to the effect of weak Van der Waal's type interactions of the desorbing 1-olefin π-complex with the surface. The contribution of these interactions needed to predict the increasing chain growth probability and the decreasing OPR is estimated to be only about 1.1 kJ/mol/CH_2, which is consistent with the effect of weak attractive forces.

The detailed kinetic model presented here, coupled with appropriate mass and energy balance equations, can therefore be used as the basis for initial design, simulations and optimization of all FTS reactor types. However, further refinements of detailed kinetic, in terms of secondary methane formation, as well as secondary 1-olefin reactivity, are possible as well and will be addressed in follow-up studies.

5. Fixed-bed FTS reactor modeling and optimization

Rational design of FTS reactors is conditioned on the scientific knowledge of chemical and physical phenomena that occur in these reactors. Different scale, number and interlinking of these phenomena make the development of mathematical models capable of simulating and predicting the behavior of FTS reactors a very demanding task. The FTS reactor models have to be able to describe the complex interplay between reaction kinetics and various physical phenomena that exist within these reactors. Even though fixed-bed reactor technology is far more present in the industrial applications, majority of reactor modeling effort in FTS research has been focused on slurry bubble column reactors [367-371]. As shown in the Chapter 2 (Literature review), most of FTS fixed-bed reactor models developed so far have been very simple.

One of their biggest drawbacks was the lack of reliable kinetic model for prediction of FTS product selectivity. Instead most of the FTS fixed-bed reactor models have utilized either heterogeneous of pseudohomogeneous one-dimensional models with simple reactant conversion, i.e. overall FTS rate, kinetic equations [241-245]. In some models averaged chain growth probability is taken into account, providing information on product selectivity. As we saw in Chapter 3, variation of process conditions can have a very big effect on product selectivity. Therefore, it is not justified to assume that in a fixed-bed reactor with a large concentration and temperature gradients throughout the bed, product selectivity (i.e. chain growth parameter) will remain unchanged at different positions within the bed.

In this chapter we will utilize the detailed kinetic model developed in this study in conjunction with a one-dimensional pseudo-homogeneous FTS fixed-bed reactor. This will provide a considerably more detailed simulations of FTS reactor, and we will be able to analyze the effect of reactors' process conditions gradients on overall product selectivity. In the second part of the chapter, we will use the developed reactor model in a rigorous optimization in order to obtain the optimal process parameters. The reactor simulations and optimization will allow us to offer guidelines for FTS fixed-bed reactor design and operation.

FTS fixed-bed reactor model

In general, fixed-bed reactor models can be divided into pseudo-homogeneous and heterogeneous, where the first assumes concentration and thermal equilibrium between the bulk of the fluid and catalyst particle, while the latter considers the transport of heat and matter to and within the catalyst particle [356]. Models can also be one- and two-dimensional, where the model complexity is increased by considering axial and radial mixing. Steynberg et al. [231] state that large catalyst particles (> 1 mm) with liquid filled pores guarantee relatively low volumetric reactions rates, meaning that the resistance of interfacial heat and mass transport (i.e. transport from fluid bulk to catalyst surface) can be neglected and that FTS fixed-bed models can be pseudo-homogeneous in that regard. They also stated that because of typically used large particle sizes (1 – 3 mm), small tube diameters (2.5 – 5 cm) and large tube lengths (6 – 12 m), plug flow can be assumed, i.e. axial mixing can be neglected in these models. Selection between one- and two-dimensional models is based on the tube diameter, where larger tube diameters mean that radial gradient cannot be neglected and two-dimensional approach is required. Since for Co-based catalyst reactors small tube diameters are typically used, in order to insure better heat transfer characteristics, in this study we assumed one-dimensional approach is adequate. We also assumed that the intra-particle mass and heat transport (i.e. transport inside the particle) can be neglected. However, this assumptions is justified only for very small catalyst particles (< 200 μm), while commercially used larger catalyst particles exhibit intra-particle resistances. This is a limitation of the reactor model, made in order to allow the use of highly detailed kinetics in reactor optimization. All molecular species inside the reactor are assumed to follow ideal gas phase behavior. Visconti et al. [372] recent study showed the over 95 mol.% of C_1-C_{30} hydrocarbons (i.e. about 99 mol.% of total hydrocarbons) is in the vapor phase under FTS conditions, which justifies the assumption of using only gas phase in the model. However, the existence of even a small amount of liquid inside the reactor can have a large effect on intensifying the heat transfer inside the reactor [248]. Therefore, we took into account an existence of a very thin liquid layer in heat transfer calculations.

The FTS fixed-bed reactor model consists of:

- **Mass balance equations**:

$$-\frac{dF_i}{dz} = A_{cs}\eta\rho_b R_i \tag{5.1}$$

where F_i is the molar flowrate of species i (i = CO, H_2, H_2O and lumped hydrocarbon groups CH_4, C_2, C_3, C_4 and C_{5+}), z is reactor length, A_{cs} is tube cross-section area, η is catalyst effectiveness, ρ_b is reactor bed density and R_i is rate of species i disappearance or formation. Rates of reactants (CO and H_2) disappearance and products (H_2O, n-paraffin and 1-olefin) formation are calculated at each point along the reactor bed using the detailed FTS kinetic model described in Chapter 4. The formation rates of n-paraffin and 1-olefin with 2, 3, 4 and above 5 are summed up, forming rates of species C_2, C_3, C_4 and C_{5+}, respectively.

- **Heat balance equation**:

$$u_s\rho c_p\frac{dT}{dz} = (-\Delta H_r)\eta\rho_b(-R_{CO}) - \frac{4U}{d_t}(T - T_w) \tag{5.2}$$

where u_s is superficial gas velocity, ρ is fluid density, c_p fluid heat capacity, T temperature, $(-\Delta H_r)$ is reaction enthalpy (assumed to be 157 kJ/mol CO for C_9 average product [239, 242, 373, 374]), U overall heat transfer coefficient, d_t is tube diameter and T_w is reactor wall temperature (assumed to be equal to the inlet temperature T_{in}).

- **Pressure drop equation:**

$$-\frac{dP_t}{dz} = f\frac{\rho u_s^2}{d_p} \tag{5.3}$$

where P_t is total pressure, f is the friction factor for fluid flow in a packed bed and d_p is the particle diameter.

The FTS fixed-bed reactor model consists of 10 ODEs that are solved in Matlab using the Runke-Kutta method with *ode15s* implicit solver for stiff problems for a step size of Δz (unless specified Δz = 0.1). The following boundary conditions for 10 system variables $F_{CO}(z)$, $F_{H2}(z)$, $F_{H2O}(z)$, $F_{CH4}(z)$, $F_{C2}(z)$, $F_{C3}(z)$, $F_{C4}(z)$, $F_{C5+}(z)$, $T(z)$ and $P(z)$ are applied:

$$F_{CO}(z=0) = F_{CO}^{in} \tag{5.4}$$

$$F_{H2}(z=0) = F_{H2}^{in} \tag{5.5}$$

$$F_{H_2O}(z=0) = 0 \tag{5.6}$$

$$F_{CH_4}(z=0) = 0 \tag{5.7}$$

$$F_{C_2}(z=0) = 0 \tag{5.8}$$

$$F_{C_3}(z=0) = 0 \tag{5.9}$$

$$F_{C_4}(z=0) = 0 \tag{5.10}$$

$$F_{C_{5+}}(z=0) = 0 \tag{5.11}$$

$$T(z=0) = T^{in} \tag{5.12}$$

$$P(z=0) = P^{in} \tag{5.13}$$

Thermodynamic properties – Correlations for the dependence of physical properties (i.e. heat capacity, density, viscosity, thermal conductivity) for various components of the system (CO, H_2, H_2O, CH_4, C_2, C_3, C_4 and C_{5+}) in their vapor phase from temperature were taken from Perry's Chemical Engineers' Handbook [375] and other literature sources [376-378]. It was assumed that the properties of C_{5+} component correspond to those of octane.

Table 5.1 – Physical properties of various system components (in ideal gas state)

Component	Property	Formula used for prediction
CO	C_p (J/mol/K)	(6.60+0.00120*T)*4.184
	μ (Pa*s)	1.1127e-6*T^0.5338/(1+94.7/T)
	λ (W/m/K)	0.00059882*T^0.6963/(1+57.13/T+501.92/T^2)
H_2	C_p (J/mol/K)	(6.62+0.000810*T)*4.184
	μ (Pa*s)	1.797e-7*T^0.685/(1-0.59/T+140/T^2)
	λ (W/m/K)	0.002653*T^0.7452/(1+12/T)
H_2O	C_p (J/mol/K)	(8.22+0.00015*T)*4.184
	μ (Pa*s)	1.7096e-8*T^1.1146
	λ (W/m/K)	6.2041e-6*T^1.3973
CH_4	C_p (J/mol/K)	(5.34+0.0115*T)*4.184
	μ (Pa*s)	5.2546e-7*T^0.59006/(1+105.67/T)
	λ (W/m/K)	8.3983e-6*T^1.4268/(1-49.654/T)
C_2	C_p (J/mol/K)	(0.4033e5+1.3422e5*(1.6555e3/T/sinh(1.6555e3/T))^2+0.7322e5*(752.87/T/sinh(752.87/T))^2)/1e3
	μ (Pa*s)	4.9054e-8*T^0.90125
	λ (W/m/K)	-1.12*T^0.10973/(1-9834.6/T-7535.8/T^2)
C_3	C_p (J/mol/K)	(0.5195e5+1.9245e5*(1.6265e3/T/sinh(1.6265e3/T))^2+1.1680e5*(723.6/T/sinh(723.6/T))^2)/1e3
	μ (Pa*s)	4.9054e-8*T^0.90125
	λ (W/m/K)	-1.12*T^0.10973/(1-9834.6/T-7535.8/T^2)
C_4	C_p (J/mol/K)	(0.7134e5+2.4300e5*(1.6300e3/T/sinh(1.6300e3/T))^2+1.5033e5*(730.42/T/sinh(730.42/T))^2)/1e3
	μ (Pa*s)	4.9054e-8*T^0.90125
	λ (W/m/K)	-1.12*T^0.10973/(1-9834.6/T-7535.8/T^2)
C_{5+}	C_p (J/mol/K)	(1.3554e5+4.43e5*(1.6356e3/T/sinh(1.6356e3/T))^2+3.0540e5*(746.4/T/sinh(746.4/T))^2)/1e3
	μ (Pa*s)	3.1191e-8*T^0.92925/(1+55.092/T)
	λ (W/m/K)	-1.12*T^0.10973/(1-9834.6/T-7535.8/T^2)

Overall heat transport coefficient (U) – Heat transport calculations take into account convective, conductive and diffusive heat transports in radial direction trough the reactor. Because the heat transfer characteristics in the central axis of the reactor are different from those at the wall of the reactor, the overall heat transfer coefficient U takes into account effective radial thermal conductivity in the reactor core (λ_{er}) along with heat transfer at the wall (h_{wall}) [241]:

$$\frac{1}{U} = \frac{1}{h_{wall}} + \frac{d_t}{8\lambda_{er}} \tag{5.14}$$

Effective radial thermal conductivity in reactor core can be calculated as [241, 379, 380]:

$$\lambda_{er} = \lambda_{er}^{s} + \lambda_{er}^{g} + \lambda_{er}^{l} \tag{5.15}$$

where λ_{er}^{s} is the static contribution of heat transport by conduction and diffusion inside the packed bed, while λ_{er}^{g} and λ_{er}^{l} are dynamic contributions of convective heat transfer in the two phases. Because diffusion transport can be considered negligible under FTS conditions, following assumption can be used:

$$\lambda_{er}^{s} = 1.5\lambda_{l} \tag{5.16}$$

where λ_{l} is thermal conductivity of the liquid layer in the reactor, which is assumed to correspond to thermal conductivity of liquid C_{20} n-paraffin. The values of λ_{er}^{g} and λ_{er}^{l} are related to the radial mixing of gas and liquid phases inside the packed bed, so they can be expressed as a function of Reynolds (*Re*) and Prantl (*Pr*) numbers:

$$\lambda_{er}^{g} + \lambda_{er}^{l} = (\alpha\beta)_{g}\,\lambda_{g}\,\mathrm{Re}_{g}\,\mathrm{Pr}_{g} + (\alpha\beta)_{l}\,\lambda_{l}\,\mathrm{Re}_{l}\,\mathrm{Pr}_{l}\ . \tag{5.17}$$

where coefficients needed for calculations are given in Table 5.2.

Table 5.2 - Coefficients needed for calculations of dynamic contributions of convective heat transfer in the gas and liquid (from Refs. [241, 380])

d_p	$(\alpha\beta)_g$	$(\alpha\beta)_l = a*(1+b*Re_g)$	
(cm)	-	*a*	*b*
0.12	0.412	0.201	$2.83*10^{-2}$
0.26	0.334	0.167	$1.34*10^{-2}$
0.43	0.290	0.152	$6.32*10^{-3}$

The effective heat transfer at the wall (h_{wall}) takes into account the interaction of the three phases with wall of the reactor (i.e. reactor tube). Because the liquid flowrate is negligible, following equation can be used [241, 356]:

$$h_{wall} = \frac{10.21\lambda_{er}^{s}}{d_{t}^{4/3}} + 0.033\frac{\lambda_{g}}{d_{p}}\mathrm{Re}_{g}\,\mathrm{Pr}_{g} \tag{5.18}$$

where the first term represents the static and the second term is dynamic contribution to heat transfer at the wall.

Fixed-bed pressure drop – The pressure drop inside the reactor was calculated using the Ergun's equation [381], where the friction coefficient (*f*) can be calculated as:

$$f = \frac{1-\varepsilon_w}{\varepsilon_w^3}(1.75 + 150\frac{1-\varepsilon_w}{\mathrm{Re}_g}) \tag{5.19}$$

where ε_w is the adjusted bed porosity, which takes into account liquid holdup inside the bed (ε_l), so that:

$$\varepsilon_w = \varepsilon_b - \varepsilon_l \tag{5.20}$$

where bed porosity (ε_b) can be calculated as a function of particle and tube geometry [382]:

$$\varepsilon_b = 0.1504 + \frac{0.2024}{\phi_p} + \frac{1.0814}{\left(\frac{d_t}{d_p} + 0.1226\right)^2} \tag{5.19}$$

where ϕ_p is particle sphericity (assumed to be 1). Contribution of the liquid holdup to bed porosity was assumed to be 1% [383].

Simulations of FTS fixed-bed reactor performance

To examine the effect of various reactor process parameters and determine whether the fixed-bed reactor model yields physically meaningful results, comparable to the industrial FTS reactors, we performed a series of simulations. Results of these simulations were meant to help in the selection of appropriate ranges for optimization of process parameters.

Model validation - The best known example of the cobalt-based multi-tubular fixed-bed reactor design is Shell's Middle Distillate Synthesis process (SMDS). Plants based on this design are the Pearl GTL in Qatar and the Bintulu plant in Malaysia. Other than the total productivity, very little is known about the specifications of the Pearl GTL plant in Qatar. Significantly more is known about the working parameters of FTS reactors

in the Binutlu GTL plant in Malaysia from a number of studies [34, 241, 384-386]. From these we can find out the following:

- Process conditions: reactor temperature is between 200 and 230 °C, pressure around 30 bar, H_2/CO feed ratio between 1.8 and 2.1;
- Reactor geometry: tube diameter between 2 - 5 cm (most likely 2.6 cm, i.e. 1 inch), particle diameter 1 – 3 mm, tube length 12.865 m and 26150 tubes in a reactor;
- Results: total syngas conversion around 80 % (Note: the single pass CO conversion is around 60 % or lower, in order to maintain low partial pressure of water, therefore, recycle of unconverted syngas is needed in order to reach higher level of total conversion), C_{5+} selectivity between 85 and 92 % and productivity of 3675 bbl/day (i.e. 144000 tonnes/y).

Using only the available data it is not possible to fully validate the proposed one-dimensional fixed-bed reactor model. However, we can perform simulations to examine whether our model performed in the ranges that would be expected under the described conditions. Figure 5.1 presents the major input (process conditions and reactor geometry) and output (species flowrates, temperature and pressure along the reactor) variables in our model. A base case reactor model setup is chosen based on available data (Table 5.3) [34, 241, 384-386].

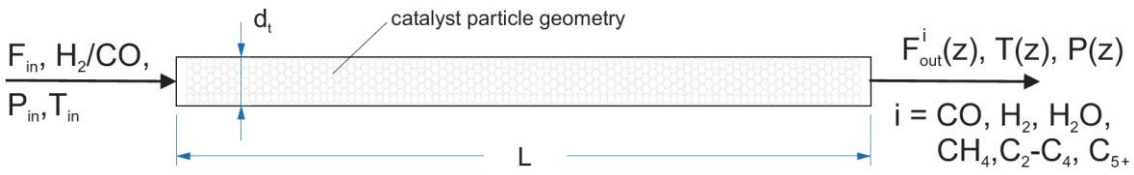

Figure 5.1 – Schematic representation of one-dimensional fixed-bed reactor with input and output variables.

Table 5.3 – Base case simulation process parameters

Process conditions		Geometry	
Inlet T (K)	475	**Tube length (m)**	12.86
Inlet P (bar)	30	**Tube diameter (cm)**	2.6
Feed H_2/CO	2.0	**Particle diameter (mm)**	2.5
Inlet syngas flowrate (mol/s)	0.15*	**Number of tubes**	26150
Wall temperature (K)	475		

*flowrate per tube is chosen to obtain approximately 60% CO conversion

Results of the simulation are shown in Figure 5.2. From these we can see that the reactor model provides reasonable predictions of reactant conversions, resulting product flowrates and temperature and pressure profiles. Calculated CH_4 and C_{5+} selectivities were 5.6 and 89.7 %, respectively, which is very similar to the industrial reactors. If we assume that the average C_{5+} product is C_9 (fuel range) we get that the reactor productivity is 151 670 tonnes/y for about 60 % single pass CO conversion level. This is comparable in the order of magnitude with the industrial plant 144 000 tonnes/y with around 80 % total conversion (with recycle). If we took into account recycle, the result for productivity would be considerably higher than the industrial plant. However, it is important to note that our model assumes 100 % catalyst effectiveness, which is not likely to be the case. The effectiveness factor for cobalt catalyst is typically in the 0.6 to 0.9 range [241]. Therefore, if one was takes all of the factors into consideration it is obvious that our model gives results representative of large scale industrial reactors and can be used in initial design, simulation and optimization of fixed-bed FTS reactors.

It is worth noting that the pressure drop within the bed was higher than expected (approximately 1 bar/m). This is likely due to the selection of pressure drop equations and catalyst particle shape [241] and will be examined in future work. However, this result did not significantly affect productivity and selectivity of FTS.

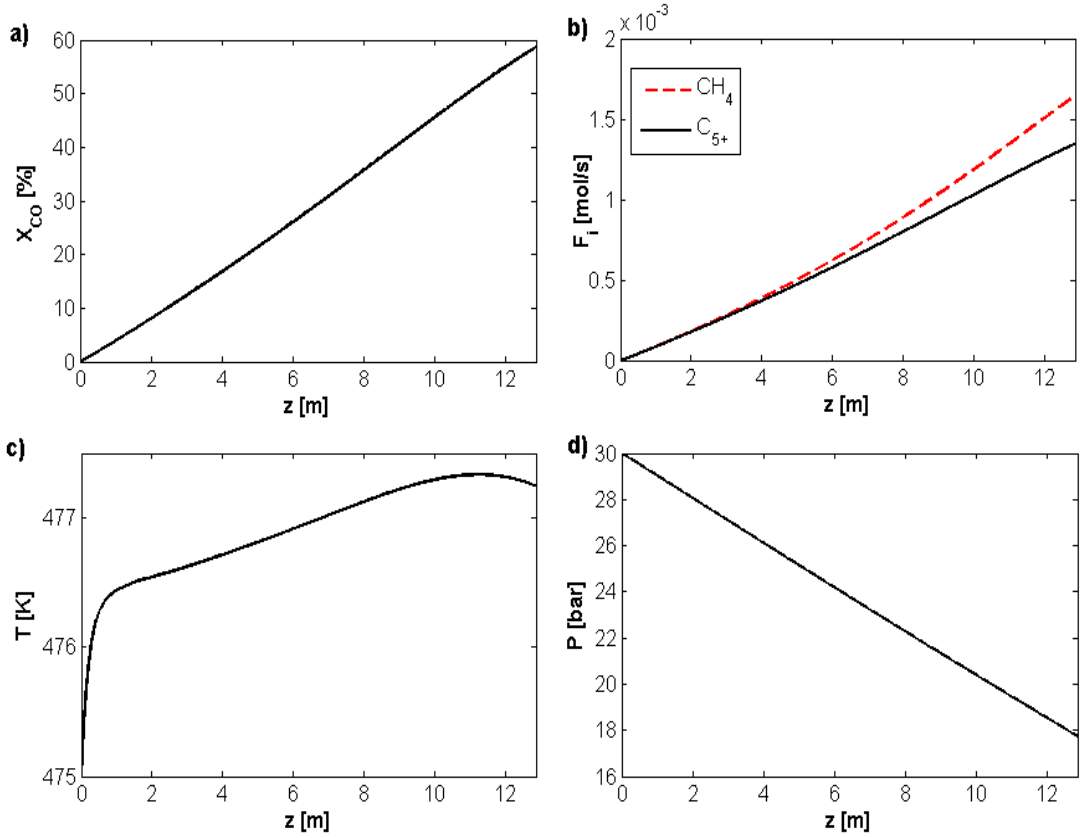

Figure 5.2 – Results of base case simulations: a) reactant conversions; b) CH_4 and C_{5+} flowrates inside the reactor; c) temperature profile inside the reactor; d) pressure drop inside the reactor. (Note: Input data given in Table 5.2)

Effect of inlet process parameters – Inlet process parameters (inlet temperature, feed ratio and flowrate) were varied for the base case geometry (Table 5.3) and the reactor behavior was analyzed. The analyzed process parameters all can have different effects, both positive and negative, on the reactor performance. For example, high temperature causes high conversion of reactants, but it also makes heat removal more difficult and product selectivity less favorable. The only process parameter whose increase does not have adverse effects is reactor pressure. The expected effect of increasing the inlet pressure is increase in both conversion and C_{5+} selectivity. Therefore, maximum allowable pressure is recommended as optimal. Other process parameters, i.e. inlet temperature, feed ratio and flowrate, all need to be carefully optimized to ensure the best possible conversion level and selectivity (i.e. reactor productivity), while maintaining good temperature control and relatively low pressure drop. Due to kinetic model

limitations, reactor inlet pressure was kept constant at 30 bar for all of the simulations and optimization.

As mentioned previously, temperature control is a major challenge in designing FTS reactors because of the reaction's high exothermity. Figure 5.3 and 5.4 show the effect of inlet temperature on model results for the base case conditions. As we showed for the base case, operating at 475 K at base conditions, results in about 60 % CO conversion and 90 % C_{5+} selectivity. Increasing the temperature results in significantly higher conversion and productivity, but lower C_{5+} selectivity. Also, the undesired methane selectivity increases. Increasing the inlet temperature can also have a detrimental effect on heat management. Figure 5.3c shows that for inlet temperature of 500 K, the temperature close to the reactor inlet increases to a point of about 520 K, but still heat is removed effectively and, after a peak, bed temperature remains relatively constant. However, simulations for inlet temperature of e.g. 510 K (not shown in figures) show much poorer heat removal and the system becomes thermally unstable unless the wall temperature is decreased to cope with the increased heat generated from the FTS reaction. Except for the increased conversion, another positive effect of increasing the inlet temperature is the decrease in fluid density, which causes a decrease in pressure drop (Figure 5.3d).

Because syngas preparation constitutes a major part of both capital and operating costs in all XTL plants, selection of appropriate syngas composition is very important. It is desired that as much as possible of the reactants (H_2 and CO) are consumed to produce hydrocarbon products, i.e. process needs to have high material efficiency. A rule of thumb here is to make the syngas H_2/CO feed ratio equal to the usage ratio (UR), where UR is the ratio of H_2 and CO consumptions [387]. Because with Co-based catalysts the extent of WGS reaction is small, UR practically equals to FTS stoichiometric ratio. This means that the value of feed ratio is typically around 2. Figure 5.5 and Figure 5.6 show the effect of varying the reactant feed ratio from 1.8 to 2.2. Because partial pressure of hydrogen has a positive effect on the rate of FTS, the conversions increase with increasing H_2/CO feed ratio (Figure 5.5a). Rates of hydrogenation reaction (i.e. paraffin formation) increased as well, as opposed to propagation, so we see more methane and light products and lower C_{5+} selectivity (Figure 5.5b and Figure 5.6). Temperature and pressure

gradients are not significantly affected by changing feed ratio, (Figure 5.5c and d). The temperature increases due to the increased conversion level and the pressure drop decreases because of the decrease in density with the higher fraction of light hydrogen.

Variations of conversion level from medium to high was analyzed by changing the inlet flowrate. Results of these simulations are shown in Figure 5.7 and Figure 5.8. The increase of inlet flowrate decreases residence time and decreases the overall reactant conversion and productivity (Figure 5.7a and b). Another negative effect of increased flowrate is a much higher pressure drop inside the reactor (Figure 5.7d). A positive effect of increased flowrate is the improved heat removal from the reactor (Figure 5.7c). According to this reactor model, increase of inlet flowrate only had a small impact on the product selectivity and resulted in higher methane and lower C_{5+} selectivity (Figure 5.8).

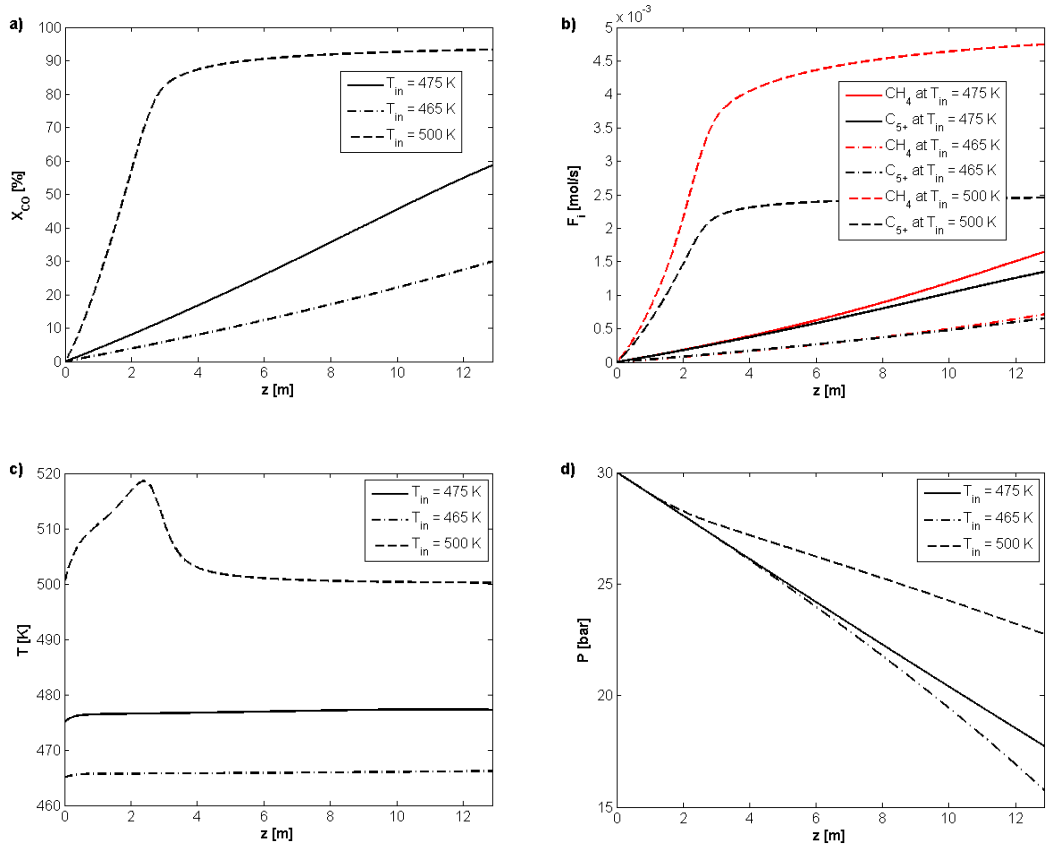

Figure 5.3 - The effect of inlet temperature on reactor model results: a) CO conversion; b) CH_4 and C_{5+} flowrates; c) temperature profile; d) pressure profile. (Process conditions P_{in} = 30 bar, feed H_2/CO ratio = 2.0, inlet flowrate 0.15 mol/s)

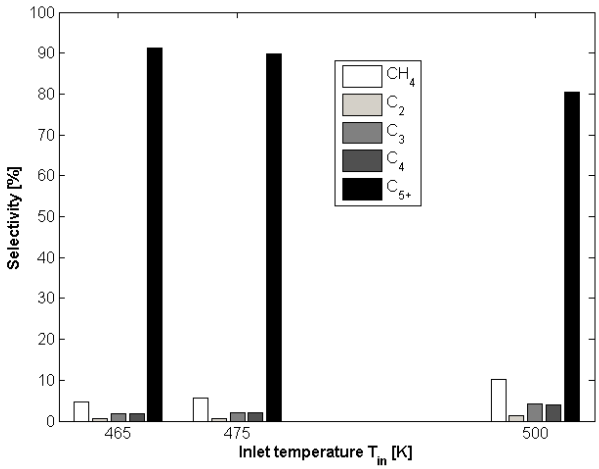

Figure 5.4 - The effect of inlet temperature on predicted product selectivities. (Process conditions P_{in} = 30 bar, feed H_2/CO ratio = 2.0, inlet flowrate 0.15 mol/s)

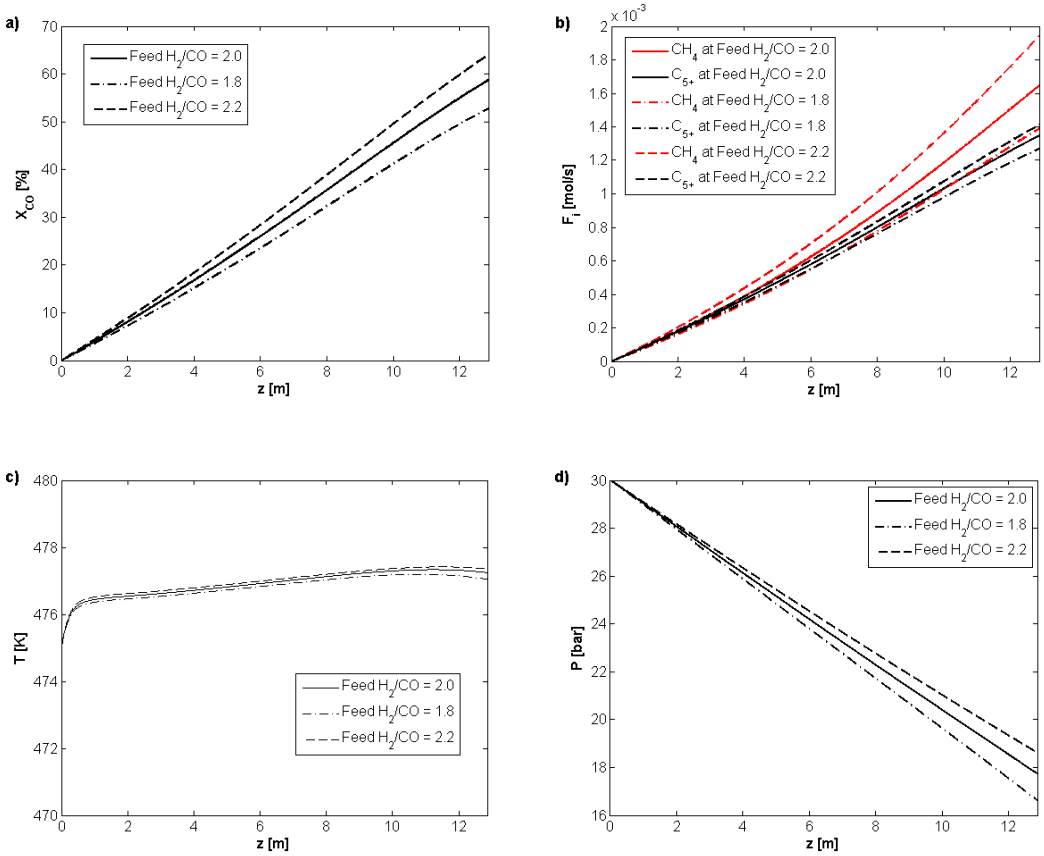

Figure 5.5 - The effect of feed H_2/CO ratio on reactor model results: a) CO conversion; b) CH_4 and C_{5+} flowrates; c) temperature profile; d) pressure profile. (Process conditions T_{in} = 483 K, P_{in} = 30 bar, inlet flowrate 0.15 mol/s)

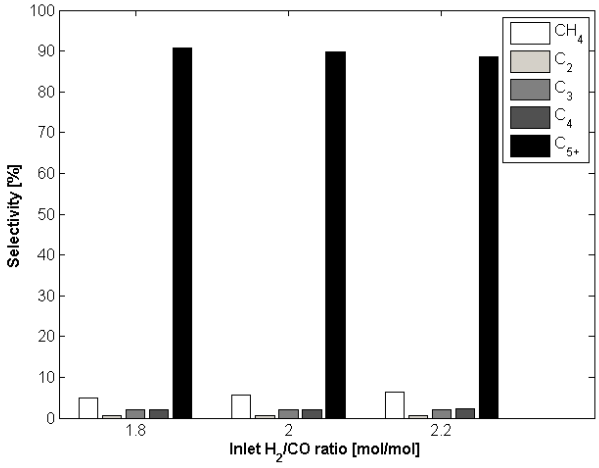

Figure 5.6 - The effect of feed H_2/CO ratio on predicted product selectivities. (Process conditions T_{in} = 483 K, P_{in} = 30 bar, inlet flowrate 0.15 mol/s)

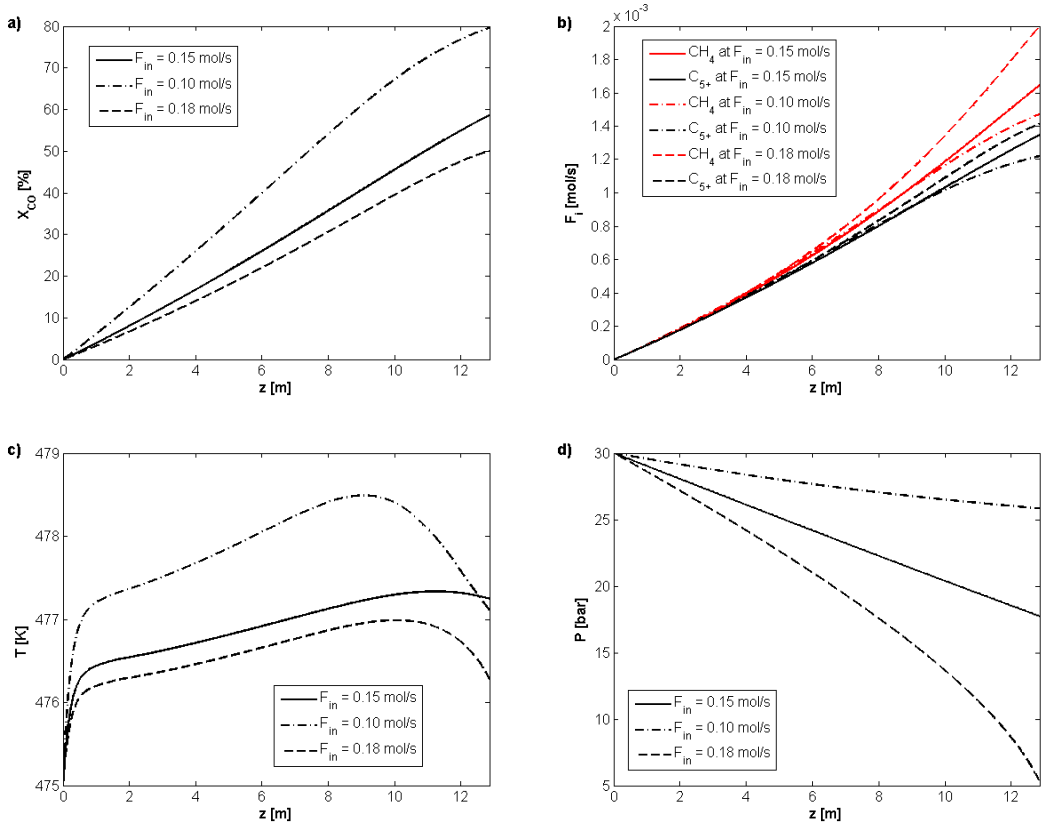

Figure 5.7 – The effect of inlet flowrate on reactor model results: a) CO conversion; b) CH_4 and C_{5+} flowrates; c) temperature profile; d) pressure profile. (Process conditions T_{in} = 483 K, P_{in} = 30 bar, feed H_2/CO ratio = 2.0)

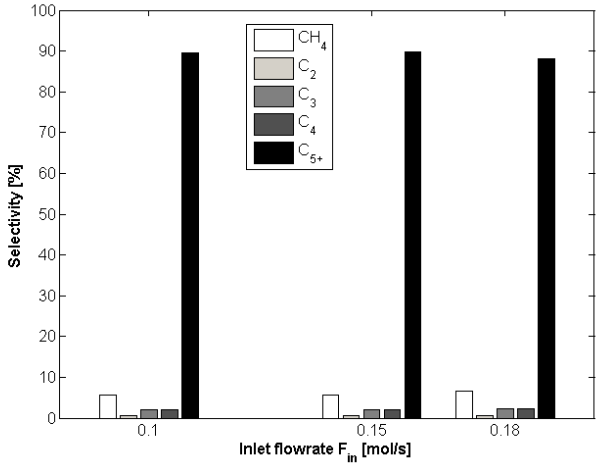

Figure 5.8 - The effect of inlet flowrate on predicted product selectivities. (Process conditions T_{in} = 483 K, P_{in} = 30 bar, feed H_2/CO ratio = 2.0)

Optimization of FTS fixed-bed reactor process parameters

Results of reactor model simulations showed that the changes of inlet process conditions (temperature, feed ratio and flowrate) can have both positive and negative effects on conversion, productivity, selectivity, heat management and pressure drop. In order to find a set of optimal process conditions that provide for a maximum productivity of desired products a reactor optimization routine was conducted. The optimization program, based on genetic algorithm, was written in Matlab with an objective function to find a maximum productivity of C_{5+} products for the defined geometry (geometry defined in Table 5.3). The algorithm of the program is shown in Figure 5.9. To ensure that the resulting optimal results produce realistic reactor performance, a series of physical reactor constraints was introduced:

- Maximum allowable temperature inside the reactor is set to 550 K;
- Maximum allowable pressure drop is set to 13 bar (i.e. approximately 1 bar/m);
- Maximum (single-pass) CO conversion is 60 %.

If any of these constraints are not met the inlet process parameters cannot be chosen as optimal. Realistic constraints were also set on the values of process parameters itself, so

the inlet temperature could have values 463 to 503 K, reactant feed ratio 1.8 to 2.2 and flowrate 0.05 to 0.5 mol/s.

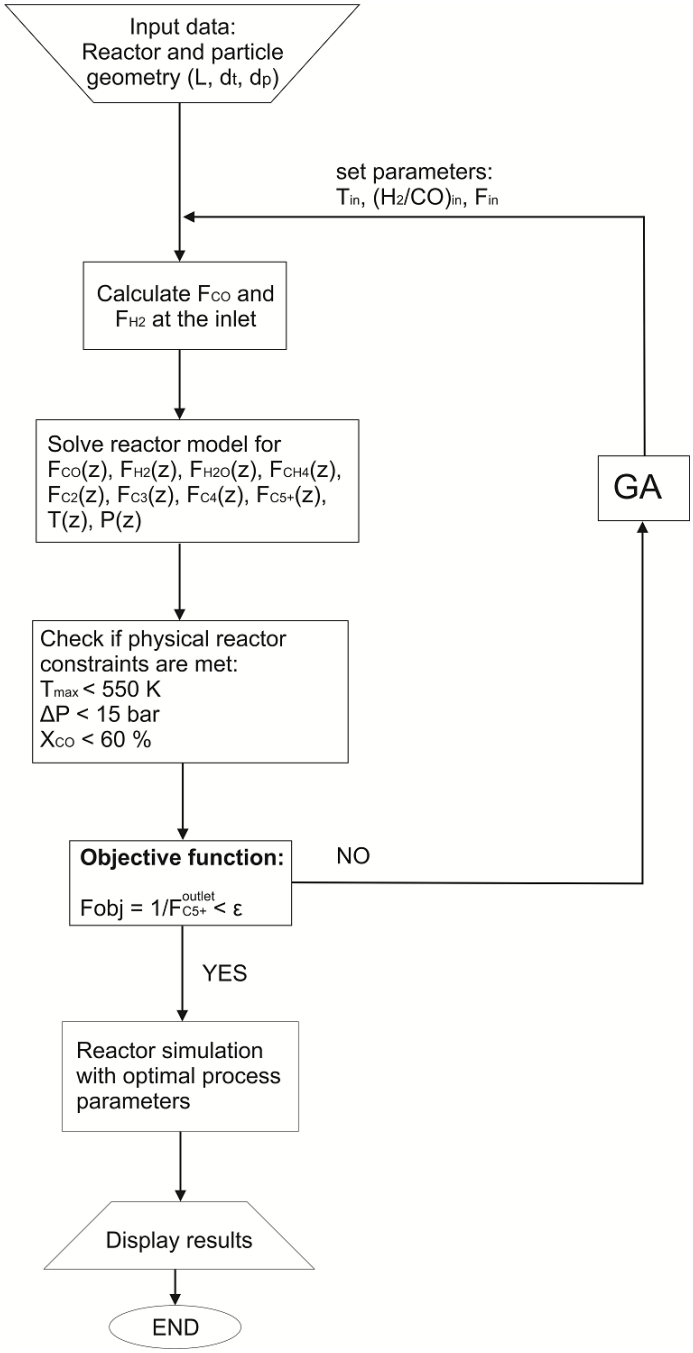

Figure 5.9 - Algorithm of reactor optimization program.

Results of process condition optimization are shown in Figure 5.10 and Table 5.4. Even though no initial guess (i.e. initial population) was set, the optimization routine found that the optimal conditions were relatively similar to those used for the base case

(T_{in} = 475 K, feed H_2/CO = 2.0 and F_{in} = 0.15 mol/s). Therefore, the comparison between the results with optimized process conditions and base case in presented in Figure 5.10 and Table 5.4. The optimized inlet temperature was 477.3 K, feed H_2/CO ratio 1.83 and inlet syngas flowrate 0.156 mol/s. The use of optimal conditions results in CO conversion of 60 %, C_{5+} selectivity of 90.2 %, productivity of 160 380 tonnes/year (for average product C_9 and 26150 tubes), mean reactor bed temperature 479.4 K and pressure drop around 13 bar (Figure 5.10). From the results we see that all of the physical restrictions on the reactor were met. Compared to the base case, the optimal inlet temperature and inlet flowrate increased slightly, from 475 to 477.3 K and 0.15 to 0.156 mol/s, respectively. Opposite to them, the optimal feed reactant ratio was lower compared to base case with 1.83 compared to 2.0.

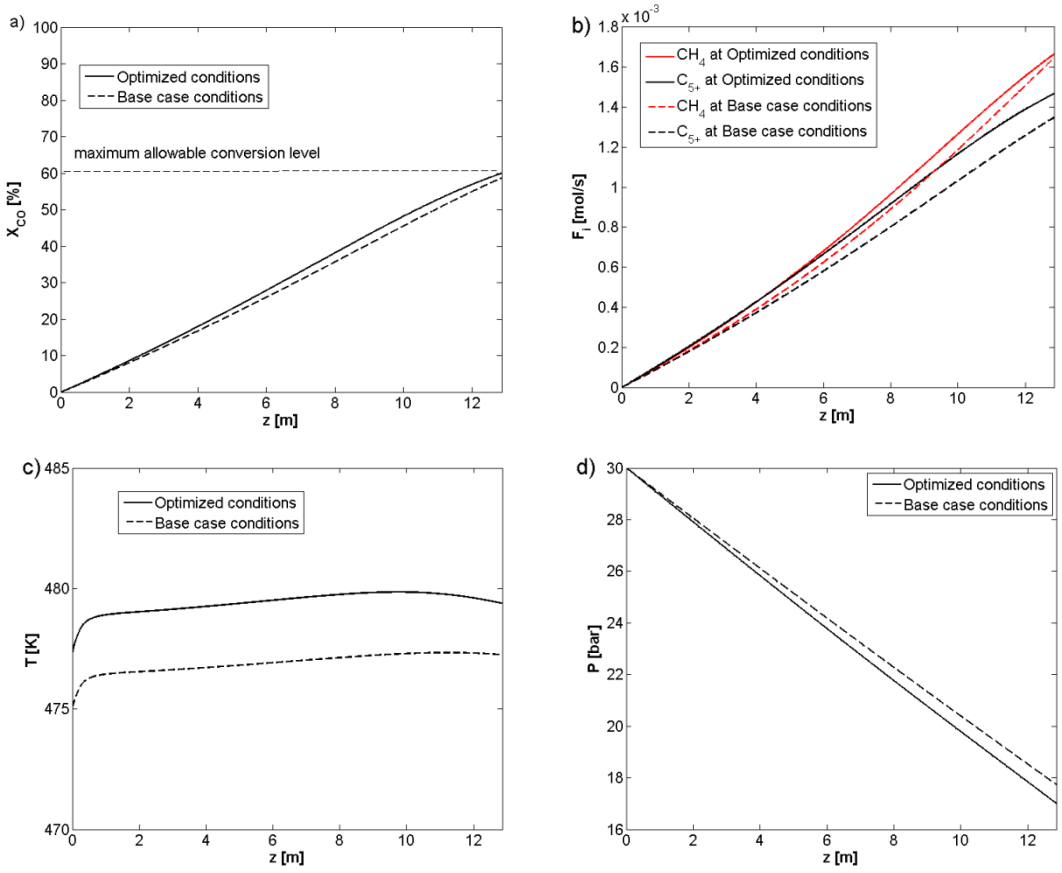

Figure 5.10 – Reactor simulation results using optimized values of process conditions and comparison to base case results (Optimized conditions: T_{in} = 474.8 K, Feed H_2/CO = 2.13 and F_{in} = 0.155 mol/s with fixed Pin = 30 bar) at defined geometry (from Table 5.3)

Table 5.4 – Comparison of optimized process conditions and results obtained with them with base case (geometry defined in Table 5.3)

Process conditions	Optimized conditions	Base case	Model results	Optimized conditions	Base case
Inlet temperature (K)	477.3	475.0	CO conversion (%)	60.0	58.7
Feed H_2/CO	1.82	2.00	C_{5+} selectivity (%)	90.2	89.7
Inlet syngas flowrate (mol/s)	0.152	0.150	C_{5+} flowrate (mmol/s)	1.47	1.35
Inlet pressure (bar)	30		Maximum bed temperature (K)	479.9	477.3
			Pressure drop (bar)	13.0	12.3

Maximum C_{5+} productivity will be achieved for the maximum conversion with the maximum inlet flowrate. Because maximum allowable conversion is set to 60 %, the optimal solution will look to maximize inlet flowrate at that conversion level. As we saw from the simulations in which the inlet flowrate was varied, increase of F_{in} causes a drop in conversion level and an increase in pressure drop. Therefore, increasing the inlet flowrate has to be accompanied with increased temperature or increased feed ratio, in order to achieve the maximum allowable conversion. Increasing the temperature will increase the conversion level, but it has a detrimental effect on heat management and product selectivity. Opposite to that, decreasing the reactant feed ratio slightly decreases the CO conversion level, but has a positive effect on product selectivity, without affecting heat removal. This is why, the optimal solution has slightly higher temperature and inlet flowrate together lower feed H_2/CO ratio.

Recommendations for fixed-bed reactor modeling and plans for future work

As shown in Chapter 3, FTS product selectivity varies with process conditions. Therefore, in order to be able to develop a reliable model of an FTS reactor, detailed kinetics has to be considered. In this part we demonstrated the application of detailed kinetic model of FTS in conjunction with the use of a pseudohomogenious fixed-bed reactor model. Simulations were performed to determine the effect of various process conditions at the reactor inlet (including temperature, reactant ratio and syngas flowrate)

on the reactor performance. The optimization of process conditions at the fixed-bed inlet showed how a proper selection these parameters can lead to the maximum value of desired C_{5+} products. Prediction of product selectivity at different process conditions inside the reactor plays an important role in determining the optimal solution, but other factors, such as maximum allowable conversion level, heat and pressure drop management need to be considered as well.

The fixed-bed reactor model presented in this Chapter was utilized to highlight the importance of using detailed kinetics in the development of FTS reactor models. However, this model includes many assumptions (e.g. no liquid flow in the reactor, maximum catalyst effectiveness, fluid plug flow etc.) and its level of detail can be significantly improved in order to get a more reliable representation of industrial FTS fixed-bed reactors. A comprehensive model of a multi-tubular FTS fixed-bed reactor would need to include the following:

- Detailed kinetic model of FTS including secondary reactions, most important of which is the secondary pathway for methane formation;
- Particle mass and heat transport model for prediction of the effect of mass and heat transfer resistances on catalyst effectiveness and selectivity;
- Prediction of vapor-liquid equilibrium (VLE) inside the reactor. This way the distribution of reactant and product components between the gas and liquid phase inside the reactor would become known, enabling for more precise modeling of the trickle bed flow pattern;
- Application of computational fluid dynamics (CFD) methods in modeling of fluid behavior inside the reactor bed.

Faculty of Technology and Metallurgy (FTM) and Texas A&M University at Qatar (TAMUQ) have received a 3 year funding from Qatar National Research Fund (QNRF, a member of Qatar Foundation), starting from February 2015., under the National Priority Research Program (NPRP) Grant No. 7-559-2-211 “Modeling, optimization and dynamic analysis of fixed bed and milli-structured reactors for Fischer-Tropsch synthesis”. Specific goal of this project is the development of a comprehensive and highly sophisticated models of conventional FTS fixed bed and novel milli-structured reactor

systems by coupling of detailed FTS surface kinetics, realistic heat and mass transfer balances inside the catalyst particle with computational fluid dynamics reactor balances for mass, heat and momentum. The obtained model will be used to determine the optimal operational parameters (reactor and particle geometries, process conditions etc.) and to study the dynamics of milli-structured reactors. In the end, based on obtained results we will provide recommendations on how to improve the reactor design and FTS process in general.

6. Conclusions

The Fischer-Tropsch synthesis technology for the production of hydrocarbons from synthesis gas has been utilized on industrial scale for almost 80 years. Currently it is used in gas-, coal- and biomass-to-liquid plants to produce liquid fuels and valuable commodity chemicals at both large and small scale. Due to this versatility of applications in different types of chemical plants, it can be expected that FTS will remain relevant throughout the 21st century. In this thesis we have comprehensively analyzed the FTS technology with focus on reaction kinetics, development of detailed kinetic models for the prediction of both reactant consumption and product formation and the application of such detailed kinetics in the modeling and optimization of fixed-bed reactors for FTS.

Chapter 2 gives an overview of the current literature on the fundamentals of FTS, including reviews of reaction mechanism, secondary reactions, effects of process conditions on the product selectivity and distribution. This Chapter also included a review of kinetic modeling, different reactor types and models of fixed-bed reactors. In the end, we discussed the opportunities for use of micro-reactors in FTS to improve reactor productivity and selectivity.

The analysis of experimental data obtained with two of the most commercially used types of FTS catalysts (cobalt and iron) was described in Chapter 3. We analyzed the effect of various process conditions, including temperature, pressure, reactant feed ratio and conversion level on the FTS product selectivity, as well as chain growth probability, ratios of products etc. Important contributions made in this chapter were the following:

- For both cobalt- and iron-based catalysts the data showed that the undesired methane selectivity can be decreased and desired C_{5+} selectivity increased by decreasing temperature and reactant feed ratio, as well as increasing pressure.
- Methane formation over cobalt catalyst proceeds over two different pathways, the primary FTS chain-growth pathway and a secondary hydrogenation pathway. Better understanding of this secondary pathway could lead to reduction of excess methane formation and significantly improved product selectivity.

- Another important observation for cobalt-based catalyst was the lack of variation of C_{2+} growth probabilities with residence time at all process conditions. This strongly suggested that secondary 1-olefin readsorption and continued chain growth do not play a significant role in determining product selectivity, as previously thought.
- Unlike for cobalt catalyst, data from iron-based catalyst showed that excess methane formation is lower and that secondary hydrogenation pathway is less important in determining the overall selectivity over this catalyst.
- Iron catalyst is highly active in the water-gas shift (WGS) reaction, which made analysis of FTS reaction kinetics additionally complex. An interesting result with iron catalyst showed that for some conditions (low H2/CO ratio of 0.67 and moderate pressure of 1.5 MPa) the partial pressure of water declines with increasing conversion level. This could have important applications for the selection of coal gasifier units that produce syngas in CTL plants.

Detailed LHHW models of FTS kinetics were developed and described in Chapter 4. Contributions made in the Chapter include:

- Derivation of detailed kinetic model of FTS based on the CO-insertion reaction mechanism. This model provided the best prediction of FTS reaction rates, over a a wide range of data used, considering various statistics and physico-chemical criteria.
- A concept of chain-length-dependent 1-olefin desorption was derived from fundamentals and introduced in the models in order to account for increasing

In Chapter 5 the developed detailed model of FTS kinetics was used to simulate performance of a fixed-bed reactor model. The original contributions highlighted for this part of the dissertation are:

- The utilization of a detailed kinetic model, including both reactant disappearance and product formation rates for FTS over cobalt catalyst, for the development of a more detailed model of fixed-bed reactor.

- An optimization of critical reactor inlet process parameters (inlet temperature, reactant feed ratio and flowrate) was conducted using the proposed reactor model. It was found that the productivity of desired C_{5+} products can be increased (compared to the base case), while maintaining the physical restrictions on reactant conversion level, maximum temperature and pressure drop, by choosing the optimal conditions.

The work on this dissertation resulted in a number of peer-reviewed publications and conference presentations, which are listed below. These included a number of potentially significant scientific contributions, such as the highlighting of secondary methane formation in determining FTS selectivity, development of detailed kinetic model for a promoted cobalt-based catalyst etc. The work presented in this dissertation will also serve as a foundation for future work under NPRP Grant No. 7-559-2-211, a collaborative project between FTM and TAMUQ funded by QNRF, which will deal with development of a comprehensive models of fixed-bed reactors for FTS and their optimization.

References

[1] U.S. Energy Information Administration, Annual Energy Outlook, 2014.
[2] M.E. Dry, Catalysis Today, 71 (2002) 227.
[3] P. Sabatier and J. Senderens, Journal of the Society of Chemical Industry, 21 (1902) 504.
[4] F. Fischer and H. Tropsch, Brennstoff-Chemie, 7 (1926) 97.
[5] F. Fischer and H. Tropsch, Brennstoff-Chemie, 4 (1923) 276.
[6] A.N. Stranges, Stud. Surf. Sci. Catal., 163 (2007) 1.
[7] C.H. Bartholomew and R.J. Farrauto, Reactors, Reactor Design, and Activity Testing - Fundamentals of Industrial Catalytic Processes, John Wiley & Sons, 2006.
[8] A. Krammer, Technology and Culture, 22 (1981) 68.
[9] BP Statistical Review of World Energy 2014, 2014.
[10] http://www.velocys.com/ (last accessed August 30, 2014)
[11] http://www.compactgtl.com/ (last accessed August 30, 2014)
[12] T. Miyazawa, T. Hanaoka, K. Shimura and S. Hirata, Kagaku Kogaku, 77 (2013) 639.
[13] E. Rytter, E. Ochoa-Fernandez and A. Fahmi, Catalytic Process Development for Renewable Materials, Conference Proceeding, 2013.
[14] M.I. Gonzalez, B. Kraushaar-Czarnetzki and G. Schaub, Biomass Convers. Biorefin., 1 (2011) 229.
[15] J. Hu, F. Yu and Y. Lu, Catalysts, 2 (2012) 303.
[16] A.Y. Krylova, Kinetics and Catalysis, 53 (2012) 742.
[17] R. Luque, A.R. de la Osa, J.M. Campelo, A.A. Romero, J.L. Valverde and P. Sanchez, Energy & Environmental Science, 5 (2012) 5186.
[18] P.K. Swain, L.M. Das and S.N. Naik, Renewable Sustainable Energy Reviews, 15 (2011) 4917.
[19] X. Hao, G. Dong, Y. Yang, Y. Xu and Y. Li, Chememical Engineering Technology, 30 (2007) 1157.
[20] M. Hook and K. Aleklett, International Journal of Energy Research, 34 (2010) 848.
[21] M.P. Dudukovic, Chemical Engineering Science, 65 (2010) 3.
[22] http://www.infomine.com/investment/metal-prices (last accessed August 30, 2014)
[23] G.P. van der Laan and A.A.C.M. Beenackers, Catalysis reviews. Science and engineering, 41 (1999).
[24] B.H. Davis, Industrial & Engineering Chemistry Research, 46 (2007) 8938.
[25] J. Yang, W. Ma, D. Chen, A. Holmen and B.H. Davis, Applied Catalysis A: General, 470 (2014) 250.
[26] F.G. Botes, J.W. Niemantsverdriet and J. van de Loosdrecht, Catalysis Today, 215 (2013) 112.
[27] M.E. Dry, Studies in Surface Science and Catalysis, 152 (2004) 533.
[28] E. Iglesia, S.C. Reyes, R.J. Madon and S.L. Soled, Advances in Catalysis, 39 (1993) 221.
[29] E. Iglesia, Applied Catalysis A: General, 161 (1997) 59.
[30] A.Y. Khodakov, W. Chu and P. Fongarland, Chemical Reviews, 107 (2007) 1692.

[31] M. Claeys and E. van Steen, Studies in Surface Science and Catalysis, 152 (2004) 601.
[32] A.A. Adesina, Applied Catalysis A: General, 138 (1996) 345.
[33] B.H. Davis, Fuel Processing Technology, 71 (2001) 157.
[34] M.E. Dry, Applied Catalysis A: General, 138 (1996) 319.
[35] M.E. Dry, Journal of Molecular Catalysis, 17 (1982) 133.
[36] R.C. Brady, III and R. Pettit, Journal of American Chemical Society, 103 (1981) 1287.
[37] H. Pichler and H. Schulz, Chemie Ingenieur Technik, 42 (1970) 1162.
[38] R.B. Anderson, R.A. Friedel and H.H. Storch, Journal of Chemcal Physics, 19 (1951) 313.
[39] P.M. Maitlis, R. Quyoum, H.C. Long and M.L. Turner, Applied Catalysis A: General, 186 (1999) 363.
[40] J.T. Kummer, T.W. DeWitt and P.H. Emmett, Journal of American Chemical Society, 70 (1948) 3632.
[41] I.M. Ciobîca, G.J. Kramer, Q. Ge, M. Neurock and R.A. van Santen, Journal of Catalysis, 212 (2002) 136.
[42] I.M. Ciobica and R.A. van Santen, The Journal of Physical Chemistry B, 106 (2002) 6200.
[43] P. Johnston and R.W. Joyner, Studies in Surface Science and Catalysis, 75 (1993) 165.
[44] P.M. Maitlis, H.C. Long, R. Quyoum, M.L. Turner and Z.-Q. Wang, Chemical Communications, 1 (1996) 1.
[45] Q. Ge, M. Neurock, H.A. Wright and N. Srinivasan, The Journal of Physical Chemistry B, 106 (2002) 2826.
[46] H.H. Storch, N. Golumbic and R.B. Anderson, The Fischer-Tropsch and Related Syntheses, John Wiley & Sons, New York, 1951.
[47] J. Schweicher, A. Bundhoo and N. Kruse, Journal of American Chemical Society, 134 (2012) 16135.
[48] J. Schweicher, A. Bundhoo, A. Frennet, N. Kruse, H. Daly and F.C. Meunier, The Journal of Physical Chemistry C, 114 (2010) 2248.
[49] M. Corral Valero and P. Raybaud, Catalysis Letters, 143 (2013) 1.
[50] R.A. van Santen, I.M. Ciobîcă, E. van Steen and M.M. Ghouri, in C.G. Bruce and K. Helmut (Editors), Advances in Catalysis, Vol. 54, Academic Press, 2011, p. 127.
[51] X.-Q. Gong, R. Raval and P. Hu, Surface Science, 562 (2004) 247.
[52] S. Storsæter, D. Chen and A. Holmen, Surface Science, 600 (2006) 2051.
[53] M. Zhuo, K.F. Tan, A. Borgna and M. Saeys, The Journal of Physical Chemistry C, 113 (2009) 8357.
[54] M. Ojeda, R. Nabar, A.U. Nilekar, A. Ishikawa, M. Mavrikakis and E. Iglesia, Journal of Catalysis, 272 (2010) 287.
[55] C.-F. Huo, J. Ren, Y.-W. Li, J. Wang and H. Jiao, Journal of Catalysis, 249 (2007) 174.
[56] C.-F. Huo, Y.-W. Li, J. Wang and H. Jiao, The Journal of Physical Chemistry C, 112 (2008) 14108.
[57] D.C. Sorescu, The Journal of Physical Chemistry C, 113 (2009) 9256.

[58] M.P. Andersson, F. Abild-Pedersen, I.N. Remediakis, T. Bligaard, G. Jones, J. Engbæk, O. Lytken, S. Horch, J.H. Nielsen, J. Sehested, J.R. Rostrup-Nielsen, J.K. Nørskov and I. Chorkendorff, Journal of Catalysis, 255 (2008) 6.
[59] S. Shetty, A.P.J. Jansen and R.A. van Santen, Journal of the American Chemical Society, 131 (2009) 12874.
[60] E. Shustorovich and H. Sellers, Surface Science Reports, 31 (1998) 1.
[61] M. Zhuo, A. Borgna and M. Saeys, Journal of Catalysis, 297 (2013) 217.
[62] J. Cheng, P. Hu, P. Ellis, S. French, G. Kelly and C.M. Lok, Journal of Catalysis, 257 (2008) 221.
[63] J. Cheng, P. Hu, P. Ellis, S. French, G. Kelly and C.M. Lok, The Journal of Physical Chemistry C, 114 (2009) 1085.
[64] J. Cheng, P. Hu, P. Ellis, S. French, G. Kelly and C.M. Lok, The Journal of Physical Chemistry C, 112 (2008) 6082.
[65] H.-J. Li, C.-C. Chang and J.-J. Ho, The Journal of Physical Chemistry C, 115 (2011) 11045.
[66] Z.-P. Liu and P. Hu, Journal of the American Chemical Society, 124 (2002) 11568.
[67] N. Kapur, J. Hyun, B. Shan, J.B. Nicholas and K. Cho, The Journal of Physical Chemistry C, 114 (2010) 10171.
[68] S. Shetty, R.A. van Santen, P.A. Stevens and S. Raman, Journal of Molecular Catalysis A: Chemical, 330 (2010) 73.
[69] O.R. Inderwildi, S.J. Jenkins and D.A. King, The Journal of Physical Chemistry C, 112 (2008) 1305.
[70] O.R. Inderwildi, D.A. King and S.J. Jenkins, Physical Chemistry Chemical Physics, 11 (2009) 11110.
[71] A.J. Markvoort, R.A. van Santen, P.A.J. Hilbers and E.J.M. Hensen, Angewandte Chemie International Edition, 51 (2012) 9015.
[72] D.-B. Cao, Y.-W. Li, J. Wang and H. Jiao, Journal of Molecular Catalysis A: Chemical, 346 (2011) 55.
[73] N.E. Tsakoumis, M. Ronning, O. Borg, E. Rytter and A. Holmen, Catalysis Today, 154 (2010) 162.
[74] D.J. Moodley, On the Deactivation of Cobalt-based Fischer-Tropsch Synthesis Catalysts, PhD Thesis, Eindhoven University of Technology, Eindhoven, 2008.
[75] M.J. van Vuuren, J. Huyser, T. Grobler and G. Kupi, Chemical Industries, 128 (2010) 229.
[76] D.B. Bukur, S.A. Patel and X. Lang, Applied Catalalysis, 61 (1990) 329.
[77] D.B. Bukur and X. Lang, Studies in Surface Science and Catalysis, 119 (1998) 113.
[78] M. Sadeqzadeh, J. Hong, P. Fongarland, D. Curulla-Ferre, F. Luck, J. Bousquet, D. Schweich and A.Y. Khodakov, Industrial & Engineering Chemistry Research, 51 (2012) 11955.
[79] J. Xu, C.H. Bartholomew, J. Sudweeks and D.L. Eggett, Topics in Catalysis, 26 (2003) 55.
[80] H.N. Pham, L. Nowicki, J. Xu, A.K. Datye, D.B. Bukur and C. Bartholomew, Industrial & Engineering Chemistry Research, 42 (2003) 4001.
[81] S.A. Eliason and C.H. Bartholomew, Applied Catalysis A: General, 186 (1999) 229.

[82] C.H. Bartholomew, Applied Catalysis A: General, 212 (2001) 17.
[83] R.M. Bowman and C.H. Bartholomew, Applied Catalysis, 7 (1983) 179.
[84] J. L. Rankin, Investigation of sulfur-tolerant catalysts for selective synthesis of hydrocarbon liquids from coal-derived gases, DOE Report, 1982.
[85] F.H. Ribeiro, A.E.S.V. Wittenau, C.H. Bartholomew and G.A. Somorjai, Catalysis Reviews: Science and Engineering, 39 (1997) 49.
[86] G.P. Van der Laan and A.A.C.M. Beenackers, Catalysis Reviews: Science and Engineering, 41 (1999) 255.
[87] A. Tavasoli, A.N. Pour and M.G. Ahangari, Journal of Natural Gas Chemistry, 19 (2010) 653.
[88] W. Qian, H. Zhang, W. Ying and D. Fang, Journal of Natural Gas Chemistry, 20 (2011) 389.
[89] A.R. de la Osa, A. De Lucas, A. Romero, J.L. Valverde and P. Sanchez, Fuel, 90 (2011) 1935.
[90] Y. Liu, B.-T. Teng, X.-H. Guo, Y. Li, J. Chang, L. Tian, X. Hao, Y. Wang, H.-W. Xiang, Y.-Y. Xu and Y.-W. Li, Journal of Molecular Catalysis A: Chemical, 272 (2007) 182.
[91] T.J. Donnelly and C.N. Satterfield, Applied Catalysis, 52 (1989) 93.
[92] R.A. Dictor and A.T. Bell, Journal of Catalysis, 97 (1986) 121.
[93] D.B. Bukur, L. Nowicki and X. Lang, Catalysis Today, 24 (1995) 111.
[94] I.C. Yates and C.N. Satterfield, Energy & Fuels, 6 (1992) 308.
[95] C.G. Visconti, E. Tronconi, L. Lietti, R. Zennaro and P. Forzatti, Chemical Engineering Science, 62 (2007) 5338.
[96] F.G. Botes, J.W. Niemantsverdriet and J. van de Loosdrecht, Catalysis Today, 215 (2013) 112.
[97] R.B. Anderson, Hydrocarbon Synthesis, Hydrogenation and Cyclization, Reinhold, New York, 1956.
[98] A. Steynberg and M. Dry, Fischer-Tropsch Technology, Studies in Surface Science and Catalysis, 152 (2004) 64.
[99] A. Dinse, M. Aigner, M. Ulbrich, G.R. Johnson and A.T. Bell, Journal of Catalysis, 288 (2012) 104.
[100] H. Schulz, Chemical Industries, 128 (2010) 165.
[101] F.G. Botes, Industrial and Engineering Chemistry, 48 (2009) 1859.
[102] A. Dinse, M. Aigner, M. Ulbrich, G.R. Johnson and A.T. Bell, Journal of Catalysis, 288 (2012) 104.
[103] B. Todic, W. Ma, G. Jacobs, B.H. Davis and D.B. Bukur, Journal of Catalysis, 311 (2014) 325.
[104] J. Patzlaff, Y. Liu, C. Graffmann and J. Gaube, Applied Catalysis A: General, 186 (1999) 109.
[105] D.B. Bukur, X. Lang, A. Akgerman and Z. Feng, Industrial & Engineering Chemistry Research, 36 (1997) 2580.
[106] D.B. Bukur, Z. Pan, W. Ma, G. Jacobs and B.H. Davis, Catalysis Letters, 142 (2012) 1382.
[107] W. Ma, G. Jacobs, Y. Ji, T. Bhatelia, D. Bukur, S. Khalid and B. Davis, Topics in Catalysis, (2011) 1.
[108] E. Iglesia, S.C. Reyes and R.J. Madon, Journal of Catalysis, 129 (1991) 238.

[109] E.W. Kuipers, C. Scheper, J.H. Wilson, I.H. Vinkenburg and H. Oosterbeek, Journal of Catalysis, 158 (1996) 288.
[110] E. Iglesia, S.C. Reyes and S.L. Soled, Computer-Aided Design of Catalysts and Reactors, 51 (1993) 199.
[111] S. Storsæter, Ø. Borg, E.A. Blekkan and A. Holmen, Journal of Catalysis, 231 (2005) 405.
[112] S. Krishnamoorthy, M. Tu, M.P. Ojeda, D. Pinna and E. Iglesia, Journal of Catalysis, 211 (2002) 422.
[113] M. Rothaemel, H.K. Firing, E.A. Blekkan, D. Schanke and A. Holmen, Catalysis Today, 38 (1997) 79.
[114] K.F. Hanssen, E.A. Blekkan, D. Schanke and A. Holmen, Studies in Surface Science and Catalysis, 109 (1997) 193.
[115] A.M. Hilmen, D. Schanke, K.F. Hanssen and A. Holmen, Applied Catalysis A: General, 186 (1999) 169.
[116] C.J. Bertole, C.A. Mims and G. Kiss, Journal of Catalysis, 210 (2002) 84.
[117] E.A. Blekkan, O. Borg, V. Froseth and A. Holmen, Catalysis, 20 (2007) 13.
[118] A.K. Dalai and B.H. Davis, Applied Catalysis A: General, 348 (2008) 1.
[119] S. Lögdberg, M. Lualdi, S. Järås, J.C. Walmsley, E.A. Blekkan, E. Rytter and A. Holmen, Journal of Catalysis, 274 (2010) 84.
[120] G.V. Schulz, Physik. Chem., B30 (1935) 379.
[121] B. Sarup and B.W. Wojciechowski, Canadian Journal of Chemical Engineering, 66 (1988) 831.
[122] G.A. Huff, Jr. and C.N. Satterfield, Journal of Catalysis, 85 (1984) 370.
[123] R. Zhang, J. Chang, Y. Xu, L. Cao, Y. Li and J. Zhou, Energy & Fuels, 23 (2009) 4740.
[124] A.P. Raje and B.H. Davis, Energy & Fuels, 10 (1996) 552.
[125] X. Zhan and B.H. Davis, Petroleum Science and Technology, 18 (2000) 1037.
[126] B. Shi and B.H. Davis, Applied Catalysis A: General, 277 (2004) 61.
[127] I. Puskas and R.S. Hurlbut, Catalysis Today, 84 (2003) 99.
[128] I. Puskas, R.S. Hurlbut and R.E. Pauls, Journal of Catalysis, 139 (1993) 591.
[129] D. Vervloet, F. Kapteijn, J. Nijenhuis and O.J.R. van, Catalysis Science & Technology, 2 (2012) 1221.
[130] S. Novak, R.J. Madon and H. Suhl, Journal of Catalysis, 77 (1982) 141.
[131] H. Schulz and M. Claeys, Applied Catalysis A: General, 186 (1999) 91.
[132] G.P. van der Laan and A.A.C.M. Beenackers, Industrial & Engineering Chemistry Research, 38 (1999) 1277.
[133] W. Zimmerman, D. Bukur and S. Ledakowicz, Chemical Engineering Science, 47 (1992) 2707.
[134] E.W. Kuipers, I.H. Vinkenburg and H. Oosterbeek, Journal of Catalysis, 152 (1995) 137.
[135] R.J. Madon and E. Iglesia, Journal of Catalysis, 139 (1993) 576.
[136] L. Nowicki, S. Ledakowicz and D. B. Bukur, Chemical Engineering Science, 56 (2001) 1175.
[137] C.N. Satterfield and G.A. Huff, Jr., Journal of Catalysis, 73 (1982) 187.
[138] C.N. Satterfield, G.A. Huff and J.P. Longwell, Industrial & Engineering Chemistry Process Design and Development, 21 (1982) 465.

[139] G.A. Huff and C.N. Satterfield, Industrial & Engineering Chemistry Process Design and Development, 24 (1985) 986.
[140] R.A. Dictor and A.T. Bell, Industrial & Engineering Chemistry Process Design and Development, 22 (1983) 678.
[141] L. Caldwell and D.S. Van Vuuren, Chemical Engineering Science, 41 (1986) 89.
[142] J. Yang, W. Shafer, V. Pendyala, G. Jacobs, D. Chen, A. Holmen and B. Davis, Catalysis Letters, 144 (2014) 524.
[143] B. Shi and B.H. Davis, Catalysis Today, 106 (2005) 129.
[144] L.M. Tau, H. Dabbagh, S. Bao and B.H. Davis, Catalysis Letters, 7 (1990) 127.
[145] Y. Yao, X. Liu, D. Hildebrandt and D. Glasser, Applied Catalysis A: General, 433-434 (2012) 58.
[146] J. Gao, B. Wu, L. Zhou, Y. Yang, X. Hao, J. Xu, Y. Xu and Y. Li, Industrial & Engineering Chemistry Research, 51 (2012) 11618.
[147] C.M. Masuku, W.D. Shafer, W. Ma, M.K. Gnanamani, G. Jacobs, D. Hildebrandt, D. Glasser and B.H. Davis, Journal of Catalysis, 287 (2012) 93.
[148] J. Yang, W. Shafer, V. Pendyala, G. Jacobs, W. Ma, D. Chen, A. Holmen and B. Davis, Topics in Catalysis, 57 (2014) 508.
[149] H.A.J.v. Dijk, The Fischer-Tropsch synthesis: A mechanistic study using transient isotopic tracing, PhD Thesis, Technische Universiteit Eindhoven, 2001.
[150] G. Botes, Kinetic and Selectivity Modelling of the Iron-Based Low-Temperature Fischer-Tropsch Synthesis, PhD Thesis, Technische Universiteit Eindhoven, 2008.
[151] C.N. Satterfield, R.T. Hanlon, D.K. Matsumoto, T.J. Donnelly and I.C. Yates, Fischer-Tropsch slurry phase process variations to understand wax formation: final technical report, 1989, p. 51
[152] T.J. Donnelly, I.C. Yates and C.N. Satterfield, Energy & Fuels, 2 (1988) 734.
[153] J. Patzlaff, Y. Liu, C. Graffmann and J. Gaube, Catalysis Today, 71 (2002) 381.
[154] J. Huyser, M.J. van Vuuren and G. Kupi, Chemical Industries, 128 (2010) 185.
[155] N.O. Egiebor and W.C. Cooper, Applied Catalysis, 14 (1985) 323.
[156] N.O. Egiebor, W.C. Cooper and B.W. Wojciechowski, Canadian Journal of Chemical Engineering, 63 (1985) 826.
[157] L. Koenig and J. Gaube, Chemie Ingenieur Technik, 55 (1983) 14.
[158] D.B. Bukur, Z. Nowicki, R.K. Manne and X. Lang, Journal of Catalysis, 155 (1995) 366.
[159] D.B. Bukur, K. Okabe, M.P. Rosynek, C. Li, D. Wang, K.R.P.M. Rao and G.P. Huffman, Journal of Catalysis, 155 (1995) 353.
[160] E. van Steen and H. Schulz, Applied Catalysis A: General, 186 (1999) 309.
[161] K.D. Kruit, D. Vervloet, F. Kapteijn and J.R. van Ommen, Catalysis Science & Technology, 3 (2013) 2210.
[162] D.B. Bukur, L. Nowicki and X. Lang, Energy & Fuels, 9 (1995) 620.
[163] E.F.G. Herington, Chememical Industries, 65 (1946) 346.
[164] H. Schulz and M. Claeys, Applied Catalysis A: General, 186 (1999) 71.
[165] L.M. Tau, H.A. Dabbagh and B.H. Davis, Energy & Fuels, 4 (1990) 94.
[166] L. Nowicki and D.B. Bukur, Studies in Surface Science and Catalysis, Vol. 119, Elsevier, 2001, p. 123.
[167] B. Todic, T. Olewski, N. Nikacevic and D.B. Bukur, Chemical Engineering Transactions, 32 (2013) 793.

[168] G.P. van der Laan and A.A.C.M. Beenackers, Studies in Surface Science and Catalysis, 119 (1998) 179.
[169] F.G. Botes, Energy & Fuels, 21 (2007) 1379.
[170] R.T. Hanlon and C.N. Satterfield, Energy & Fuels, 2 (1988) 196.
[171] A.W. Weitkamp, H.S. Seelig, N.J. Bowman and W.E. Cady, Journal of Industrial Engineering Chemistry, 45 (1953) 343.
[172] V. Sage and N. Burke, Catalysis Today, 178 (2011) 137.
[173] L.-M. Tau, H.A. Dabbagh, J. Halasz and B.H. Davis, Journal of Molecular Catalysis, 71 (1992) 37.
[174] H. Schulz, Topics in Catalysis, 26 (2003) 73.
[175] M.K. Gnanamani, R.A. Keogh, W.D. Shafer and B.H. Davis, Applied Catalysis A: General, 393 (2011) 130.
[176] B. Shi, G. Jacobs, D. Sparks and B.H. Davis, Fuel, 84 (2005) 1093.
[177] H. Schulz, B.R. Rao and M. Elstner, Erdöl und Kohle – Erdgas – Petrochemie, 23 (1970).
[178] H. Schulz, E. van Steen and M. Claeys, Topics in Catalysis, 2 (1995) 223.
[179] C. Aaserud, A.-M. Hilmen, E. Bergene, S. Eric, D. Schanke and A. Holmen, Catalysis Letters, 94 (2004) 171.
[180] K. Krishna and A. Bell, Catalysis Letters, 14 (1992) 305.
[181] A.A. Adesina, R.R. Hudgins and P.L. Silveston, Applied Catalysis, 62 (1990) 295.
[182] J.H. Boelee, J.M.G. Cüsters and K. Van Der Wiele, Applied Catalysis, 53 (1989) 1.
[183] F.G. Botes and N.S. Govender, Energy & Fuels, 21 (2007) 3095.
[184] W.H. Zimmerman and D.B. Bukur, The Canadian Journal of Chemical Engineering, 68 (1990) 292.
[185] G.A. Huff and C.N. Satterfield, Industrial & Engineering Chemistry Process Design and Development, 23 (1984) 696.
[186] R. Zennaro, M. Tagliabue and C.H. Bartholomew, Catalysis Today, 58 (2000) 309.
[187] T.K. Das, W.A. Conner, J. Li, G. Jacobs, M.E. Dry and B.H. Davis, Energy & Fuels, 19 (2005) 1430.
[188] G. Bub and M. Baerns, Chemical Engineering Science, 35 (1980) 348.
[189] M.E. Dry, Industrial & Engineering Chemistry Process Design and Development, 15 (1976) 282.
[190] H.E. Atwood and C.O. Bennett, Industrial & Engineering Chemistry Process Design and Development, 18 (1979) 163.
[191] W.D. Deckwer, R. Kokuun, E. Sanders and S. Ledakowicz, Industrial & Engineering Chemistry Process Design and Development, 25 (1986) 643.
[192] S. Ledakowicz, H. Nettelhoff, R. Kokuun and W.D. Deckwer, Industrial & Engineering Chemistry Process Design and Development, 24 (1985) 1043.
[193] B. Sarup and B.W. Wojciechowski, The Canadian Journal of Chemical Engineering, 67 (1989) 62.
[194] B. W. Wojciechowski, The kinetics of the Fischer-Tropsch synthesis, Taylor & Francis, Colchester, 1988.
[195] I.C. Yates and C.N. Satterfield, Energy & Fuels, 5 (1991) 168.
[196] A. Outi, I. Rautavuoma and H.S. van der Baan, Applied Catalysis, 1 (1981) 247.

[197] F.G. Botes, B. van Dyk and C. McGregor, Industrial & Engineering Chemistry Research, 48 (2009) 10439.
[198] T. Bhatelia, W. Ma, B. Davis, G. Jacobs and D. Bukur, ChemicaI Engineering Transactions, 25 (2011) 707.
[199] G.P. van der Laan and A.A.C.M. Beenackers, Applied Catalysis A: General, 193 (2000) 39.
[200] W. Ma, G. Jacobs, D.E. Sparks, R.L. Spicer, B.H. Davis, J.L.S. Klettlinger and C.H. Yen, Catalysis Today, 228 (2014) 158.
[201] O. Levenspiel, Chemical Engineering Science, 57 (2002) 4691.
[202] M. Boudart, Industrial & Engineering Chemistry Fundamentals, 25 (1986) 656.
[203] T. Komaya and A.T. Bell, Journal of Catalysis, 146 (1994) 237.
[204] A.-M. Hilmen, O.A. Lindvag, E. Bergene, D. Schanke, S. Eri and A. Holmen, Studies in Surface Science and Catalysis, 136 (2001) 295.
[205] J.J.C. Geerlings, J.H. Wilson, G.J. Kramer, H.P.C.E. Kuipers, A. Hoek and H.M. Huisman, Applied Catalysis A: General, 186 (1999) 27.
[206] C. Erkey, J.B. Rodden and A. Akgerman, Energy & Fuels, 4 (1990) 275.
[207] R.J. Madon and E. Iglesia, Journal of Molecular Catalysis A: Chemical, 163 (2000) 189.
[208] H. Pichler, H. Schulz and M. Elstner, Brennstoff-Chemie, 48 (1967) 78.
[209] L.E. Murillo, N.A. Khan and J.G. Chen, Surface Science, 594 (2005) 27.
[210] B.A. Sexton and A.E. Hughes, Surface Science, 140 (1984) 227.
[211] K. Miyabe and M. Suzuki, AIChE Journal, 41 (1995) 548.
[212] K. Miyabe and M. Suzuki, AIChE Journal, 41 (1995) 536.
[213] T.R. Rybolt, M.D. Wall, H.E. Thomas, J.W. Bramblett and M. Phillips, Journal of Colloid Interface Science, 138 (1990) 113.
[214] E.S. Lox and G.F. Froment, Industrial & Engineering Chemistry Research, 32 (1993) 71.
[215] E.S. Lox and G.F. Froment, Industrial & Engineering Chemistry Research, 32 (1993) 61.
[216] X. Guo, Y. Liu, J. Chang, L. Bai, Y. Xu, H. Xiang and Y. Li, Journal of Natural Gas Chemistry, 15 (2006) 105.
[217] B.-T. Teng, J. Chang, C.-H. Zhang, D.-B. Cao, J. Yang, Y. Liu, X.-H. Guo, H.-W. Xiang and Y.-W. Li, Applied Catalysis A: General, 301 (2006) 39.
[218] B.-T. Teng, C.-H. Zhang, J. Yang, D.-B. Cao, J. Chang, H.-W. Xiang and Y.-W. Li, Fuel, 84 (2005) 791.
[219] Y.-N. Wang, W.-P. Ma, Y.-J. Lu, J. Yang, Y.-Y. Xu, H.-W. Xiang, Y.-W. Li, Y.-L. Zhao and B.-J. Zhang, Fuel, 82 (2003) 195.
[220] B. Teng, J. Chang, H. Wan, J. Lu, S. Zheng, Y. Liu, Y. Liu and X. Guo, Chinese Journal of Catalysis, 28 (2007) 687.
[221] J. Chang, L. Bai, B. Teng, R. Zhang, JunYang, Y. Xu[a], H. Xiang and Y. Li[a], Chemical Engineering Science, 62 (2007) 4983.
[222] J. Yang, Y. Liu, J. Chang, Y.-N. Wang, L. Bai, Y.-Y. Xu, H.-W. Xiang, Y.-W. Li and B. Zhong, Industrial & Engineering Chemistry Research, 42 (2003) 5066.
[223] C.G. Visconti, E. Tronconi, L. Lietti, P. Forzatti, S. Rossini and R. Zennaro, Topics in Catalysis, 54 (2011) 786.
[224] C.G. Visconti, L. Lietti, E. Tronconi, P. Forzatti, R. Zennaro and S. Rossini, Catalysis Today, 154 (2010) 202.

[225] S.-H. Kwack, J.W. Bae, M.-J. Park, S.-M. Kim, K.-S. Ha and K.-W. Jun, Fuel, 90 (2011) 1383.
[226] S.-H. Kwack, M.-J. Park, J.W. Bae, S.-J. Park, K.-S. Ha and K.-W. Jun, Fuel Processing Technology, 92 (2011) 2264.
[227] S.-H. Kwack, M.-J. Park, J.W. Bae, K.-S. Ha and K.-W. Jun, Reaction Kinetics, Mechanisms and Catalysis, 104 (2011) 483.
[228] B. Todic, W. Ma, G. Jacobs, B.H. Davis and D.B. Bukur, Catalysis Today, 228 (2014) 32.
[229] B. Todic, T. Bhatelia, G.F. Froment, W. Ma, G. Jacobs, B.H. Davis and D.B. Bukur, Industrial & Engineering Chemistry Research, 52 (2013) 669.
[230] J. Anfray, M. Bremaud, P. Fongarland, A. Khodakov, S. Jallais and D. Schweich, Chemical Engineering Science, 62 (2007) 5353.
[231] A.P. Steynberg, M.E. Dry, B.H. Davis and B.B. Breman, Studies in Surface Science and Catalysis, 152 (2004) 64.
[232] B.H. Davis, Catalysis Today, 71 (2002) 249.
[233] S.T. Sie and R. Krishna, Applied Catalysis A: General, 186 (1999) 55.
[234] S. Chambrey, P. Fongarland, H. Karaca, S. Piche, A. Griboval-Constant, D. Schweich, F. Luck, S. Savin and A.Y. Khodakov, Catalysis Today, 171 (2011) 201.
[235] M.E. Dry, Catalysis Today, 6 (1990) 183.
[236] M.E. Dry and A.P. Steynberg, Studies in Surface Science and Catalysis, 152 (2004) 406.
[237] R. Guettel and T. Turek, Chemical Engineering Science, 64 (2009) 955.
[238] A.M. Hilmen, E. Bergene, O.A. Lindvåg, D. Schanke, S. Eri and A. Holmen, Catalysis Today, 105 (2005) 357.
[239] A. Jess, R. Popp and K. Hedden, Applied Catalysis A: General, 186 (1999) 321.
[240] X. Lang, A. Akgerman and D.B. Bukur, Industrial & Engineering Chemistry Research, 34 (1995) 72.
[241] K.M. Brunner, J.C. Duncan, L.D. Harrison, K.E. Pratt, R.P.S. Peguin, C.H. Bartholomew and W.C. Hecker, International Journal of Chemical Reactor Engineering, 10 (2012).
[242] A. Jess and C. Kern, Chemical Engineering Technology, 32 (2009) 1164.
[243] T.S. Lee and J.N. Chung, Energy & Fuels, 26 (2012) 1363.
[244] A.R. Miroliaei, F. Shahraki, H. Atashi and R. Karimzadeh, Journal of Industrial Engineering Chemistry, 18 (2012) 1912.
[245] A. Sharma, R. Philippe, F. Luck and D. Schweich, Chemical Engineering Science, 66 (2011) 6358.
[246] C. Hou, Q. Yang, G. Xia, X. Sun, K. Wang, S. Zeng, Y. Wu, C. Jin, Z. Yan, M. Li, R. Xu and Z. Hu, China, SINOPEC Research Institute of Petroleum Processing, 2013, p. 11
[247] Y.-N. Wang, Y.-Y. Xu, Y.-W. Li, Y.-L. Zhao and B.-J. Zhang, Chemical Engineering Science, 58 (2003) 867.
[248] J.W.A. De Swart, R. Krishna and S.T. Sie, Studies in Surface Science and Catalysis, 107 (1997) 213.
[249] H. Adib, R. Haghbakhsh, M. Saidi, M.A. Takassi, F. Sharifi, M. Koolivand, M.R. Rahimpour and S. Keshtkari, Journal of Natural Gas Science and Engineering, 10 (2013) 14.

[250] R.C. Baliban, J.A. Elia and C.A. Floudas, Industrial & Engineering Chemistry Research, 52 (2013) 3381.
[251] R.C. Baliban, J.A. Elia, R. Misener and C.A. Floudas, Computers & Chemical Engineering, 42 (2012) 64.
[252] A. Rafiee and M. Hillestad, Chemical Engineering Technology, 36 (2013) 1729.
[253] M. Panahi, A. Rafiee, S. Skogestad and M. Hillestad, Industrial & Engineering Chemistry Research, 51 (2012) 425.
[254] S.K. Mazidi, M.T. Sadeghi and M.A. Marvast, Chemical Engineering Technology, 36 (2013) 62.
[255] M.R. Rahimpour, M.H. Khademi and A.M. Bahmanpour, Chemical Engineering Science, 65 (2010) 6206.
[256] M. Bayat and M.R. Rahimpour, Journal of Natural Gas Science and Engineering, 11 (2013) 52.
[257] M. Panahi and S. Skogestad, Industrial & Engineering Chemistry Research, 51 (2012) 10179.
[258] Q.-S. Liu, Z.-X. Zhang and J.-L. Zhou, Journal of Natural Gas Chemistry, 8 (1999) 238.
[259] Q.-S. Liu, Z.-X. Zhang and J.-L. Zhou, Journal of Natural Gas Chemistry, 8 (1999) 137.
[260] A.I. Stankiewicz and J.A. Moulijn, Chemical Engineering Progress, 1 (2000) 13.
[261] J. Yang, Y. Qi, J. Zhu, Y.-A. Zhu, D. Chen and A. Holmen, 308 Journal of Catalysis, 37.
[262] I.I. Chernobaev, M.N. Yakubovich, A.I. Tripolskii, N.V. Pavlenko and V.L. Struzhko, Theoretical and Experimental Chemistry, 33 (1997) 38.
[263] W.H. Lee and C.H. Bartholomew, Journal of Catalysis, 120 (1989) 256.
[264] H. Schulz, Catalysis Today, 214 (2013) 140.
[265] V.R.R. Pendyala, M.K. Gnanamani, G. Jacobs, W. Ma, W.D. Shafer and B.H. Davis, Applied Catalysis A: General, 468 (2013) 38.
[266] G. Jacobs, P.M. Patterson, Y. Zhang, T. Das, J. Li and B.H. Davis, Applied Catalysis A: General, 233 (2002) 215.
[267] J. Li, G. Jacobs, T. Das, Y. Zhang and B. Davis, Applied Catalysis A: General, 236 (2002) 67.
[268] J. Li, G. Jacobs, T. Das and B.H. Davis, Applied Catalysis A: General, 233 (2002) 255.
[269] M. Claeys and E. van Steen, Catalysis Today, 71 (2002) 419.
[270] J.P. den Breejen, P.B. Radstake, G.L. Bezemer, J.H. Bitter, V. Froseth, A. Holmen and K.P. de Jong, Journal of the American Chemical Society, 131 (2009) 7197.
[271] G.L. Bezemer, J.H. Bitter, H.P.C.E. Kuipers, H. Oosterbeek, J.E. Holewijn, X. Xu, F. Kapteijn, D.A.J. van and J.K.P. de, Journal of the American Chemical Society, 128 (2006) 3956.
[272] Z. Pan, M. Parvari and D.B. Bukur, Applied Catalysis A: General, 480 (2014) 79.
[273] W. Ma, G. Jacobs, R.A. Keogh, D.B. Bukur and B.H. Davis, Applied Catalysis A: General, 437-438 (2012) 1.
[274] D. Reay, C. Ramshaw and A. Harvey, Process Intensification, Butterworth-Heinemann, Oxford, 2008, p. 103.
[275] A. Renken and L. Kiwi-Minsker, Advances in Catalysis, Vol. 53, Academic Press, 2010, p. 47.

[276] R.M. de Deugd, F. Kapteijn and J.A. Moulijn, Topics in Catalysis, 26 (2003) 29.
[277] J.A. Moulijn, M.T. Kreutzer, T.A. Nijhuis and F. Kapteijn, Advances in Catalysis, Vol. 54, Academic Press, 2011, p. 249.
[278] K. Pangarkar, T.J. Schildhauer, J.R. Van Ommen, J. Nijenhuis, F. Kapteijn and J.A. Moulijn, Industrial and Engineering Chemistry Research, 47 (2008) 3720.
[279] M.T. Kreutzer, F. Kapteijn, J.A. Moulijn and J.J. Heiszwolf, Chemical Engineering Science, 60 (2005) 5895.
[280] A.M. Hilmen, E. Bergene, O.A. Lindvåg, D. Schanke, S. Eri and A. Holmen, Catalysis Today, 69 (2001) 227.
[281] A.M. Hilmen, E. Bergene, O.A. Lindvag, D. Schanke, S. Eri and A. Holmen, Studies in Surface Science and Catalysis, 130B (2000) 1163.
[282] L.C. Almeida, F.J. Echave, O. Sanz, M.A. Centeno, G. Arzamendi, L.M. Gandía, E.F. Sousa-Aguiar, J.A. Odriozola and M. Montes, Chemical Engineering Journal, 167 (2011) 536.
[283] R. Krishna and S.T. Sie, Chemical Engineering Science, 49 (1994) 4029.
[284] R.M. de Deugd, R.B. Chougule, M.T. Kreutzer, F.M. Meeuse, J. Grievink, F. Kapteijn and J.A. Moulijn, Chemical Engineering Science, 58 (2003) 583.
[285] R.M. de Deugd, F. Kapteijn and J.A. Moulijn, Catalysis Today, 79-80 (2003) 495.
[286] F. Kapteijn, R.M. de Deugd and J.A. Moulijn, Catalysis Today, 105 (2005) 350.
[287] C.G. Visconti, E. Tronconi, L. Lietti, G. Groppi, P. Forzatti, C. Cristiani, R. Zennaro and S. Rossini, Applied Catalysis A: General, 370 (2009) 93.
[288] C.G. Visconti, E. Tronconi, G. Groppi, L. Lietti, M. Iovane, S. Rossini and R. Zennaro, Chemical Engineering Journal, 171 (2011) 1294.
[289] A. Holmen, H.J. Venvik, R. Myrstad, J. Zhu and D. Chen, Catalysis Today, 216 (2013) 150.
[290] S. Farzad, A. Rashidi, A. Haghtalab and M.A. Mandegari, Fuel, 132 (2014) 27.
[291] C.L. Kibby, R.J. Saxton, Jr., K. Jothimurugesan, T.K. Das, H.S. Lacheen, M. Bartz and A. Has, US Patent 2013/0210942 Al, 2013.
[292] A. Zamaniyana, Y. Mortazavi, A.A. Khodadadi, F. Bahadoran and S. Dialameh, Pazhuhesh Naft, 22 (2012) 66.
[293] W. Liu, Y. Wang, W. Wilcox and S. Li, AIChE Journal, 58 (2012) 2820.
[294] Y. Wang and W. Liu, US Patent 20090215911A1, 2009.
[295] W. Liu, J. Hu and Y. Wang, Catalysis Today, 140 (2009) 142.
[296] M. Bakhtiari, F. Khorasheh, A. Zamanian, A. Nakhaeipour and M. Irani, Petroleum & Coal, 50 (2008) 56.
[297] R. Guettel, J. Knochen, U. Kunz, M. Kassing and T. Turek, Industrial & Engineering Chemistry Research, 47 (2008) 6589.
[298] Y. Wang, J. Hu, D. Rector and W. Liu, Proceedings of Annual International Pittsburgh Coal Conference, 24th (2007) 441/1.
[299] L.C. Almeida, O. Gonzalez, O. Sanz, A. Paul, M.A. Centeno, J.A. Odriozola and M. Montes, Studies in Surface Science and Catalysis, 167 (2007) 79.
[300] R. Guettel, J. Knochen, U. Kunz and T. Turek, Chemie Ingenieur Technik, 79 (2007) 1295.
[301] L.C. Almeida, O. Sanz, D. Merino, G. Arzamendi, L.M. Gandía and M. Montes, Catalysis Today, 215 (2013) 103.
[302] J. Zhu, J. Yang, A.H. Lillebø, Y. Zhu, Y. Yu, A. Holmen and D. Chen, Catalysis Today, 215 (2013) 121.

[303] Z. Yu, O. Borg, D. Chen, B.C. Enger, V. Froseth, E. Rytter, H. Wigum and A. Holmen, Catalysis Letters, 109 (2006) 43.
[304] C. Cao, D.R. Palo, A.L.Y. Tonkovich and Y. Wang, Catalysis Today, 125 (2007) 29.
[305] A.L. Tonkovich, K. Jarosch, S. Fitzgerald, B. Yang, D. Kilanowski, J. McDaniel and T. Dritz, Microchannel Gas-to-Liquids for Monetizing Associated and Stranded Gas Reserves, Velocys Inc, White Paper, 2011.
[306] S. LeViness, A.L. Tonkovich, K. Jarosch, S. Fitzgerald, B. Yang and J. McDaniel, Improved Fischer-Tropsch Economics Enabled by Microchannel Technology, Velocys Inc., White Paper, 2011.
[307] A.L. Tonkovich, T. Mazanec, K. Jarosch, S. Fitzgerald, B. Yang, R. Taha, D. Kilanowski, J. Lerou, J. McDaniel, D. Atkinson and T. Dritz, Gas-to-Liquids Conversion of Associated Gas Enabled by Microchannel Technology Velocys Inc., White Paper, 2009.
[308] E. Klemm, H. Döring, A. Geisselmann and S. Schirrmeister, Chemical Engineering & Technology, 30 (2007) 1615.
[309] Y. Wang, D.P. VanderWiel, A.L.Y. Tonkovich, Y. Gao and E.G. Baker, US Patent, 6558634 B1, 2003.
[310] J. Knochen, R. Guettel, C. Knobloch and T. Turek, Chemical Engineering and Processing, 49 (2010) 958.
[311] H.A.J. van Dijk, J.H.B.J. Hoebink and J.C. Schouten, Topics in Catalysis, 26 (2003) 111.
[312] B.C. Enger, V. Froeseth, J. Yang, E. Rytter and A. Holmen, Journal of Catalysis, 297 (2013) 187.
[313] N.S. Govender, F.G. Botes, M.H.J.M. de Croon and J.C. Schouten, Journal of Catalysis, 260 (2008) 254.
[314] M. Arsalanfar, A.A. Mirzaei, H.R. Bozorgzadeh and H. Atashi, Journal of Industrial and Engineering Chemistry, 18 (2012) 2092.
[315] F.E.M. Farias, F.G. Sales and F.A.N. Fernandes, Journal of Natural Gas Chemistry, 17 (2008) 175.
[316] S. Ozkara-Aydinoglu, O. Atac, O.F. Gul, S. Kinayyigit, S. Sal, M. Baranak and I. Boz, Chemical Engineering Journal, 181-182 (2012) 581.
[317] B.W. Wojciechowski, Canadian Journal of Chemical Engineering, 64 (1986) 149.
[318] L.M. Tau, H.A. Dabbagh, J. Halasz and B.H. Davis, Journal of Molecular Catalysis, 71 (1992) 37.
[319] S. Soled, E. Iglesia, S. Miseo, B. DeRites and R. Fiato, Topics in Catalysis, 2 (1995) 193.
[320] G.A. Huff, Fischer-Tropsch synthesis in a slurry reactor, Ph.D. Thesis, MIT, 1982.
[321] B.H. Davis, Industrial & Engineering Chemistry Research, 46 (2007) 8938.
[322] H. Kolbel and P. Ackermann, Chemie Ingenieur Technik, 28 (1956) 381.
[323] A.P. Steynberg, M.E. Dry, M.E. Davis, B.H. Davis and B.B. Breman, Studies in Surface Science and Catalysis, 152 (2004) 64.
[324] A.K. Dalai and B.H. Davis, Applied Catalysis A: General, 348 (2008) 1.
[325] D.J. Duvenhage, R.L. Espinoza and N.J. Coville, Studies in Surface Science and Catalysis, 88 (1994) 351.
[326] D.J. Duvenhage and N.J. Coville, Applied Catalysis A: General, 298 (2006) 211.

[327] D.B. Bukur and X. Lang, Industrial and Engineering Chemistry Research, 38 (1999) 3270.
[328] D.B. Bukur, X. Lang and L. Nowicki, Industrial & Engineering Chemistry Research, 44 (2005) 6038.
[329] D.B. Bukur, L. Nowicki and X. Lang, Chemical Engineering Science, 49 (1994) 4615.
[330] K. Aasberg-Petersen, T.S. Christensen, I. Dybkjaer, J. Sehested, M. Østberg, R.M. Coertzen, M.J. Keyser and A.P. Steynberg, Studies in Surface Science and Catalysis, 152 (2004) 258.
[331] D. Gray, M. Lytton, M. Neuworth and G. Tomlinson, Impact of developing technology on indirect liquefaction, DOE Technical Report, 1980.
[332] D. Gray and G.C. Tomlinson, Assessing the economic impact of indirect liquefaction process improvements: Volume 1, Development of the integrated indirect liquefaction model and baseline case, DOE Technical Report, 1990.
[333] D. Gray, G.C. Tomlinson and A. ElSawy, Quantification of Progress in Indirect Coal Liquefaction, DOE Technical Report, 1990.
[334] D. Gray and G. Tomlinson, Studies in Surface Science and Catalysis, 107 (1997) 145.
[335] J. Neathery, D. Gray, D. Challman and F. Derbyshire, Fuel, 78 (1999) 815.
[336] D. Gray, J. Plunkett, S. Salerno, C. White and G. Tomlinson, Proceedings of 31st International Technical Conference on Coal Utilization and Fuel Systems, (2006) 253.
[337] B.L. Bhatt, R. Frame, A. Hoek, K. Kinnari, V.U.S. Rao and F.L. Tungate, Topics in Catalysis, 2 (1995) 235.
[338] J.P. den Breejen, P.B. Radstake, G.L. Bezemer, J.H. Bitter, V. Frøseth, A. Holmen and K.P.d. Jong, Journal of the American Chemical Society, 131 (2009) 7197.
[339] E. Rytter, S. Eri, T.H. Skagseth, D. Schanke, E. Bergene, R. Myrstad and A. Lindvåg, Industrial & Engineering Chemistry Research, 46 (2007) 9032.
[340] Ø. Borg, P.D.C. Dietzel, A.I. Spjelkavik, E.Z. Tveten, J.C. Walmsley, S. Diplas, S. Eri, A. Holmen and E. Rytter, Journal of Catalysis, 259 (2008) 161.
[341] A.-M. Hilmen, O.A. Lindvg, E. Bergene, D. Schanke, S. Eri and A. Holmen, Studies in Surface Science and Catalysis, 136 (2001) 295.
[342] C.A. Mims, J.J. Krajewski, K.D. Rose and M.T. Melchior, Catalysis Letters, 7 (1990) 119.
[343] R.J. Madon, S.C. Reyes and E. Iglesia, Journal of Physical Chemistry, 95 (1991) 7795.
[344] O. Borg, S. Eri, E.A. Blekkan, S. Storsaeter, H. Wigum, E. Rytter and A. Holmen, Journal of Catalysis, 248 (2007) 89.
[345] G. Jacobs, M.C. Ribeiro, W. Ma, Y. Ji, S. Khalid, P.T.A. Sumodjo and B.H. Davis, Applied Catalysis A: General, 361 (2009) 137.
[346] T. Jermwongratanachai, G. Jacobs, W. Ma, W.D. Shafer, M.K. Gnanamani, P. Gao, B. Kitiyanan, B.H. Davis, J.L.S. Klettlinger, C.H. Yen, D.C. Cronauer, A.J. Kropf and C.L. Marshall, Applied Catalysis A: General, 464–465 (2013) 165.
[347] H. Schulz, M. Claeys and S. Harms, Studies in Surface Science and Catalysis, 107 (1997) 193.
[348] S. Krishnamoorthy, M. Tu, M.P. Ojeda, D. Pinna and E. Iglesia, Journal of Catalysis, 211 (2002) 422.
[349] C.J. Bertole, C.A. Mims and G. Kiss, Journal of Catalysis, 210 (2002) 84.

[350] S. Storsaeter, O. Borg, E.A. Blekkan, B. Totdal and A. Holmen, Catalysis Today, 100 (2005) 343.
[351] J. Cheng, T. Song, P. Hu, C.M. Lok, P. Ellis and S. French, Journal of Catalysis, 255 (2008) 20.
[352] C.M. Nguyen, B.A. De Moor, M.-F. Reyniers and G.B. Marin, The Journal of Physical Chemistry C, 115 (2011) 23831.
[353] A.M. Goda, M. Neurock, M.A. Barteau and J.G. Chen, Surface Science, 602 (2008) 2513.
[354] H.A.J. van Dijk, J.H.B.J. Hoebink and J.C. Schouten, Topics in Catalysis, 26 (2003) 163.
[355] J. Cheng, P. Hu, P. Ellis, S. French, G. Kelly and C.M. Lok, The Journal of Physical Chemistry C, 112 (2008) 1308.
[356] K.B.B. Gilbert F. Froment, Juray De Wilde, Chemical Reactor Analysis and Design, John Wiley & Sons, New York, 2011.
[357] T.-Y. Park and G.F. Froment, Computers and Chemical Engineering, 22 (1998) 103.
[358] B. Wang, D.W. Goodman and G.F. Froment, Journal of Catalysis, 253 (2008) 229.
[359] W.J. Lee and G.F. Froment, Industrial & Engineering Chemistry Research, 47 (2008) 9183.
[360] M.A. Vannice, S.H. Hyun, B. Kalpakci and W.C. Liauh, Journal of Catalysis, 56 (1979) 358.
[361] M.A. Vannice, Journal of Catalysis, 37 (1975) 462.
[362] Y. Kim, D.-Y. Hwang, S. Song, S. Lee, E. Park and M.-J. Park, Korean Journal of Chemical Engineering, 26 (2009) 1591.
[363] D.J. Lavrich, S.M. Wetterer, S.L. Bernasek and G. Scoles, Journal of Physical Chemistry B, 102 (1998) 3456.
[364] G. Blyholder, D. Shihabi, W.V. Wyatt and R. Bartlett, Journal of Catalysis, 43 (1976) 122.
[365] J.J.C. Geerlings, M.C. Zonnevylle and G.C.P.M. De, Surface Science, 241 (1991) 302.
[366] G.A. Beitel, C.P.M. de Groot, H. Oosterbeek and J.H. Wilson, Journal of Physical Chemistry B, 101 (1997) 4035.
[367] G. Lozano-Blanco, J.W. Thybaut, K. Surla, P. Galtier and G.B. Marin, AIChE Journal, 55 (2009) 2159.
[368] J.W.A. de Swart and R. Krishna, Chemical Engineering and Processing, 41 (2002) 35.
[369] C. Maretto and R. Krishna, Catalysis Today, 52 (1999) 279.
[370] N. Rados, M.H. Al-Dahhan and M.P. Dudukovic, Industrial & Engineering Chemistry Research, 44 (2005) 6086.
[371] G.P. Van der Laan, A.A.C.M. Beenackers and R. Krishna, Chemical Engineering Science, 54 (1999) 5013.
[372] C.G. Visconti and M. Mascellaro, Catalysis Today, 214 (2013) 61.
[373] W.H. Zimmerman, J.A. Rossin and D.B. Bukur, Industrial & Engineering Chemistry Research, 28 (1989) 406.
[374] P. Chaumette, C. Verdon and P. Boucot, Topics in Catalysis, 2 (1995) 301.
[375] D. Green and R. Perry, Perry's Chemical Engineers' Handbook, Eighth Edition, McGraw-Hill Education, 2007.

[376] B. Poling, J. Prausnitz and J.O. Connell, The Properties of Gases and Liquids, McGraw-Hill Education, 2000.
[377] W.M. Haynes, CRC Handbook of Chemistry and Physics, 95th Edition, Taylor & Francis, 2014.
[378] U.S. National Institute of Standards and Technology, NIST Chemistry Webbook, U.S. Secretary of Commerce, 2003.
[379] S. Yagi and D. Kunii, AIChE Journal, 3 (1957) 373.
[380] A. Matsuura, Y. Hitaka, T. Akehata and T. Shirai, Heat Transfer - Japanese Research, 8 (1979) 44.
[381] S. Ergun, Chemical Engineering Progress, 48 (1952) 89.
[382] F. Benyahia and K.E. O'Neill, Particulate Science and Technology, 23 (2005) 169.
[383] C. Knobloch, R. Güttel and T. Turek, Chemie Ingenieur Technik, 85 (2013) 455.
[384] A. Hoek and L.B.J.M. Kersten, in B. Xinhe and X. Yide, Studies in Surface Science and Catalysis, 147 (2004) 25.
[385] S.T. Sie, M.M.G. Senden and H.M.H. Van Wechem, Catalysis Today, 8 (1991) 371.
[386] V.M.H. van Wechem and M.M.G. Senden, Studies in Surface Science and Catalysis, 81 (1994) 43.
[387] M.E. Dry, Studies in Surface Science and Catalysis, 152 (2004) 196.

List of tables

List of figures

List of symbols and abbreviations

A_{cs} : reactor tube cross-section area (m^2)

A_i : preexponential factor of rate constant for elementary step i

BTL : biomass-to-liquids

c : constant determining chain length dependence

c_p : fluid heat capacity

[CO-S]: surface coverage of adsorbed CO

CTL : coal-to-liquid

d_t : tube diameter (m)

d_p : the particle diameter (m)

E_i : activation energy of elementary step i (kJ/mol)

ΔE : change in 1-olefin desorption activation energy caused by weak force interactions (kJ/mol/CH_2 group)

$E_{d,o}^{n}$: overall activation energy for the 1-olefin desorption step (kJ/mol)

f : friction factor for fluid flow in a packed bed

F_i : molar flowrate of species

F_{obj} : multi-response objective function

FTS : Fischer-Tropsch synthesis

GTL : gas-to-liquids

H_2/CO : reactant feed ratio, mol/mol

ΔH_i : enthalpy of elementary step i (kJ/mol)

[H-S] : surface coverage of adsorbed atomic hydrogen

h_{wall} : heat transfer coefficient at the wall

k_i : reaction rate constant for elementary step i

K_i : equilibrium constant for elementary step i

N_{resp} : number of responses

N_{exp} : number of experimental balances

OPR : olefin-to-paraffin ratio

P : pressure, MPa

P_i : partial pressure of species i, MPa

Pr : Prantl number

R : universal gas constant, kJ/kmol/K

Re : Reynolds number

R_i : reaction rate of species i, mol/g_{cat}/h

[R-S] : surface coverage of growing hydrocarbon chains

S : vacant active site

S_n : selectivity to hydrocarbons with n carbon atoms

T : temperature, K

T_w : reactor wall temperature (K)

TOS : time on stream, h

U :overall heat transfer coefficient

u_s : surface velocity (m/s)

W : catalyst mass, g_{cat}

WHSV: weight hourly space velocity, $NL/g_{cat}/h$

X_{CO} : CO conversion

y_n : molar fraction of hydrocarbon with n carbon atoms

z : reactor length coordinate

Greek symbols

α_0 : chain growth probability for the low hydrocarbon range (double-alpha theory)

α_{inf} : chain growth probability for the high hydrocarbon range (double-alpha theory)

α_n : chain growth probability for carbon number n ($n \geq 1$)

β_n : probability 1-olefin with n carbon numbers readsorption

λ_{er} : effective radial thermal conductivity in reactor core

ρ : fluid density

ρ_b : reactor bed density

Subscripts and Superscripts

cal : calculated value

exp : experimental value

M : methane

E : ethene

n : number of carbon atoms

List of publications

Scientific publications published in top international journals (category M21):

1. Branislav Todic, Vitaly V. Ordomsky, Nikola M. Nikacevic, Andrei Y. Khodakov and Dragomir B. Bukur, "Opportunities for intensification of Fischer–Tropsch synthesis through reduced formation of methane over cobalt catalysts in microreactors", Catalysis Science & Technology, **2015**, 5, 1400. (**IF = 4.760**)
2. Tomasz Olewski, Branislav Todic, Lech Nowicki, Nikola Nikacevic and Dragomir B. Bukur, "Hydrocarbon selectivity models for iron-based Fischer–Tropsch catalyst", Chemical Engineering Research and Design, **2015**, 95, 1. (**IF = 2.281**)
3. Branislav Todic, Wenping Ma, Gary Jacobs, Burtron H. Davis, Dragomir B. Bukur, "Effect of process conditions on the product distribution of Fischer–Tropsch synthesis over a Re-promoted cobalt-alumina catalyst using a stirred tank slurry reactor", *Journal of Catalysis*, **2014**, 311, 325. (**IF = 5.787**)
4. Branislav Todic, Wenping Ma, Gary Jacobs, Burtron H. Davis, Dragomir B. Bukur, "CO-insertion mechanism based kinetic model of the Fischer–Tropsch synthesis reaction over Re-promoted Co catalyst", *Catalysis Today*, **2014**, 228, 32. (**IF = 2.980**)
5. Gary Jacobs, Wenping Ma, Pei Gao, Branislav Todic, Tejas Bhatelia, Dragomir B. Bukur, Syed Khalid, Burtron H. Davis, "The application of synchrotron methods in characterizing iron and cobalt Fischer–Tropsch synthesis catalysts", *Catalysis Today*, **2013**, 214, 100. (**IF = 2.980**)
6. Branislav Todic, Tejas Bhatelia, Wenping Ma, Gary Jacobs, Burtron H. Davis, Dragomir B. Bukur, "Kinetic Model of Fischer−Tropsch Synthesis in a Slurry Reactor on Co−Re/Al_2O_3 Catalyst", *Industrial and Engineering Chemistry Research*, **2013**, 52, 669. (**IF = 2.206**)
7. Gary Jacobs, Wenping Ma, Pei Gao, Branislav Todic, Tejas Bhatelia, Dragomir B. Bukur, Syed Khalid, Burtron H. Davis, "Fischer-Tropsch synthesis: differences observed in local atomic structure and selectivity with Pd compared to typical promoters (Pt, Re, Ru) of Co/Al_2O_3 catalysts", *Topics in Catalysis*, **2012**, 55, 811. (**IF = 2.608**)

Scientific publications published in leading journals of national importance (category M51):

1. Branislav Todic, Tomasz Olewski, Nikola Nikacevic, Dragomir B. Bukur, "Modeling of Fischer-Tropsch product distribution over Fe-based catalyst", *Chemical Engineering Transactions*, **2013**, 32, 793. (**IF = N/A**)

Conference presentations (category M34):

1. Branislav Todic, Lech Nowicki, Nikola Nikacevic, Dragomir B. Bukur, "Effect of process conditions on Fischer-Tropsch synthesis over an industrial iron-based catalyst", Syngas Convention 2, March 29 – April 1, 2015, Cape Town, South Africa.
2. Branislav Todic, Tejas Bhatelia, Wenping Ma, Gary Jacobs, Burtron H. Davis and Dragomir B. Bukur, "Importance Of methane formation in determining overall selectivity of Fischer-Tropsch synthesis over cobalt-based catalyst", 249th ACS National Meeting & Exposition, March 22-26, 2015, Denver, US.
3. Branislav Todic, Tomasz Olewski, Nikola Nikacevic, Dragomir B. Bukur, "Modeling of Fischer-Tropsch product distribution over Fe-based catalyst", 11th International Conference on Chemical & Process Engineering, June 2-5, 2013, Milan, Italy
4. Wenping Ma, Gary Jacobs, Branislav Todic, Dragomir B. Bukur and Burtron H. Davis, "Fischer-Tropsch synthesis: Influence of process conditions on deactivation of Ru and Re promoted 25%Co/Al_2O_3 catalysts", 23rd North American Catalysis Society Meeting, June 2-7, 2013, Louisville, US.
5. Branislav Todic, Nikola Nikacevic, Dragomir B. Bukur, "Application of detailed kinetics in a fixed bed reactor model for the Fischer-Tropsch synthesis", 9th European Congress of Chemical Engineering, April 21–25, 2013, The Hague, Nederland.
6. Branislav Todic, Wenping Ma, Gary Jacobs, Burtron H. Davis and Dragomir B. Bukur, "Detailed kinetic model of Fischer-Tropsch synthesis over a cobalt-based catalyst", 9th European Congress of Chemical Engineering, April 21–25, 2013, The Hague, Nederland.
7. Gary Jacobs, Wenping Ma, Branislav Todic, Dragomir B. Bukur and Burtron H. Davis, "Fischer-Tropsch synthesis: linking cobalt catalyst promoter performance parameters to catalyst structure: an EXAFS investigation", NGCS 10, March 2–7, 2013, Doha, Qatar.
8. Branislav Todic, Wenping Ma, Gary Jacobs, Burtron H. Davis and Dragomir B. Bukur, "CO-insertion mechanism based comprehensive kinetic model of Fischer-Tropsch Synthesis over Re-promoted Co catalyst", NGCS 10, March 2–7, 2013, Doha, Qatar.
9. Wenping Ma, Gary Jacobs, Branislav Todic, Dragomir B. Bukur and Burtron H. Davis, "Fischer-Tropsch synthesis: Activity and selectivity of 0.48% Re-25%Co/Al_2O_3 catalyst in a 1L slurry-phase reactor", AIChE Annual Meeting, October 28 – November 2, 2012., Pittsburg, US.
10. Branislav Todic, Tejas Bhatelia, Wenping Ma, Gary Jacobs, Burtron H. Davis and Dragomir B. Bukur, "Comprehensive kinetic model of Fischer-Tropsch

synthesis in a slurry reactor", SynFuel2012 Symposium, June 29-30, 2012, Munich, Germany.

11. Branislav Todic, Tejas Bhatelia, Wenping Ma, Gary Jacobs, Burtron H. Davis and Dragomir B. Bukur, "Kinetic modeling of GTL product distribution on Co catalyst", Research Poster, Research-Industry Partnership Showcase, May 21, 2012, Doha, Qatar.
12. Jacobs, G., Ma, W., Davis, B.H., Todic, B., Bhatelia, T., Bukur, D.B, "The application of synchrotron methods in characterizing iron and cobalt Fischer-Tropsch synthesis catalysts," Keynote Lecture, Syngas Convention 2012, April 1-4, 2012, Cape Town, South Africa.
13. Branislav Todic, Tejas Bhatelia, Wenping Ma, Gary Jacobs, Burtron H. Davis and Dragomir B. Bukur, "Comprehensive kinetic model for Fischer-Tropsch synthesis over a Re promoted Co/Al_2O_3 catalyst", AIChE Spring National Meeting, April 1-5, 2012., Houston, US.
14. Tejas Bhatelia, Branislav Todic, Dragomir Bukur, Wenping Ma, Burtron Davis and Gary Jacobs, "Detailed kinetics of the Fischer-Tropsch reaction over a Ru-promoted Co/Al_2O_3 catalyst", Qatar Foundation Annual Research Forum, November 20-22, 2011, Doha, Qatar.

Biography

Branislav Todić was born on 21.10.1987. in Sremska Mitrovica, where we finished elementary and high school. He enrolled at the Faculty of Technology and Metallurgy (FTM), University of Belgrade, in academic year 2006/2007., Department of Chemical Engineering. He finished the undergraduate studies in September of 2010., with a grade point average of 9,34. He graduated from Master Studies at FTM (Chemical Process Engineering) in August of 2011. with a grade point average of 9,50 and mark 10 for a Master Thesis "Analysis of GTL – Fischer-Tropsch process for the production of liquid hydrocarbons from natural gas" with mentor Professor Dr. Dejan Skala.

In academic year 2011/12. he enrolled in the Doctoral studies at the Faculty of Technology and Metallurgy, academic program Chemical Engineering, under the supervision of Dr. Nikola Nikačević, Associate Professor at FTM.

Biografija

Branislav Todić je rođen 21.10.1987. godine u Sremskoj Mitrovici, gde je završio osnovnu i srednju školu. Na Tehnološko-metalurški fakultet (TMF), Univerziteta u Beogradu, upisao se školske 2006/2007. godine, na odsek za Hemijsko inženjerstvo. Osnovne studije je završio u septembru 2010. godine sa prosečnom ocenom 9,34. Master studije TMF-a (smer Hemijsko procesno inženjerstvo) završio je u avgustu 2011. godine sa prosečnom ocenom 9,50 i ocenom 10 sa Master radom na temu „Analiza GTL – Fišer-Tropšovog (Fischer-Tropsch) procesa dobijanja tečnih ugljovodonika iz prirodnog gasa" kod mentora prof. dr Dejana Skale.

Školske 2011/12. upisao se na doktorske studije na Tehnološko-metalurškom fakultetu, studijski program Hemijsko inženjerstvo, pod rukovodstvom dr. Nikole Nikačevića, vanrednog profesora TMF.

Прилог 1.

Изјава о ауторству

Потписани-а Бранислав Тодић

број индекса 4028/2011

Изјављујем

да је докторска дисертација под насловом

Моделовање хемијске кинетике и оптимизација реактора са пакованим слојем за Фишер-Тропш синтезу (енг. Kinetic modeling and optimization of fixed-bed reactor for Fischer-Tropsch synthesis)

- резултат сопственог истраживачког рада,
- да предложена дисертација у целини ни у деловима није била предложена за добијање било које дипломе према студијским програмима других високошколских установа,
- да су резултати коректно наведени и
- да нисам кршио/ла ауторска права и користио интелектуалну својину других лица.

Потпис докторанда

У Београду, 16.2.2015.

Todić Branislav

Прилог 2.

Изјава о истоветности штампане и електронске верзије докторског рада

Име и презиме аутора Бранислав Тодић

Број индекса 4028/2011

Студијски програм Хемијско инжењерство

Наслов рада Моделовање хемијске кинетике и оптимизација реактора са пакованим слојем за Фишер-Тропш синтезу (енг. Kinetic modeling and optimization of fixed-bed reactor for Fischer-Tropsch synthesis)

Ментор др. Никола Никачевић

Потписани/а Бранислав Тодић

Изјављујем да је штампана верзија мог докторског рада истоветна електронској верзији коју сам предао/ла за објављивање на порталу **Дигиталног репозиторијума Универзитета у Београду.**

Дозвољавам да се објаве моји лични подаци везани за добијање академског звања доктора наука, као што су име и презиме, година и место рођења и датум одбране рада.

Ови лични подаци могу се објавити на мрежним страницама дигиталне библиотеке, у електронском каталогу и у публикацијама Универзитета у Београду.

Потпис докторанда

У Београду, 2.16.2015.

Todić Branislav

Прилог 3.

Изјава о коришћењу

Овлашћујем Универзитетску библиотеку „Светозар Марковић" да у Дигитални репозиторијум Универзитета у Београду унесе моју докторску дисертацију под насловом:

Моделовање хемијске кинетике и оптимизација реактора са паковањем слојем за Фишер-Тропш синтезу (енг. Kinetic modeling and optimization of fixed-bed reactor for Fischer-Tropsch synthesis)

која је моје ауторско дело.

Дисертацију са свим прилозима предао/ла сам у електронском формату погодном за трајно архивирање.

Моју докторску дисертацију похрањену у Дигитални репозиторијум Универзитета у Београду могу да користе сви који поштују одредбе садржане у одабраном типу лиценце Креативне заједнице (Creative Commons) за коју сам се одлучио/ла.

1. Ауторство

2. Ауторство - некомерцијално

3. Ауторство – некомерцијално – без прераде

4. Ауторство – некомерцијално – делити под истим условима

5. Ауторство – без прераде

6. Ауторство – делити под истим условима

(Молимо да заокружите само једну од шест понуђених лиценци, кратак опис лиценци дат је на полеђини листа).

Потпис докторанда

У Београду, 2.16.2015.

Jodić Branislav

1. Ауторство - Дозвољавате умножавање, дистрибуцију и јавно саопштавање дела, и прераде, ако се наведе име аутора на начин одређен од стране аутора или даваоца лиценце, чак и у комерцијалне сврхе. Ово је најслободнија од свих лиценци.

2. Ауторство – некомерцијално. Дозвољавате умножавање, дистрибуцију и јавно саопштавање дела, и прераде, ако се наведе име аутора на начин одређен од стране аутора или даваоца лиценце. Ова лиценца не дозвољава комерцијалну употребу дела.

3. Ауторство - некомерцијално – без прераде. Дозвољавате умножавање, дистрибуцију и јавно саопштавање дела, без промена, преобликовања или употребе дела у свом делу, ако се наведе име аутора на начин одређен од стране аутора или даваоца лиценце. Ова лиценца не дозвољава комерцијалну употребу дела. У односу на све остале лиценце, овом лиценцом се ограничава највећи обим права коришћења дела.

4. Ауторство - некомерцијално – делити под истим условима. Дозвољавате умножавање, дистрибуцију и јавно саопштавање дела, и прераде, ако се наведе име аутора на начин одређен од стране аутора или даваоца лиценце и ако се прерада дистрибуира под истом или сличном лиценцом. Ова лиценца не дозвољава комерцијалну употребу дела и прерада.

5. Ауторство – без прераде. Дозвољавате умножавање, дистрибуцију и јавно саопштавање дела, без промена, преобликовања или употребе дела у свом делу, ако се наведе име аутора на начин одређен од стране аутора или даваоца лиценце. Ова лиценца дозвољава комерцијалну употребу дела.

6. Ауторство - делити под истим условима. Дозвољавате умножавање, дистрибуцију и јавно саопштавање дела, и прераде, ако се наведе име аутора на начин одређен од стране аутора или даваоца лиценце и ако се прерада дистрибуира под истом или сличном лиценцом. Ова лиценца дозвољава комерцијалну употребу дела и прерада. Слична је софтверским лиценцама, односно лиценцама отвореног кода.